# LIQUID SLOSH AND ITS INFLUENCE ON BRAKING AND ROLL RESPONSES OF PARTLY FILLED TANK VEHICLES

Guorong Yan

A Thesis

in

The Department

of

Mechanical and Industrial Engineering

Presented in Partial Fulfillment of the Requirements
For the Degree of Doctor of Philosophy at
Concordia University
Montreal, Quebec, Canada

April 2008

*Your file Votre référence*
*ISBN: 978-0-494-37766-6*
*Our file Notre référence*
*ISBN: 978-0-494-37766-6*

# ABSTRACT

## Liquid Slosh and Its Influence on Braking and Roll Responses of Partly Filled Tank Vehicles

Guorong Yan, Ph.D.

Concordia University, 2008

Liquid cargo contained in a partly-filled tank is known to experience the sloshing movement when subjected to manoeuvre-induced disturbances. Large amplitude slosh can be induced within a partly-filled road tank vehicle under mild to severe directional manoeuvres, which could severely degrade the vehicle stability and directional control limits. A three-dimensional computational fluid dynamics slosh model is implemented for the partly-filled cleanbore and baffled tanks on the basis of the Navier-Stokes equations incorporating the VOF technique. A comprehensive experimental study is conducted to analyze the fluid slosh within a scale model tank with and without the baffles under continuous as well as single-cycle sinusoidal lateral and longitudinal acceleration excitations. The three-dimensional fluid slosh responses are further investigated for full scale baffled and unbaffled vehicle tanks using the validated fluid slosh model. The fluid slosh characteristics are analyzed under different fill volumes corresponding to a constant load and subjected to excitations representing steady-turning, straight-line braking, braking-in-turn and path change maneuvers. The fluid slosh analyses are also carried out to explore the anti-slosh effectiveness of baffles and to evaluate the effects of baffle design factors, such as equalizer and the orifice size.

The influences of transient fluid slosh on the tank vehicle stability and responses are studied by incorporating the fluid slosh model to in-plane vehicle models. The two-

dimensional roll-plane slosh models of partly-filled tanks of different cross-sections are integrated with the roll moment equilibrium of an articulated vehicle to derive the vehicle roll stability limits. The roll stability analyses are performed for circular and "Reuleaux triangular" tanks under the conditions of constant and variable cargo loads. The results attained are compared with the quasi-static solutions to demonstrate the role of transient slosh loads on the roll stability limits. The three-dimensional slosh model of a partly-filled tank is also integrated into a 7-DOF pitch plane model of a tridem truck to analyze its straight-line braking characteristics in the presence of fluid slosh. The straight-line braking responses of the coupled tank-vehicle model with and without baffles are analyzed under different fill volumes but constant load for different magnitudes of braking treadle pressure and road surface adhesion limits.

# ACKNOWLEDGEMENTS

The author is sincerely grateful to his supervisors Dr. S. Rakheja and Dr. K. Siddiqui for their continued intellectual guidance and encouragement throughout the course of this research. The financial supports provided by the Ministère des Transport du Québec, the Natural Sciences and Engineering Research Council of Canada, and the Concordia University are appreciated.

The assistance provided by Jose Esteves and K. Modaressi-Tehrani in the experiments of this research is acknowledged.

The author also wishes to thank his family for their love, encouragement and many sacrifices which made this work possible.

# TABLE OF CONTENTS

## CHAPTER 3

## MODELING OF THREE-DIMENSIONAL FLUID SLOSH AND VALIDATION



## CHAPTER 4

## FLUID SLOSH ANALYSIS OF FULL-SCALE VEHICLE TANKS AND BAFFLE DESIGN FACTORS

## CHAPTER 5

## EFFECT OF FLUID SLOSH ON ROLLOVER THRESHOLD ANALYSIS OF PARTLY FILLED TANK TRUCKS

## CHAPTER 6

## EFFECT OF TRANSIENT FLUID SLOSH ON BRAKING PERFORMANCE ANALYSIS

# LIST OF FIGURES

# LIST OF TABLES

# NOMENCLATURE

| | |
|---|---|
| $A$ | Amplitude of acceleration |
| $\vec{A}_i$ | Area vector of the $i^{th}$ face in the wall zones of slosh model |
| $a_x$, $a_y$ | Longitudinal ($x$), lateral ($y$) accelerations |
| $a_y^*$ | Lateral acceleration corresponding to vehicle rollover threshold |
| $\vec{a}$ | Acceleration vector attributed to a vehicle maneuver |
| B$i$ | Baffles used in the corresponding tanks T$i$ ($i$=1 to 5) |
| $cg$ | Centre of gravity |
| C1, C2, C3 | Fluid cargos corresponding to different fill volumes but at a constant load: Sulfuric acid ('C1', 38.1% fill volume); Dichloromethane ('C2', 52.1% fill volume); Water ('C3', 69.5% fill volume) |
| $C_{Fy}$, $C_{Fz}$ | The ratios of the lateral ($y$) and vertical ($z$) sloshing forces at the instant of the maximum roll moment, to the corresponding mean or steady-state values |
| $c_{si}$ | Damping coefficients of the suspension at the $i^{th}$ axle |
| $c_{ti}$ | Tire damping coefficient at the $i^{th}$ axle |
| DLF | Dynamic load factor |
| $F$ | Volume fraction function of fluid |
| $f$ | Frequency |
| $f_b$ | Beating frequency |
| $f_e$ | Excitation frequency |
| $\vec{f}$ | Body force vector |
| $F_x$, $F_y$, $F_z$ | Slosh force components in the longitudinal ($x$), lateral ($y$) and vertical ($z$) directions |

| | |
|---|---|
| $F_{xbf}$ , $F_{xbr}$ | The braking forces developed at the front (*f*) and rear (*r*) tire-road interfaces |
| $F_{zsf}$ , $F_{zsr}$ | Vertical forces developed due to the front (*f*) and rear (*r*) suspensions |
| $\overline{F}_y$, $\overline{F}_z$ | Lateral (*y*) and vertical (*z*) forces of steady-state slosh |
| $\overline{F_{xl}}$ , $\overline{F_{zl}}$ | The resultant longitudinal (*x*) and vertical (*z*) forces due to sloshing liquid cargo |
| $F_{zti}$ | Vertical force due to the tires on the $i^{\text{th}}$ axle |
| $\vec{g}$ | Gravity acceleration vector |
| $H_s$ | Sprung mass *cg* vertical position at the static state |
| $h_l$, $h_{ST}$, $h_T$ | Height of liquid mass *cg*, semitrailer *cg*, tank *cg* |
| $h_{rci}$ | Roll center height of the $i^{th}$ axle |
| $h_0$ | Equivalent rigid "frozen" liquid *cg* height |
| $I_{yys}$ , $I_{yyl}$ | Mass moment of inertias of the sprung mass and the floating fluid mass |
| $I_i$ | Polar mass moment of the tire-wheel assembly *i* |
| $i_s$ | Longitudinal slip in percentage |
| $K$ | Calibration factor for the resultant slosh roll moment determined through calibration performed with the empty tank. |
| $K_{Si}^*$ , $K_{Ti}^*$ | Equivalent roll stiffnesses of the $i^{th}$ axle suspension springs and tires |
| $k_{si}$ , $k_{ti}$ | Vertical stiffness coefficients due to suspension springs and tires |
| $K_{\phi i}$ | Auxiliary roll stiffness of the $i^{th}$ axle |
| $L$ | Longitudinal distance between the front dynamometer and the lateral axis passing through the centers of the rear dynamometers |
| $L_f$ , $L_r$ | Longitudinal positions of the front and rear axles from the static sprung mass *cg* |

| | |
|---|---|
| $M_X$, $M_Y$, $M_Z$ | Roll, pitch and yaw moments |
| $M_{Fy}$ , $M_{Fx}$, $M_{Fz}$ | Normalized lateral, longitudinal and vertical slosh forces |
| $M_{Mx}$, $M_{My}$, $M_{Mz}$ | Normalized roll, pitch and yaw moments due to liquid slosh |
| $\overline{M}_x$ | Roll moment of steady-state slosh |
| $\overline{M_{yl}}$ | The resultant pitch moment due to the fluid slosh |
| $M_{1i}$ | Primary overturning moment arising from the centrifugal acceleration for the $i^{th}$ composite axle ($i$=1,2,3) |
| $M_{2i}$ | Lateral displacement moment caused by lateral *cg* translation due to roll deflection of the sprung weight for the $i^{th}$ composite axle ($i$=1,2,3) |
| $M_{3i}$ | Restoring moment due to the lateral transfer of vertical load from inner to outer tires for the $i^{th}$ composite axle ($i$=1,2,3) |
| $m$ , $m_l$ | Mass ($l$: liquid) |
| $m_{uf}$, $m_{ur}$ | The front and rear unspung masses |
| $N_Y$, $N_X$ | Lateral and longitudinal load shifts due to fluid slosh |
| $N_Y^e$ | Lateral load shift measured for the empty tank and structure |
| $p$, $P_i$ | Pressure ($i^{th}$ face centroid in the wall zones of fluid slosh model) |
| QS | Quasi-static method |
| $R_i$ | The effective rolling radius of wheel $i$ |
| $S_i$ | Half suspension track of the $i^{th}$ composite axle ($i$=1,2,3) |
| $T$ | Period |
| $T_i$ | (1) Half tire tracks of the $i^{th}$ composite axles ($i$=1,2,3)<br>(2) Braking torque applied to the $i^{th}$ wheel |
| TC | Tank of circular cross-section |
| TR | Tank of "Reuleaux triangular" shape |

| | |
|---|---|
| T0 | Cleanbore tank without baffle |
| T1 | Tank equipped with single-orifice baffles of flat or spherical surface |
| T2 | Tank equipped with multiple-orifice baffles of flat or spherical surface |
| T3 | Tank equipped with single half-circular orifice baffles of spherical curvature |
| T4 | Tank equipped with half-opened baffles of spherical curvature |
| T5 | Tank equipped with single circular orifice baffles of conical shape |
| $\vec{u}$ | Velocity vector |
| VOF | Volume of fluid |
| $W$ | (1) Sprung weight<br>(2) Lateral spacing between rear left and rear right dynamometers |
| $(XYZ)$, $(xyz)$ | Longitudinal, lateral and vertical axles of Cartesian coordinate systems |
| $(xyz)^B$ | The floating reference system moving with vehicle body |
| $(xyz)^L$ | The Cartesian coordinate system in the fluid slosh model |
| $(xyz)^S$ | The floating reference system moving with vehicle sprung mass *cg* |
| $X_{fi}$ , $Y_{fi}$, $Z_{fi}$ | Longitudinal, lateral and vertical coordinates of the centroid of the $i^{th}$ face cell along the liquid wetted wall and baffle boundaries |
| $x_s, \dot{x}_s, \ddot{x}_s$ | Position, velocity and acceleration of the sprung mass *cg* in the longitudinal direction |
| $z_s, \dot{z}_s, \ddot{z}_s$ | Position, velocity and acceleration of the sprung mass *cg* in the vertical direction |
| $z_{ui}$ | Vertical displacement of the unsprung mass *i* from its respective static position |
| $\phi$ | Liquid free surface gradient |
| $\phi_1$, $\phi_2$ | Physical properties of given fluid |
| $\alpha_s, \dot{\alpha}_s, \ddot{\alpha}_s$ | Pitch deflection, angular velocity and angular acceleration of the sprung mass |

| | |
|---|---|
| $\theta_s$ | Roll angle of tank |
| $\theta_{si}^*$ | roll angle of the $i^{th}$ composite axle ($i$=1,2,3) |
| $\mu$ | Viscosity |
| $\rho$ | Density |
| $\Omega$ | Domain of the liquid occupied cells of slosh model |
| $\partial\Omega$ | Domain of liquid-wetted faces on the wall boundary of slosh model |
| $\nabla$, $\nabla\cdot$, $\nabla^2$ | The gradient, divergence, Laplace operators |
| $\sum$ | Summation operator |

# CHAPTER 1

# INTRODUCTION AND LITERATURE REVIEW

## 1.1 GENERAL

Liquid slosh in a moving container plays a crucial role in the stability of vehicles transporting bulk liquid. Liquid cargo transportation systems, such as road tank trucks and oil tanker ships, when partially loaded and subject to external excitations, could be at higher risk of overturning than the rigid cargo transporting vehicles. Furthermore, liquid slosh is also a big concern in many other engineering applications: for instance, fuel slosh can cause the flight destabilization of aircrafts, rockets and spacecrafts. Furthermore, the seismic excitations arising from a earthquake may yield large-amplitude slosh of liquid contained in large storage tanks and reservoirs, resulting in damages to the structure.

Liquid cargo partially filled in a moving road tank usually experiences slosh in large or small amplitude depending on the manoeuvre and road surface conditions. Large amplitude sloshing can be induced when a vehicle undergoes braking/accelerating, cornering or lane-change manoeuvres. Liquid cargo road containers are often partially filled because the axle loads are subject to regulatory limits but the weight densities of the liquid products transported vary from one case to another. For the tanks employed in fuel delivery, the partial fill situation may occur in the route. Road tanks are often used to transport dangerous liquids, for example, flammable or toxic chemical goods. Accidents involving such vehicles may thus result in serious environment pollution in addition to the fatalities and damages.

Road tank vehicles are mostly in the category of either articulated (i.e., separated tractor and trailer units) or non-articulated (i.e., straight truck) heavy-duty vehicles. Heavy-duty vehicles, due to their higher centre of gravity (*cg*) and weights and large dimensions, are known to have lower directional stability and controllability limits than those of other road vehicles. Roll instability is the most dangerous instability mode that happens more frequently. An examination of yearly heavy truck safety trends in United States from 1984 to 1987 showed that the rollover was the most harmful event, accounting for 41.4% of the fatalities [1]. Winkler [2] also reported that there are more than 15,000 rollovers of commercial trucks each year in US and about 62.67% of these rollovers are from tractor-semitrailers. For every four million miles of truck travel, there is about one rollover.

In comparison with other heavy vehicles (e.g. rigid cargo vehicles), partially filled road tanks exhibit even lower stability limit. This is attributed to the dynamic interactions between the sloshing liquid and the moving vehicle, which has adverse impact on the vehicle stability. The destabilization is directly attributed to the dynamic slosh forces and moments that arises from a directional manoeuvre [3]. Strandberg's study [3] showed that the overturning acceleration threshold of a 50%-volume filled elliptic tank during a steady turn could reduce to half as compared to the 100% filled tank. Since the rollover limits of tank vehicles are usually very low, a moderate manoeuvre, such as cornering, lane-change or braking-in-a-turn, may cause rollover. A study of highway accidents in Canada [4] showed that the rollover was the main cause of 1874 reported incidents of dangerous goods transportation vehicles during 1990 and 1998. The 43% of these

reported incidents were associated with the rollover, and 85% of the rollover incidents were from the tank trucks [4].

Although liquid slosh has been identified as a significant factor that can destabilize tank vehicles, the dynamic interactions between the liquid motion and vehicle stability has not been sufficiently investigated and thus, not well understood. The relevant studies reported in the literature are limited either in the development of methodologies for predicting the liquid slosh in various containers or in the analysis of vehicle stability based upon simplified models of liquid cargo motion without sufficient consideration of the dynamic slosh effect. The stability analyses are considerably underestimated assuming steady-state slosh, while the transient dynamic slosh is not sufficiently evaluated. The magnitudes of transient slosh forces are considerably larger than the inertia forces derived from the equivalent "frozen" liquid mass [5]. The dissertation research focuses on the development of an accurate method to model dynamic fluid slosh within tanks, and the analyses of transient slosh effects on the roll stability and braking performance of the coupled tank-vehicle system.

## 1.2 LITERATURE REVIEW

### 1.2.1 Direction Dynamics of Heavy Vehicles

The instability of road vehicles, in most cases, occurs when the vehicles are performing manoeuvres, such as braking, cornering, lane-change, and braking-in-turn. Roll instability is known to be the most dangerous instability mode that results in relatively large number of rollover related accidents. Heavy-duty vehicles generally tend to be unstable when subjected to a lateral acceleration over 0.3g [6, 7]. Road vehicles may roll over when the

overturning moment exceeds the maximum restoring moment [11]. The overturning moment is yielded by the centrifugal force arising from the directional manoeuvre, while the restoring moment is generated by the lateral transfer of vertical load on tires. For articulated heavy vehicles, the roll instability originates from the trailer axles that experience large magnitudes of lateral load shift. The roll instability can be evaluated from the point of view of relative instability or absolute instability [8]. A relative instability does not imply the actual occurrence of a tip- or roll-over, but relates to the onset of a probable instability, while an absolute instability refers to the absolute rollover.

Vehicles may experience loss of directional control and/or yaw instability when the wheels experience lockup during a braking-related directional manoeuvre [9, 19]. The braking characteristics of an articulated combination are quite complex, particularly when a moving load is considered. The load transfer during a braking manoeuvre depends not only on the deceleration, but also on the braking force generated from the semitrailer. The partially filled articulated tank vehicles impose additional load transfer arising from the cargo motion, which can adversely affect the braking performance even in the presence of anti-lock braking system. The identification of an optimal braking force distribution in the presence of varying axle loads in a partly-filled liquid cargo vehicle is extremely complex. Jacknifing may occur during a turning manoeuvre when the tractor rear tires experience lockup, while trailer swing may happen when the trailer tires are locked [9, 19]. Jacknifing is usually the most severe form of instability, which yields high yaw velocity of the trailer. Trailer swing has little influence on the stability of the tractor but could pose highway safety risks for other vehicles. In addition, the rapid steering inputs

or external perturbations at higher speeds may cause the trailer to oscillate about its equilibrium position in the lateral direction.

The roll and yaw stabilities have been widely analyzed on the basis of roll plane models and yaw plane models, respectively [8, 11-15]. The uncoupled roll or yaw plane models, however, are considered insufficient for the study of vehicle stability and directional response during steering and/or braking manoeuvres. The complex dynamic responses of tractor-semitrailers, thus, need to be evaluated using three-dimensional vehicle models. A number of yaw, roll and yaw/roll models have been developed and extensively reviewed by Kang [10].

The roll stability of heavy-duty vehicles has been widely investigated in terms of the static rollover threshold, which is evaluated on the basis of the equilibrium of roll moment about a roll centre assuming that the vehicle is subjected to a steady turn. The suspensions and tires are usually lumped into a single roll plane or multi-axle roll planes. Although the rollover accidents in reality are never static, the static roll stability is the dominant measure that determines the propensity to rollover potential of a vehicle [8, 11]. The static rollover threshold can be interpreted as the maximum value of the lateral acceleration that a vehicle can tolerate without rollover, and is a measure of the relative instability of a vehicle. Liu *et al.* [8] pointed out that the static rollover threshold of articulated heavy vehicles in most cases, is slightly (normally no more than 5%) higher than the dynamic rollover threshold for rigid cargo vehicles, while the relationship between static and dynamic rollover limits of partly-filled liquid cargo vehicles is not yet known.

A simplified method for predicting the static rollover threshold for tractor-semitrailers is a two-dimensional static roll plane model developed by Ervin [11]. In this model, the tires and suspensions of a five-axle vehicle were lumped into single or three composite axles, while the articulation effect from the fifth wheel was not considered. From the static roll moment equilibrium, it was shown that the estimated rollover thresholds correlated well with the rollover accident data from BMCS (Bureau of Motor Carrier Safety of US DOT) over the years from 1976 to 1979.

Verma and Gillespie [12] proposed a roll plane model to study the dynamic roll response of commercial vehicles by lumping all axles into a single one. The model allowed large displacements and rotations, and coupled motions in roll and vertical directions. The study showed that a vehicle may rollover at a lateral acceleration lower than the static rollover threshold, owing to the roll resonance of the vehicle. Liu *et al.* [8] derived the dynamic rollover threshold of articulated freight vehicles using a roll plane model and a relative roll instability criterion based on load transfer ratio of the axles that experience lift-off from the ground. The roll moment equilibrium was established while the instantaneous vertical motions of the centres of sprung and unsprung masses were taken into account. The effective lateral acceleration (ELA) was defined to represent the dynamic rollover threshold for the condition of unity value of lateral load transfer, referred to as Roll Safety Factor (RSF). It was concluded that the dynamic roll threshold values of articulated vehicles are very close to the static rollover threshold (SRT) in most cases, suggesting that SRT can serve as a good measure of dynamic roll stability.

The yaw and lateral directional response characteristics of heavy vehicles have been widely studied using linear and non-linear yaw plane models. The cornering

properties and articulation effects are usually incorporated in yaw-plane modeling. Jindra [13] developed a yaw plane model to study the directional response of various articulated trucks subject to a steady turning at a constant forward speed, assuming linear cornering characteristics of tires. The linear yaw-plane model was extended by Mallikarjunarao and Fancher [14] to further study the yaw and lateral directional response characteristics of articulated vehicles. The model considered the differential longitudinal slip of dual tire sets, while assuming linear cornering characteristics. The natural oscillation modes and directional stability limits of the vehicle were examined through eigenvalue analysis of the characteristic equations. A comprehensive yaw-plane model with non-linear cornering properties of tires was proposed by Vallurupalli [15] to investigate the directional response of an articulated vehicle with external articulation dampers under lane change and evasive manoeuvres at high speeds.

The uncoupled roll or yaw plane models cannot adequately describe the dynamic response of a vehicle under most directional manoeuvres. Moreover, when a vehicle manoeuvre contains the frequency content (e.g. lane-change) in the vicinity of the roll natural frequency of the vehicle, the measure of dynamic response becomes a more significant parameter for the roll stability. A tractor-semitrailer could reach a roll natural frequency as low as 0.5 Hz when heavily loaded and suspension is not sufficiently stiff [16]. This could lead to a potentially dangerous situation since an emergency type of evasive manoeuvre could approach this frequency. The dynamics of a tractor-semitrailer under the frequency-related manoeuvre is featured by a time lag of lateral acceleration action between the tractor and semitrailer, and large rearward amplification of the semitrailor acceleration [17, 18]. The study of roll stability is incomplete if it is only

based on the roll plane modeling without considering these phenomena. Moreover, when a vehicle is negotiating a directional manoeuvre at variable forward speeds, e.g., braking-in-turn, neither a roll-plane model nor the yaw-plane model analysis could be considered adequate.

Mikulcik [19] studied the braking characteristics of tractor-semitrailer combinations by formulating a three-dimensional (3-D) non-linear model. The tractor and trailer units possessed degrees-of-freedom (DOF) in the pitch, yaw, roll, longitudinal, lateral and vertical directions. The study showed that jackknifing is directly related to the nonlinearities of the vehicle system, and the linear and non-linear theories could yield significantly different predictions of jackknife behaviour. Comprehensive 3-D vehicle model of various vehicle combinations, referred to as the Constant Velocity Yaw/Roll model, were developed by Mallikarjunarao *et al.* [20, 21]. The generalized model has been widely used to study directional responses of various heavy vehicle configurations. In this model, sprung masses are represented as rigid units, each of which has 5-DOF (except the longitudinal motion), while each axle is restrained to roll and bounce. The model considers non-linear tire cornering and suspension properties, and the suspension roll centres are assumed to be located at a constant height beneath the sprung mass *cg*. The pitch motion of the sprung masses and the relative roll angles between sprung and unsprung masses are assumed to be small. It has been shown that the model is capable of predicting directional and roll dynamic responses of various articulated heavy vehicle combinations under constant forward speed directional maneuvers. Subsequently, Phase IV model was developed to study vehicle responses under simultaneous braking and steering manoeuvres [22]. The model is regarded as the most comprehensive vehicle

model, applicable for various heavy vehicle combinations. The model could have as many as 71-DOF for all units and axles of a vehicle combination.

### 1.2.2 Liquid Slosh Dynamics

Any disturbance to partially filled liquid-containers can induce sloshing. Depending on the type of disturbance and container shape, the free liquid surface can experience different types of slosh motion, such as simple planar, non-planar, rotational, irregular beating, symmetric, asymmetric, quasi-periodic or chaotic [23]. The liquid motion within a container has infinite number of natural frequencies, but only the few lowest modes are generally excited by the motion of the containers.

The amplitude of liquid slosh is influenced by a large number of factors, namely, the amplitude and frequency of the tank motion, liquid-fill depth, liquid properties and tank geometry. When the frequency of the tank motion approaches one of the natural frequencies of the fluid, the large amplitude slosh occurs together with swirling motion of the fluid [24-26]. For road tank vehicles, the lowest natural frequency is of paramount concern due to low spectral components of steering manoeuvres and steering-induced motion. It would thus be desirable to conceive a tank geometry that will result in a natural frequency under critical fill levels distant from the frequency of possible steering manoeuvres. The frequency of steering manoeuvres is typically well below 0.5 Hz [27], while an emergency evasive manoeuvre may approach this frequency [16].

The natural frequencies of the fluid slosh within a tank are dependent on the tank geometry and fill depth, and could be predicted from by the linear flow equations. In spite of the nonlinear characheristics of slosh, it has been reported that the linear theory

can yield reasonably good prediction of the natural frequencies. Budiansky [28] proposed the formulations based on the hydrodynamic theory to calculate the natural frequencies of liquid slosh within horizontal cylindrical and spherical containers for various fill depths. It was reported that the fundamental slosh frequency of a 50% filled cylindrical tank under a transverse excitation lies in the vicinity of 0.56 Hz, which further decreases under lower fill levels. A study of typical tanks used in articulated vehicle showed that the fundamental slosh frequency ranges from 0.52 to 0.67 Hz for 40% to 70% fill heights [29]. Silvermann and Abramson [30] proposed a methodology to predict the slosh natural frequencies for rectangular tanks, which was further extended by Romero *et al.* [31] to study the slosh natural frequencies for different tank geometries. These approximations were observed to be in fair agreement with the experimental results obtained from very small size tanks. The study showed that the slosh frequencies for the circular cross-section tanks are higher than those for the elliptical tanks. A generic shape tank, proposed by Kang [10], behaved similar to the elliptical tank for lower fill levels and like the circular tank for higher fill levels.

The directional and roll stability of moving tankers is directly affected by the hydrodynamic pressure and thus the slosh forces and moments, apart from the slosh frequency. The dynamic pressure is composed of non-impulsive and impulsive components. Su *et al.* [32] found that high magnitude impulsive pressures occur locally over short durations (1 to 10 ms), which are caused by the impact of liquid against the tank structure. Such impacts are associated with the occurrence of hydraulic jumps and traveling waves [32, 33]. Large amplitude, near-resonance standing waves can also cause impulsive impact pressures due to a rapid but continuous build-up of liquid surface.

However, such pulses last for relatively longer time (about 1/10 of the slosh period). The standing waves can cause slowly varying non-impulsive pressures variations.

The slosh forces are calculated through the integration of hydrodynamic pressure acting on the tank walls, and depend on the fill level, tank geometry and excitation amplitude. A higher fill level does not necessarily yield larger slosh forces when all other conditions are held fixed. On the basis of a quasi-static slosh model, it has been reported that the liquid load shift reaches its maximum near the fill level of 70% [7, 34]. Popov [35] studied the transient slosh response within a rectangular and a circular container, and concluded that the maxima of the dynamic force and moment coefficients (defined as the ratios of the peak dynamic forces or moments to the corresponding steady state forces or moments) occur at medium fill level ratio (defined as the ratio of the fill level to the characteristic length) for the rectangular container, but at relatively smaller fill level ratio for the circular container. However, Modaressi's [36] study showed that the amplification factor of lateral load transfer (defined as the ratio of transient maximum to mean value) reaches maximum in the vicinity of 60% fill level for the circular tank subject to a ramp step lateral acceleration excitations, irrespective of the excitation magnitude. In terms of the excitation effect, obviously the slosh forces tend to be larger as the tank excitation becomes more severe.

The slosh forces and moments have been evaluated in terms of dynamic load shift, which is related to the instantaneous *cg* coordinates. The liquid *cg* coordinates have been determined from the shape of free surface and the tank geometry, using kineto-static liquid motion. The waveform of free surface could also be an important parameter for estimating transient liquid slosh forces. The characteristics of the liquid slosh waves

depend on the liquid fill depth and the frequency of oscillations. Standing waves, traveling waves, hydraulic jumps and a combination of the latter two could be induced by the motion of a container [32]. A shallow liquid (i.e., at low fill level), when oscillates at a frequency much lower than its resonance frequency, yields standing waves. As the frequency is increased, the waves are converted into traveling waves of short wavelength. Hydraulic jumps may occur when the oscillations approach the resonance frequency. As the frequency is further increased, the jump wave becomes a solitary wave. For the liquid at higher fill level, sloshing near resonance is characterized by the formation of large amplitude standing waves, which could add to the traveling waves during large amplitude excitations.

The magnitude of liquid slosh is also dependent on the damping. The slosh damping generally arises from kinematic viscosity of the liquid, liquid fill height, tank geometry and additional damping devices. The viscosity of commonly transported fluids in general has negligible contribution to the magnitudes of slosh forces and the damping [36]. The fundamental sloshing frequency and the mode shapes are virtually unaffected by the liquid viscosity [37, 38].

The slosh amplitude is largely controlled by the tank shape and the properties of damping devices. Damping mostly takes place at the rigid walls, which is closely related to the shape of the container. For instance, the damping of lateral slosh in a circular cylinder is about 18% less than that yielded in a square tank of the same cross-sectional area [39]. Popov [35] pointed out that in the range of fill levels of practical interest (50%-100%), the dynamic slosh force and moment coefficients are sufficiently close for the rectangular and circular containers. The conventional road tankers are generally of either

circular or modified-elliptic cross-sections. Typically, the former exhibits smaller lateral *cg* motion but higher *cg* height, while the latter has relatively lower *cg* height but larger lateral *cg* variations. Kang [10] examined the existing tank shapes and proposed novel tank designs of "Reuleaux triangle" cross-section shapes to minimize the liquid cargo motion. He compared the performance of his proposed designs with conventional tanks using quasi-static slosh model, and showed that the "Reuleaux triangle" cross-sectional tanks exhibit greater roll stability limits than the current designs.

A closed separating wall is considered to be the most effective choice to curb the slosh amplitude. Popov *et al.* [40] reported that the overturning moment of a tank could be decreased by 30% with a rigid separating wall, as compared to a baffle. Berlamont [41] suggested that the optimal compartment length is the half of the length of the free surface wave. Wang *et al.* [42] studied the influence of number and size of compartments on the longitudinal load transfer and braking performance of a partially filled tank truck using the kineto-static fluid model. They concluded that equally spaced compartments yield minimum longitudinal load shift under straight-line braking manoeuvres, irrespective of the fill level.

The use of closed solid separating walls however, adds excessive structural weight and causes inconvenience for cleaning and loading/unloading. Various baffles, such as ring, vertical cruciform baffles, perforated, and flexible baffles, are considered as acceptable alternative that provide reasonable damping effects with the addition of only small structural weight. The effectiveness of the rigid baffles depends on their geometry, spacing and the orifice locations with respect to the liquid free surface. Only a few studies have investigated the influences of baffles on the nature of fluid slosh and the

majority of these studies involved tanks other than those employed for road transportation. The studies involving cylindrical, spherical and propellant tanks have shown that the flexible baffles might be more effective than the rigid baffles to damp slosh in the moving containers [43-47]. Lloyd *et al.* [48] investigated various rigid baffles, including solid dished, oblique, spiral, round, and perforated designs and concluded that the lightweight perforated baffle was the best among the designs. Popov *et al.* [40] studied the effect of size and location of baffle orifice on the slosh control within a rectangular tank. The results showed that an orifice opening equal to 5% of the cross-section area yields a significant increase (by 29%) in the peak overturning moment for a fill depth ratio of 70%, when compared to that caused by separating wall. An increase in the orifice opening, up to 20% of the cross-section area, showed negligible influence on the moment change. The lateral slosh force along the axis of the baffle, however, was nearly independent of the variations in the orifice sizes studied.

**Methods of Slosh Analyses**

The slosh motion of the liquid free surface has been extensively studied since early 1960's. In view of the methodology used, these studies can be grouped into the following categories: experimental, numerical, mechanical analogy, quasi-static hydrodynamic, and analytical. Numerical methods have been proven to be useful for simulating large-amplitude fluid slosh within a tank of complex geometry [32, 35]. Mechanical analogy provides a good approach that can be conveniently integrated with vehicle models, but the non-linearity of slosh is very difficult to model by using the parameters of the equivalent mechanical system [101]. The quasi-static hydrodynamic model is a simpler

method for deriving the static and steady-state liquid surface position [109, 112]. Analytical methods can only be applied to predict the sloshing with small amplitude oscillations [86, 87, 94]. Relatively few experimental investigations have been conducted due to complexity of measurements and applying excitations. The recent experimental efforts were mostly limited to ships and the data were used to validate the computational results under harmonic inputs [57, 77].

**(1) CFD Methods**

In computational fluid dynamics, the fluid within a rigid container is typically described as a viscous laminar flow by using the incompressible time-averaged Navier-Stokes equations. In some cases, it is also described as the potential flow represented by the Laplace equation. Wiesche [49] presented a detailed review of the flow theories that have been applied in computational slosh dynamics. In view of the discretization of governing equations, the slosh modeling of viscous fluid was usually realized in finite difference [35, 50-54], finite volume [55-57] and finite element [58-60] approximation methods, while solving the potential fluid slosh was associated with the use of finite element [61, 62, 124] and boundary element [63-67] methods.

Finite difference methods (FDM) refer to the discretization of the governing differential equations with the approximation of derivatives using Taylor series expansion. The discretizations are typically based on the structured mesh. Since finite difference techniques are restricted in the use of the structured mesh, the implementation of the complicated boundary conditions poses difficulties. These methods thus, do not perform well in predicting the slosh within a container of complex geometry. The finite

volume methods (FVM) are applied to the integral form of the governing equations and do not require structured meshes for the spatial discretization. The mesh elements could be arbitrary polygons or arbitrary polyhedra for 2-D and 3-D spatial domains respectively. Thus, the FVM could be applied for the slosh problems within the tanks of complex shape. In finite element methods (FEM), the governing differential equation is first reformulated into an equivalent variational form. Then the finite dimensional space is constructed through finite element discretization and the solutions are obtained by solving the minimization problem of the finite-dimensional space. Finite element methods do not require the space to be discretized into the structured mesh, and the implementation of the boundary condition is simpler. The FEM formulations for fluid slosh have been established on the basis of either potential flows or viscous flows, whereas, the FDM and FVM consider viscous flows. In boundary element methods (BEM), the slosh problems are formulated in terms of boundary integral equations on the basis of the potential flow theory. The discretization involves the boundary only, not necessarily the whole fluid domain; thus the reduction in one dimension is realized for the modeling.

While the field variables of slosh flows can be calculated by using any of the above solvers without difficulty, the special techniques are required to determine the advection of the moving boundary interface. This poses a great difficulty for the slosh predication, especially when a wave breaking occurs [51, 69]. From the point of view of CFD, the liquid within a partially filled tank is represented by the two-phase (air and liquid) flow, where the difference in the density of the two phases is very large. Owing to the very low density of air, its inertia force, when compared with that of liquid, is

negligible. This causes the phase interface a moving boundary. The determination of free surface position is an essential but complex task for handling the slosh problems in numerical methods. Considerable efforts, however, have been made in developing robust techniques for deriving the free surface of the moving fluid.

The earliest successful numerical technique to determine the advection of free surface boundary was the Marker and Cell (MAC) technique originally developed at the Los Alamos National Laboratory [50]. MAC was the first numerical integration scheme that was successfully applied to handle the complicated free surface problems. The MAC technique is mainly characterized by the use of "massless" marker particles to denote the location of the liquid phase. The marker particles move with the local velocity as the computation proceeds. The marker particles are initially placed in the cells that are associated with the liquid. The cells without markers (i.e., empty cells) represent the region where no liquid is present. Therefore, the cells with markers that neighbour the empty cells represent the free surface positions. Free surface boundary conditions are applied by assigning the air pressure to all grid cells on the surface. The velocity components (or velocity gradients) at and immediately adjacent to the surface should satisfy the conditions of incompressibility and zero surface shear-stress. The surface tension has also been considered for some specific applications [68]. The original MAC technique was associated with the finite difference approximation of the unsteady viscous incompressible Navier-Stokes equations based on a fixed Eulerian mesh. It was also characterized by the use of a staggered grid and the conservation forms of the equations.

The MAC technique, however, has been primarily applied for solving the 2-D free surface problems due to large memory and CPU cost required for storing the number of

marker particles. The treatment of free surface motion in large-amplitude slosh typically requires about 16 markers for each grid cell. The method was subsequently refined by many researchers, which evolved into a number of improved algorithms, such as SOLA [51-53, 69], SIMAC [70, 71], SUMMAC [72], and TUMAC [73]. The SOLA algorithm [52] was derived with significant simplifications of original marker and cell method but was considered suitable for the slosh problems with gentle free surface motion. The SOLA-SURF scheme [51, 53, 69], an extension of SOLA, utilized the free surface function to represent the surface evolutions, assuming a single-valued profile of surface shape. The scheme is not valid for handling wave breaking or flow separation and the liquid impact against the tank ceiling. Kim [69] proposed a concept of buffer zone in the vicinity of the tank ceiling such that the contact of the free surface with the top wall can be computed. The slosh-induced impulsive pressure was calculated for the 2-D and 3-D rectangular tanks with and without baffles. The results were well correlated with the experimental data and other simulation solutions. In a similar fashion, Popov [35, 40] developed a nonlinear 2-D slosh model to examine the transient slosh within the rectangular and circular tanks (baffled and un-baffled) under braking/acceleration and steady turning. The Navier-Stokes equations were formulated by using primitive variables, including velocities, pressure, and free surface height. The interpolation-reflection technique was employed to deal with the complex boundary conditions for arbitrary tank geometry. The simulation results were verified using the experimental data.

In the majority of MAC modified versions, the explicit updating of the velocity field does not provide accurate solutions for the viscous stress at the solid boundaries, even if non-uniform grids are employed [70]. It was mainly due to the diffusive

constraint on the time step. The method was thus limited to the viscous flows where viscous stress at the interfaces could be neglected. Armenio *et al.* [54, 70] developed a Semi-Implicit Marker and Cell algorithm (SIMAC) to overcome the above deficiency of the MAC method. The algorithm was used to analyze the sloshing of water in rectangular containers. It was reported that both the free surface evolution and the boundary layer at the rigid walls could be predicted accurately, and the hydraulic jumps and traveling waves were well captured by the simulations.

There are two other modifications of the MAC technique: SUMMAC [72] and TUMAC [73]. The SUMMAC has been successfully implemented to analyze incompressible flows with a free surface under transient conditions, which indicates the possibility of solving a wide range of water wave problems. The TUMAC was developed to simulate nonlinear wave formation in the near-field of the ships of arbitrary three-dimensional configuration advancing in the deep water. However, the implementation of these two techniques for the sloshing problems within a moving container has not been reported.

The volume of fluid (VOF) technique [74, 75] has now been viewed as the most powerful technique to successfully track the complex free surface motion. This technique is based on the concept of a fractional volume of fluid. A special step function called the volume of fluid function F is used, whose value is unity at any point occupied by the liquid, and zero elsewhere. Thus, a unit value of F indicates that the cell is fully occupied by the liquid, while a zero value indicates an empty cell. The value of this function that lies between zero and one then represents the fractional volume of the cell occupied by the liquid near free surface. The method uses only one storage word for each cell instead

of the number of marker particles used in MAC, which considerably reduces the memory requirement and computational cost.

The VOF technique has been incorporated with finite difference, finite volume and finite element approximation methods to solve various liquid slosh problems. Su *et al.* [32] and Celebi and Akyildiz [76] combined the finite difference based SOLA algorithm with the VOF technique to solve a 2-D viscous liquid slosh in a moving rectangular baffled tank. In the SOLA-VOF model, a moving coordinate system fixed to the tank was used to simplify the boundary conditions on the fluid-tank interface during large-amplitude tank motion. A donor-acceptor method was used for the transportation of the VOF function. The study showed that the vertical baffles provide better damping effect for the cases at low fill levels, while the horizontal baffles are more effective under high fill situations. It was pointed out that the numerical model works well only for short time, but not for long time simulation of the slosh in large amplitude after turbulence or secondary flows may be introduced.

Owing to its simplicity, the VOF algorithm has been incorporated into many commercial software, such as FLUENT [77], NASA-VOF [78], FLOW-3D [79] and Comet [57]. Hadzic *et al.* [77] used the built-in VOF model of the finite volume based FLUENT software to predict the slosh within a rectangular tank subjected to sinusoidal excitations. The study compared the time history of static pressure variations at 14 different monitoring locations and the free surface position obtained from the numerical simulations with the experimental data. Although good agreement was shown in overall trends, the sharp peaks were observed in the predicted static pressure. It was argued to be attributed to the impulsive pressure and consideration of laminar flow. Sames *et al.* [57]

analyzed the validity of the application of the Comet software in predicting fluid slosh within rectangular and cylindrical tanks. High Resolution Interface Capturing (HRIC) scheme and the blending of upwind and downwind schemes were implemented in Comet for discretization of the volume fraction conservation equation. The validity of the code in the slosh simulations was demonstrated for a rectangular tank in 60% fill level and a circular tank in 50% fill level, subjected to a harmonic excitation in the vicinity of the resonance frequency. The effect of grid refinement was also systematically studied and it was reported that different grids could lead to different solutions. It was suggested that grid refinement would be necessary for specific slosh problems, particularly those involving flow separation. The time histories of simulated pressures and forces were compared with the available measurement results. It was further suggested that the accurate prediction of complicated free surface (such as spray and air bubbles) needs special treatment in the discretization of advection term of the volume fraction conservation equation.

The VOF evolution function, in most cases, is solved in the advection manner on the Eulerian frame of reference. The majority of VOF algorithms have thus been limited to the re-construction of free surface with the first order accuracy. This would most likely be inadequate for the free surface flows involving delicate physics or the free surface flows within complex-geometry. Shahbazi *et al.* [80] developed a new type of VOF algorithm through the re-mapping of irregular triangular meshes based upon the Lagrangian-Eulerian (LE) methods and achieved the second order accuracy. Unlike the typical advection algorithms, their method consisted of three parts – a Lagrangian phase, a reconstruction phase and a re-mapping phase. The algorithm was only examined for

translation and rotation test problems, and was not applied in combination with an incompressible Navier-Stokes solver to handle a wide range of physical flows. The authors suggested that the high curvature and thin filament regions of flows could be accurately and efficiently captured by the use of an adaptation technique.

The consideration of surface tension can allow the VOF based scheme to deal with more subtle and complicated free surface problems, such as the processes of merging and break-up of fluid drops. The simple way to model the surface tension is to calculate the interface curvature and then add a force to the fluid momentum balance. Lafaurie *et al.* [81] proposed a new method, which is called SURFER, to introduce a correction of surface tension to the stress tensor. The corrector was constructed from the local gradients of the VOF fraction. The test runs were carried out for the liquid droplet collisions in 2-D and 3-D. Although the simulations provided reasonably good results, the presence of small undesirable pathological effects was noted, such as parasite currents, especially when the surface tension is high.

Alternatively, Lagrangian adaptive grid technique has been used to capture the free surface motion [58, 82]. In this method, the mesh moves with the fluid to attain a description of the free surface. The method, however, is not suitable for large-amplitude slosh, due to excessive deformation and deterioration of the mesh [58, 82]. A re-meshing method based on the combination of Lagrangian and Eulerian approaches was developed for capturing the free surface [59, 60, 83]. In this method, each element vertices can undergo three different motions: moving with the fluid using Lagrangian description; remaining fixed using Eulerian description; or moving in an arbitrarily prescribed way.

The method, referred to as arbitrary Lagragian-Eulerian (ALE), limited for analysis involving complex free surface motions such as wave breaking.

The free surface height remains the simplest approach to capture the evolution of the moving interface elevation in some numerical studies [40, 84, 85] and for almost all analytical methods (summarized in the next section). The equation of free surface has been used for the advection of freely moving boundary. The surface height, however, is usually assumed as a single-value function of spatial coordinates for simplicity, which would obviously not be applicable for aggressive slosh encountered during the wave-braking situations, since the assumption does not hold.

**(2) Analytical Methods**

The analytical solutions of fluid slosh are usually obtained through considerable simplification of the flow governing equations. The typical analytical methods used to study slosh are formulated on the basis of the linear or nonlinear potential flow theories, where the fluid flows are assumed to be homogeneous, incompressible, inviscid and irrotational. The velocity, pressure, forces, moments and wave elevation are expressed in terms of the velocity potential. The potential theories are described by the Laplace equation. The free surface is tracked by the time-evolution of the surface height relative to a given reference elevation, while the evolution is governed by the free surface equation. Linear theories are formulated to treat small amplitude slosh at frequencies far away from the resonance frequencies [5, 86]. The fluid slosh problems, however, exhibit considerable nonlinearities arising from various factors, such as complex tank geometry, large amplitude excitation and couplings between various slosh modes [24].

Analytical solutions of the nonlinear slosh problems have been attempted on the basis of the theory of nonlinear liquid vibration developed by Moiseev [88]. The fundamental idea was established on the basis of the potential theory of incompressible fluid, while the free boundary was assumed to evolve following the kinematic and dynamic free-surface conditions [25, 79, 86, 87]. The free surface shape was described by the free surface height which is the function of time and space. Mathematically, it was expressed by the time dependent coefficients and the excitation amplitude ratio, defined as the ratio of the excitation amplitude to the cross dimension of the tank. The tank motion is generally assumed to be small compared to the cross dimension of the tank. The free-boundary problem was reduced to a finite sequence of asymptotic approximations that could be solved analytically.

The slosh in the vicinity of the resonance frequency within a 2-D rectangular open tank was predicted by Faltinsen [87] on the basis of Moiseev's theory [88]. The fluid slosh was investigated under forced harmonic oscillations of small amplitudes but in the vicinity of the fundamental slosh natural frequency. The study also derived parameters describing the wave amplitude and dynamic pressures at two monitoring points. The analytical solutions were shown to be in good agreement with the experimental data. A combined analytical and numerical method was derived by Solaas and Faltinsen [79] to solve 2-D sloshing in a tank of general shape. The boundary element method was used to determine the eigenfrequencies of the liquid slosh within the arbitrary tanks, while the non-linear analytical method based on Moiseev's theory [88] was applied to obtain the nonlinear velocity potential. This combined analytical and numerical method was

restricted to slosh within a tank in which the walls are vertical at the mean free surface line and was not valid for shallow water slosh problems.

More recently, a number of the multi-modal models have been developed and extensively used to predict fluid slosh in various containers [89-94]. Faltinsen *et al.* [89] constructed a multi-dimensional modal model using the Bateman-Luk (pressure-integral Lagrangian) variational principle. Based on the potential theory, the nonlinear free boundary problem was formulated using the velocity potential, free surface function and the fluid velocity vector. The general form of a discrete infinite-dimensional modal system was derived on the basis of the theory originally proposed by Miles [95] and Lukovsky [96]. The free surface elevation function and velocity potential were expanded in generalized Fourier series by a set of natural surface modes and domain modes, respectively. A finite-dimensional asymptotic modal model with multiple degrees of freedom was further derived by truncating the infinite system to solve for small amplitude 2-D slosh in a smooth rectangular tank. It was pointed out that the method is not valid for shallow water problems. The obvious difference was observed for the damping rate of the transient fluid motion between the analytical solution and the experimental results.

The multi-modal model was further applied by Faltinsen and Timokha [90, 93], Rognebakke and Faltinsen [91] and Faltinsen *et al.* [92] to predict slosh problems under different situations. The analytical modal methods, however, were limited to tank shapes with the vertical walls. The modal models were further extended by Lukovsky and Timokha [94] to treat the nonlinear slosh within tanks with non-vertical walls. A non-conformal mapping technique proposed by Lukovsky [97] was used in the analysis. In all

modal methods mentioned above, the slosh waves were assumed to be non-breaking and non-overturning type. Moreover, the ceilings of the containers were assumed infinite in height.

**(3) Mechanical Equivalent Models**

The dynamic fluid slosh and its interaction with a structure have also been represented by analogous mechanical system models. The analogous systems are usually constructed on the basis of the assumption that the liquid in a moving container can be divided into two distinct parts: a component that stays stationary with respective to the container structure; and a moving fluid part that creates the slosh forces against the structure. The latter component is often modeled by either a mass-spring system or a pendulum. Dashpots are also added to the mass-spring system to represent the energy dissipation. The model parameters, such as, equivalent masses, spring constant, moments of inertia, natural frequencies, pendulum length, etc., are the significant factors for the construction of the mechanical analogy of the fluid slosh. The methods for calculating model parameters for fluid slosh within rectangular, cylindrical and ellipsoidal tanks were presented by Abramson [24] and Dodge [98]. Ibrahim *et al.* [23] presented the detailed theory of mechanical equivalent modeling of fluid slosh and model parameter estimations.

The mechanical-equivalent models evolved in the fifties and sixties for spacecraft applications [24, 98-100]. Its applications, however, have been limited due to difficulties associated with identification of model parameters, particularly when nonlinear slosh is considered for wide ranges of fill and geometry conditions. In the early models, the model parameters were derived using either the experimental methods or the linear slosh

theory. The mechanical analogous models thus cannot accurately predict the nonlinearity and damping effect of dynamic slosh. The study of nonlinear fluid oscillation in spherical containers carried out by Sayar and Bauengaten [101] revealed that the pendulum model could not duplicate the nonlinear response of the fluid motion except for a particular fluid height, where the parameters could be considered valid.

The equivalent mechanical models, however, have been employed in many studies on liquid slosh within partially filled tanks, since they can be conveniently integrated with the vehicle model for dynamic analyses. Khandelwal and Nigam [102] studied the liquid slosh within a rigid rectangular container mounted on a railway wagon by means of an equivalent pendulum model of the liquid slosh. The model included a fixed mass representing the stationary portion of the liquid and an infinite number of pendulums corresponding to the odd fluid modes. Khandelwal's previous study [103] showed that the even modes did not contribute to the forces and moments. The excitation was represented by constant horizontal and vertical harmonic accelerations. It was reported that the model could effectively predict the natural frequencies, free surface elevation near the walls, and slosh forces and moment acting on the structure. The model parameters, however, were derived assuming small displacement and steady-state free surface condition. Ranganathan *et al.* [104] and Mantriota [105] utilized the pendulum theory to model liquid oscillations inside a cylindrical tank. In the former study [104], the liquid cargo was divided into a fixed mass and a simple pendulum representing the moving mass. In the latter study [105], the liquid was broken into numerous uniformly and longitudinally distributed transversal elementary sections represented by pendulums of constant weight. The results showed the oscillations in roll and lateral acceleration

responses of the tank-vehicle about the mean values obtained from the quasi-static model, while the magnitudes of oscillations and the transient responses could not be validated.

Ranganathan *et al.* [106] developed a spring-mass equivalent mechanical model for a partially filled horizontal cylindrical tank in the longitudinal pitch plane under application of a longitudinal deceleration representing a straight-line braking manoeuvre. The parameters of the model were estimated using the potential flow theory and the approximate summation technique based on Dodge's [98] formulation for rectangular tanks. The fluid in the cylindrical tank was broken into finite rectangular elements. The constant longitudinal acceleration input was limited to small magnitudes (less than 0.1g). The slosh forces and moment in the pitch plane were evaluated, while the model validity was only demonstrated in terms of fundamental slosh frequency against the available experimental results. The longitudinal load shift was validated on the basis of the results attained from a steady-state liquid model [107]. In a similar fashion, Xu and Dai [108] performed a mechanical-equivalent model of fluid slosh within a cylindrical tank in the longitudinal-pitch plane. The mechanical model (a linear mass-spring combination) incorporated an impact effect to allow prediction of the large-amplitude slosh. The impact effect was evaluated by calculating the impact force based on the potential energy function, while no attempts were made to validate the model.

**(4) Quasi-static Hydrodynamic Model**

Quasi-static hydrodynamic model (QS) is a simplified method that can be used for quick prediction of the steady-state liquid surface position (i.e., the stationary state that the time-dependent slosh evolves into). In this approach, it is assumed that the fluid is invisid

and the free surface assumes a straight-line configuration at every instant, and the fluid moves as a bulk. The fluid surface position is determined from the applied centrifugal force in the roll plane or the inertia force in the pitch plane. The associated liquid *cg* translations are computed as a function of the tank geometry, fill level and gradient of the free surface with reference to a fixed coordinate system. The quasi-static slosh model is effective for estimating the steady-state load shift resulting from the liquid cargo motion inside a tank. However, this method does not allow predictions of dynamic slosh forces and moments, especially the transient peak values. Since the method provides a convenient means to derive the free surface position and steady-state forces and moments, it has been used in several studies for the dynamic stability analyses of the tank-vehicles [10, 109-113].

**(5) Experimental Studies**

Relatively few experimental studies have been reported on fluid slosh within moving containers. The reported studies have contributed greatly to enhancing understanding of the nature of fluid slosh and serves as a means for the validation of computational models. Most of these studies, however, have been limited to harmonic inputs and small-scaled models. Since the dynamic similarity of slosh is very complex [35], only few efforts have been made to transform the experimental results of scaled models to the full-scaled tanks [3]. Most of the experimental studies on fluid slosh were conducted to validate the results of the numerical models [35, 51, 74, 114, 115]. The experimental studies have also been performed to obtain reliable boundary conditions for the numerical

models [35]. The experimental studies have reported slosh forces [3, 24, 35, 116], surface wave height [24, 116, 117], and hydrodynamic pressure at specific locations [77, 116].

The nonlinearity of the slosh was experimentally studied by Abramson *et al.* [24] for a vertically-placed small size cylindrical tank (inside diameter = 19.6 cm) and a spherical tank (inside diameter = 19.3 cm). The liquid free surface displacements and forces were measured using height transducers and strain-sensing devices, respectively. Fluid slosh in both cylindrical and spherical tanks was investigated for the cleanbore design, and with a vertical splitter plate installed in the direction parallel to the excitation in order to reduce the complex swirl motion in the vicinity of the resonance frequency. The measured data revealed the presence of the jump phenomena under excitations near the resonance frequencies, irrespective of the tank geometry.

Strandberg [3] was probably the first to extensively study liquid slosh within scaled-model tanks representative of tank vehicles. Four small-scale model tanks of circular, elliptic, super-elliptic and rectangular cross-sections (approximate cross-sectional area = 0.025 $m^2$) were used for the study. The tanks were installed in a specially designed test set-up and subjected to lateral motion. The slosh forces and acceleration were measured using force transducers and an accelerometer, respectively. The measured forces, transformed to the full-scale tanks based on the dynamic similarity, were applied to the tank-vehicle model for lateral stability analyses. The study provided some significant knowledge related to roll stability of tank vehicles.

Kobayashi *et al.* [116] conducted experiments to analyze the dynamic liquid slosh response in horizontal cylindrical tanks, particularly the natural frequency, surface wave height, hydrodynamic pressure and resultant slosh force. Four model tanks of identical

cross-sectional area (diameter = 0.47 m) but different lengths (1 to 4 times the diameter) and different end shapes, were used in the experiments. The natural frequencies were obtained through the frequency sweep tests under small excitation amplitudes. The resonance tests under a displacement excitation of 0.032 times the tank diameter showed that the maximum slosh forces in the longitudinal and lateral excitation directions occur at 75% and 50% fill ratio (defined as the ratio of fill height to diameter), respectively. The peak magnitudes of longitudinal and lateral forces were reported approximately 0.28 and 0.16 times the liquid weight for 80% fill ratio, respectively.

Pal *et al.* [117] presented a simple experimental set-up to measure some fundamental sloshing parameters, including slosh frequency, free surface displacement and damping due to slosh within a vertical cylindrical container. The free surface height was detected using 16 position sensors located near the periphery of the container wall. The natural frequency was measured by forcing the tank to oscillate at low amplitudes, similar to the method employed by Kobayashi *et al.* [116]. The measured liquid surface profiles and natural frequencies showed reasonably good agreement with the results obtained from the finite element simulation by Pal *et al.* [62] and Abramson's analytical method [5], respectively.

The reported experimental studies have generally employed very small size tanks, thus the coupling between the tank and the vehicle could not be investigated. Rakheja *et al.* [118] conducted field tests to validate the directional response of a two-axle truck with a cylindrical tank (1.22 m in diameter and 1.73 m in length). The tank was filled to its 50% capacity with water, while a dye was mixed with water to visualize the fluid slosh. The experiments were conducted under typical lane change maneuvers under different

forward speeds and gate sizes, and constant radius turns at different forward speeds. The road-measured data were analyzed to determine the directional response characteristics in the presence of the fluid slosh, namely, the lateral load transfer, free surface coordinates, lateral acceleration, and yaw and roll rates. The data were used to validate a directional dynamics model based on the quasi-static fluid slosh analysis.

### 1.2.3 Dynamics of Tank-vehicle Combination

Owing to the destabilizing forces and moments arising from the dynamic liquid cargo motion, partly-filled road tank vehicles are known to exhibit lower stability limits than rigid cargo vehicles. The destabilization arises from the dynamic load shift in both the lateral and longitudinal directions, attributed to liquid cargo slosh under directional manoeuvres. Although a great number of studies have been conducted to predict the liquid slosh within various containers, only limited efforts have contributed to the stability analysis of tank-vehicle combinations by considering the dynamic liquid cargo motion. The effect of transient liquid cargo sloshing on road tanks is not well understood yet, which is mainly due to the difficulties associated with the modeling of complex interactions between the liquid slosh and the moving tank vehicle.

The directional responses of partially filled tank-vehicle combinations could be studied using the available rigid cargo vehicle models by incorporating the effect of liquid cargo slosh. The roll stability limits of tank vehicles during steady turns have been widely investigated using static/kineto-static roll-plane models of fluid motion [10, 34, 109, 111, 112]. The directional responses of tank vehicles under typical steering manoeuvres at constant forward speeds have also been investigated using roll/yaw plane

models of the vehicle coupled with the kineto-static fluid model [105, 119]. Furthermore, variable speed 3-D tank vehicle model was used to study the tank vehicle's response to braking-in-turn manoeuvres [10, 105]. These studies may be grouped in three categories based on the method of fluid slosh analysis, namely: experimental [3, 118], equivalent mechanical analogy [102, 104-106, 119], quasi-static hydrodynamic model [10, 109-113], and CFD model [7, 55].

The earliest research on the stability of tank-vehicle combinations was probably performed by Strandberg [3], as described in the previous subsection. The roll stability of various tank vehicles was analyzed by integrating the measured dynamic slosh forces, based on the dynamic similarity, into a simplified single-DOF vehicle model. The lateral stability was analyzed by examining the overturning tendencies under steady cornering and transient lane-change manoeuvres. The results revealed that the elliptic and super-elliptic tank vehicles exhibit lower values of overturning limits than the circular tank vehicle under transient lane-change manoeuvres. This suggested that the stability losses are greater for wider tank shapes, while the corresponding gains from the lower *cg* height of the elliptic and super-elliptic tanks would be small compared with the circular tank. It was further deduced that the overturning limit of a 50% volume filled elliptic tanker during the lane-change manoeuvre reduces to 2.4 $m/s^2$ from 5.4 $m/s^2$ when completely filled. Addition of three longitudinal walls resulted in considerable increase in the overturning limit for a rectangular tank. Winkler [2] adapted Strandberg's results to further analyze the roll stability of tank vehicles and showed that the rollover threshold of partly-filled cylindrical tank trucks tends to decline as the fill load increases. For a rectangular tank, the minimum rollover threshold was observed near 40% fill condition.

The results suggested that rollover threshold of a circular tank (minimum near 50% fill) is higher than that of the rectangular one (occurring at about 40% fill). Although the study considered the nonlinear slosh effect, the dynamic interaction between the liquid slosh and the container was not considered.

Rakheja *et al.* [109] formulated a static roll plane model of a partially filled articulated cylindrical tank vehicle to predict the rollover threshold during a steady turning manoeuvre. The liquid cargo slosh within the compartmented and cleanbore cylindrical tanks was evaluated using the quasi-static approach. The study employed a comprehensive static roll model of an articulated tractor-semitrailer combination, developed by Mallikarjunarao and Fancher [126, 127]. The study demonstrated that the rollover threshold decreases due to the liquid cargo motion within the tank. The effect of compartments within the tank and an optimal order of unloading were also evaluated. Kineto-static roll plane model was further used by Ranganathan *et al.* [111] and Rakheja *et al.* [113] to study the static roll stability and dynamic roll responses of articulated tank vehicles with different tank geometries. These studies further confirmed the findings of Strandberg [3] that the magnitude of the lateral liquid *cg* translation in the wider modified oval and modified square tanks was considerably larger than that in the circular tank, leading to considerably larger overturning moment for the wider cross-section tanks. Assuming constant payload, the modified square and oval tanks revealed higher thresholds when transporting lighter liquid cargos, while the circular tank showed higher stability limits when carrying denser cargos. On the basis of the static equilibrium between the total overturning and the restoring moments that was proposed by Ervin [11], Rakheja *et al.* [112] formulated a simplified approach to estimate the rollover thresholds

of partially filled tank vehicles under a steady turn. The validity of the proposed simplified approach was demonstrated by comparing the results attained for multi-axle vehicle with those deduced from the comprehensive static roll model.

Kang [10] developed a constant speed 3-D yaw/roll model of a partly filled tank vehicle, on the basis of the Yaw/Roll model developed by Gillespie and MacAdam [21] and the quasi-static roll-plane fluid slosh model. The model was analyzed to evaluate the directional dynamic responses of a 5-axle tractor-semitrailer vehicle equipped with tanks of different cross-section, including the optimal cross-section. The analyses were performed under the steady turning and lane-change manoeuvres as functions of fill volume, tank cross-sectional shape, and the nature of the manoeuvre. It was shown that the load shift that arises from the cargo motion is a dominant factor that adversely affects the dynamic response of a tank vehicle, especially for a relatively low fill volume. It was also pointed out that the *cg* height of liquid cargo has moderate influence on the vehicle response for the high fill volume state, and it tends to be insignificant when the fill volume is low. A comprehensive variable speed 3-D tank-vehicle model incorporating a 3-D quasi-static fluid slosh model was further developed to investigate the response to braking and braking-in-turn manoeuvres. The vehicle model was based upon the Phase IV model developed by MacAdam *et al.* [22]. The braking system for each axle was described by the input pressure and the output torque characterized with time lag, rise time and braking torque ratio. The study presented comprehensive dynamic response analyses under various fill volumes, road conditions, manoeuvres and tank shapes. It was reported that the lateral load transfer ratio tends to be considerably higher on a dry road during a simultaneous braking and turning manoeuvre, which yields lower rollover limit

of the vehicle. The results also showed that the effect of fluid motion on the yaw response of the vehicle is generally small, even though the asymmetric load shift causes lockup of the inner trailer wheels only. A lockup of both the inner and outside trailer wheels occurs under excessive load transfer, when such a manoeuvre is negotiated on a wet or slippery road condition. This causes a sharp decrease in the lateral cornering force which results in a serious yaw instability that is observed well before the rollover limit is reached.

Aquaro *et al.* [120] presented a finite element modeling approach to determine the rollover threshold of a partially filled tank vehicle. The beam elements were used to describe the torsional and bending stiffness of the tank. The vehicle model incorporated non-linear force deflection properties of the leaf spring suspension by a non-linear spring/damper element, while the tire stiffness was assumed to be linear. The fluid slosh within the tank was simulated by an analogous pendulum model presented by Ranganathan *et al.* [106]. The roll stability of the tank truck was analyzed under the constant radius turning manoeuvres and ATC (Aberdeen Test Center of U.S. Army) double lane change manoeuvres using ANSYS finite element code. The study reported forward speeds corresponding to the overturning limit, which differed nearly 10% from the reported measured data [121]. The results attained for the ATC double lane change showed agreement in trend alone.

Mantriota [105] proposed a linear 2-DOF tank-vehicle model of an articulated tank-vehicle incorporating the dynamic liquid slosh effect by a pendulum model to study the vehicle yaw stability. The linear model was formulated in the yaw plane using the Lagrange's energy method, which was previously developed for an articulated vehicle transporting suspended rigid cargo [122, 123]. The pitch and roll motions of the rigid

portion of the sprung mass were neglected, while the analysis was performed assuming constant forward velocity and small angular motion. The liquid bulk, assumed to be inviscid, was divided into numerous uniform longitudinally distributed transversal elements. Each element was modeled by a pendulum of constant weight undergoing only the roll motion. The study concluded that a 70% filled tank vehicle exhibits considerably lower directional stability under 0.38 Hz steering manoeuvres.

A pitch-plane vehicle model employing a mechanical analogy of the fluid slosh was developed by Ranganathan *et al.* [106] to study the straight-line braking performance of a partly-filled tank truck. The natural frequency of the mechanical-equivalent model of the sloshing fluid was consistent with the experimental data. The normal load was observed to oscillate about the static value obtained from the quasi-static slosh model, which has also been reported on the basis of the road-measured data [118]. Ranganathan *et al.* [119] further developed a pitch plane model of an articulated vehicle employing a quasi-static liquid slosh model to study the braking characteristics of the vehicle with a partially filled cylindrical tank. The study concluded that the braking efficiency of a half filled tank vehicle reduced to nearly 55%, which was nearly 100 for an equivalent rigid cargo vehicle under identical braking inputs. A 3-D vehicle model was integrated with a pendulum model of the moving fluid in the roll-plane, by Ranganathan *et al.* [104] to further study the directional response of a cylindrical tank vehicle under a lateral acceleration excitation. The dynamic slosh forces and moments were calculated from the analogous mechanical slosh model. The results showed that the dynamic responses oscillate about the steady-state values, which were comparable with those attained from the kineto-static fluid model [112].

Owing to the computational complexity of the coupled vehicle-fluid system in the presence of dynamic fluid slosh, Ranganathan [7] developed an iterative methodology to update the vehicle state on the basis of slosh forces and moments derived from the transient fluid slosh analysis using a 2-D SOLA CFD code for a scaled tank, while the vehicle was represented by a 3-D vehicle model. The directional response characteristics of a partly filled tractor-semitrailer tank vehicle were investigated and compared to those of the vehicle derived from the quasi-dynamic model. The results showed that the quasi-dynamic model overestimates the response characteristics for low frequency steer inputs and high fill conditions. Rumold [55] developed a similar methodology to fully integrate the tank-vehicle models, by taking into account the transient slosh behaviour, to study the braking dynamics of a two-axle tank truck with a rectangular container. The integration of the tank and vehicle models was realized through a unique parallel modular simulation method for the two-dimensional case. The global tank truck system was decomposed into a fluid subsystem and a rigid body subsystem containing the container structure, which were coupled by updating the variable values for the two models each iteration step. The dynamic fluid slosh within the fluid subsystem was analyzed by solving the Navier-Stokes equations using the finite volume approximation coupled with the VOF free surface tracking technique. The tire properties were reported on the basis of the magic formula proposed by Pacejka [125], while the suspension was neglected.

## 1.3 MOTIVATION AND OBJECTIVES

Through the review of the literature relevant to the studies on directional stability of road tank vehicles, it is evident that the studies of the transient fluid slosh within partly filled

containers have been insufficient and incomplete. Although analytical and numerical methods have greatly contributed to the understanding of fluid slosh within different types of containers, the impact of transient large amplitude fluid slosh on dynamic responses of the vehicle is not yet fully understood. Moreover, the studies on the effectiveness of baffles in limiting the fluid slosh have been severely limited.

While many studies have suggested the presence of a strong coupling between the dynamic slosh and the directional dynamics of the vehicle, the dynamic interaction between the fluid and the vehicle has been mostly limited to the use of either quasi-static or mechanical-equivalent methods in the fluid slosh analyses. The role of transient forces and moments on the vehicle's directional response mostly remains unknown, particularly in the presence of baffles. The development of a mechanical analogy of the fluid, however, is quite complex in view of nonlinearity of slosh. Although considerable efforts have been made to study fluid slosh through experimental means, the studies have mostly employed very small size model tanks subjected to highly idealized disturbances, while little evidences of a dynamic similarity exist. The slosh phenomena would be largely different for different sizes of the tanks. A need to obtain measured data for sizes representative of the road tanks thus exists in order to obtain a more objective validation of the dynamic fluid slosh models and a better understanding of the slosh physics within the full size tanks. Furthermore, baffles within a tank tend to greatly alter the fluid slosh, depending on the geometry and location of the baffle.

The present dissertation research thus aims at conducting a detailed investigation of dynamic fluid slosh within partly-filled cleanbore as well as baffled tanks, which involves the analyses of fundamental natural frequency, transient nature of fluid slosh

forces and moments caused by time-varying external excitations, and their effects on the roll and pitch dynamic behavior of a partly-filled tank vehicle. This will contribute to a better understanding of the complex phenomenon that will lead to the improved stability of road tank vehicles. The specific objectives of the proposed study are:

a) Perform laboratory experiments on a scale model of a "Reuleaux triangle" cross-sectional tank with and without baffles to measure dynamic slosh forces and moments arising from fluid slosh under excitations applied in the lateral and longitudinal directions.

b) Conduct a thorough analysis of the laboratory-measured data to build an understanding of the fluid slosh behavior under various fill conditions, and frequency and severity of the tank motion, and effectiveness of different baffles.

c) Develop a CFD fluid slosh model for the scale model tank and examine its validity against the experimental results under different conditions, such as tank configuration, fill level and excitation.

d) Analyze transient fluid slosh effects within a partly filled full scale tank of "Reuleaux triangular" cross-section coupled with different types of baffles.

e) Explore a few concepts in anti-slosh mechanisms in the pitch and roll planes, such as lateral and longitudinal partial baffles and evaluate the effectiveness of different baffle design concepts.

f) Investigate the impact of transient slosh forces and moments on the rollover threshold of a multiple axle vehicle combination using the simplified moment equilibrium approach.

g) Develop a pitch plane vehicle model integrated with the CFD slosh model, and evaluate the dynamic braking performance of a partially filled cleanbore and baffled tank truck under straight braking maneuvers.

## 1.4 STRUCTURE OF PRESENTATION

The first chapter introduces the historical review of the researches on heavy vehicle dynamics, fluid slosh dynamics and dynamics of tank-vehicle combination. In this chapter, previous researches in the above fields are grouped and discussed in accordance with the methodology utilized. These methodologies are analyzed by presenting the conclusions and the main limitations of these studies. The literature study then leads to the motivation of the present research.

Chapter 2 describes the experimental setup, methodology and the result discussion for the laboratory fluid slosh study. The three-dimensional forces resulting from the fluid slosh in a tank with a "Reuleaux triangle" cross-section are measured for different tank configurations, fill levels and excitations. The roll, pitch and yaw moments are calculated using the force data. The peak slosh forces and moments are then analyzed as function of tank configuration, fill level and excitation frequency and magnitude. Furthermore, frequency analysis is presented for the forced and free slosh experiments. The slosh frequency is studied through the frequency content analysis of slosh force components, and the estimation of slosh natural frequency.

A three-dimensional CFD slosh model and the validations are presented in Chapter 3. The CFD slosh model is built based upon the VOF technique. The model is numerically verified for different tank configurations regarding the mesh influence and

convergence. Afterwards it is substantially validated against the experiment results discussed in Chapter 2. The validations are composed of the comparisons of results, including natural frequency, forces and moments, from the two approaches for both transient and steady state slosh. The comparisons are presented for different tank configurations at different fill volumes and under different excitation magnitudes and frequencies.

Chapter 4 presents the fluid slosh analysis of a full scale tank for a two-axle tridem tank truck using the CFD slosh model introduced in Chap. 3. The three-dimensional slosh are simulated for unbaffled and baffled tank configurations at different fill conditions and subjected to the manoeuvres of steady turning, straight braking, braking-in-a-turn, and path change. The transient peak forces and moments are analyzed with relation to the quasi-static solutions. A few of novel baffle concepts are also evaluated based on the transient fluid slosh analysis with the CFD model. Furthermore, several baffle design factors, such as equalizer and baffle opening, are investigated.

In Chapter 5, the CFD slosh model is incorporated into a roll plane vehicle model to predict the rollover threshold of a six-axle semitrailer tank vehicle. The peak slosh forces and moments and liquid *cg* coordinates in the roll plane are calculated from the slosh model and then applied to vehicle roll moment equilibrium to derive the roll stability limit. The analyses are performed for two different tank geometries (circular and "Reuleaux triangle" cross-section) under different fill volumes and excitation magnitudes. The predictions are compared with the results obtained from the quasi-static approach and the results of the equivalent rigid cargo transporting vehicle.

The CFD slosh model is further integrated into a pitch plane vehicle model in Chapter 6 to explore the transient braking performance of a two-axle tridem truck in straight braking maneuvers. The integration is achieved through the parallel calculations and the input parameter updating for the CFD slosh model and the vehicle model. It thus permits the real-time simulation of dynamic fluid-structure interaction for tank vehicles during maneuvers. The stopping distance and the dynamic load factor are derived from the integrated tank-vehicle model for unbaffled and baffled tank configurations at different fill volumes under different braking efforts.

The main conclusions from the dissertation research are summarized in Chapter 7. A few recommendations and suggestions are also presented for the purpose of future work in the relevant field.

# CHAPTER 2

# EXPERIMENTAL STUDY OF LIQUID SLOSH DYNAMICS IN A PARTIALLY FILLED TANK

## 2.1 INTRODUCTION

Fluid slosh within a tank is known to be quite complex, particularly under the influence on multiple-axis excitations, as encountered in moving vehicles. The fundamental properties of slosh and effects of anti-slosh devices, such as baffles, could be effectively investigated through laboratory experiments under controlled conditions. Such experiments can provide considerable insight into the fluid slosh and associated forces and moments. The majority of the experimental investigations on the fluid slosh have been conducted in model tanks which are small in size compared to the fullscale tanks of cross-section area in the order of 3.5 $m^2$. The cross-sectional areas of the model tanks employed in the reported studies were in the order of 0.2 $m^2$ [3, 24, 31, 116]. Since the similarity of sloshing fluid flows is very complex, the slosh behavior would be expected to differ for different tank sizes. Moreover, some of the reported slosh studies were limited to measurements of hydrodynamic pressure at given points or only one component of the slosh forces [116, 133]. The stability of a road tank vehicle, however, is strongly dependent on the resultant slosh forces and moments arising in all the translational and rotational axes. Furthermore, experimental studies on tanks with baffles have been extremely limited [48, 134].

In this chapter, the three-dimensional fluid slosh is experimentally investigated in a test tank in the laboratory. The measurements were performed with and without baffles to evaluate fundamental slosh frequencies, and dynamic slosh forces and moments under the influence of harmonic lateral and longitudinal acceleration fields. The measured data are analyzed to build an understanding of the conditions of beating phenomenon and swirling motion of the free surface, magnitudes of slosh forces and moments developed, and the role of primary influencing factors.

## 2.2 EXPERIMENTAL METHOD

### 2.2.1 Experimental Setup

The experiments were conducted in a scale model tank of cross-section, similar to the "Reuleaux triangle" with variable arc widths, as shown in Figure 2.1*a*. The tank cross-section was realized on the basis of the optimal tank geometry proposed by Kang [10] with the goal of suppressing liquid slosh in the roll plane. The model tank was designed with sufficiently large dimensions to reduce the effects of boundary constraints on the fluid slosh. The resulting tank design is considerably larger than those employed in the earlier reported studies [3, 24, 31, 116]. The total length and cross-section area of the test tank were 1.85 m and 0.426 $m^2$, respectively. The transverse width of the tank was approximately 1/3 of a typical full scale tank in road tank vehicles. The tank was made of 12.7 mm thick transparent plexiglass material to facilitate flow visualization (Figure 2.2*a*).

The tank was designed in three modular sections of equal length that allowed to conveniently insert different baffle designs between the flanges of the modular sections

(Figure 2.1*a*). Two different baffle designs were considered: (*i*) a single-orifice baffle (245.5 mm diameter); and (*ii*) a multiple-orifice baffle comprising 34 small orifices (38.1 mm diameter) and a large 101.6 mm diameter orifice at the geometric center, as shown in Figure 2.1*b*. The porosity of the two baffles was approximately 11% of the entire cross-sectional area. The baffles were made of transparent rigid PVC. Three different configurations of the test tank were realized, namely: the cleanbore tank (no baffles), is denoted as 'T0' tank; tank with two single-orifice baffles, denoted as tank 'T1'; and tank with two multiple-orifice baffles, denoted as tank 'T2'.

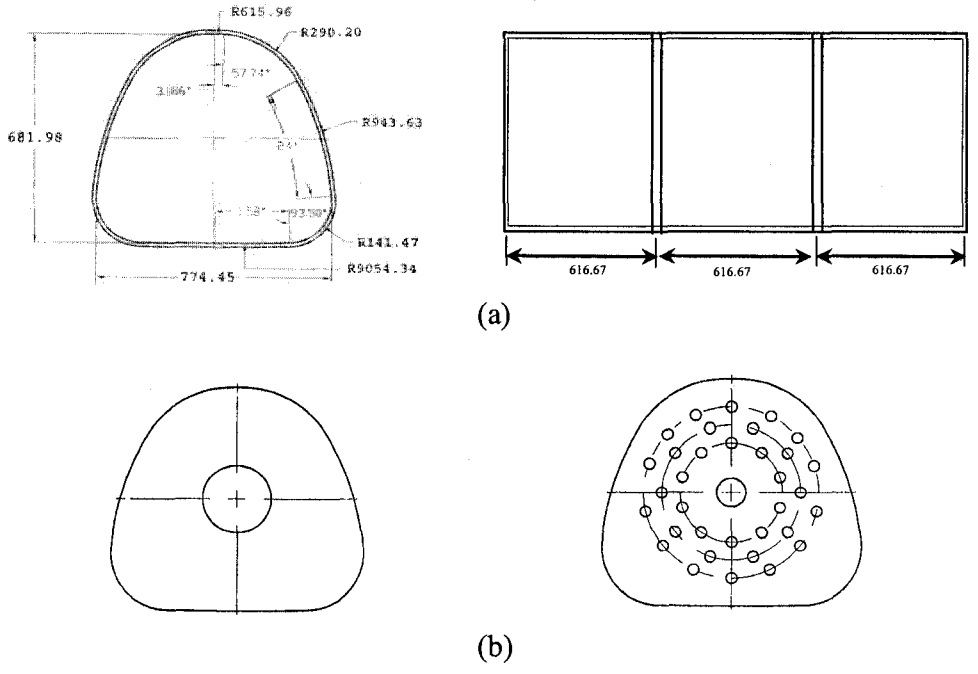


Figure 2.1: Schematic of: (a) the test tank (all dimensions are in mm); (b) the single-orifice ('T1') and multiple-orifice ('T2') baffles.

The tank (with or without baffles) was mounted on an aluminum plate that was fixed on a horizontal shake table through three three-axes force dynamometers to measure dynamic forces developed along the longitudinal ($X$), lateral ($Y$) and vertical ($Z$)

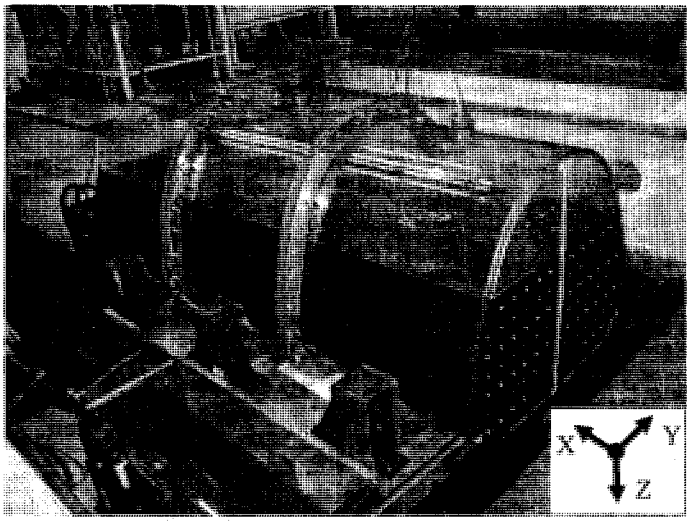


(a)

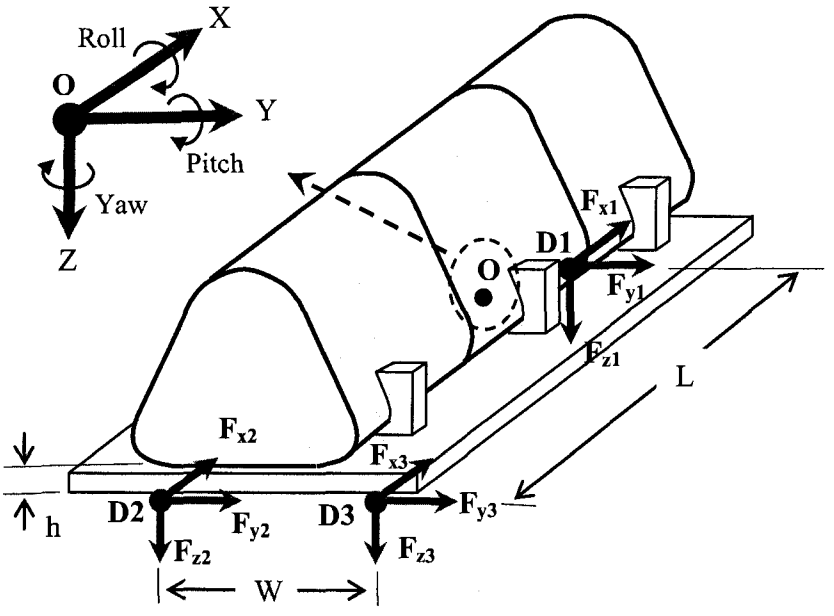


(b)

Figure 2.2: (a) a pictorial view of the experimental setup; (b) schematic of the tank illustrating local and global coordinate systems and locations of the three dynamometers (D1, D2 and D3).

axes. The three dynamometers were installed in a triangular manner, as shown in Figure 2.2*b*. Two of the dynamometers (D2 and D3) were mounted in the rear end of the plate, while a single dynamometer (D1) was used at the leading edge of the plate. The single dynamometer was located underneath the tank geometric centre in the roll plane. The forces acquired by the dynamometers were manipulated to compute roll, pitch and yaw moments developed due to fluid motion. The shake table was connected to a 40 cm stroke hydraulic servo-actuator and placed on a fixed granite slip table. The motion of the slip table was constrained by a pair of guides on the sides of the table. During the experiments, the surface of the slip table was fully covered with oil to achieve smooth motion of the shake table with minimal friction. The oil film was maintained on the table surface through an oil circulation system. The hydraulic actuator was controlled by a servo controller (MTS 407), while the tank with its support structure could be mounted either along or normal to the actuator axis. This allowed achieving either lateral or longitudinal excitation to the tank. Water was used as the test liquid within the tank and a food dye was added to visualize the flow.

The acceleration and displacement of the platform with the tank were measured using an accelerometer and a linear variable differential transformer (LVDT), respectively. The force, acceleration and displacement signals were acquired using a National Instrument PCI-6036E DAQ board. A total of 11 channels were used for the acquisition of nine force components from three dynamometers, and the platform acceleration and displacement. The data were acquired at a rate of 256 Hz using the Labview 7.0 software.

### 2.2.2 Test Conditions

The experiments were designed to measure three components of the dynamic force arising from the liquid slosh within the test tank with or without baffles. The test matrix included three fill volumes (30, 50 and 70% of the tank volume) and various amplitudes and frequencies of acceleration excitation. The fill depth corresponding to each fill volume was computed from the tank geometry and is summarized in Table 2.1. A grid was marked on the tank cross-section to monitor the fill height and volume, as illustrated in the photograph of the tank in Figure 2.2*a*. The static free surface of the liquid in the single-orifice baffle tank configuration ('T1') with 30% fill volume occurred slightly below the orifice opening. This resulted in entrapment of the fluid within different segments of the tank, due to absence of equalizers within the test tank. The 30% fill volume for 'T1' tank was thus excluded.

Table 2.1: Test matrix including tank configurations and types of the lateral (Y) and longitudinal (X) excitations.

| Tank configuration | Percent fill volume (fill depth, cm) | | | Type and direction of excitation | |
|---|---|---|---|---|---|
| | 30% (17.96) | 50% (29.39) | 70% (41.79) | Harmonic (continuous) | Single-cycle |
| 'T0' (un-baffled) | √ | √ | √ | Y, X | Y |
| 'T1' (single-orifice baffle) | — | √ | √ | Y, X | Y |
| 'T2' (multiple-orifice baffle) | √ | √ | √ | Y, X | Y |

The experiments were performed under different amplitudes of harmonic acceleration excitations at various discrete frequencies in order to study steady-state slosh behavior and the dependency of slosh forces on the excitation frequency and magnitude.

The test matrix illustrating the frequencies and magnitudes of excitation is shown in Table 2.2. The ranges of excitation frequencies were selected on the basis of expected fundamental slosh frequencies, which were estimated using the methodology presented by Romero *et al.* [31]. The lateral acceleration excitations were synthesized at different discrete frequencies in 0.5 to 3 Hz range and four different amplitudes (0.5, 1, 2 and 3 $m/s^2$). The higher acceleration amplitudes at lower frequencies, however, were not attempted in order to limit the peak displacement of the tank assembly within the stroke of actuator, as evident in Table 2.2. The longitudinal excitations were synthesized to yield three different amplitudes of acceleration (0.25, 0.5 and 1 $m/s^2$) in the frequency range of 0.25 to 1.5 Hz, as summarized in Table 2.2. Considering different longitudinal mode resonant frequencies for different tank configurations, 'T0' tank was subject to excitations in 0.25 to 1 Hz frequency range, while 'T1' and 'T2' tanks were subject to excitations in the 0.5 Hz to 1.5 Hz frequency range.

Table 2.2: Test matrix illustrating frequencies and magnitudes of continuous lateral and longitudinal excitations.

| $A$ | Lateral acceleration excitation frequency (Hz) | | | | | | | | | | | | |
|---|---|---|---|---|---|---|---|---|---|---|---|---|---|
| ($m/s^2$) | 0.5 | 0.6 | 0.7 | 0.8 | 0.9 | 1 | 1.1 | 1.2 | 1.3 | 1.5 | 2 | 2.5 | 3 |
| 0.5 | √ | √ | √ | √ | √ | √ | √ | √ | √ | √ | √ | √ | √ |
| 1 | √ | √ | √ | √ | √ | √ | √ | √ | √ | √ | √ | √ | √ |
| 2 | | | √ | √ | √ | √ | √ | √ | √ | √ | √ | √ | √ |
| 3 | | | | | √ | √ | √ | √ | √ | √ | √ | √ | √ |

| $A$ | Longitudinal acceleration excitation frequency (Hz) | | | | | | | | | | | | | | | | | |
|---|---|---|---|---|---|---|---|---|---|---|---|---|---|---|---|---|---|---|
| ($m/s^2$) | 0.25 | 0.3 | 0.36 | 0.4 | 0.45 | 0.5 | 0.55 | 0.6 | 0.65 | 0.7 | 0.8 | 0.9 | 1 | 1.1 | 1.2 | 1.3 | 1.4 | 1.5 |
| 0.25 | √ | √ | √ | √ | √ | √ | √ | √ | √ | √ | √ | √ | √ | √ | √ | √ | √ | √ |
| 0.5 | | | √ | √ | √ | √ | √ | √ | √ | √ | √ | √ | √ | √ | √ | √ | √ | √ |
| 1 | | | | | | √ | √ | √ | √ | √ | √ | √ | √ | √ | √ | √ | √ | √ |

Apart from the harmonic excitations, a single-cycle sinusoidal acceleration excitation was synthesized to study the transient lateral slosh behavior. It has been suggested that the centrifugal acceleration encountered during a path change can be approximated by a single-sinusoid [132]. The single-cycle sinusoidal lateral acceleration was constructed using the following piecewise functions:

$$a_y(t) = \begin{cases} 0.5A(1-\cos(4\pi ft)) & t \le 0.25T \\ A\sin(2\pi ft) & 0.25T < t \le 0.75T \\ -0.5A(1-\cos(4\pi ft)) & 0.75T < t \le T \\ 0 & t > T \end{cases} \tag{2.1}$$

where $T$ is the period, $f$ is frequency and $A$ is the amplitude of acceleration. Equation (2.1) was integrated to obtain displacement excitation signal, which was smoothened to eliminate the effects of discontinuities. The resulting displacement signal was used as the input for the electro-hydraulic exciter. The sampling rate of the displacement signal was varied to achieve two different fundamental frequencies of the resulting acceleration excitations: 1 and 1.5 Hz. Figure 2.3 shows the time history of the single sinusoidal

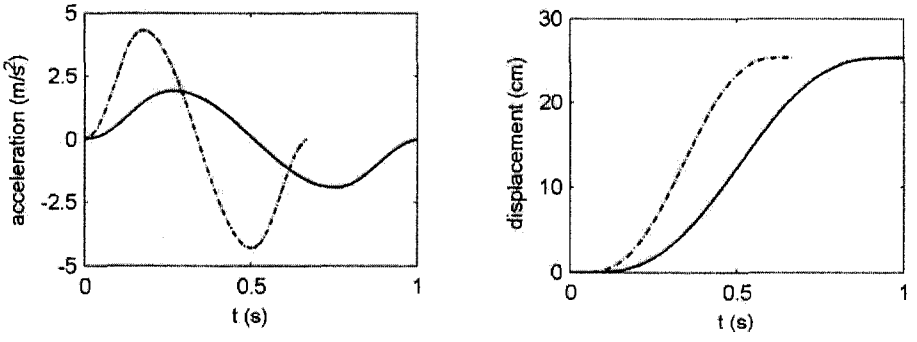


Figure 2.3: The single-cycle sinusoidal acceleration and the corresponding displacement along the lateral (Y) axis. Solid line - 1 Hz; dash-dotted line - 1.5 Hz.

lateral acceleration excitation and the corresponding displacement signal at the selected excitation frequencies of 1 and 1.5 Hz. The variations in displacement signal suggest that such a signal can represent a path change maneuver.

### 2.2.3 Test and Data Analysis Methodology

Two series of measurements were conducted under lateral acceleration excitations, with objectives to measure steady-state slosh response to harmonic excitation and transient slosh response to single-cycle sinusoidal acceleration. The measurements were initially performed with desired configurations of the empty tank for both baffled and un-baffled configurations. The measured forces along the three orthogonal axes were stored and later applied to perform corrections for the inertial forces due to the tank and supporting structure of the resultant forces arising from the fluid slosh in the partially filled tank. The dynamic responses of the tank and structure alone were measured under each excitation, which revealed constant mass of the assembly, approximately equal to 347 kg.

For each fill volume condition and each tank configuration, the tank was filled to the desired liquid fill level and the slip table was positioned in its mid-stroke. Under each harmonic excitation, the data acquisition was initiated when steady-state motion of the free surface was observed. A low frequency swirl at the free surface was observed under excitations in the vicinity of the fundamental slosh frequency. The data were thus acquired for the duration of 40 seconds in order to capture this low frequency swirling behavior. Under single-cycle sinusoidal excitations, the data acquisition was started prior to the initiation of the excitation in order to track the starting instant of the tank motion and to acquire the transient slosh response.

The data acquired by the three dynamometers were analyzed to determine the resultant slosh forces and moments. The measured forces under each excitation frequency revealed the presence of a 13 Hz component in both lateral and longitudinal directions. This frequency was attributed to the natural frequency of the coupled slip table and actuator system, and was judged to be sufficiently high compared to the highest excitation frequency of interest (3 Hz). The acquired signals were low-pass filtered using an $8^{th}$ order Butterworth digital low-pass filter with cutoff frequency of 6 Hz in order to attenuate the 13 Hz component.. The filtered data showed notable variations in the amplitudes of different cycles of oscillations. The steady-state amplitudes were thus calculated using a confidence treatment to reduce the uncertainty. The steady-state signal over a period of 20 seconds was extracted and the peak amplitude was identified over the 96% confidence interval. The peak slosh forces developed under single-cycle sinusoidal inputs, however, were taken directly from the filtered signal.

Under excitations along the lateral direction, the resultant slosh forces developed along the three axes were computed by the summation of force components measured from the three dynamometers, such that:

$$
\begin{aligned}
F_X(t) &= \sum_{i=1}^{3} F_{xi}^{f}(t) \\
F_Y(t) &= \sum_{i=1}^{3} F_{yi}^{f}(t) - m_e \cdot a_Y(t) \qquad (i = 1, 2 \text{ and } 3) \\
F_Z(t) &= \sum_{i=1}^{3} F_{zi}^{f}(t)
\end{aligned}
\tag{2.2}
$$

where $F_X, F_Y$ and $F_Z$ are resultant dynamic forces due to the sloshing fluid; $F_{xi}$, $F_{yi}$ and $F_{zi}$ are three force components measured by the $i^{th}$ dynamometer; $i = 1$, 2 and 3 refer to the front, rear-left and rear-right dynamometers, as illustrated in Figure 2.2*b*. The

superscript $f$ refers to the case of liquid filled tank; $m_e$ is the equivalent mass of rigid structure including the empty tank and its mounting plate identified from the empty tank tests; and $a_Y$ is the lateral excitation acceleration. The subscripts $X$, $Y$ and $Z$ indicate the global coordinate system of the tank with origin 'O' located at the geometric centre of the tank projected at its base (Figure 2.2*b*), while $x$, $y$ and $z$ represent the local coordinate systems of dynamometers. It should be noted that each dynamometer was zeroed prior to each trial. The measured lateral slosh force due to fluid and the tank structure was subsequently corrected by subtracting the contribution from the rigid structure, including the platform and empty tank. The magnitude of the inertial force component measured in the $X$ direction was found to be significantly small. In the vertical ($Z$) direction the inertial force equaled the fluid and structure weight, which was zeroed prior to measurements. The inertial force corrections in the $X$ and $Z$ directions were thus not attempted.

The roll ($M_X$), pitch ($M_Y$) and yaw ($M_Z$) moments due to fluid slosh were computed from the measured force components in the following manner:

$$\begin{aligned} M_X(t) &= \left(\frac{W}{2}N_Y\right)K - hF_Y \\ M_Y(t) &= \frac{L}{2}N_X + hF_X \\ M_Z(t) &= \frac{L}{2}(F_{y1} - F_{y2} - F_{y3}) + \frac{W}{2}(F_{x2}^f - F_{x3}^f) \end{aligned} \tag{2.3}$$

where $L$ is the longitudinal distance between the front dynamometer and the lateral axis passing through the centers of the rear dynamometers; $W$ is the lateral spacing between centers of the rear left and rear right dynamometers (Figure 2.2*b*); $h$ is the height of the origin "O" from the top surface of the dynamometers; $K$ is a calibration factor for the

resultant roll moment that was determined through calibration performed with the empty tank. This calibration factor was used to account for the spacing of individual force sensors within each dynamometer. $N_Y$ and $N_X$ are the lateral and longitudinal load shifts, respectively, attributed to fluid slosh, determined from:

$$\begin{aligned} N_Y(t) &= (F_{z3}^f - F_{z2}^f) - N_Y^e \\ N_X(t) &= (F_{z2}^f + F_{z3}^f) - F_{z1}^f \end{aligned} \tag{2.4}$$

where $N_Y^e$ is the lateral load shift measured for the empty tank and structure, which is linearly dependent on the lateral excitation acceleration $a_Y$.

The resultant slosh forces under longitudinal acceleration excitations ($a_X$) are also derived in a similar manner, where the inertial force correction is applied only in the longitudinal direction, such that:

$$\begin{aligned} F_X(t) &= \sum_{i=1}^{3} F_{xi}^f(t) - m_e \cdot a_X(t) \\ F_Y(t) &= \sum_{i=1}^{3} F_{yi}^f(t) \qquad (i = 1, 2 \text{ and } 3) \\ F_Z(t) &= \sum_{i=1}^{3} F_{zi}^f(t) \end{aligned} \tag{2.5}$$

The moments due to fluid slosh are derived from Equation (2.3), where the lateral and longitudinal load shifts are determined from:

$$\begin{aligned} N_Y(t) &= F_{z3}^f - F_{z2}^f \\ N_X(t) &= (F_{z2}^f + F_{z3}^f - F_{z1}^f) - N_X^e \end{aligned} \tag{2.6}$$

where $N_X^e$ is the longitudinal load shift measured for the empty tank and structure, which is linearly dependent on the longitudinal excitation acceleration ($a_X$).

The dynamic responses of the partly filled tank to excitations in the lateral and longitudinal directions were assessed in terms of the resultant normalized slosh forces

and moments. Under a lateral acceleration excitation, the resultant lateral force $F_Y$ is normalized with respect to that developed by an equivalent rigid load, such that:

$$M_{Fy} = \frac{F_Y}{m_l a_Y} \tag{2.7}$$

where $m_l$ is the liquid mass and $M_{Fy}$ is the normalized lateral slosh force that has been termed as an amplification factor of lateral slosh force [128].

The resultant forces developed along the $X$ and $Z$ directions were normalized with respect to the weight of the liquid alone, such that:

$$M_{Fx} = \frac{F_X}{m_l g}; \quad M_{Fz} = \frac{F_Z}{m_l g} \tag{2.8}$$

The roll, pitch and yaw moments were normalized by the roll moment developed by the equivalent rigid "frozen" liquid which the *cg* height is $h_0$:

$$M_{Mi} = \frac{M_i}{m_l a_Y h_0} \qquad (i = x, y, z) \tag{2.9}$$

Similarly, under the longitudinal acceleration excitations, the amplification factors in slosh forces and moments are defined as:

$$M_{Fx} = \frac{F_X}{m_l a_X}; \quad M_{Fy} = \frac{F_Y}{m_l g}; \quad M_{Fz} = \frac{F_Z}{m_l g} \tag{2.10}$$

$$M_{Mi} = \frac{M_i}{m_l a_X h_0} \qquad (i = x, y, z) \tag{2.11}$$

The frequencies of fluid slosh within the baffled and cleanbore tanks were also measured from the free oscillations of the fluid surface. For this purpose, the signals from the dynamometers were acquired soon after the acceleration excitation was terminated. The gradual decay in the free surface oscillations was observed, which was considered to

occur near the fundamental slosh frequency. The measured force signals revealed gradual decay related to the free surface oscillation. The fundamental natural frequencies of fluid slosh in the lateral and longitudinal directions were subsequently computed from the frequency spectra of the forces measured under the free oscillations. The resolution of spectra is 0.0156 Hz. The spectra invariably revealed a single dominant peak and the corresponding frequency was considered as the fundamental slosh natural frequency.

## 2.3 SLOSH FREQUENCIES

The fundamental frequencies of lateral and longitudinal fluid slosh in a partly-filled highway tank vehicle may occur in the vicinity of 0.6 Hz and 0.3 Hz, respectively [16]. Under low fill volumes, the lateral model slosh frequency may lie close to the steering frequency corresponding to an emergency type of maneuver, which may induce resonant oscillations of the free surface and thus severe slosh forces. The slosh frequencies, however, strongly depend upon the fill volume and the number of baffle partition. In this study, the measured slosh forces are analyzed to identify important slosh frequencies that cause high magnitude of slosh forces.

Figure 2.4*a* shows the fundamental natural frequencies obtained from the frequency spectra of measured forces in both lateral and longitudinal directions for the cleanbore tank ('T0') for the three fill volume cases considered in the study. Three free oscillation tests were conducted for each fill volume and the same results were attained for the three tests. The figure shows that the slosh frequency increases with the fill volume. This trend is consistent with those reported by Budiansky [28], Lamb [130] and Kobayashi *et al.* [116] for cylindrical and rectangular tanks. The fundamental frequencies

corresponding to different fill levels were also computed using the analytical method proposed by Romero *et al.* [31], which was based upon wave length and wave speed of the free surface. The measured frequencies agree reasonably well with the computed frequencies in both lateral and longitudinal directions for all the fill levels, as shown in Figure 2.4*a*. The measured frequencies, however, tend to be slightly higher than the calculated ones, particularly in the lateral mode. The deviations in both lateral and longitudinal mode frequencies tend to increase with high fill volume. The maximum difference between the measured and computed frequencies was found to be approximately 4% at 70% fill volume. This deviation is mostly attributed to the assumption of constant free surface length considered in the estimation method. The length of free surface of the liquid varies considerably in the lateral plane and may lead to the estimation errors.

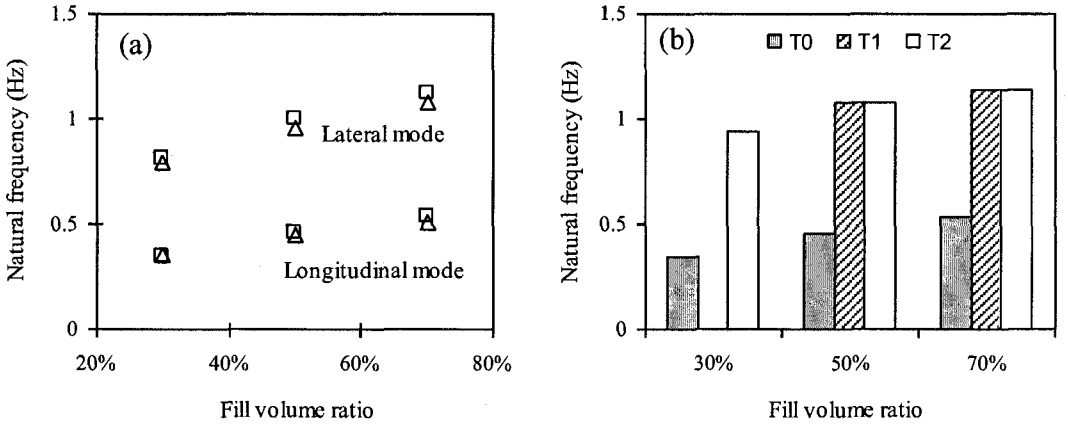


Figure 2.4: (a) Comparisons of the measured and estimated natural frequencies of lateral and longitudinal fluid slosh in the cleanbore tank (□, measured; Δ, estimated); (b) comparisons of the fundamental longitudinal slosh natural frequencies in different tanks configurations.

The presence of lateral baffles tends to increase the longitudinal mode frequencies considerably with only little or no effect on the lateral mode frequencies. Figure 2.4*b*

shows the effect of transverse baffles on the longitudinal mode natural frequencies measured for the three fill conditions. It should be noted that the data for 30% filled 'T1' tank was not acquired for the reason described in section 2.2. The results show that the addition of baffles yields significantly higher natural frequencies, irrespective of the fill volume, which increase by nearly 173%, 138% and 115% for 'T2' tank under 30%, 50% and 70% fill volumes, respectively, when compared to those attained for 'T0' tank. Both types of baffles yield identical gains in the longitudinal mode natural frequencies. The results also show that the natural frequency increases with the fill level, as observed for the cleanbore tank ('T0'). The measured data further revealed that baffles do not affect the lateral mode natural frequency.

The frequency spectra of slosh forces revealed a number of important spectral components in the power spectral density (PSD) of the forces as illustrated in Figure 2.5. The figure shows the spectra of lateral, longitudinal and vertical slosh forces measured for 50%-filled baffled and un-baffled tanks subject to 1 $m/s^2$ lateral acceleration excitation at 0.7 Hz. The spectra of forces measured for the baffled 'T1' tank were similar to those of the 'T2' tank, and thus not presented. The tank configurations 'T0' and 'T2' revealed similar magnitudes of the spectral energy of the lateral and vertical slosh forces, while considerable differences could be seen in the longitudinal force responses. Two predominant peaks are observed in the lateral force spectrum near the excitation frequency ($f_e \approx 0.7$ Hz) and the lateral mode fundamental frequency ($f_{n,y} \approx 1$ Hz), as evident in Figure 2.5*a*. The spectra of the longitudinal slosh force (Figure 2.5*b*) show prominent peaks near the excitation frequency ($f_e$), longitudinal mode resonant frequency ($f_{n,x} \approx 0.45$ Hz) and lateral mode frequency ($f_{n,y} \approx 1$ Hz). The longitudinal mode resonance

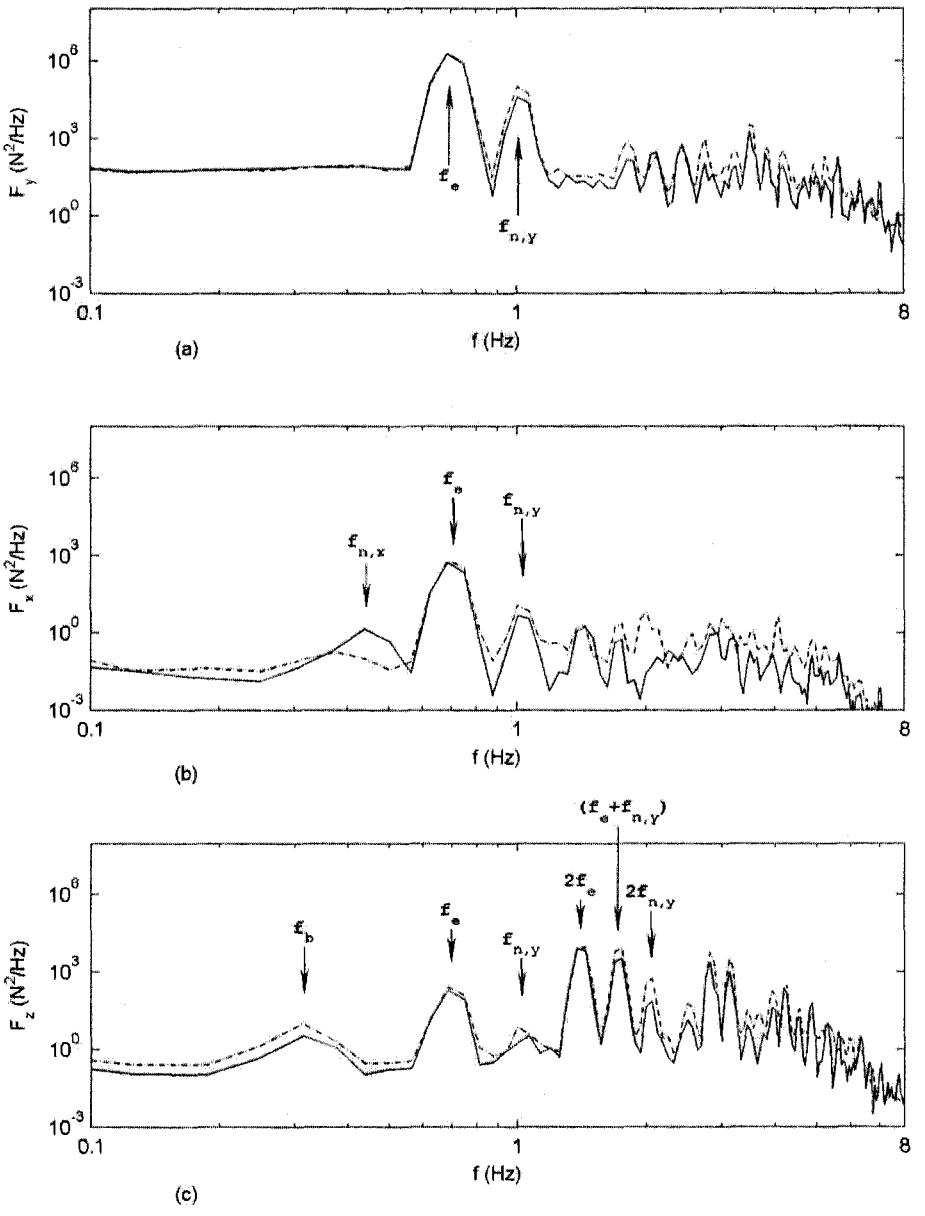


Figure 2.5: Frequency spectra of slosh force components measured on the 50%-filled un-baffled ('T0') and baffled ('T2') tanks subject to the 1 m/s$^2$ lateral acceleration excitation at 0.7 Hz: (a) lateral force; (b) longitudinal force; (c) vertical force. Solid line, 'T0' tank; dash-dotted line, 'T2' tank.

of the baffled 'T2' tank occurred near 1.1 Hz (Figure 2.4*b*). It lies in the close proximity of the lateral mode resonance of 1 Hz. The results suggest coupling between the longitudinal and lateral slosh, even though the excitation is applied along the lateral direction alone. The peak in $F_x$ near the excitation frequency is also partly attributed to slight misalignment of the tank with respect to the lateral axis of excitation. This coupling was clearly evident for the baffled tanks. The free surface undergoes considerable longitudinal and rotational motions after impacting against the baffle or end caps. The spectra also exhibit several high frequency peaks, which may be related to higher slosh modes and structural modes. The data corresponding to these modes were not analyzed in this study.

The spectra of the vertical forces (Figure 2.5*c*) show several prominent peaks. The peak occurring at the very low frequency of 0.3 Hz corresponds to the beating frequency ($f_b$), which is equal to the difference between the fundamental mode resonance frequency ($f_{n,y}$) and the excitation frequency ($f_e$). The beating phenomenon of the free surface was clearly observed during the experiments, particularly within the baffled tanks. The spectral energy of the peak at the beating frequency, however, was relatively small compared to other peaks. This peak corresponding to the beating frequency, however, is not evident in the spectra of the lateral forces. This is due to the reason that the beating is reflected less apparently in the lateral force than in the vertical force. This is also evident in the time-histories of lateral and vertical forces shown in Figure 2.6. The figure shows the variations in the measured lateral and vertical forces in the 50%-filled 'T0' tank subject to 0.5 m/s$^2$ lateral acceleration excitation at 1.3 Hz. The results clearly show the presence of beating frequency, $f_b = |f_e - f_{n,y}|$, and the beating period $T_b$ of

approximately 3.3 s. The beating phenomenon could be attributed to modulation of the excitation frequency with the resonant frequency [131].

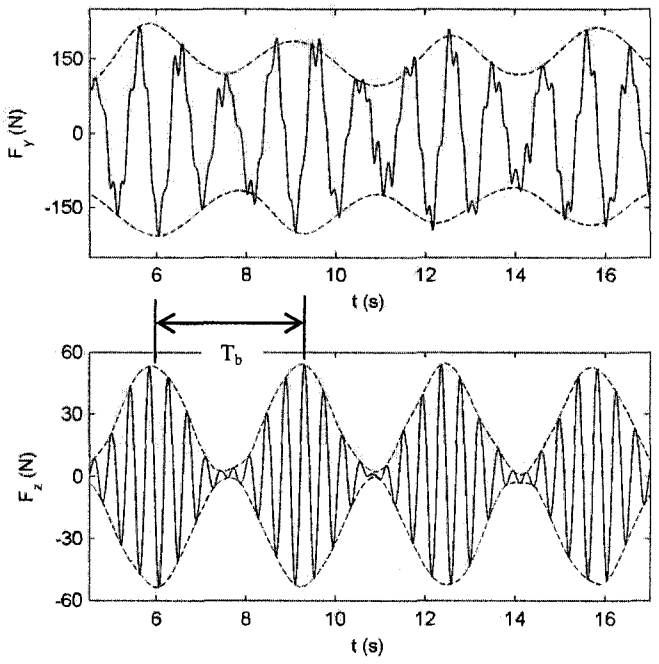


Figure 2.6: Time histories of lateral ($F_y$) and vertical ($F_z$) slosh forces developed in the 50%-filled cleanbore tank ('T0') under 0.5 m/s$^2$ lateral acceleration excitation at 1.3 Hz. The dashed line illustrates the wave envelop attributed to the beating phenomenon in slosh.

The spectra of vertical forces in Figure 2.5*c* also show peaks near the excitation ($f_e$) and resonant ($f_{n,y}$) frequencies. The oscillation in lateral and vertical forces occur near the lateral mode resonance ($f_{n,y} \approx 1$ Hz) and the vibration frequency ($f_e+f_{n,y}$), respectively. The spectra also exhibit additional important peaks in the 1 to 2 Hz frequency range. The peaks occur near 1.4, 1.7 and 2.0 Hz. The frequencies of the first and last peaks in this range correspond to twice the excitation and lateral mode frequencies. The largest peak in

this range occurs at twice the excitation frequency (≈1.4 Hz) suggesting that the liquid oscillates like a pendulum. A peak near twice the resonant frequency (≈2 Hz) is also evident. The peak near 1.7 Hz corresponds to twice of the mean of the excitation and resonant frequencies ($f_e+f_{n,y}$), and has been referred to as the vibration frequency in the presence of beating [131]. The frequency spectra of the vertical force at the excitation magnitudes greater than 1 m/s$^2$ also revealed identical trends. However, at the lower excitation magnitude of 0.5 m/s$^2$, the largest peak in vertical force occurred at the vibration frequency, as opposed to twice the excitation frequency observed at higher magnitude excitations. This suggests that more pronounced beating is likely to occur at lower excitation magnitudes.

The largest peak in a given frequency spectrum could be related to the dominant mode of the corresponding slosh force component. The results in Figure 2.5 show that the dominant frequency mode is not identical for all the slosh force components. The relationship between the dominant mode frequency and the excitation frequency was further investigated from the data acquired under different excitations. The data were analyzed to identify correlations between the frequency of the dominant peak ($f_p$) and the excitation frequency. Figure 2.7 illustrates the variations in the dominant mode frequency ($f_p$) of the lateral and vertical forces, respectively with respect to the lateral acceleration excitation frequencies for the 50%-filled 'T1' tank subject to two different lateral acceleration excitation magnitudes (0.5 and 2 m/s$^2$). The results clearly show that the dominant mode of the lateral forces occur near the excitation frequency (i.e. $f_p=f_e$) for the higher excitation of 2 m/s$^2$, while it could be the resonant frequency for the lower excitation magnitude (0.5 m/s$^2$). The dominant modes of the vertical forces occur at twice

the excitation frequency (i.e. $f_p=2f_e$), under the higher excitation magnitude. The dominant modes corresponding to the lower excitation of 0.5 m/s$^2$, however, generally occur near the vibration frequency ($f_e+f_{n,y}$).

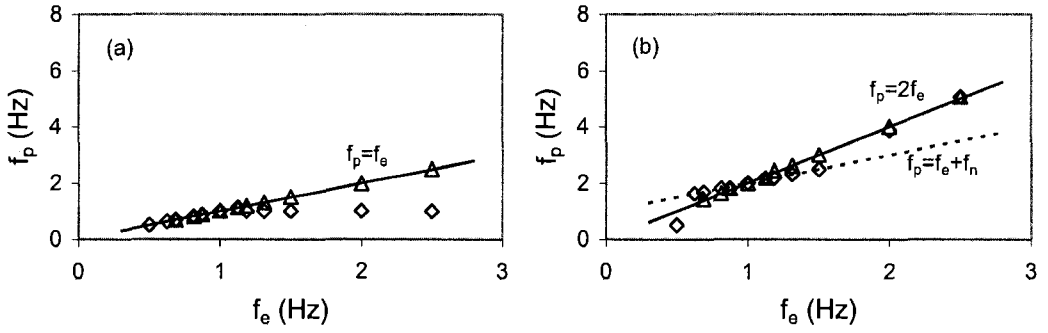


Figure 2.7: Relationships between the dominant mode frequency of slosh force ($f_p$) and the excitation frequency ($f_e$) for the 50%-filled baffled tank 'T1'. (a) lateral force; (b) vertical force. (◊, A=0.5 m/s$^2$; Δ, A= 2 m/s$^2$)

Similar trends could also be observed in the measured slosh forces under longitudinal excitations. Figure 2.8*a* presents the variations in the longitudinal slosh forces for the 50%-filled cleanbore tank ('T0') under a 0.5 m/s$^2$ longitudinal excitation at 0.6 Hz, in the vicinity of the first mode near 0.45 Hz. The longitudinal slosh force response attained under a 0.5 m/s$^2$ longitudinal excitation at 1 Hz, near the second mode resonance, is shown in Figure 2.8*b*. The second mode frequency was also estimated using the relationship described in [116] for the equivalent rectangular tank in the same fill level. The second mode frequency was estimated as 1.09 Hz, which lies close to the measured value. The results clearly show the beating phenomenon under both excitations, where the beating frequencies occur near 0.16 Hz and 0.063 Hz, which are approximately

equal to the difference between the excitation frequency and the resonant frequencies of first and second modes, respectively.

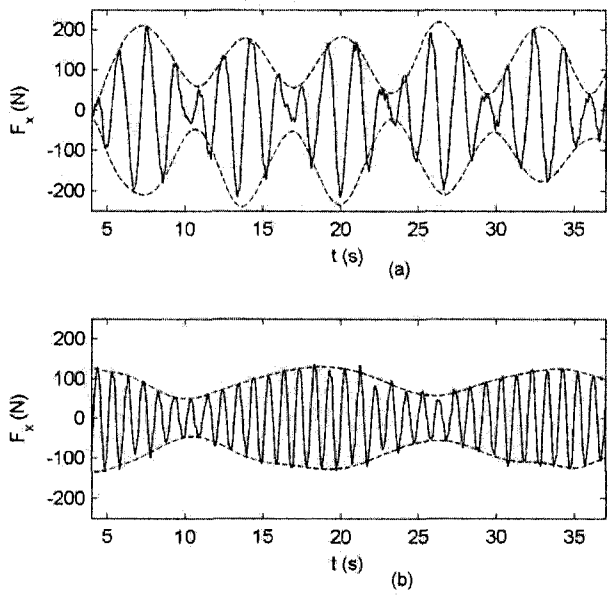


Figure 2.8: Time histories of the longitudinal slosh force ($F_x$) measured on the 50%-filled cleanbore tank subject to longitudinal acceleration excitations: (a) A=0.5 m/s$^2$ at 0.6 Hz; (b) A=0.5 m/s$^2$ at 1 Hz.

The relationship between the beating frequency and the excitation frequency was further explored from the data acquired under different excitations. As an example, Figure 2.9 illustrates the variations in the beating frequency with the excitation frequency for the forces measured on the 50% and 70%-filled 'T0' tanks subject to a 0.5 m/s$^2$ lateral acceleration excitation. The beating frequency estimated from the relation $f_b = |f_e - f_{n,y}|$ are also plotted in the figure. The results clearly show good agreements between the estimated and measured beating frequencies, irrespective of the fill volume

and excitation frequency considered. The results reveal that the beating phenomenon could be clearly observed for $|f_e - f_n| \leq 0.4$ Hz. It has been reported that the steering frequency in a path-change maneuver is typically in the order of 0.3 Hz, and may approach as high as 0.5 Hz in an emergency type of directional maneuver [16]. Considering that the fundamental lateral mode slosh frequencies for a partly-filled full size tank employed in highway transportation lies in the 0.5–0.6 Hz range in the roll plane [128], the fluid oscillation within the tank may yield beating phenomenon. Similar degrees of agreements (not shown here) were also observed under longitudinal acceleration excitation, while the intensity of beating was considerably small for the 30%-filled tanks under excitation along both the axes. Moreover, the beating phenomenon was not clearly observable under higher magnitudes of excitations, where the slosh forces along longitudinal and lateral axes primarily oscillate at the excitation frequency.

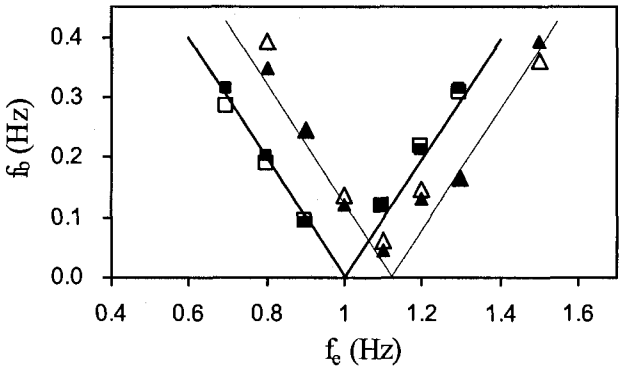


Figure 2.9: Relationship between the beating frequency ($f_b$) and the excitation frequency ($f_e$) for the cleanbore tank subjected to the lateral acceleration excitation of 0.5 m/s$^2$ at different frequencies. (□, 50% fill volume; Δ, 70% fill volume; open symbols, lateral force; solid symbols, vertical force; the estimated beating frequencies are shown by continuous lines: solid line, 50% fill volume; dashed line, 70% fill volume).

## 2.4 SLOSH FORCES AND MOMENTS

The influence of excitation magnitude and frequency on the severity of fluid slosh are investigated in terms of normalized amplification factors in forces and moments, using Equations (2.7) to (2.11). The results attained for the three tank configurations and three fill conditions under lateral and longitudinal excitations are discussed below.

### 2.4.1 Lateral Harmonic Excitations

Figure 2.10 shows variations in the magnitude of the steady state forces and moments amplification factors for the 50%-filled 'T0' tank subject to lateral harmonic excitations of different amplitude at various frequencies. The figure shows that the maxima of the normalized force components lie in the vicinity of the lateral mode natural frequency ($\approx$1 Hz), irrespective of the excitation magnitude. Abramson *et al.* [129] reported that the slosh resonant frequency decreases as the excitation amplitude increases for the compartmented upright cylindrical tanks. The results also suggest shift in the peak towards slightly higher frequencies, as the excitation magnitude is increased. This trend, however, could not be observed consistently. This could be attributed to the resolution of the test frequencies considered in the experiments.

Since the lateral force is normalized by the inertial force generated by the equivalent rigid mass of fluid, the responses can be interpreted as the amplification factor arising from the dynamic slosh effect. The results show that the peak amplification factor in lateral force could reach as high as 4. The slosh amplification factor decreases as the excitation magnitude increases, which is attributed to boundary effects. It is interesting to note that the amplification factor approaches a value less than unity at frequencies above

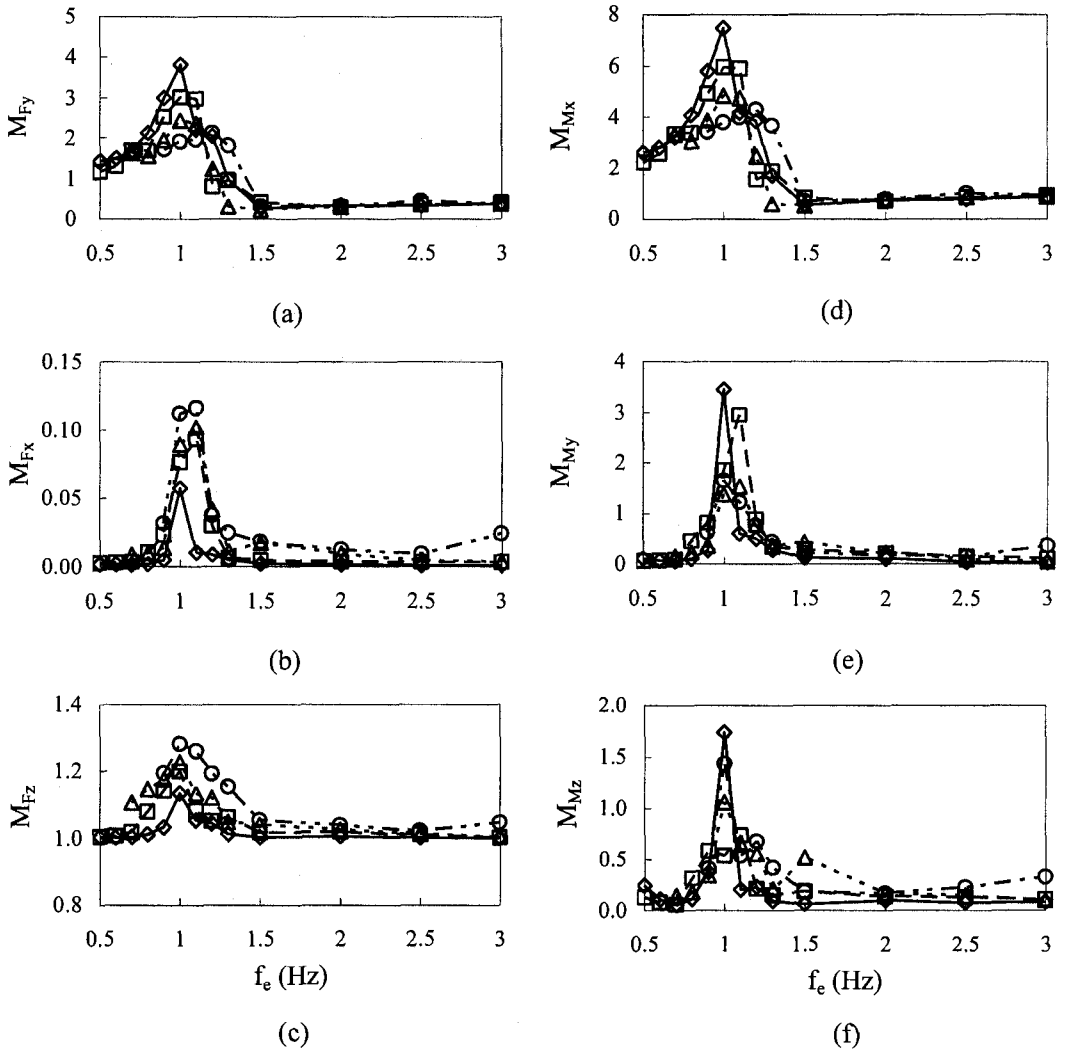


Figure 2.10: Variations in the normalized slosh force and moment components with the excitation frequency for the 50%-filled cleanbore tank under lateral acceleration excitations: (a) lateral force; (b) longitudinal force; (c) vertical force; (d) roll moment; (e) pitch moment; (f) yaw moment. (◊, A= 0.5 m/s$^2$; □, A= 1 m/s$^2$; Δ, A= 2 m/s$^2$; ○, A= 3 m/s$^2$).

1.4 Hz. This suggests that magnitude of lateral slosh force under excitations at higher frequencies would be considerably smaller than that caused by an equivalent rigid mass. The lower magnitude of lateral force at higher frequencies is attributed to relatively

smaller magnitude of the free surface oscillation. The results do not show peaks in the forces and moments corresponding to higher modes of fluid slosh. On the basis of formulation presented by Budiansky [28], the second and third lateral mode frequencies of a 50%-filled cylindrical tank of cross-section area identical to that of the given test tank were estimated as 1.78 and 2.31 Hz, respectively. The higher mode frequencies of the test tank were expected to be in the vicinity of these estimated frequencies despite the difference in the geometrical shape. The absence of peaks in the forces and moments near these frequencies was attributed to two factors: (*i*) the chosen excitation frequencies were not in the close proximity of the higher mode frequencies; and (*ii*) the magnitudes of slosh forces near these higher mode frequencies were relatively small. The latter is also evident from nearly unity magnitude of the normalized vertical slosh force, shown in Figure 2.10*c*.

The peak magnitudes of the normalized vertical slosh force also occur in the vicinity of the resonant frequency and increase with the excitation magnitude. The normalized magnitude, however, remains slightly above 1.0 at frequencies greater than 1.4 Hz, suggesting small magnitude of fluid slosh. The peak amplification factor is observed to be near 1.3 for the 3 $m/s^2$ lateral acceleration excitation. This indicates that the variations in the vertical force arising from dynamic slosh are up to 30% greater than the liquid weight under the excitations considered.

Figure 2.10*b* shows that the magnitude of the normalized longitudinal force $M_{Fx}$ is significantly smaller than the other force components indicating that the amplification in the longitudinal force is small under lateral excitation. The peak $M_{Fx}$, however, occurs in the vicinity of the resonant frequency as observed for $M_{Fy}$, while the peak magnitude and

the corresponding frequency tend to increase with the excitation magnitude. A sharp increase in longitudinal force is observed when the excitation approaches the natural frequency, suggesting the presence of 3D swirling motion. The results also show that the maximum force developed in the longitudinal direction is less than 13% of the liquid weight for the given excitations. The results also suggest that the slosh behaves in the two-dimensional manner when the excitation is away from the resonant frequency.

The swirling of the free surface under excitations in the vicinity of the fundamental frequency was clearly observed during the experiments. The swirling motion can also be observed from the time histories of the measured forces. As an example, Figure 2.11 illustrates the time histories of the measured slosh forces under 1 m/s$^2$ lateral acceleration excitation at 1 Hz (i.e. at resonance). The results suggest that the lateral and vertical force components have approached their respective nearly steady state, when the data acquisition was initiated. The magnitude of the longitudinal force component is almost negligible for the initial duration ($t \leq 8$ s), and approaches a relatively higher magnitude thereafter. The increase in the longitudinal force magnitude after a time lag is attributed to the swirling motion of the free surface in the $x$-$y$ plane, which was visually observed during the experiments. Such 3D flows also cause variations in the magnitudes of vertical and lateral forces, as seen in the figure. The oscillations in the lateral and longitudinal forces exhibit considerable distortion of the harmonic shape, which can be attributed to the large-amplitude slosh. The oscillations in $F_x$ and $F_y$ seem to be symmetric about the zero mean force. The variations in the vertical force, however, are asymmetric. The magnitude of vertical force along the downward direction (positive) is greater than that along the upward direction (negative). This asymmetric behavior is due to fluid inertia

effect, which tends to be greater under large magnitude slosh. The variations in magnitudes of $F_y$ and $F_z$ with that of $F_x$ suggest the presence of strong coupling among the three force components.

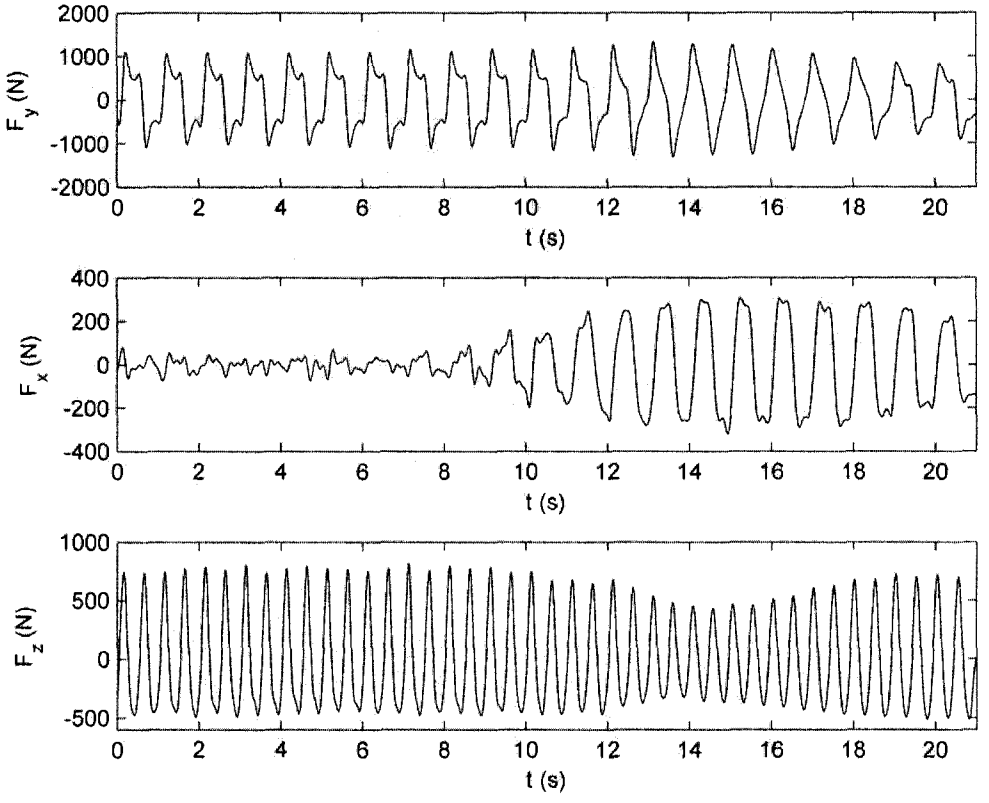


Figure 2.11: Time-histories of slosh force components developed in the 50%-filled cleanbore tank subjected to 1 m/s$^2$ lateral acceleration excitation at 1 Hz.

The roll and pitch moments amplification factors, illustrated in Figure 2.10 show the trend similar to those of lateral and longitudinal forces, respectively. The maxima of normalized roll and pitch moments are 7.5 and 3.4, respectively, at the excitation magnitude of 0.5 m/s$^2$ occurring near the resonance. Figure 2.10*f* shows that the yaw

moment due to fluid slosh also reaches the peak near the resonance, which is attributed to the swirling fluid motion in the vicinity of the resonance. The peak of the normalized yaw moment approaches 1.7 at the excitation magnitude of 0.5 m/s$^2$, occurring at the resonant frequency.

The influence of excitation magnitudes on the peak lateral fluid slosh forces and roll moments are further evaluated for all the tank configurations with 30%, 50% and 70% fill volumes. Figure 2.12 illustrates the peak amplification factors in lateral force and roll moment under different magnitudes of lateral acceleration excitation. It should be noted that the peak responses were attained in the vicinity of the lateral mode resonance. The results show that 30% fill volume yields the highest values of $M_{Fy}$ and $M_{Mx}$, while these factors are the lowest for 70% fill volume, irrespective of the excitation magnitude and tank configuration. The results also show that for a given fill volume, $M_{Fy}$ and $M_{Mx}$ decreased with an increase in the acceleration excitation magnitude. The peak vertical slosh force and roll moment tend to be the largest under 50% fill volume and lowest for 30% fill volume, when fluid mass effect is taken into account. A few studies on rectangular and cylindrical tanks have also concluded that the largest slosh forces occur in the proximity of 50%-fill condition [35, 36]. The figure further shows a larger amplification factor in roll moment than in the lateral force, especially under lower fill volume. For example at 30% fill volume, $M_{Mx}$ is nearly three times the $M_{Fy}$ for all the excitation magnitudes considered. This can be attributed to the fact that not only lateral force but also the load shift caused by liquid cg oscillation and the vertical slosh force contribute to the total roll moment. It was, however, observed that the peak values of vertical and longitudinal force amplification factors ( $M_{Fz}$ and $M_{Fx}$ ) increased with in the

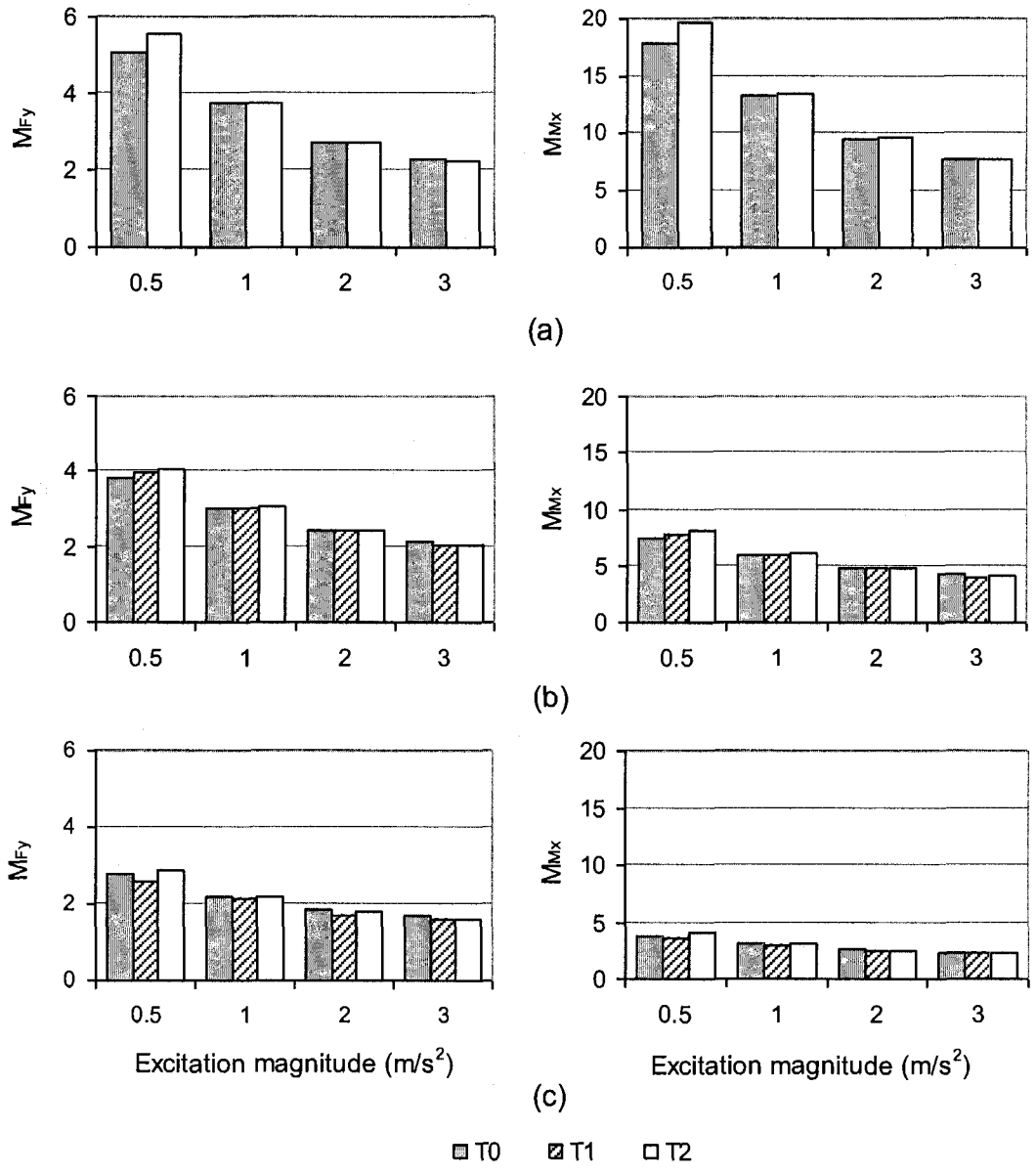


Figure 2.12: Variations in peak amplification factors of lateral force ($M_{Fy}$) and roll moment ($M_{Mx}$) with the lateral acceleration excitation magnitude for all the tank configurations: (a) 30%; (b) 50%; (c) 70% fill volume.

acceleration excitation magnitude, irrespective of the fill volume and tank configuration, as illustrated in Figure 2.13. The figure shows the variation of peak amplification factors of longitudinal and vertical slosh forces with the acceleration excitation magnitude for all the tank configurations at the 50% fill volume. This is attributed to the normalization with respect to $mg$ which is constant (Equation (2.8)), whereas the lateral slosh force is normalized by $ma_y$ which is dependent upon the acceleration magnitude (Equation (2.7)). This thus indicates that the absolute magnitudes of peak fluid slosh forces increase with the acceleration magnitude.

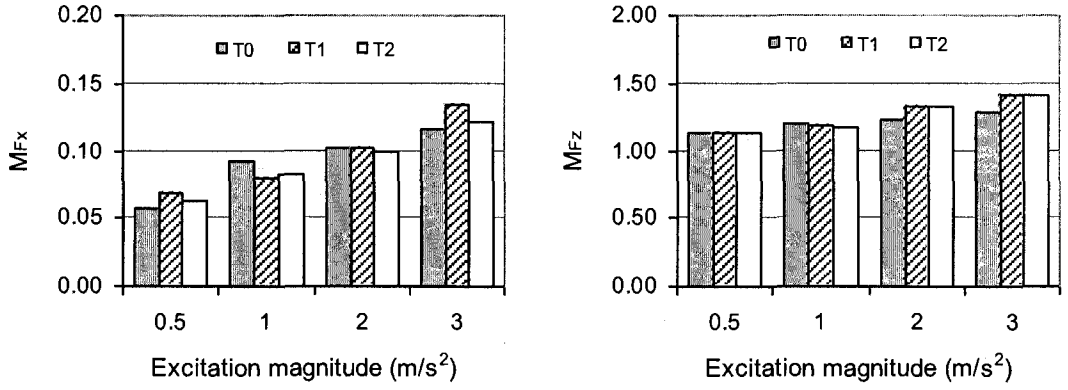


Figure 2.13: Variations of peak amplification factors of longitudinal ($M_{Fx}$) and vertical ($M_{Fz}$) slosh forces with the acceleration excitation magnitude for all the three tank configurations at the 50% fill volume.

The maxima of the normalized longitudinal and vertical slosh forces as well as pitch and yaw moments for given lateral harmonic excitations are presented in Figure 2.14 for all the fill volumes and tank configurations. The maxima generally occurred in the vicinity of the respective fundamental slosh frequency, irrespective of the excitation magnitude. The results show that the peak forces and moments vary with the fill level in

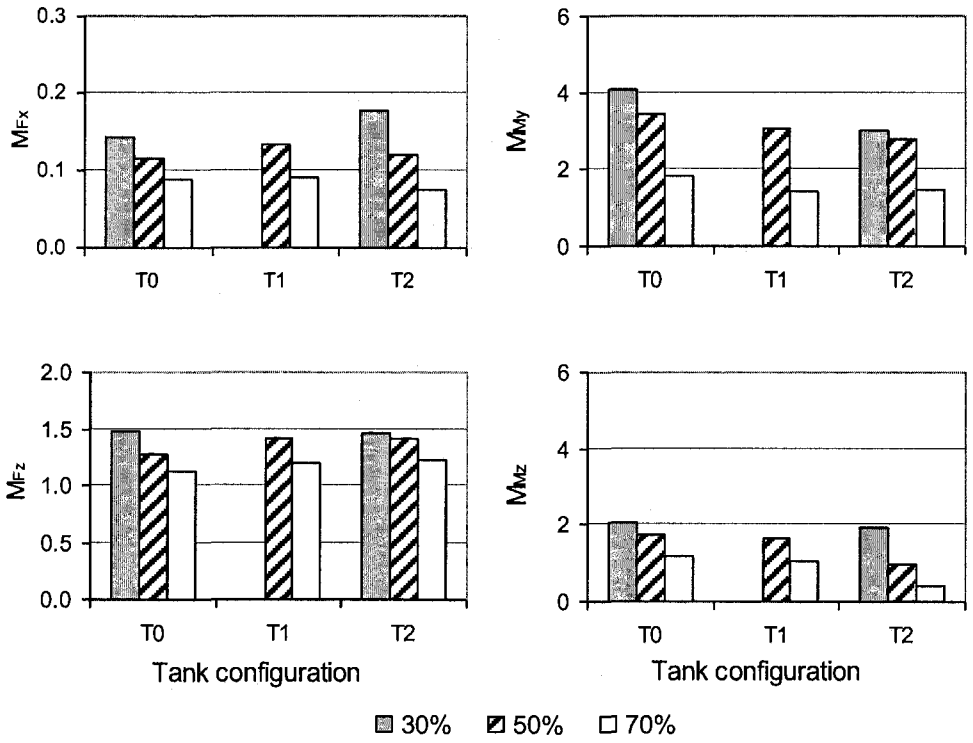


Figure 2.14: Peak amplification factors of longitudinal ($M_{Fx}$) and vertical ($M_{Fz}$) slosh forces, and pitch ($M_{My}$) and yaw ($M_{Mz}$) moments due to fluid slosh in the selected tank configurations and fill volumes.

a manner similar to that observed for lateral force and roll moment (Figure 2.12). The results also suggest a considerably larger amplification factor in pitch moment than in the longitudinal force. The peak normalized longitudinal forces developed in both baffled and un-baffled tanks occur under 30% fill volume, but remain well below 0.2 for the given experimental conditions. The peak normalized pitch moment, however, approached as high as 4. This is attributed to the fact that the peak moment is mostly caused by the longitudinal load shift, which tends to be higher due to fluid swirl. The results also show that the baffled tanks yield lower normalized pitch moment ($M_{My}$) than the cleanbore tank, suggesting that the baffles help to suppress the longitudinal load shift. The results further show considerably smaller peak normalized vertical forces, where the effect of

baffles is relatively small. The peak yaw moment is also considerably smaller than the pitch moment.

### 2.4.2 Longitudinal Harmonic Excitations

Figure 2.15 shows the amplification factors in longitudinal and lateral slosh forces, and pitch moment for the 50%-filled un-baffled ('T0') and baffled ('T2') tanks subjected to longitudinal harmonic excitations of different frequencies and magnitudes. The results reveal that the peak normalized longitudinal force ($M_{Fx}$) occurs in the vicinity of the longitudinal mode natural frequencies (i.e. 0.45 Hz and 1.08 Hz, for the un-baffled and baffled tanks, respectively). However, the baffled tank ('T2') yields considerably lower peak force than the un-baffled tank ('T0'), suggesting that the baffles could effectively suppress longitudinal slosh. The results show that the peak longitudinal force tends to decrease as the excitation magnitude increases for the un-baffled tank, as it was observed for $M_{Fy}$ under lateral harmonic excitations. This trend, however, is not evident for the baffled tank in Figure 2.15*b*. These results suggest that the longitudinal slosh force magnitude is nearly linearly dependent on the acceleration magnitude for the baffled tanks, particularly with the multiple-orifice baffles. It was also observed that a higher fill volume yields relatively larger variations in the peak longitudinal slosh force, particularly for the 'T1' tank, where the single orifice baffles permit greater flows across the baffles. The results also show that the magnitudes of $M_{Fx}$ tend to be less than unity, when the excitation frequency is larger than the resonant frequency for both the baffled and un-baffled tanks.

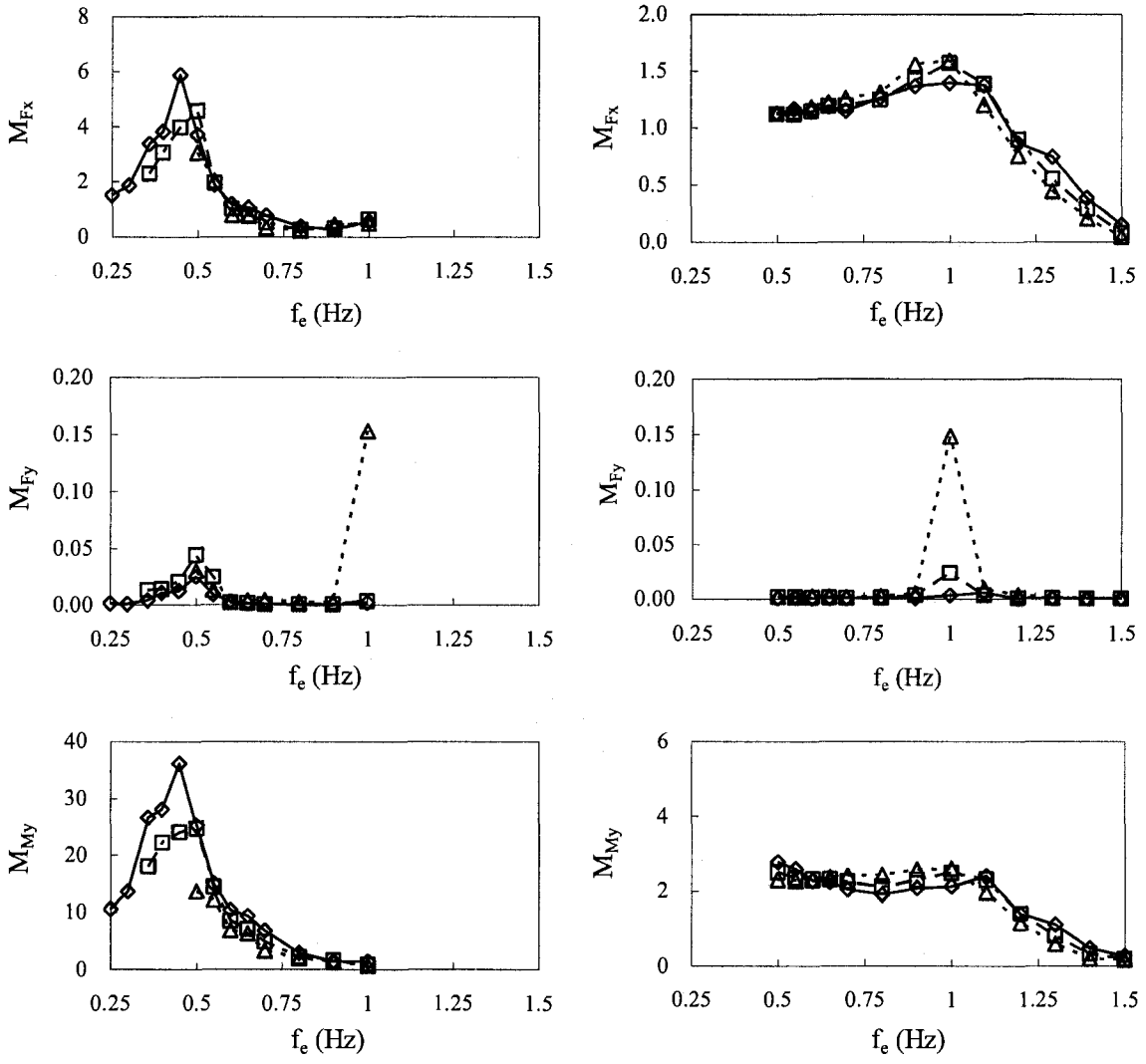


Figure 2.15: Variation of peak amplification factors of longitudinal and lateral forces, and pitch moment with the excitation frequency for the 50% filled tanks (a) 'T0' tank, and (b) 'T2' tank (◊, = 0.25 m/s$^2$; □, = 0.5 m/s$^2$; Δ, = 1 m/s$^2$).

The variations in lateral force amplification factor suggest that the peak lateral force occurs in the vicinity of the longitudinal mode resonant frequency, irrespective of the excitation magnitude for both the un-baffled and baffled tanks. The largest peak value approaches 0.15 for both the tanks, suggesting that the peak lateral force is approximately 15% of the liquid weight. This suggests the presence of coupling between the longitudinal and lateral motions of the fluid, as discussed in the previous section. For the baffled tank, the fundamental lateral mode resonant frequency is quite close to the lateral mode resonance ($\approx$1.08 Hz). Very little variations in the normalized vertical force $M_{Fz}$ were observed under longitudinal excitations for all the tank configurations and fill volumes considered.

The peak amplification factors in longitudinal force and pitch moment at different longitudinal excitation magnitudes are plotted in Figure 2.16 for all the fill volumes and tank configurations. It should be noted that the peak forces developed in the 30% filled un-baffled tank could not be derived under the excitation magnitude of 1 m/s$^2$, since the lowest excitation frequency was limited to 0.5 Hz, which was well above the resonant frequency of 0.36 Hz (see Table 2.2). The results thus show relatively lower $M_{Fx}$ for the un-baffled tank under 30% fill condition.

Similar to the longitudinal force, the baffles greatly suppress the peak pitch moment caused by fluid slosh. Figure 2.15 shows that the peak values of $M_{My}$ due to fluid motion in 'T0' tank are significantly greater than those for 'T2' tank, irrespective of the excitation magnitude. This is attributed to greater longitudinal load shift in 'T0' tank under a longitudinal excitation, which tends to be largest under lower fill volume of 30%

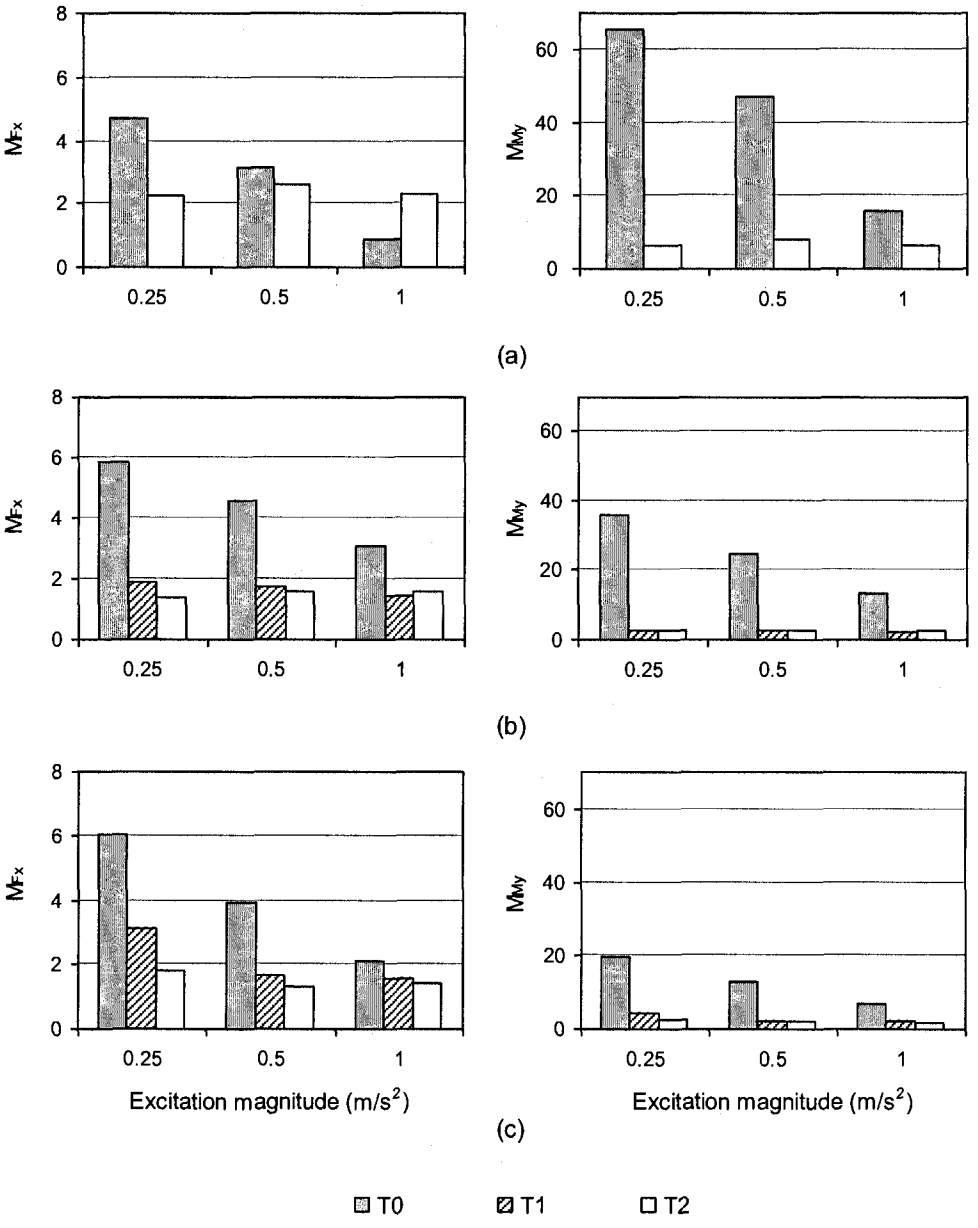


Figure 2.16: Variation of peak amplification factors of longitudinal slosh force and pitch moment with the excitation magnitude for three tank configurations under longitudinal acceleration excitations: (a) 30%; (b) 50%; (c) 70% fill volume.

(see Figure 2.16*a*). The baffled 'T2' tank yields nearly constant magnitude of $M_{My}$ at frequencies up to 1.1 Hz, irrespective of the excitation magnitude, which is mostly caused by relatively small load shifts in the 'T2' tank. The magnitudes of $M_{My}$, however, decrease rapidly at frequencies greater than the respective resonant frequencies for both tanks. The single-orifice baffle tank also reveals similar degree of effectiveness in suppressing the peak magnitude of $M_{My}$, as evident in Figures 2.16*a* and *c* for the 50%- and 70%-fill volumes, respectively. The results for the 70%-filled tank clearly show that multiple-orifice baffles provide relatively greater benefit in suppression of longitudinal slosh force and pitch moment.

Figure 2.17 presents the maxima of the normalized roll and yaw moments for given longitudinal harmonic excitations for all the fill volumes and tank configurations. The results show that the $M_{Mx}$ and $M_{Mz}$ decrease as the fill volume increases, irrespective of the tank configuration, which is consistent with the trends observed under lateral acceleration excitations. The higher longitudinal load shift coupled with greater swirling motion of the fluid in 'T0' tank results in significantly larger yaw moment amplification ($M_{Mz}$). The magnitude of $M_{Mz}$, however, tends to be significantly lower for both the baffled tanks, irrespective of the fill volume. These results indicate that the baffles also help in suppressing the roll and yaw moments under longitudinal excitations. For the 50% fill volume, the roll and yaw moments developed by fluid slosh in the baffled 'T2' tank are 65.7% and 49.6% lower than those generated in the un-baffled 'T0' tank, respectively.

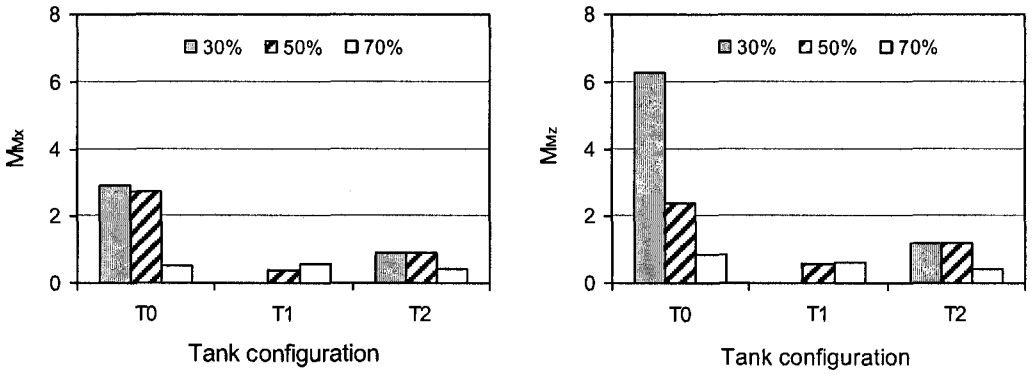


Figure 2.17: Peak amplification factors of roll and yaw moments versus tank configurations for three fill volumes subjected to longitudinal acceleration excitations.

### 2.4.3 Lateral Single-cycle Sinusoid Excitations

As described in section 2.2, the single cycle sinusoid excitation along the lateral axis were performed to study the transient slosh in partly filled tank vehicles under motions caused by a lane change type of maneuver. Figure 2.18 shows the transient peak normalized lateral and vertical slosh forces for all the tank configurations and fill volumes subject to the lateral single-cycle sinusoidal excitations. Two cases are considered, one with the peak acceleration of 1.9 m/s$^2$ at 1 Hz (Figure 2.18*a*) and the other with the peak acceleration of 4.3 m/s$^2$ at 1.5 Hz (Figure 2.18*b*). The corresponding amplification factors in roll, pitch and yaw moments ($M_{Mx}$, $M_{My}$ and $M_{Mz}$) are illustrated in Figure 2.19. It should be noted that the former excitation is in the vicinity of the lateral mode resonance for the 50%-filled tank. The results show negligible effect of tank

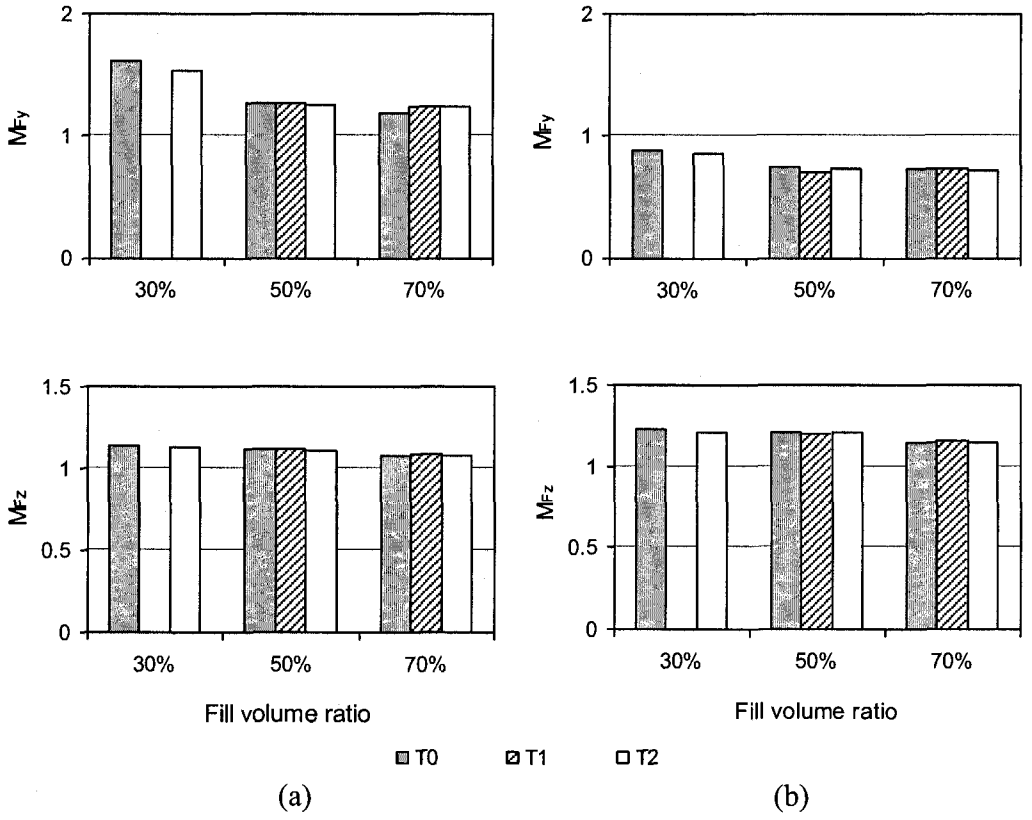


Figure 2.18: Peak amplification factors of lateral and vertical slosh forces versus the fill volume for the three tank configurations subjected to single-cycle lateral acceleration excitations: (a) 1.9 m/s$^2$ at 1 Hz; (b) 4.3 m/s$^2$ at 1.5 Hz.

configuration and fill volume on the peak value of $M_{Fz}$ under both excitations. The variations in $M_{Fx}$ (not shown here) were also found to be negligible suggesting that the liquid slosh is a two-dimensional motion of the free surface under these conditions. The peak $M_{Fy}$, however, tends to be higher under the 1 Hz excitation, which is close to the fundamental lateral mode resonance. The magnitude of $M_{Fy}$ under the 1 Hz excitation is significantly higher than that under the 1.5 Hz excitation, irrespective of the fill volume. The peak magnitude of $M_{Fy}$ under the higher frequency excitation (1.5 Hz) is less than

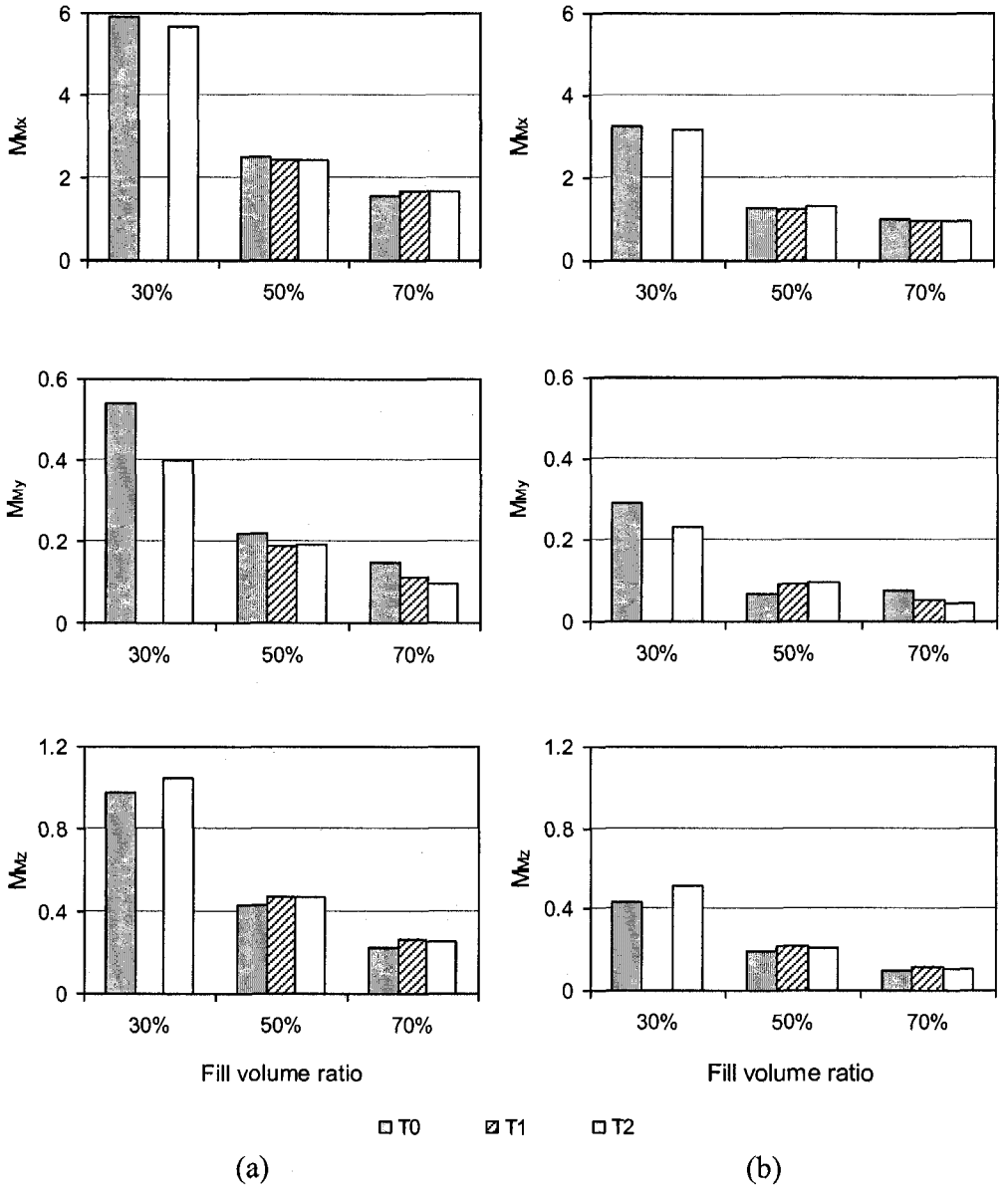


Figure 2.19: Peak amplification factors of roll, pitch and yaw moments versus the fill volume for three tank configurations subjected to single-cycle lateral acceleration excitations: (a) 1.9 m/s$^2$ at 1 Hz; (b) 4.3 m/s$^2$ at 1.5 Hz.

unity. Furthermore, the 30% fill volume yields slightly higher peak values of $M_{Fy}$, as it was observed under lateral harmonic excitation (Figure 2.12). The amplification in roll moment, $M_{Mx}$, however, is considerably large for the 30% fill volume under both excitations, while the contribution of baffles is very small. The magnitudes of $M_{My}$ and $M_{Mz}$ are also relatively small but tend to be higher for the 30% fill volume. These trends are comparable with those obtained under lateral harmonic excitations.

## 2.5 SUMMARY

Liquid slosh in a scaled tank with cross-section similar to a 'Reuleaux triangle' has been investigated in the laboratory for un-baffled and baffled configurations under three different fill conditions. The experiments involved the analyses of slosh frequencies, forces and moments under lateral and longitudinal acceleration excitations of different magnitudes and frequencies. The results have shown that the slosh is a complex phenomenon, containing a number of frequency contents. Predominant peak in the spectrum of a slosh force component may occur in the vicinity of the excitation frequency, natural frequency or the vibration frequency. The lateral and longitudinal force components generally oscillate at a frequency close to the excitation or the natural frequency, whereas, the oscillations in the vertical force invariably occur at a frequency twice the excitation or natural frequency. The spectra of force components also show the presence of beating frequency, when the excitation frequency is close to the natural frequency of slosh, which is more evident under lower excitation magnitudes.

The fundamental frequencies of fluid slosh estimated from the spectra of the dominant force component under free oscillation, agreed reasonably well with those

estimated using the reported analytical method based upon wave length and wave speed of the free surface [31]. The fundamental natural frequency of slosh was observed to be dependent on the fill level and the tank configuration. This frequency, in both lateral and longitudinal modes, increased with the fill level for all three tank configurations considered. The addition of transverse baffles caused a significant increase in the longitudinal mode natural frequency, while the lateral mode frequency was not affected by the baffles. For the 50% fill volume, the longitudinal mode frequency increased from 0.45 Hz for the un-baffled tank to 1.08 Hz for the baffled tanks.

The measured data and flow visualization revealed the three-dimensional nature of the fluid motion under excitations along either lateral or longitudinal axis of the tank for both baffled and un-baffled configurations, which suggests a coupling between the lateral and longitudinal fluid slosh. The peak slosh forces and moments generally occurred in the vicinity of slosh natural frequency in the respective mode, which was manifested under continuous as well as single-cycle sinusoidal excitations. The dynamic slosh could yield largely amplified resulting forces and moments near the resonance, when compared to those of the equivalent rigid mass. The slosh amplification factors in lateral and longitudinal forces under respective excitations, however, decreased as the fill level or excitation magnitude increased. The slosh amplification effect was reflected more significantly in roll and pitch moments than in the forces. The amplification factors in both longitudinal and lateral forces at an excitation frequency above the resonant frequencies are generally below unity, which suggests that the magnitude of fluid slosh force is less than the inertial force developed by an equivalent rigid mass subject to the same excitation. The transient lateral slosh measured under single-cycle lateral

acceleration excitation revealed predominantly two-dimensional motion of the free surface for all tank configurations considered.

The peak magnitudes of longitudinal slosh force and pitch moment developed under a longitudinal acceleration excitation decreased significantly in the presence of lateral baffles. This was clearly evident for both single-orifice and multiple-orifice baffles, although multiple-orifice baffles resulted in slightly greater reductions in peak force and moment. The baffles also helped to reduce the magnitudes of corresponding pitch moment. The addition of lateral baffles, however, did not affect the peak magnitudes of lateral slosh force or roll moment under lateral acceleration excitations.

# CHAPTER 3

# MODELING OF THREE-DIMENSIONAL FLUID SLOSH AND VALIDATION

## 3.1 INTRODUCTION

As the literature review in Chapter 1 indicates, the CFD simulation incorporating the VOF technique is the most effective approach for predicting fluid slosh in tanks. Most of the previous studies on fluid slosh within tanks have been considered two-dimensional (2-D) flows [32, 57, 77, 136, 137]. When a tank is excited at a frequency near the resonance, the swirling motion may be induced and superimposed on the normal slosh motion [24], which cannot be adequately captured by the 2-D model. The laboratory experiments performed on a scale model tank have clearly shown the presence of 3-D fluid slosh even under excitations along a single axis (Chapter 2). Moreover, highway tanks commonly encounter simultaneous excitations along all axes, which would cause 3-D slosh. Only a few studies [57, 135] have reported the 3-D slosh analysis for very limited parameters. Thus, the 3-D slosh behavior in tanks has not been well understood.

In this Chapter, a 3-D CFD slosh model is established using the FLUENT software package. In view of the limitations of the previous studies, the model has been systematically verified for the three-dimensional water slosh in a cleanbore tank and two baffled tanks. The validation was extensively performed against the experimental results for three different fill volumes and various excitations. The three components of fluid slosh forces and moments, which are significant for the analysis of vehicle stability, are

examined. Moreover, the slosh natural frequency is also evaluated for the validity of the model.

## 3.2 CFD SLOSH MODELING

The fluids contained in a partially-filled tank, can be regarded as a two-phase (gas-liquid) flow with identical or different species. The density of the two fluids is largely different. Taking the air-water mixture as an example, the density of water is approximately 815 times that of air. In such flows, the inertial forces are dominant relative to the viscous force and the viscous effect could be negligible [139]. Majority of the previous slosh analyses have thus been made in the scope of laminar flows. The turbulence effect has been considered in only a few applications of VOF model [137,138]. With the applications in the slosh analysis, Armenio and La Rocca [137] are probably the only researchers that have taken turbulence into account. A SubGrid Scale turbulence model was used in solving the Novier-Stokes equations, coupled with the Semi-Implicit Marker and Cell method (SIMAC), an earlier version of VOF model. In order to obtain the high resolution required for turbulence, a fine boundary layer was treated near the wall, while the effects of the turbulence model were not discussed.

In this dissertation research, a laminar flow is assumed since the fluid slosh under typical directional maneuvers occurs at low velocities. The flow is considered to comprise of two fluids: air as the gas phase fluid and water as the liquid phase fluid. In the model, air is regarded as the primary phase and water as the secondary phase. The liquid flow is described by the unsteady incompressible continuity and Navier-Stokes (N.S.) momentum equations:

$$\nabla \cdot \vec{u} = 0 \tag{3.1}$$

$$\rho\left(\frac{\partial \vec{u}}{\partial t} + (\vec{u} \cdot \nabla)\vec{u}\right) = -\nabla p + \mu \nabla^2 \vec{u} + \vec{f} \tag{3.2}$$

where "$\nabla$" is the gradient operator; "$\nabla \cdot$" is the divergence operator; "$\nabla^2$" is the Laplace operator; $p$ is the pressure; $\rho$ is the density of fluid; $\mu$ is the fluid viscosity; $\vec{u}$ is the velocity vector and $\vec{f}$ is the body force vector representing the forces arising from accelerations due to gravity and external disturbances, such as vehicle maneuvers, such that:

$$\vec{f} = \rho\vec{g} + \rho\vec{a} \tag{3.3}$$

where $\vec{g}$ is the acceleration due to gravity and $\vec{a}$ is the acceleration attributed to a vehicle maneuver. For example, a lane change maneuver may be idealized by a single-cycle sinusoidal acceleration input, while a ramp-step function can represent a steady turning or a breaking input. These acceleration functions are incorporated into the governing momentum equation, Equation (3.2), by the user-defined momentum source function.

The air-water interface is tracked by solving the volume fraction equation:

$$\frac{\partial F}{\partial t} + \nabla \cdot (\vec{u}F) = 0 \tag{3.4}$$

where $F$ is the volume fraction function. In the computation domain, the unity value of $F$ is assigned as unity for all grid cells completely occupied by the liquid, while zero value is assigned for all grid cells completely occupied by the gas. The grid cells partially occupied by water assume values of $F$ ranging from zero to one, depending on the

fractions of both fluids in the cells. The gas-liquid interface is thus determined by the cells with $F$ values lying between zero and unity.

Although the flow was treated as a two phase flow, only one set of the governing equations, Equations (3.1) and (3.2), coupled with the volume fraction equation (Equation (3.4)), are solved [151]. The fluid properties, such as density and viscosity, for different phase fluids in the N.S. equations are determined by the evolution of volume fraction for a grid cell. For example, since the liquid phase is the interest of tracking, the liquid density in each cell can be determined by a general expression:

$$\phi = F_2\phi_2 + (1-F_2)\phi_1, \quad (\phi = \rho \text{ or } \mu) \tag{3.5}$$

where $\phi_1$ and $\phi_2$ indicate the densities or viscosities of air and water, respectively. $F_2$ is the value of volume fraction of the liquid phase for a cell.

The above modeling was realized using the FLUENT 6.2.16 software package. The software uses the finite volume method to discretize the integral form of the governing equations, Equations (3.1) and (3.2). In the present modeling, the segregated solver was activated, so the governing equations could be solved sequentially. The flow equations are solved based on the pressure correction and pressure-velocity coupling technique, Pressure-Implicit with Splitting of Operators (PISO) [140]. This scheme requires dramatically less number of iterations to reach convergence, particularly for the transient flow. The first order upwind scheme was chosen for the spatial discretization because the second order scheme resulted in a poor convergence. Considering the large body forces involved in the two-phase flow, the body-force-weighted scheme was adopted for the pressure interpolation. Due to the large body forces arising from the liquid, the body force and pressure gradient terms in the momentum equation are in near

equilibrium, while the contributions of convective and viscous terms are small. In this situation, the segregated algorithm yields poor convergence [151]. The implicit body force treatment was thus used to achieve the partial equilibrium of pressure gradient and body forces, and obtain a good convergence. The first order implicit scheme was chosen for the temporal discretization, since the higher order schemes were not available for the multi-phase models in the FLUENT software. No slip condition was selected for all the tank walls.

The geometric reconstruction (Geo-Reconstruct) scheme was used for the calculation of face fluxes near the interface between two fluids for the VOF model. The Geo-Reconstruct scheme is a special interpolation treatment to the cells that lie near the interface between two phases. The scheme assumes that the interface has a linear slope within each cell, and uses this linear shape for the calculation of fluid advection through the cell faces in the vicinity of the interface [151]. A smooth interface shape could be formed using this interpolation scheme, even for an unstructured grid.

Since the FLUENT software uses the gauge pressure in the calculations, the location of reference pressure is very important. It should be kept constant and not be interfered during the calculations. In the present two phase VOF application, the reference pressure is located in the lighter air phase within the tank ceiling. High magnitude spikes in forces were observed in case of severe slosh due to the interference of the reference pressure by the liquid phase fluid. In order to avoid this disturbance, a small tube was added to the tank at the top and the reference pressure location was shifted into the tube.

Since the FLUENT software does not give the output of the parameters of interest, namely the instantaneous coordinates of liquid centre of gravity (*cg*), slosh forces and resulting moments; these were calculated at each instant using the user defined functions (UDF). Figure 3.1 shows the coordinate system used for the calculation of these parameters, together with a perspective view of the baffled tanks considered for the analysis of fluid slosh.

The slosh force components, $F_y$ (lateral), $F_x$ (longitudinal) and $F_z$ (vertical), can be derived from the integration of the pressure over the liquid wetted wall and baffle boundaries, such that:

$$F_y(t) = \sum_{\partial\Omega} (P_i \vec{A}_{yi}) \tag{3.6}$$

$$F_x(t) = \sum_{\partial\Omega} (P_i \vec{A}_{xi}) \tag{3.7}$$

$$F_z(t) = \sum_{\partial\Omega} (P_i \vec{A}_{zi}) \tag{3.8}$$

where $P_i$, is the pressure at the $i^{th}$ face centroid in the wall zones, $\vec{A}_i$, is the area vector of the $i^{th}$ face in the wall zones, and $\partial\Omega$ is the domain of liquid-wetted faces on the wall boundary.

The roll ($M_x$), pitch ($M_y$) and yaw ($M_z$) moments can be derived from the integration of product of force vectors and the position vectors from the reference origin, that is,

$$M_x(t) = \sum_{\partial\Omega} \vec{F}_{zi} Y_{fi} - \sum_{\partial\Omega} \vec{F}_{yi} Z_{fi} \tag{3.9}$$

$$M_y(t) = \sum_{\partial\Omega} \vec{F}_{xi} Z_{fi} - \sum_{\partial\Omega} \vec{F}_{zi} X_{fi} \tag{3.10}$$

$$M_z(t) = \sum_{\partial\Omega} \vec{F}_{yi} X_{fi} - \sum_{\partial\Omega} \vec{F}_{xi} Y_{fi} \tag{3.11}$$

where $Y_{fi}$, $X_{fi}$ and $Z_{fi}$ are the lateral, longitudinal and vertical coordinates of the centroid of the $i^{th}$ face cell along the liquid wetted wall and baffle boundaries, respectively. $\vec{F}_{yi}$, $\vec{F}_{xi}$ and $\vec{F}_{zi}$ are the lateral, longitudinal and vertical force components acting on the the $i^{th}$ face on the liquid wetted wall and baffle boundaries, respectively. These force components are equal to the product of the local pressure and the face area.

## 3.3 ANALYSIS METHODS

The CFD model is derived for the tanks that are the same as the test tank employed in the laboratory experiments, namely the cleanbore ('T0') and baffled ('T1' and 'T2') tanks. The model simulations are performed under different fill and excitation conditions considered for the experiments. The validity of the model is examined by comparing the slosh natural frequency and the slosh forces and moments predicted by the model with those obtained from the experiments for different tank configurations with different fill levels and excitations. Figure 3.2 illustrates the tank configurations with single- and multiple-orifice baffles, which are notated as 'T1' and 'T2' tanks, respectively. The geometries of the tank and baffles are identical to those described in Chapter 2.

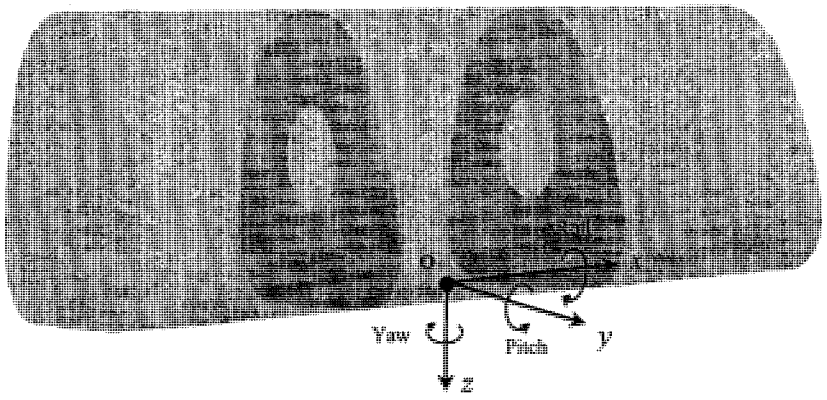


(a)

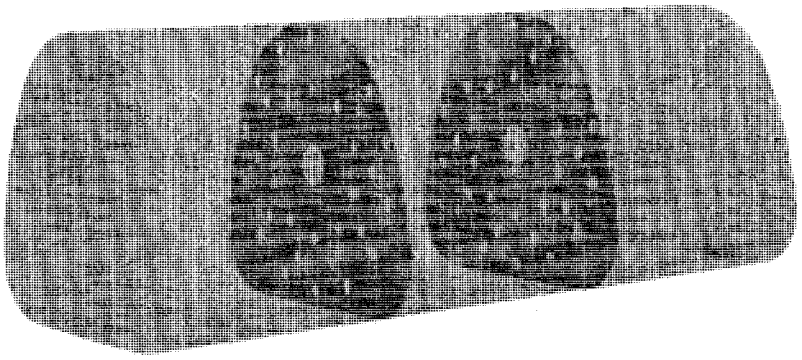

(b)

Figure 3.1: The perspective views of the baffled tanks: (a) 'T1'; (b) 'T2'. The reference coordinate system (*xyz*) used for the calculations of simulation parameters originates at the geometry centre of tank bottom.

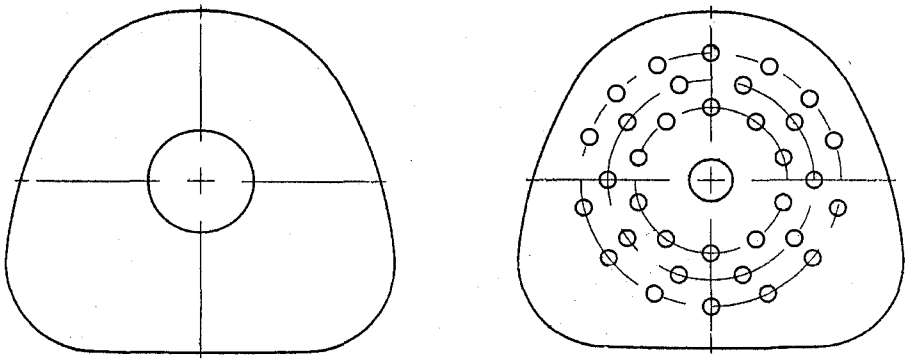


Figure 3.2: The baffles considered in the simulations: (a) single-orifice baffle ; (b) multiple-orifice baffle .

The simulations are performed under excitations that were employed in the experimental study, namely, the single-cycle sinusoidal, idealized ramp-step and the harmonic acceleration inputs. The first two were used for the verification of the transient slosh flows, while the last one was used for the validation of the flow in the steady state. The simulation matrices are summarized in Tables 3.1 and 3.2. The single-cycle sinusoidal excitations, as shown in Figure 2.3, were applied to tank 'T1' in the lateral direction. The simulations for tank 'T2' were not performed under these excitations since the experiment results showed very similar responses of both that the two types of transverse baffles. The ramp-step excitations are idealized by piecewise exponential functions, as illustrated in Figure 3.3, which were applied along the longitudinal direction in both baffled and unbaffled tanks. For the lateral harmonic excitations, the simulations were conducted under excitations at different frequencies ranging from 0.6 Hz to 1.5 Hz at two acceleration magnitudes: $1 m/s^2$ and $2 m/s^2$. The simulations for tank 'T2' were limited to excitations at resonant frequencies alone due to requirement of finer mesh. Table 3.3 summarizes the simulation matrix corresponding to longitudinal harmonic

excitations at various resonant frequencies. It should be noted that the simulations for the 30%-fill 'T1' tank were omitted, for the reasons described in Chapter 2.

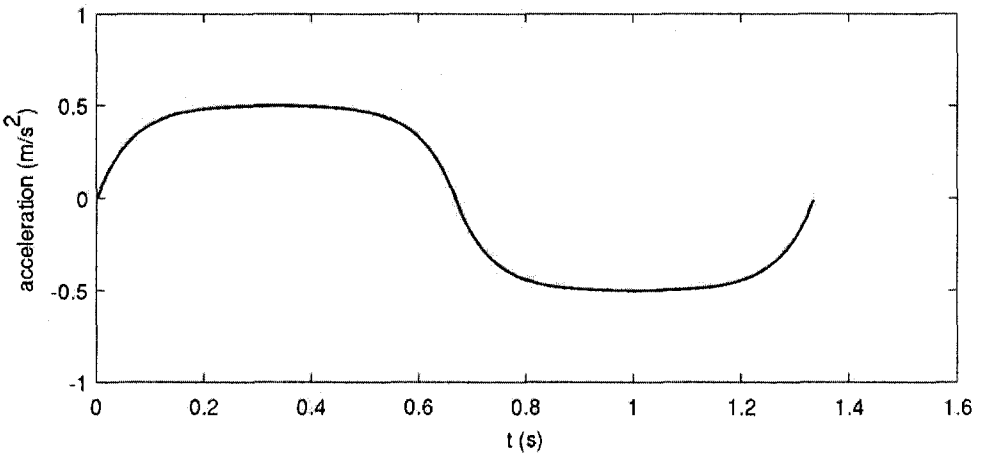


Figure 3.3: The idealized ramp-step excitation utilized for the evaluation of transient slosh simulations in the longitudinal direction.

Table 3.1: The simulation matrix for the tanks subjected to the single-cycle sinusoidal (in lateral direction) and idealized ramp-step excitations (in longitudinal direction).

| Excitation direction | $A$ (m/s$^2$) | $f$(Hz) | Tank & fill volume |
|---|---|---|---|
| lateral | 1.93 | 1 | 'T0' (30%) |
| | 4.34 | 1.5 | 'T1' (50%, 70%) |
| longitudinal | 0.5 | 0.75 | 'T0'&'T2' (30%, 50%, 70%) |
| | 0.89 | 1 | 'T1' (50%, 70%) |

Table 3.2: The simulation matrix for tanks 'T0' and 'T1' at 50% and 70% fill volumes subjected to the lateral harmonic excitation.

| $A$ (m/s$^2$) | $f$(Hz) | | | | | Fill volume |
|---|---|---|---|---|---|---|
| | 0.6 | 0.8 | 1 | 1.2 | 1.5 | |
| 1 | √ | √ | √ | √ | √ | 50% |
| 2 | -- | √ | √ | √ | √ | 50%, 70% |

Table 3.3: The simulation matrix for all three tank configurations at 30%, 50% and 70% fill volumes subjected to the longitudinal harmonic excitation of 1 m/s$^2$ magnitude.

| Tank | Fill volume | f (Hz) |
|---|---|---|
| 'T0' | 30% | 0.36 |
| | 50% | 0.5 |
| | 70% | 0.5 |
| 'T1' & 'T2' | 30% | 0.9 |
| | 50% | 1 |
| | 70% | 1.1 |

The fluid slosh under a linear frequency sweep was simulated for estimating the natural frequencies of fluid slosh within 'T0' and 'T1' tanks with the three fill volumes. Owing to the high computational time, the frequency sweep simulations were not performed for the 'T2' tank configuration. For the lateral direction sweep excitation, the frequency is increased linearly at the rate of 0.025 Hz/s, while a constant acceleration magnitude of 0.5 m/s$^2$ is considered. Considering the differences in the longitudinal mode natural frequencies between the baffled and unbaffled tanks, different swept frequency ranges were selected for the baffled and unbaffled tanks. For the cleanbore tank, the excitation frequency was swept from 0.001 Hz to 2 Hz at the rate of 0.025 Hz/s. For both the baffled tanks, the frequency sweep range was selected identical to that of the lateral direction since their longitudinal mode fundamental frequencies are close to the lateral mode frequencies.

The fluid slosh responses are known to depend greatly on the mesh size, time step and convergence criterion. Systematic simulations were initially performed to assess the dependence of solution on these factors and identify appropriate mesh size, time step, and convergence criterion. Tank 'T2' with small size multiple orifice baffles required a much finer mesh than the other two tanks 'T0' and 'T1'. Due to the complexity of the baffle's pattern, the triangular grid cell was utilized for the cross-section face meshing, as seen in Figure 3.4*b*, which was subsequently extended into the third dimension, i.e., longitudinal direction, to form the volume mesh using the Cooper technique. For tanks 'T0' and 'T1', the same strategy was utilized for the 3D meshing but the quadrilateral grid cell was used for the cross-sectional plane (see Figure 3.4*a*). The resulting mesh sizes were thus much smaller than that of tank 'T2'. Three different grids were evaluated for each tank configuration, as summarized in Table 3.4.

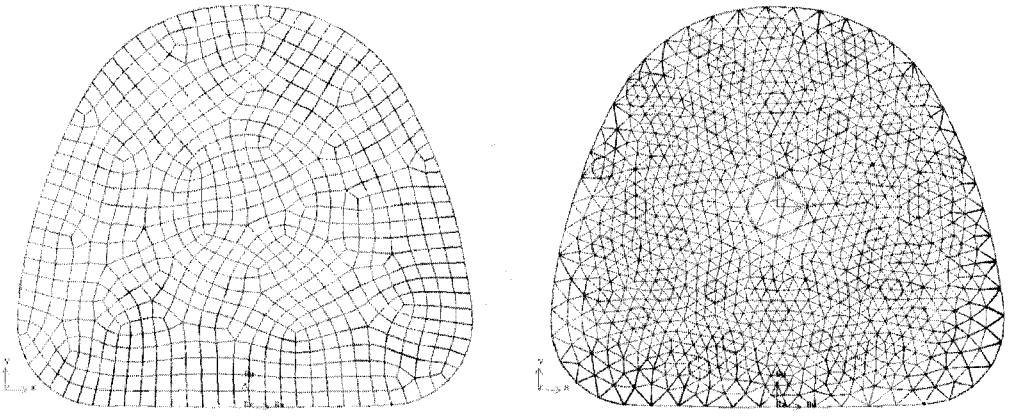

(a) (b)

Figure 3.4: The mesh scenarios applied in the tank cross-section plane. (a) 'T1' tank; (b) 'T2' tank.

Table 3.4: The mesh sizes adopted for assessing the mesh dependence of solutions for different tank configurations.

| Tank | Number of cells | | | Cell shape |
|---|---|---|---|---|
| | Grid I | Grid II | Grid III | |
| 'T0' | 24,800 | 45,414 | 86,800 | Hexahedral |
| 'T1' | 25,170 | 46,201 | 85,398 | Hexahedral |
| 'T2' | 74,232 | 134,604 | 232,876 | Wedge |

Figure 3.5 shows the dependence of the simulation results on the grid size for tank 'T2' with 50% fill volume subjected to the lateral harmonic excitation of 1 Hz, near the lateral mode resonant frequency and magnitude of 1 $m/s^2$. The results show that the three grids yield relatively smaller difference in the resulting lateral force, which the influence is quite significant on the longitudinal force. The finer mesh tends to capture the low frequency variation in the slosh force attributed to the beat phenomenon observed from the experimental data. Comparison of the transient simulation results with the experimental data further confirmed that the finest mesh (Grid III) is most appropriate for fluid slosh analysis for tank 'T2' (see Figures 3.23 and 3.24). For tanks 'T0' and 'T1', from the comparisons of the simulation results with the experimental data, it was deduced that the medium fine Grid II would be appropriate for the selected simulation matrix.

The convergence criterion was assessed for three different residual levels ($10^{-4}$, $10^{-5}$ and $10^{-6}$) for the fluid slosh in the vicinity of the resonance. The results attained with the three residuals showed nearly negligible differences in the slosh forces and moments. The value of $10^{-4}$ was thus considered as the residual tolerance. The converged solution could be obtained with the time step size in the range of 1~4 ms.

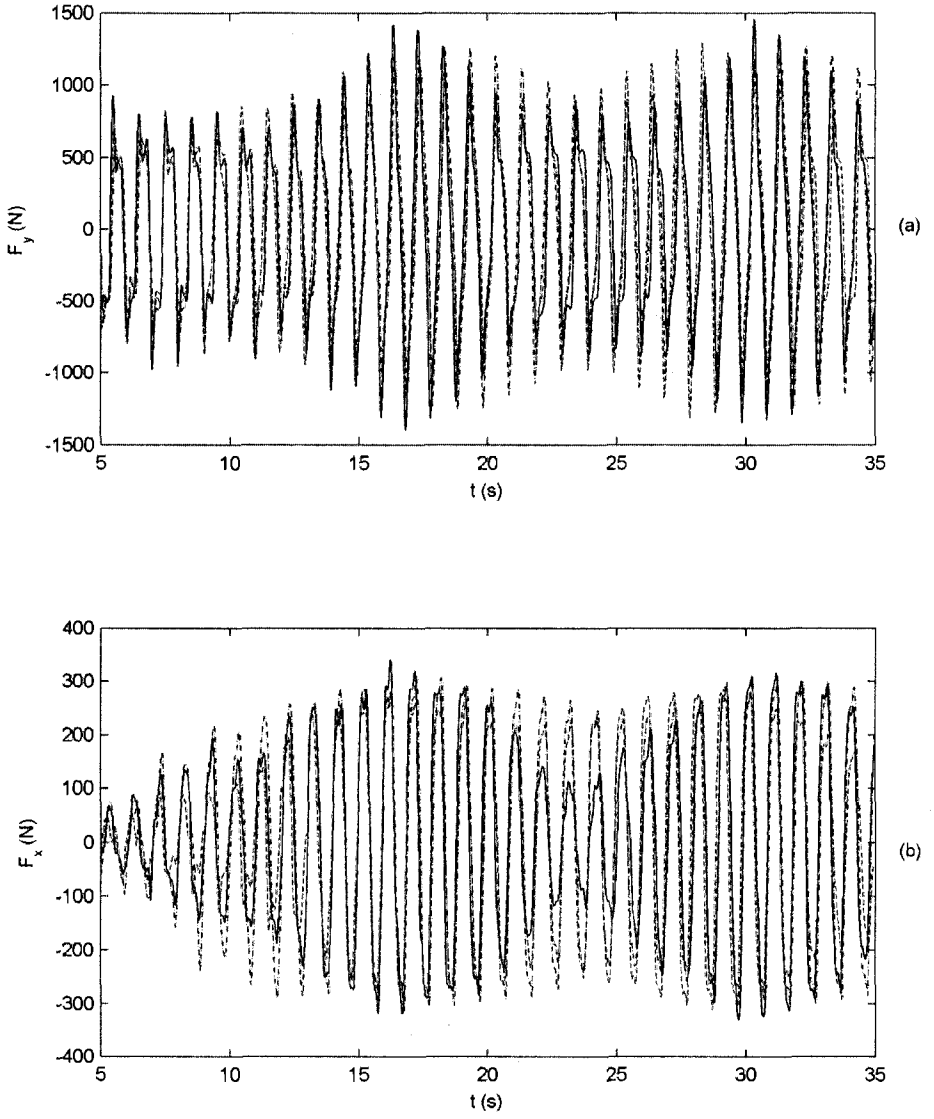


Figure 3.5: The dependence of the simulation results on the grid size for the baffled 'T2' tank with 50% fill volume subjected to 1 m/s$^2$ lateral harmonic excitation at 1 Hz: (a) lateral force; (b) longitudinal force. –·–·–, Grid I; -----, Grid II; ——, Grid III.

## 3.4 MODEL VALIDATIONS

The analyses of the CFD model were performed using the refined mesh size, step size and tolerance for different tank configurations. The results are compared with the experimental data in order to demonstrate the model validity.

### 3.4.1 Slosh Natural Frequency

The natural frequencies of fluid slosh are derived through spectral analysis of the slosh force responses to frequency sweep excitations. The Fast Fourier Transform technique was used to derive the power spectra with a frequency resolution of 0.0305 Hz. The power spectral densities (PSD) of the slosh forces generally revealed a single predominant peak, which was believed to correspond to the fundamental slosh frequency. Figure 3.6 illustrates the typical plot spectra of the lateral forces of tank 'T0' with three different fill volumes subjected to linear frequency sweep excitation along the lateral axis. The results clearly show a single dominant peak for each fill volume, while the 50% fill volume yields the highest magnitude, suggesting the most severe slosh among the three fill volumes.

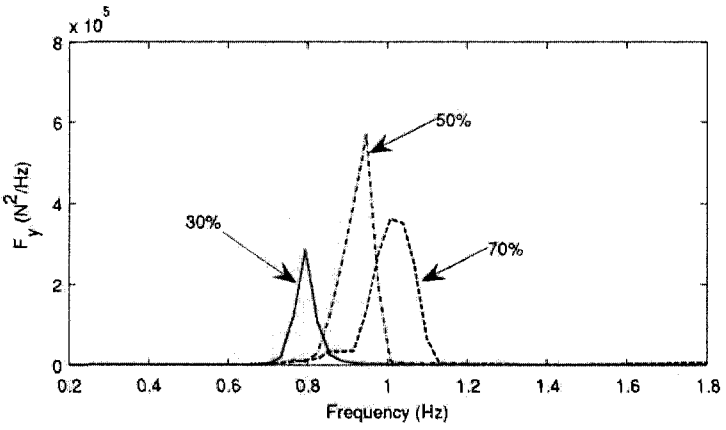


Figure 3.6: Power spectral density of the lateral slosh force under swept harmonic lateral excitation and 30%, 50% and 70% fill volumes.

Figure 3.7 shows the variations in the fundamental frequency identified from frequency spectra of lateral and longitudinal forces for the cleanbore tank 'T0' with 30%, 50% and 70% fill volumes. The results are also compared with the measured data presented in Chapter 2. For both the lateral and longitudinal modes, the predicted frequencies agree reasonably well with the experiment results for all the fill conditions. The results are also compared with the estimated data using the analytical method [31]. The comparison again shows good agreements with both the simulated and measured data. The differences between the simulation results and the measured data are less than 8%, while the peak difference from the analytical estimations is below 4%. The simulation results attained for the baffled 'T1' tank also showed good agreements with the experimental results for different fill volumes, as seen in Table 3.5. It is observed that the peak difference between the simulation and experiment results of fundamental slosh frequencies is less than 8% for the 50% and 70% fill volumes in the lateral mode, and less than 4% in the longitudinal mode.

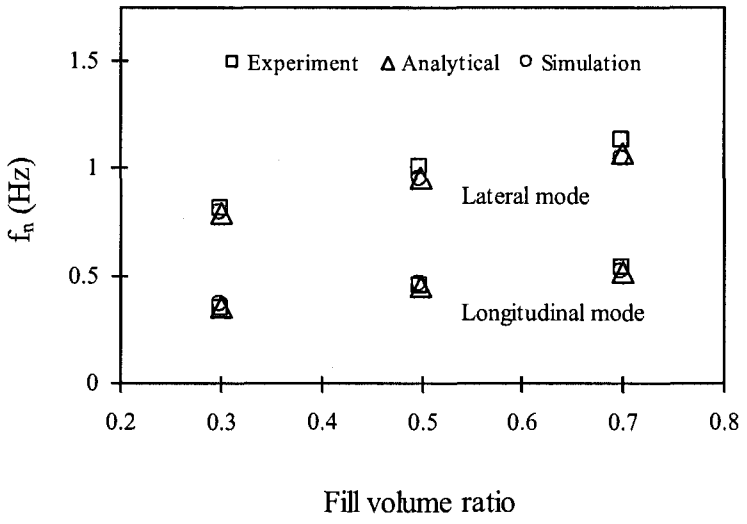


Figure 3.7: Comparison of fundamental natural frequencies estimated from the simulation, experimental and analytical methods. ○, simulation; □, Experimental; Δ, Analytical [31].

Table 3.5. Comparison of lateral and longitudinal mode fundamental slosh frequencies derived from simulation and experiment results for tank 'T1' at 50% and 70% fill volumes.

| Mode direction | Method | Fill volume | |
|---|---|---|---|
| | | 50% | 70% |
| Y | Sim. | 0.9460 | 1.0376 |
| | Exp. | 1.0000 | 1.1250 |
| X | Sim. | 1.0376 | 1.0986 |
| | Exp. | 1.0781 | 1.1406 |

### 3.4.2 Transient Slosh Forces and Moments

The magnitudes of transient slosh forces and moments strongly depend upon the nature of excitation (i.e., direction, frequency and magnitude), and tank geometry and fill volume, as it was evidenced in the laboratory-measured data. Furthermore, the magnitudes of transient peak slosh forces and moments can be significantly larger than those in the steady-state values. It is thus essential to analyze the applicability of the CFD model in predicting the transient fluid slosh. The analysis of the model validity in this study is conducted for unbaffled and baffled tanks with three different fill volumes (30%, 50% and 70%) under both transient lateral and longitudinal single-cycle acceleration excitations.

The previous experimental results (Chapter 2) showed that the transverse planar baffles have negligible effect on the fluid slosh under a pure lateral single-cycle excitation, and thus the slosh in tanks 'T0', 'T1' and 'T2' under this type of excitations yielded similar results. Due to this fact and experimental data not available for 30% fill volume, the model validation is thereby presented for the cleanbore tank 'T0' with the low fill volume, while the influences of the intermediate and high fill volumes are discussed with respect to the baffled tanks. Figures 3.8 and 3.9 show comparison of slosh forces and moments obtained from the model with the experimental data for the cleanbore tank ('T0') with the low fill volume (30%) and subjected to the excitation of 1.93 m/s$^2$ magnitude at 1 Hz. The figures show time histories of the forces and moments, respectively, along the three axes. Reasonably good agreements are observed in the lateral and vertical forces ($F_y$ and $F_z$), and the roll moment ($M_x$) responses, while the magnitudes of the longitudinal force ($F_x$), and the pitch and yaw moments ($M_y$ and $M_z$)

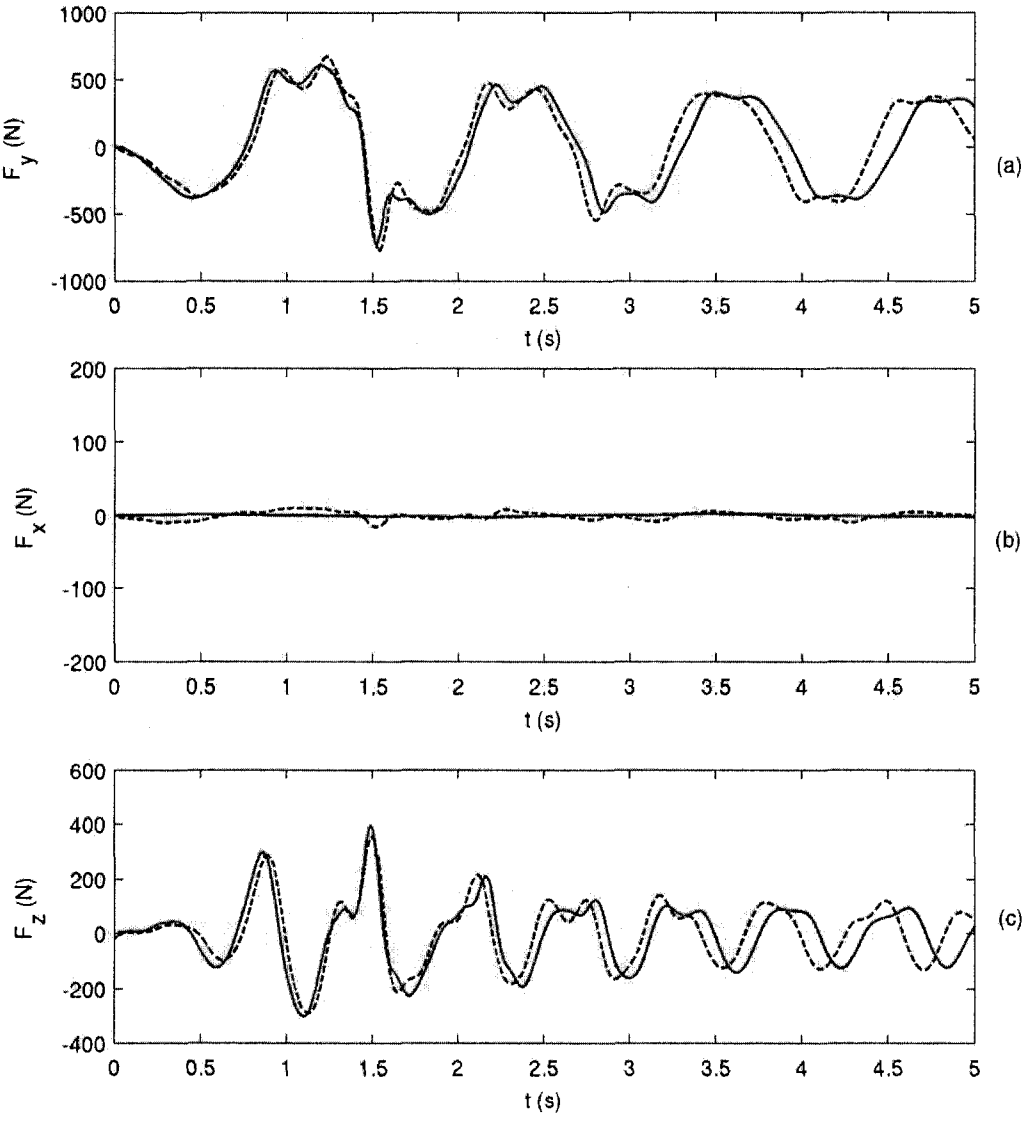


Figure 3.8: Comparison of slosh force components derived from the model with the measured data: (a) lateral force ($F_y$); (b) longitudinal force ($F_x$); (c) vertical force ($F_z$). ——, simulation; -----, experiment. (Tank: 'T0'; fill volume: 30%; lateral single-cycle sinusoidal excitation of 1.93 m/s$^2$ magnitude at 1Hz)

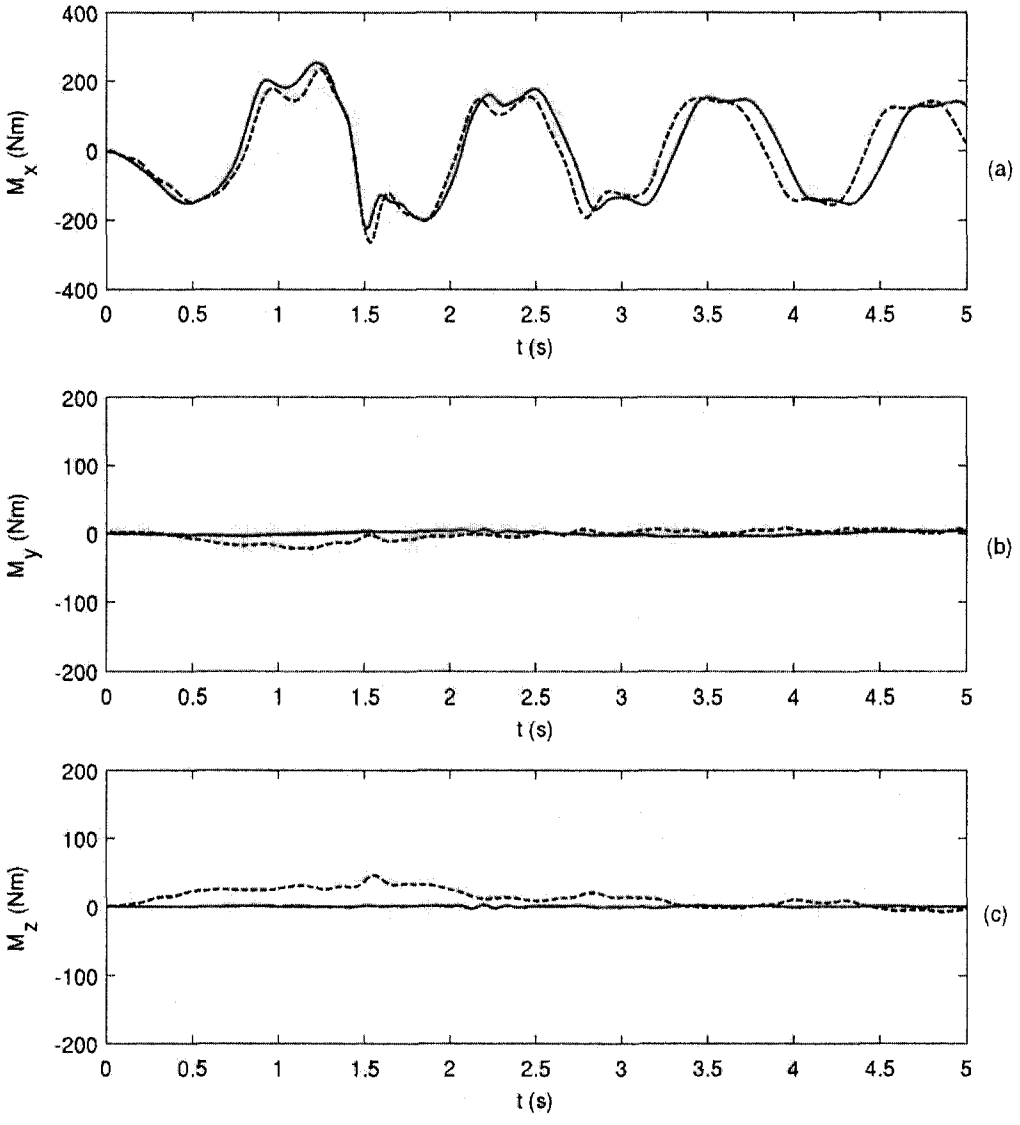


Figure 3.9: Comparison of slosh moments derived from the model with the measured data: (a) roll ($M_x$); (b) pitch ($M_y$); (c) yaw ($M_z$). ——, simulation; -----, experiment. (Tank: 'T0'; fill volume: 30%; excitation: lateral single-cycle sinusoidal excitation of 1.93 m/s$^2$ magnitude at 1Hz)

.

tend to be very small. Both the compared results show slowly dampening magnitudes of $F_y$, $F_z$ and $M_x$, while very small deviations are observed in the response variations, including the subtle characteristics of peaks and valleys. The comparisons show some discrepancies in the longitudinal forces, and pitch and yaw moments, while their magnitudes are very small compared to $F_y$, $F_z$ and $M_x$. The deviations are most likely associated with the limitations of the measurement systems subject to low magnitude signals, namely the signal to noise ratio and resolution. The small magnitude of longitudinal force identically shown in both the model and experimental responses suggests that the slosh is predominantly two-dimensional in the roll plane.

The model responses for the intermediate and high fill volumes (50% and 70%) under the same excitation are illustrated in Figure 3.10. In the figure only the transient roll moment ($M_x$) is plotted for comparison since it reflects the combined effects of both the lateral and vertical forces. Again, the comparisons show reasonably good agreement between the two for both the fill volumes. The model responses tend to capture the global trends reasonably well, including the transient peak behaviors. Recalling the results under 30% fill volume, both the model and experimental results tend to exhibit larger roll moment as fill volume increases due to the increased fluid load. Furthermore, the model responses again show a lower variation frequency than the respective experiment data, which is consistent with that observed for the low fill volume (30%).

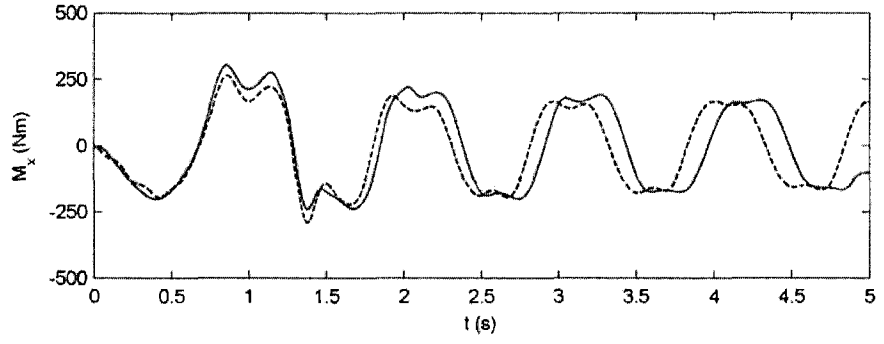


(a)

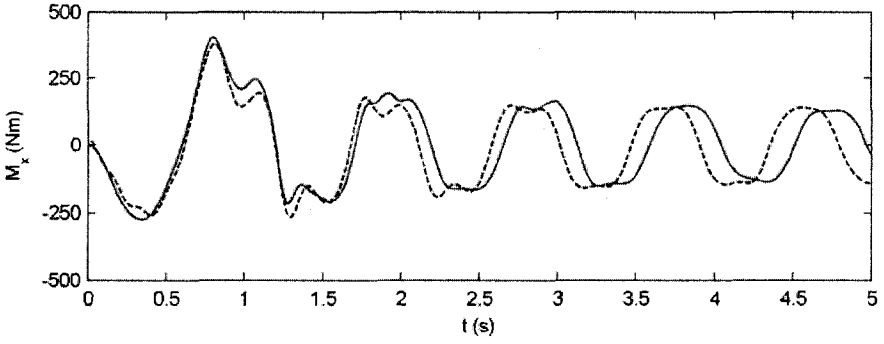


(b)

Figure 3.10: Comparison of roll moment ($M_x$) derived from the model with the measured data for tank 'T1' with fill volume (a) 50% and (b) 70% under lateral single-cycle sinusoidal excitation of 1.93 m/s$^2$ magnitude at 1 Hz. ——, simulation; -----, experiment.

The model validity is further examined under a similar excitation of higher magnitude (4.34 m/s$^2$) and frequency (1.5 Hz). Figure 3.11 illustrates comparisons of model responses in terms of time-histories of $F_y$, $F_z$ and $M_x$ with the corresponding measured data for 30%-filled 'T0' tank under this excitation. The comparisons are limited only to $F_y$, $F_z$ and $M_x$ responses due to the very small magnitudes of the other parameters. The compared results show the trends similar to those observed under the excitation of lower magnitude and frequency shown in Figures 3.8 and 3.9. While the

comparisons show reasonably good agreements between the simulation results and the measured data, the model results generally suggest slightly lower slosh frequency than that of the experiment results. This tendency was observed in the slosh force as well as moment responses, and is discussed at the end of this section. The model responses under this high magnitude excitation for the baffled tanks show a similar behavior, and are thus not presented.

The model validity is also analyzed for the three tank configurations ('T0', 'T1' and 'T2') under an idealized ramp-step excitation along the longitudinal $x$-axis, as depicted in Figure 3.3. Figure 3.12 illustrates the comparisons of the model and experiment results for the cleanbore tank 'T0' with 30% fill volume and subjected to an idealized longitudinal ramp-excitation of 0.89 m/s$^2$ magnitude. The comparisons are limited only to the longitudinal and vertical forces ($F_x$, $F_z$) and pitch moment ($M_y$), since the magnitudes of lateral force ($F_y$) and roll ($M_x$) and yaw ($M_z$) moments were observed to be very small. The same as the results under the lateral excitations, very good agreements are shown between the model and experimental results. Both the results consistently show that, while variation of $F_z$ is in small magnitude and at high frequency, $F_x$ and $M_y$ vary at low variation frequency and with very small decaying rate of magnitude. The small slosh frequencies and damping rate in $F_x$ and $M_y$ is due to the longer length of the tank, relative to the width. The high frequency presented in $F_z$ is probably due to the effect of traveling wave of free surface along the longitudinal direction. It is also clearly seen that the model responses closely imitate the highly non-

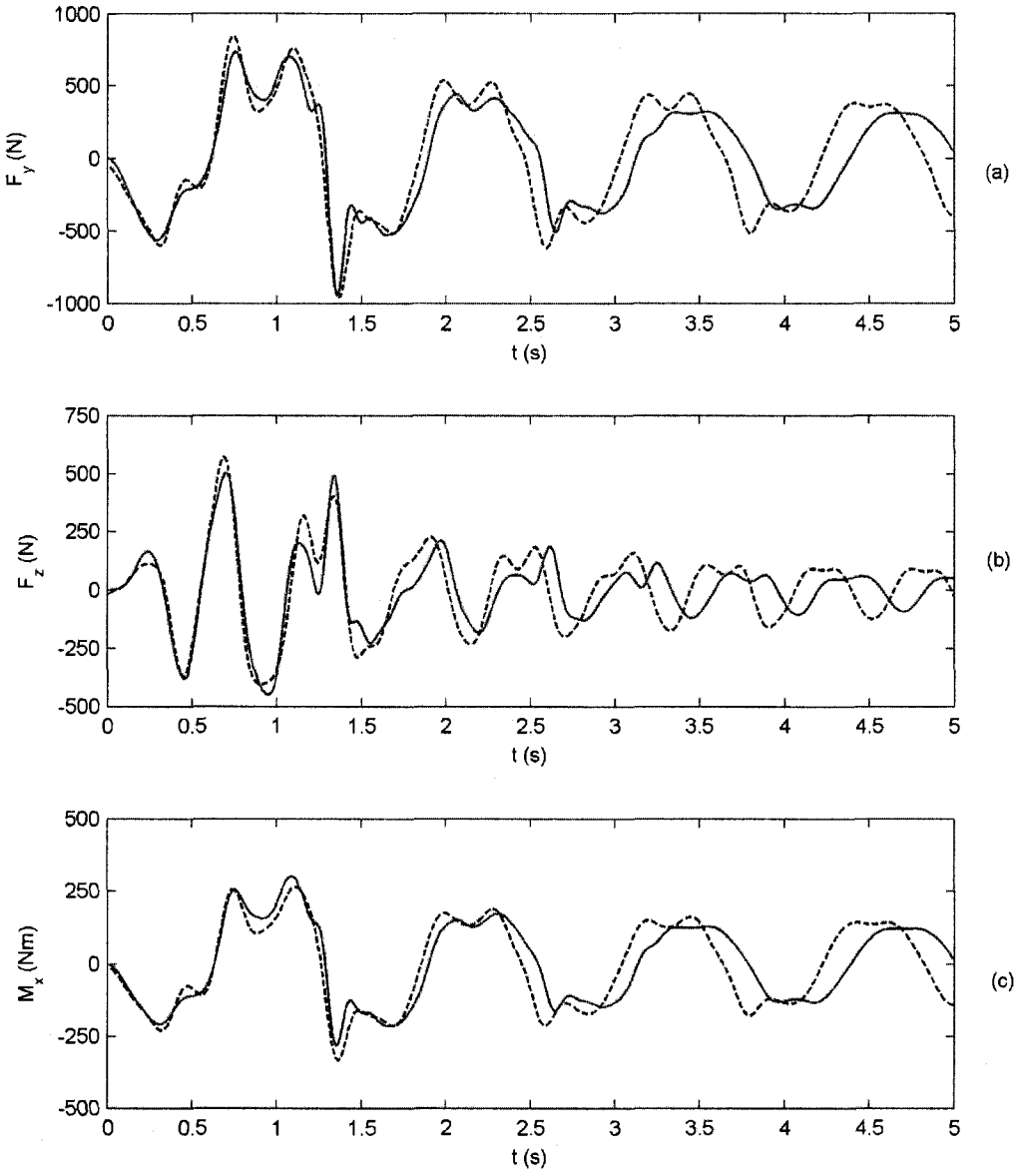


Figure 3.11: Comparison of slosh forces and moment derived from the model with the measured data: (a) lateral force ($F_y$); (b) vertical force ($F_z$); (c) roll moment ($M_x$). ——, simulation; -----, experiment. (Tank: 'T0'; fill volume: 30%; lateral single-cycle sinusoidal excitation of 4.34 m/s$^2$ magnitude at 1.5 Hz)

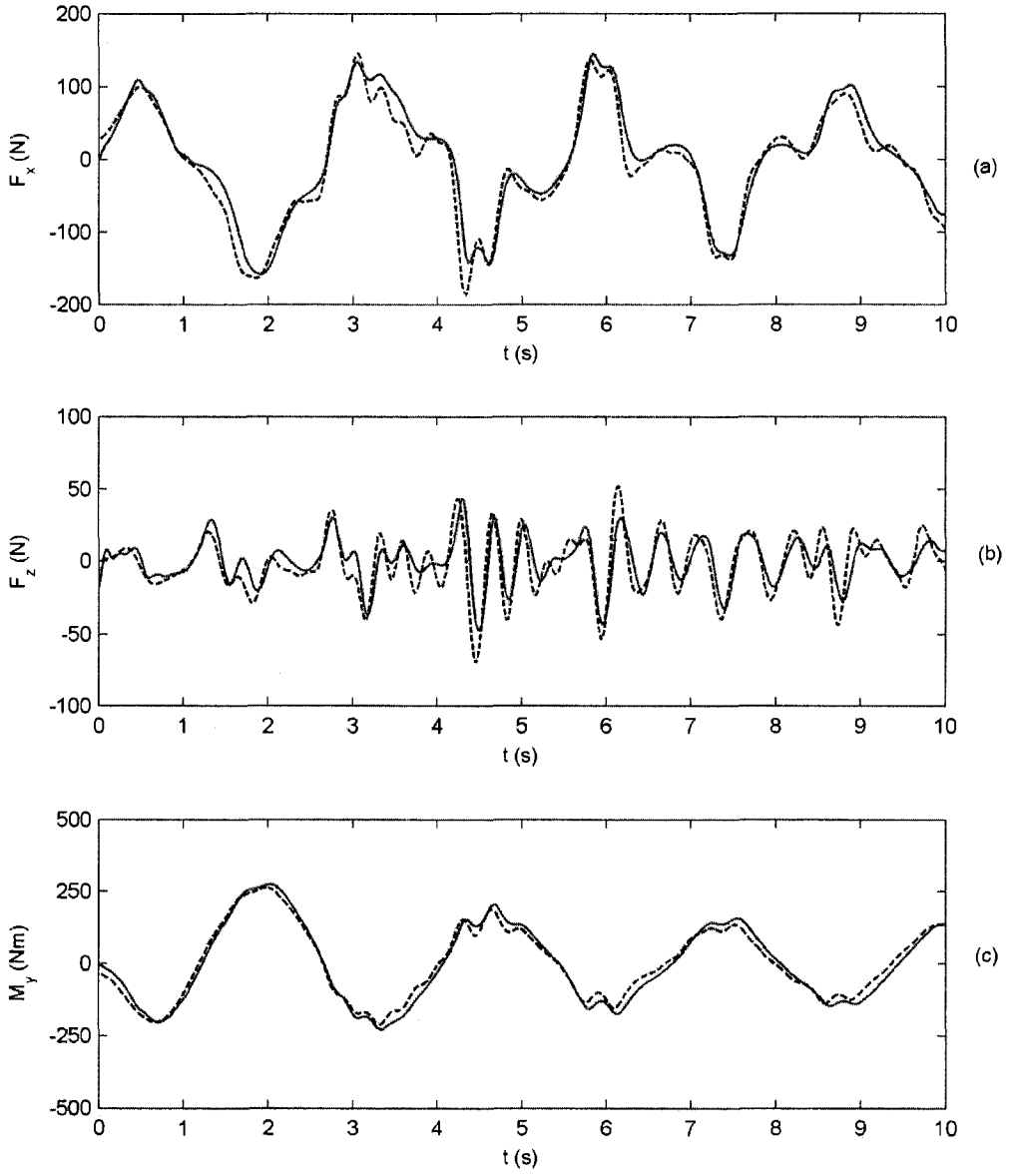


Figure 3.12: Comparison of slosh forces and moment derived from the model with the measured data: (a) longitudinal force ($F_x$); (b) vertical force ($F_z$); (c) pitch moment ($M_y$). ——, simulation; -----, experiment. (Tank: 'T0'; fill volume: 30%; longitudinal idealized ramp-step excitation of 0.89 m/s$^2$).

linear slosh behavior exhibited by the corresponding experimental data, including every subtle transient feature and the global trend. In addition, the model and experimental results show the identical slosh frequency responses.

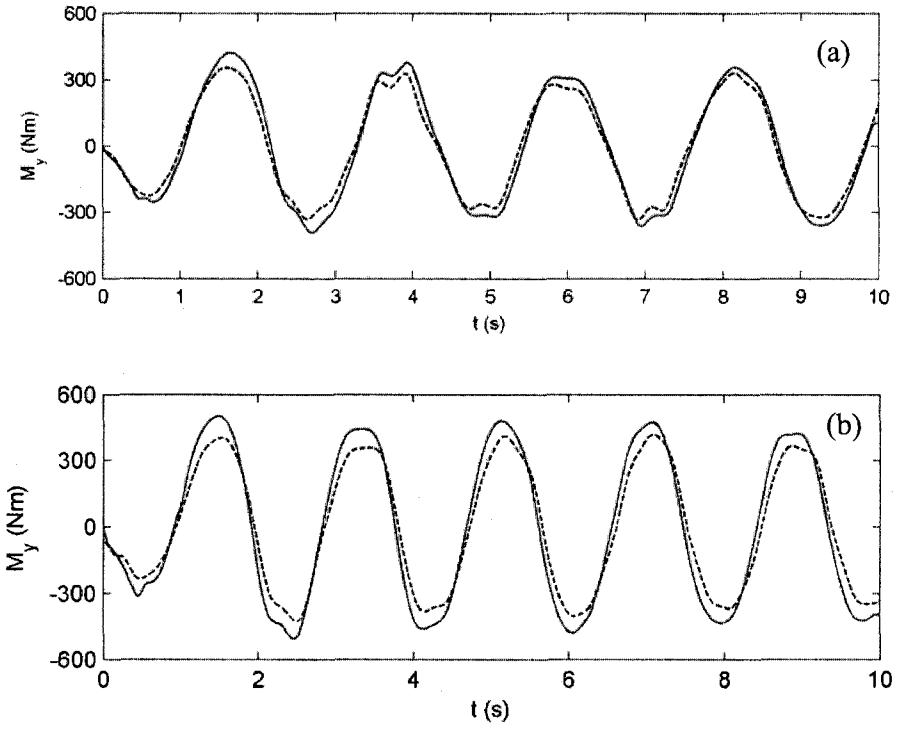


Figure 3.13: Comparisons of pitch moment ($M_y$) derived from the model with the measured data for tank 'T0' with fill volume (a) 50% and (b) 70% subjected to longitudinal idealized ramp-step excitation of 0.89 m/s$^2$. ——, simulation; -----, experiment.

The pitch moment results obtained from the model under the same excitation for the intermediate and high fill volumes are shown in Figure 3.13. Both the results demonstrate the same slosh frequency, and it tends to increase as fill volume increases. Moreover, variation magnitude decays very slowly, while it tends to be higher for a higher fill volume due to the larger fluid load. A slight larger deviation is observed between the model and experiment results for the intermediate and high fill volumes, as

compared to those for the low fill volume (Figure 3.12*c*). The peak-to-peak differences are 15.5% and 21.6% for the comparisons with respect to the intermediate and high fill volumes, respectively. This relatively large deviations are most likely attributed to complex flows associated separation of the free surface under the intermediate fill volume and above, where the first order scheme in spatial discretization may not give the accurate solutions.

The model responses to the longitudinal excitation are also examined for the baffled tanks ('T1' and 'T2') to evaluate the applicability of the model in predicting the fluid slosh in complex tank configurations. Figure 3.14 shows the comparisons of the model responses in the pitch moment ($M_y$) with the corresponding measured data under the same longitudinal idealized ramp-step excitation as above. In contrast to the slosh behavior in the cleanbore tank shown in Figures 3.12 and 3.13, the model and experiment results for both the baffled tanks ('T1' and 'T2') show a rapid decaying in the magnitudes of slosh forces and moment due to the damping effect of the baffles. The compared results further show that the presence of the baffles (both 'T1' and 'T2') yields significant reduction in the magnitude of the slosh pitch moment ($M_y$), as compared to the results of tank 'T0' with the same fill volume in Figure 3.12. While the comparisons show reasonably good agreements in the frequency responses and global damping trend of variation magnitude for both the baffled tanks, considerably large deviations in the peak magnitudes are also evident with the model responses overestimated. The peak-to-peak differences for the slosh pitch moment ($M_y$) are 27.9% and 15.1% for tank 'T1' and 'T2'. Such large deviation, however, were not evident from the steady-state slosh analysis of the baffled tanks (presented in the next section).

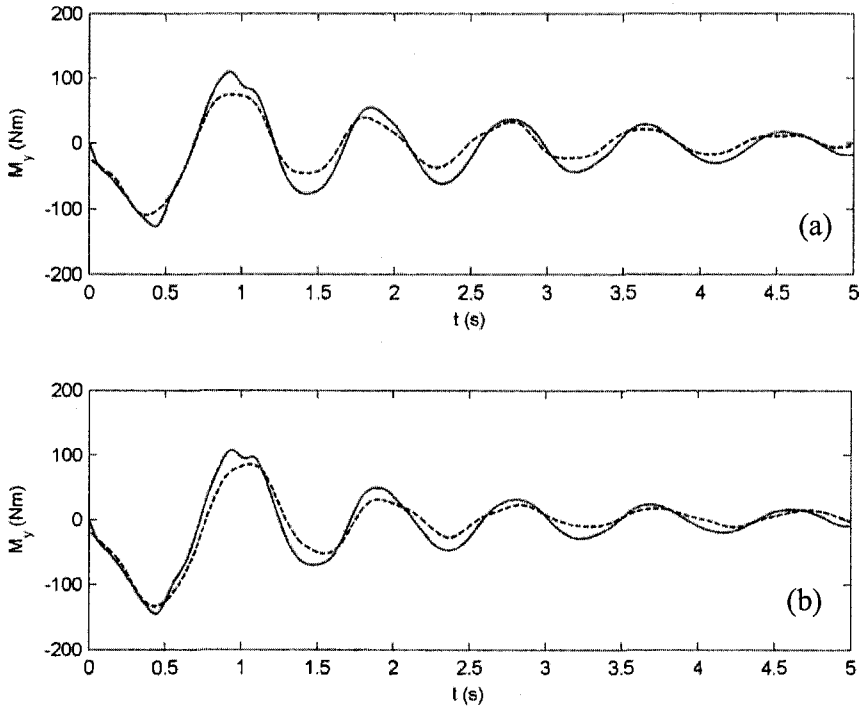


Figure 3.14: Comparison of slosh pitch moment ($M_y$) derived from the model with the measured data for baffled tank (a) 'T1' and (b) 'T2' with the intermediate fill volume (50%) subjected to longitudinal idealized ramp-step excitation of 0.89 m/s$^2$. ——, simulation; -----, experiment.

As a summary, the model results showed reasonably good agreements with the experimental data in terms of the predominant slosh forces and moments associated with the excitations. The agreements lie generally in the peak responses and transient variation trends of the slosh parameters. Slightly larger deviations in peak values were observed for the intermediate and high fill volumes. Considerably large discrepancies (15%-30%) were shown in the comparisons of the results for the baffled tank configurations when subjected to a longitudinal excitation. While the model and experimental responses showed identical slosh frequency under the longitudinal excitations, a slight frequency difference (<5%) was consistently observed under the lateral excitations, irrespective of

fill volume. The frequency difference is probably due to the inherent distinction between the laboratory experiment and numerical simulation. The tank is ideally treated as a completely rigid structure body in simulations, while it is not the case in the experiment. As shown in Chapter 2, the experiment tank is mounted on three dynamometers positioned in triangular locations (Figure 2.2). The lateral spacing (i.e., "*W*" in Figure 2.2) between the supporting dynamometers is considerably smaller than the longitudinal spacing ("L"). Due to the smaller lateral spacing of the supports, the empty tank experienced a high frequency mechanical vibration (13 Hz) when subjected to a lateral excitation, which is believed to be responsible for the relatively higher frequencies of the experiment results. However, due to the larger longitudinal spacing of the dynamometers and thus the more solid supporting in the longitudinal direction, the mechanical vibration was not observed when subjected to a longitudinal excitation.

### 3.4.3 Steady-state Slosh Force and Moments

A disturbed fluid is known to eventually settle down to its corresponding steady-state. The experimental fluid slosh analysis (Chapter 2) has shown that a liquid, when subjected to a harmonic excitation near resonant frequency (even along a single-axis direction), tends to slosh in a three-dimensional manner. This is different from the transient two-dimensional slosh characterized under a one-cycle sinusoidal excitation. While the analysis of transient 2-D slosh is performed to evaluate the model's applicability in capturing the short term transient fluid slosh phenomena, the analysis of steady-state slosh is essential for examining the model's capability of predicting the long term slosh phenomena, particularly the 3-D swirling motion. Since the resonance is the harshest

slosh phenomena, the validation of the model thus highlights on the fluid slosh responses to harmonic excitations near resonant frequency.

Figures 3.15 and 3.16 show the comparisons of steady-state slosh forces and moments derived from the model with the experiment data. The results are obtained for the clearbore tank ('T0') with 50% fill volume and subjected to the lateral harmonic excitation of 1 $m/s^2$ magnitude at the resonant frequency 1 Hz. The figures show reasonably good agreement between the model and experiment results for every component of forces and moments. The agreement lies not only in the high frequency contents shown in all the transient force and moment components, but also in the low frequency variations presented in the longitudinal slosh force ($F_x$) and pitch moment ($M_y$). The compared results also show that the longitudinal force $F_x$ is developed in a considerably long time. Furthermore, the peak values of the slosh forces and moments are very close between the model and experimental data, while the varying magnitudes also show the same trends for all the parameters. It is seen that the agreements are particularly good in the late times of the time-histories of the six parameters. It should be noted that the simulation and experiment were not carried out under the same initial condition. The simulations were started for the fluid at rest, while the experiments were initiated under the condition that the disturbed fluid was not fully settled down. The compared results show very small differences (<3%) in the peak values of the predominant lateral force ($F_y$) and roll moment ($M_x$). While the discrepancy in the peak $F_x$ is negligible, relatively large deviations are shown for the peak magnitudes of the vertical force ($F_z$), and pitch and yaw moments ($M_y$ and $M_z$), which are in the order of 10%.

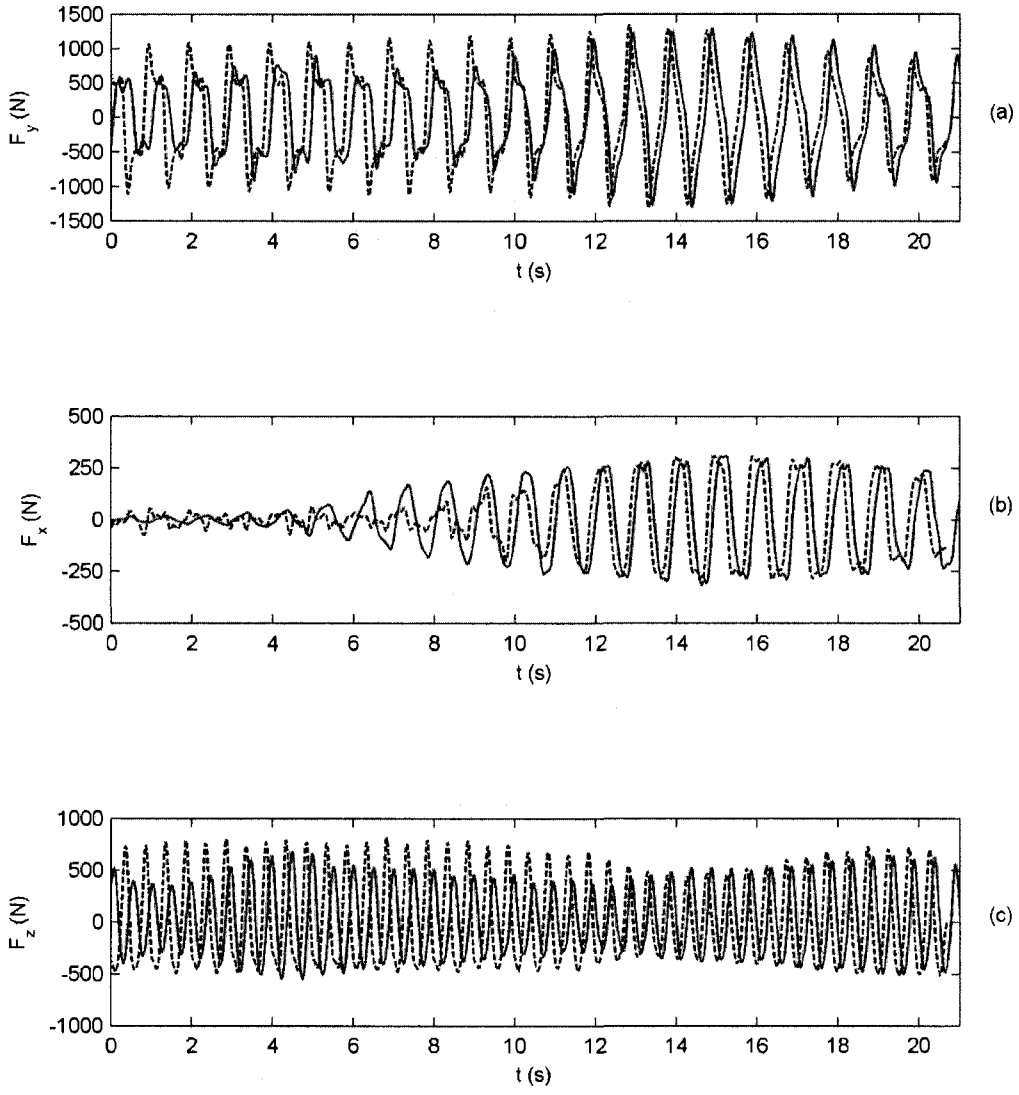


Figure 3.15: Comparison of steady-state slosh forces derived from the model with the measured data: (a) lateral force ($F_y$); (b) longitudinal force ($F_x$); (c) vertical force ($F_z$). ——, simulation; -----, experiment. (Tank: 'T0'; fill volume: 50%; excitation: lateral harmonic excitation of magnitude 1 m/s$^2$ at 1 Hz).

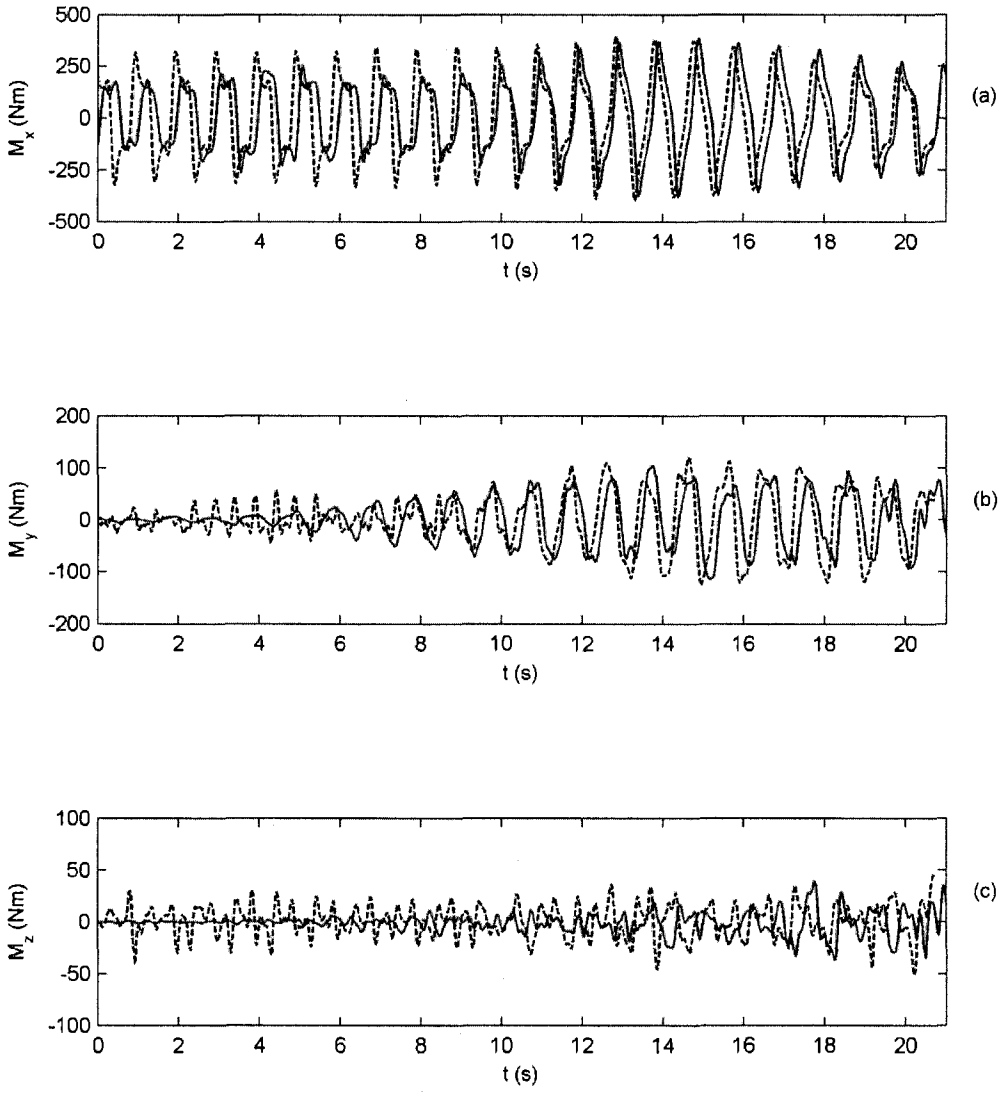


Figure 3.16: Comparison of steady-state slosh moments derived from the model with the measured data: (a) roll ($M_x$); (b) pitch ($M_y$); (c) yaw ($M_z$). ——, simulation; -----, experiment. (Tank: 'T0'; fill volume: 50%; excitation: lateral harmonic excitation of magnitude 1 m/s$^2$ at 1 Hz).

Good agreements are also shown in the comparisons of the model responses and experiment results for the baffled tank 'T1', as evident in Figure 3.17, which depicts the results obtained under the same intermediate fill volume (50%) and subjected to the same harmonic excitation at resonance. The comparisons in the figure are limited to the slosh forces ($F_y$, $F_x$ and $F_z$) since the behaviors of roll and pitch moments are similar to those of $F_y$ and $F_x$, and the yaw moment is very small. Again, the model and experimental results agree well in terms of the variation frequencies and magnitudes. The frequency responses are observed nearly the same between the two, whereas highly non-linear trends in the varying magnitudes are identified to be similar. While the transient peaks and valleys derived from the model are consistent with the experiment data, the corresponding peak shapes are also "mimic". The model response in the longitudinal force shows relatively small variation with time, while significantly large variation is observed for the corresponding experimental results. This deviation can be due to the relatively coarse mesh used in the model simulation for this tank because the low frequency magnitude variation behavior is strongly related to the mesh size, as demonstrated in Figure 3.5*b*. Again, better agreements are shown in the late times of the time-series signals due to the different initial fluid conditions used in both the model simulation and laboratory experiment. It is seen that the difference in the peak values of the dominant lateral force $F_y$ is negligible, while the deviations in the peak $F_x$ and $F_z$ are slightly large, which are 15.1% and 11.7%, respectively.

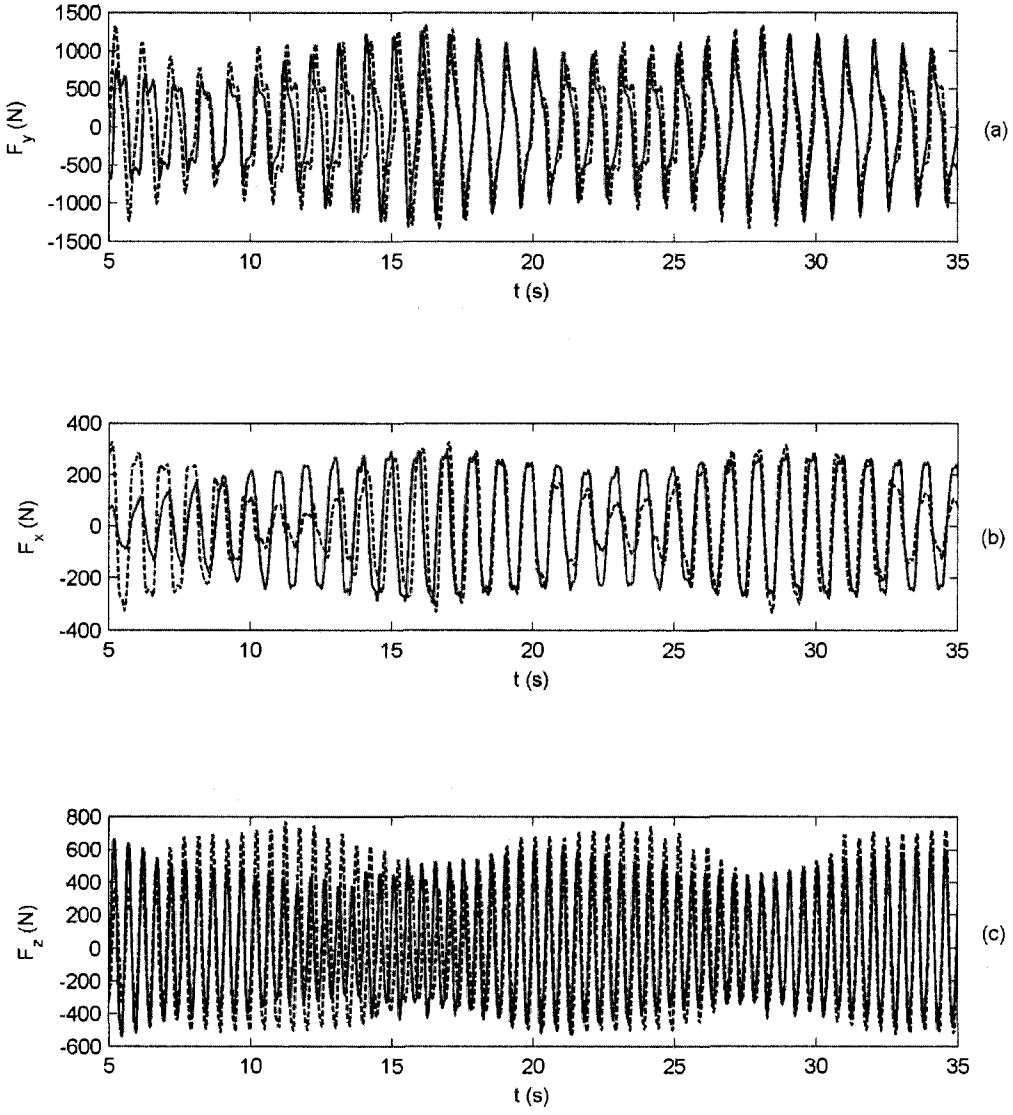


Figure 3.17: Comparison of steady-state slosh forces derived from the model with the measured data: (a) lateral force ($F_y$); (b) longitudinal force ($F_x$); (c) vertical force ($F_z$). ——, simulation; -----, experiment. (Tank: 'T1'; fill volume: 50%; excitation: lateral harmonic excitation of magnitude 1 m/s$^2$ at 1 Hz).

While the three-dimensional fluid slosh can be quantitatively observed in the slosh force responses of the model, the non-linear slosh characteristics can also be clearly demonstrated by the visual slosh free surface evolvement, as evident in Figure 3.18. Figure 3.18 presents the five free surface patterns evolved from t = 41.25 s ~ 42.25 s covering one slosh period in the steady-state range for the baffled tank 'T1' under the same conditions as Figure 3.17. The slosh resulting lateral and longitudinal forces are also presented in Figure 3.20*f* to show the corresponding force behavior. The free surface images shown in Figures 3.18*a* to *d* clearly present different patterns. The patterns at t = 40.25 s and 42.25 s, shown in Figures 3.20*a* and *e* and corresponding to negative peaks of $F_x$, are practically the same, indicating that the slosh is a periodic phenomenon. Asymmetrical patterns are presented at t = 41.75 s and 42.25 s (Figures 3.20*a* and *c*) corresponding to the positive and negative $F_x$ peaks, respectively, and at t = 42 s and 42.5 s (Figures 3.20*b* and *d*) when $F_y$ is near the negative and positive peaks, respectively. This suggests that the fluid oscillates in both the longitudinal and lateral directions and thus the whole fluid bulk is characterized by a three-dimensional motion. Since the free surface motion was not recorded in the experiment, no experiment imaging data can be available for the comparison.

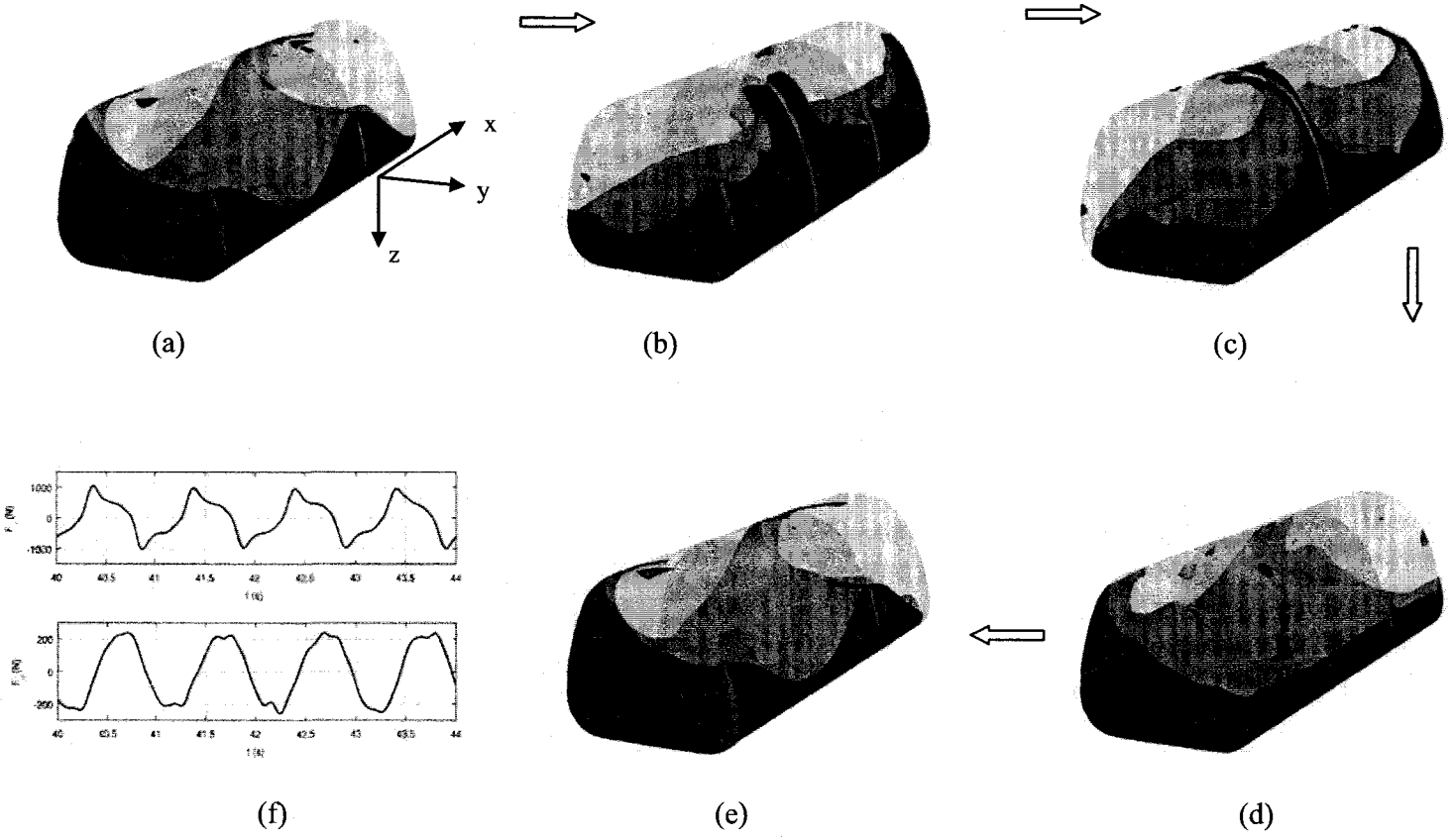


Figure 3.18: The free surface patterns evolved at different instants: (a) 41.25 s; (b) 41.5 s; (c) 41.75 s; (d) 42 s; (e) 42.25 s; (f) corresponding transient slosh forces (*Fy* and *Fx*). (Tank: 'T1'; fill volume: 50%; excitation: lateral harmonic excitation of 1 Hz and 1m/s$^2$)

The model responses for the complex tank configuration 'T2'are also reasonably consistent with the experiment results near the resonance, as illustrated in Figure 3.19. Figure 3.19 shows the slosh forces derived from the model for 50%-filled tank 'T2' under the lateral harmonic excitation of 1 $m/s^2$ magnitude at the resonant frequency (1 Hz), in comparison of the experiment data. The comparisons in the three force components show the agreement in the order similar to those observed for tanks 'T0' and 'T1'. The slosh forces, especially the longitudinal force, derived from the model, exhibit practically the same trend of varying magnitudes as that of the experiment. Furthermore, the deviations in the peaks of all force components are negligible. Comparison of the figure with Figures 3.19 shows that the model gives much better results for tank 'T2' than tank 'T1'. This difference is probably due to a finer mesh utilized in the model simulation for tank 'T2'. The model results show some overshoot peaks in the vertical slosh force which are not visible for the corresponding experimental data. Since these abnormal peaks correspond to the variation peaks of lateral and longitudinal forces and the reference pressure location in this simulation was placed near the tank roof, this model behavior is probably attributed to the disturbance of the reference pressure by the separated flow surface.

As a summary, the resonant slosh analyses with the model showed that the CFD VOF slosh model is capable of capturing the complex swirling slosh happened at the resonance, and can give reasonably accurate solutions in all the slosh resulting forces and moments during the steady-state slosh. Moreover, the model can be applied to the relatively simple geometrical cleanbore tank, as well as the complex baffled tank configurations.

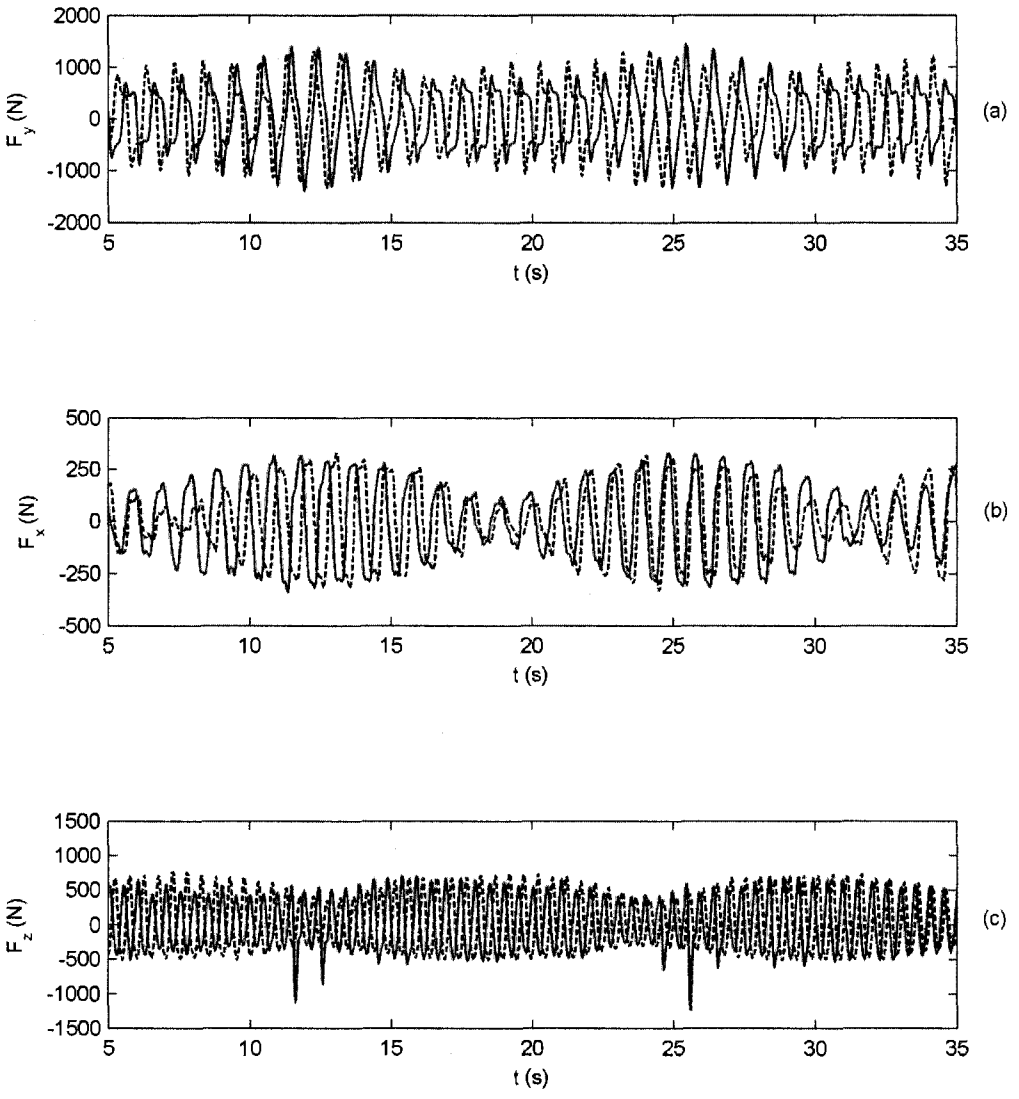


Figure 3.19: Comparison of steady-state slosh forces derived from the model with the measured data: (a) lateral force ($F_y$); (b) longitudinal force ($F_x$); (c) vertical force ($F_z$). ——, simulation; -----, experiment. (Tank: 'T2'; fill volume: 50%; excitation: lateral harmonic excitation of magnitude 1 m/s$^2$ at 1 Hz).

While the analyses of the resonant slosh (the most severe slosh phenomena) serve to be the essential part of the model validation, it may be also desirable to evaluate the model's responses to harmonic excitations of different frequencies and magnitudes. Figures 3.20 and 3.21 illustrate variations of the maxima of slosh forces and moments in the steady-state derived from the model simulations with the excitation frequency, which are compared to the corresponding experimental results. The results are obtained for the cleanbore tank ('T0') with the intermediate fill volume (50%) and subjected to the lateral harmonic excitations of 1 and 2 $m/s^2$ magnitudes at the frequency ranging from 0.6 to 1.5 Hz. The maximum values of the slosh forces and moments are calculated on the basis of confidence treatment which is the same as those introduced in Chapter 2 for the experiment data analysis.

The model results invariably show the peaks occurring at the resonant frequency for all the slosh forces and moments, irrespective of the excitation magnitude, which is exactly the same as the experimental behavior. Both the model and experimental results consistently show small longitudinal slosh force and pitch moment when the excitation frequency is rather than the resonant frequency, suggesting that slosh is predominantly two-dimensional under this condition. It is also seen that the deviation in the predominant parameters (lateral force and roll moment) of the resonant slosh between the compared results is significantly small (< 3%) for the two excitation magnitudes considered (1 and 2 $m/s^2$). A considerably large difference is observed in the longitudinal resonant slosh force and pitch moment for the high magnitude excitation (2 $m/s^2$), which are 23.3% and 14.7%, respectively. Under the high excitation magnitude at resonance, the yaw moment, due to the small magnitude, also shows considerably large difference

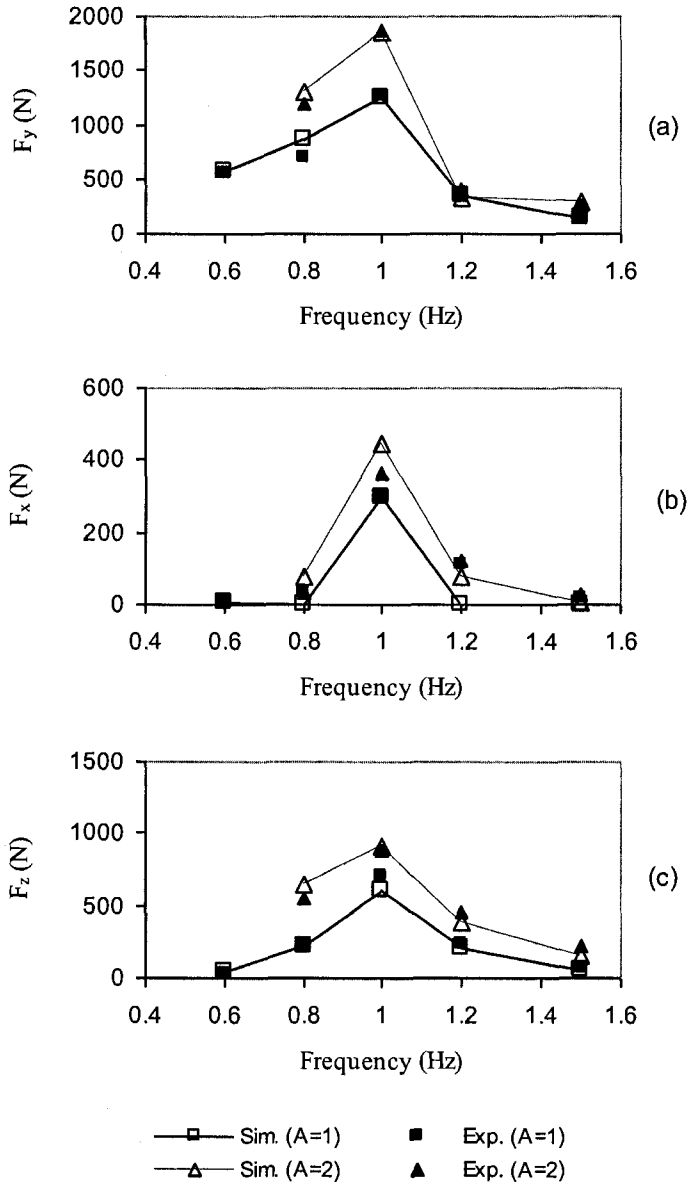


Figure 3.20: Comparisons of the maximum slosh forces in the steady-state derived from the model with the experimental results for tank 'T0' with the intermediate fill volume (50%) and subjected to lateral harmonic excitations of different frequencies and magnitudes. (a) lateral force ($F_y$), (b) longitudinal force ($F_x$), (c) vertical force ($F_z$).

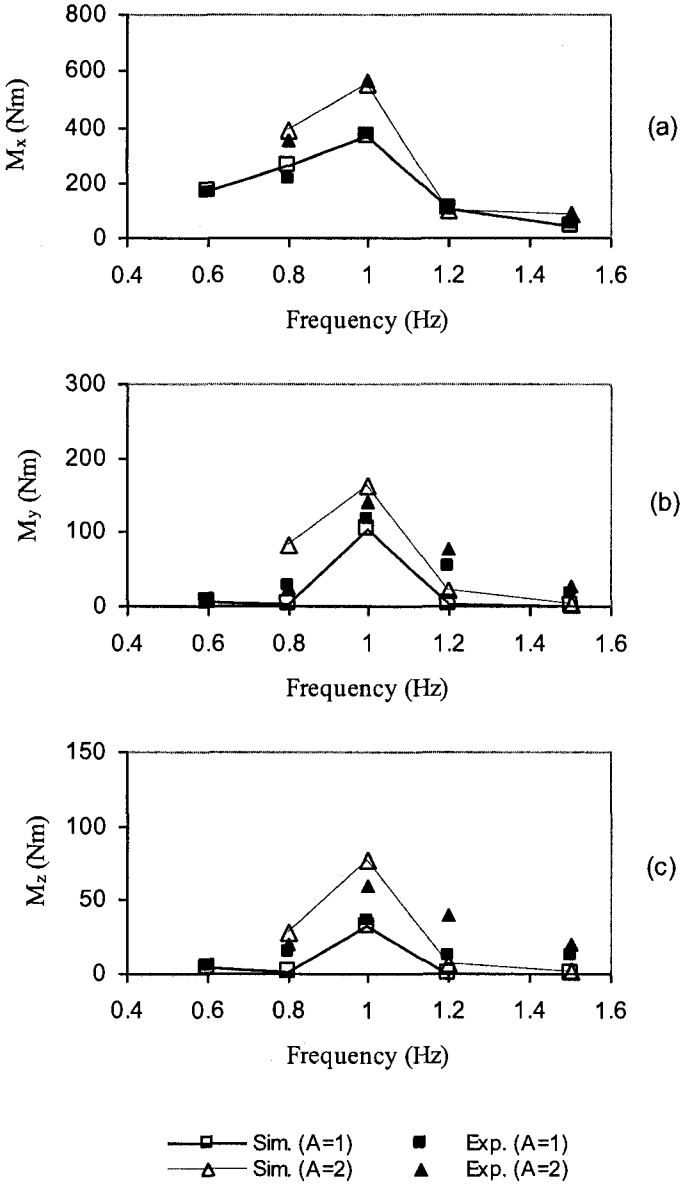


Figure 3.21: Comparisons of the maximum slosh moments in the steady-state derived from the model with the experimental results for tank 'T0' with the intermediate fill volume (50%) and subjected to lateral harmonic excitations of different frequencies and magnitudes. (a) roll ($M_x$), (b) pitch ($M_y$), (c) yaw ($M_z$).

(nearly 30%) between the two. For all the other off-resonance excitations, the predominant lateral force and roll moment derived from the model are in nice agreements with the corresponding experiment data. Slightly large deviations are visible for the pitch and yaw moments at 1.2 Hz and above. This is probably because they are in small magnitude and this may cause high uncertainty of the experimental results. The model responses to the same variable frequency harmonic excitations for the baffled tank 'T1' also present a similar trend, as compared with the corresponding experiment data.

## 3.5 SUMMARY

A three-dimensional CFD slosh model is developed on the basis of VOF technique and validated against the experiments for a wide range of conditions. The model validity was analyzed for tank configurations 'T0', 'T1' and 'T2' with three fill volumes (30%, 50% and 70%). The analyses comprise the evaluation of the model's applicability in the transient and steady-state fluid slosh, which were conducted under the single-cycle sinusoidal and idealized ram-step, and harmonic sinusoidal excitations, respectively.

The analysis of model validity was performed by examining the model responses in the slosh natural frequency and slosh resulting forces and moments, in comparison with the experimental data and analytical solutions. The model results showed small deviations (<8%) from the experimental data and analytical calculations in the slosh natural frequencies in both the lateral and longitudinal modes, irrespective of the tank configuration and fill volume.

The model results in both the transient and steady-state slosh consistently exhibited good agreement with the experiment data in the slosh resulting forces and

moments. Small deviations were shown between the two in the transient peak values of forces and moments, particularly the predominant parameters. Moreover, the agreement also lies in both global trend and local subtle features in the time histories of these parameters for: (*i*) the 2-D slosh observed under single-cycle sinusoidal and idealized ramp-step excitations, and (*ii*) the 3-D slosh presented under harmonic excitations at resonance. These trends were consistently observed for the cleanbore tank 'T0' and baffled tanks 'T1' and 'T2' with three different fill volumes (30%, 50% and 70%). The model results showed a slightly lower slosh frequency, compared to the experiment data which were probably affected by a high frequency mechanical vibration of the tank setup. Furthermore, the model's responses to harmonic excitations of variable frequencies further demonstrated that the model is applicable to the fluid slosh which frequency is less than 1.5 Hz. It can be concluded that the model is capable of predicting the 2-D and 3-D liquid slosh phenomena in the unbaffled and baffled tanks regardless of fill volume, within the frequency range of possible vehicle maneuvers (usually less than 0.5 Hz).

The results using different meshes showed that both wedge and hexahedral grid cells are appropriate for the application to the model simulations. The results using different mesh sizes further show that the accuracy of capturing a three-dimensional slosh is strongly dependent on the mesh size. The analysis of one parameter component is incomplete when the slosh is characterized by three-dimensional motion. The analysis of mesh independence showed that the tank equipped with multiple-orifice baffles ('T2'), due to relatively complex geometry, requires considerably finer mesh than the cleanbore tank ('T0') and the tank with single-orifice baffles ('T1').

# CHAPTER 4

# FLUID SLOSH ANALYSIS OF FULL-SCALE VEHICLE TANKS AND BAFFLE DESIGN FACTORS

## 4.1 INTRODUCTION

As previously described in Chapter 1, the CFD simulation approach, owing to its inexpensiveness, convenience and effectiveness, has gained an increased attention for the analysis of dynamic fluid slosh. The majority of CFD efforts, however, have contributed to explore numerical algorithms [50, 52, 69, 70, 83] and evaluate the validity of numerical modeling [32, 77, 57] of the fluid slosh. The fluid slosh models were rarely implemented for the fluid slosh analysis. Even so, they were limited to the simple 2-D fluid slosh applications [32, 40, 141] and very small scale tank models [32, 40]. There is a scarcity in the literature of the 3-D fluid slosh analysis, particularly within baffled full-scale tanks. One study reported in the literature on 3-D analysis of fluid slosh is by Modaressi-Tehrani *et al.* [128]. They analyzed the 3-D slosh in a full scale cylindrical tank using Fluent software. However, the analysis was conducted with variable cargo load and no equalizer considered.

In this Chapter, a 3-D full-scale tank with an optimized "Reuleaux triangular" cross-section has been designed to match with a full-scale triden tank truck. The dynamic fluid slosh within the tanks is simulated with the CFD VOF slosh model developed and validated in Chapter 3. The tank has six configurations in order to evaluate the influence of different baffle designs and baffle design factors on the slosh forces and moments. The

three components of fluid slosh force and moment are examined for the tank filled with three different fill volumes of fluid cargos corresponding to a constant load and subjected to the acceleration excitations representing different types of vehicle maneuvers.

## 4.2 DESIGN OF FULL-SCALE TANK

The tank considered in the simulations is designed to match with a full-scale tridem tank truck (Figure 4.1). The tank cross-section is an optimized "Reuleaux triangle" shape, which was proposed by Kang [10]. This tank shape is designed to minimize the fluid cargo slosh roll moment, which has been evaluated with the quasi-static method [10]. To match with the truck, the designed tank has 7.62 m length, 3.3 $m^2$ cross-section and 23.67 $m^3$ volume. A full load capacity of approximately 16,400 kg can be attained with the 100% fill volume of gasoline ($\rho$=693.4 $kg/m^3$), under which the axle loads of the tank truck are within the maximum limits.

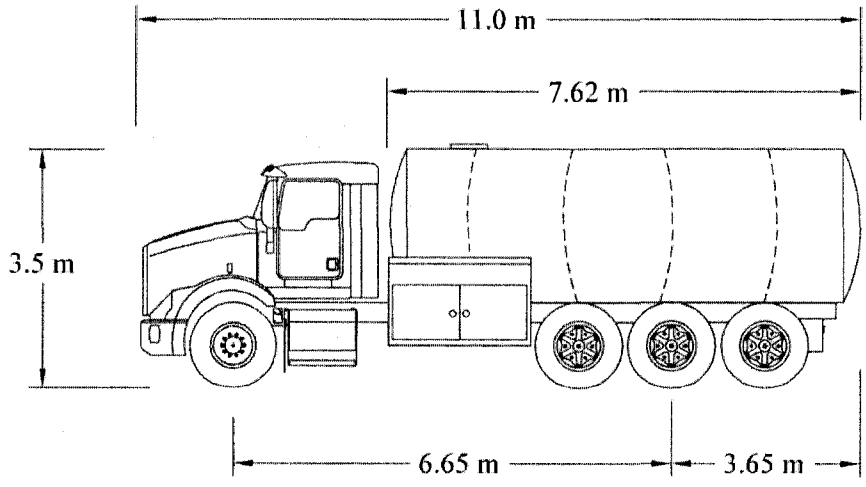


Figure 4.1: Schematic and dimension of the full scale tridem tank truck.

Six tank configurations are considered in the present study which comprise of one cleanbore and five baffled arrangements as described below:

(i) Cleanbore unbaffled tank, hereafter referred to as tank 'T0'

(ii) Tank equipped with single circular orifice baffles of spherical curvature, hereafter referred to as tank 'T1'

(iii) Tank equipped with multiple circular orifice baffles of spherical curvature, hereafter referred to as tank 'T2'

(iv) Tank equipped with single half-circular orifice baffles of spherical curvature, hereafter referred to as tank 'T3'

(v) Tank equipped with half-opened baffles of spherical curvature, hereafter referred to as tank 'T4'

(vi) Tank equipped with single circular orifice baffles of conical shape, hereafter referred to as tank 'T5'

The six tank configurations have the same tank shell, while the difference lies in the layout and shape of the baffles. The designs of the tank configurations are devised in accordance with the CFR codes (49 CFR Part 178) and ASME rules (Boiler and Pressure Vessel Code, Section VIII). The cleanbore tank is designed to have dished heads. The crown radius of the heads is 1.6295 m, which is 80% of the diameter of the equivalent circular tank with the same cross-section area. Out of the five baffled configurations, tanks 'T1' to 'T4' are equipped with the baffles of spherical curvature. The curvature of these baffles is the same as that of the tank heads, as shown in Figure 4.2*a*. The baffle for tank 'T5' has the conical shape of cone angle of 45° (see Figure 4.2*b*). In all the baffled configurations, four transverse baffles are installed within the cleanbore tank frame with

the same longitudinal spacing of 1.4046 m, which is less than the maximum baffle spacing required in the CFR codes (60 in., i.e., 1.524 m).

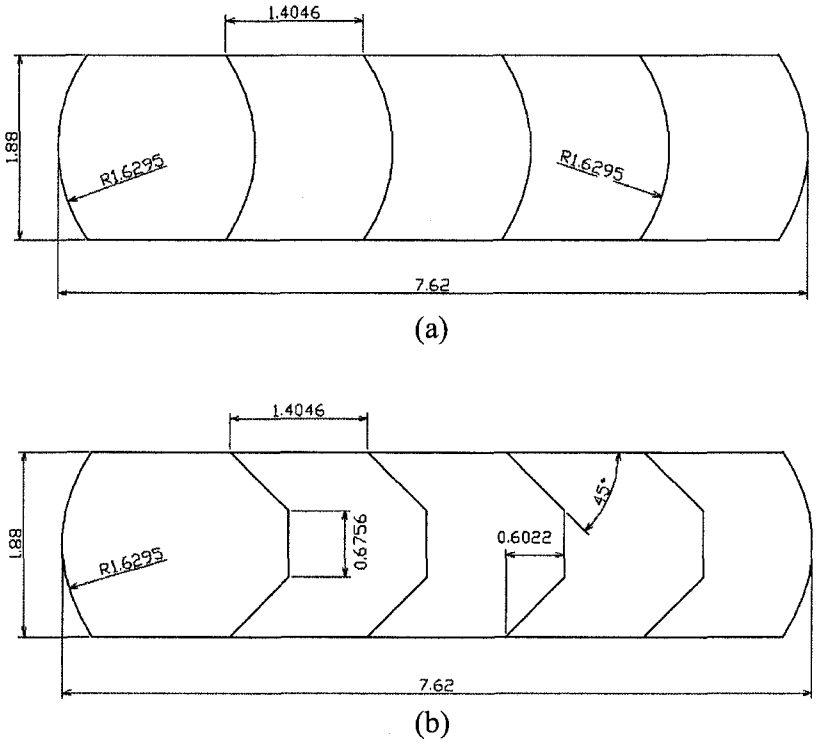


Figure 4.2: Side view of the geometries of the baffled tanks: (a) 'T1' to 'T4'; (b) 'T5'.

The layout and shape of orifices are different for different baffles, as depicted in Figure 4.3. For simplicity, the baffles of tanks 'T1' to 'T5' are denoted as 'B1' to 'B5', respectively. The baffles 'B1' and 'B2' are designed to have the conventional layout similar to those introduced in Chapter 2 but at the full scale. The single orifice baffle ('B1') has a circular orifice of 0.6756 m diameter at the geometric center of the tank cross-section, as illustrated in Figure 4.3*a*. The multiple-orifice baffle ('B2') is composed of one circular orifice of 0.3028 m diameter located at the geometric center of the tank cross-section and 29 circular orifices of 0.1122 m diameter distributed around, as shown

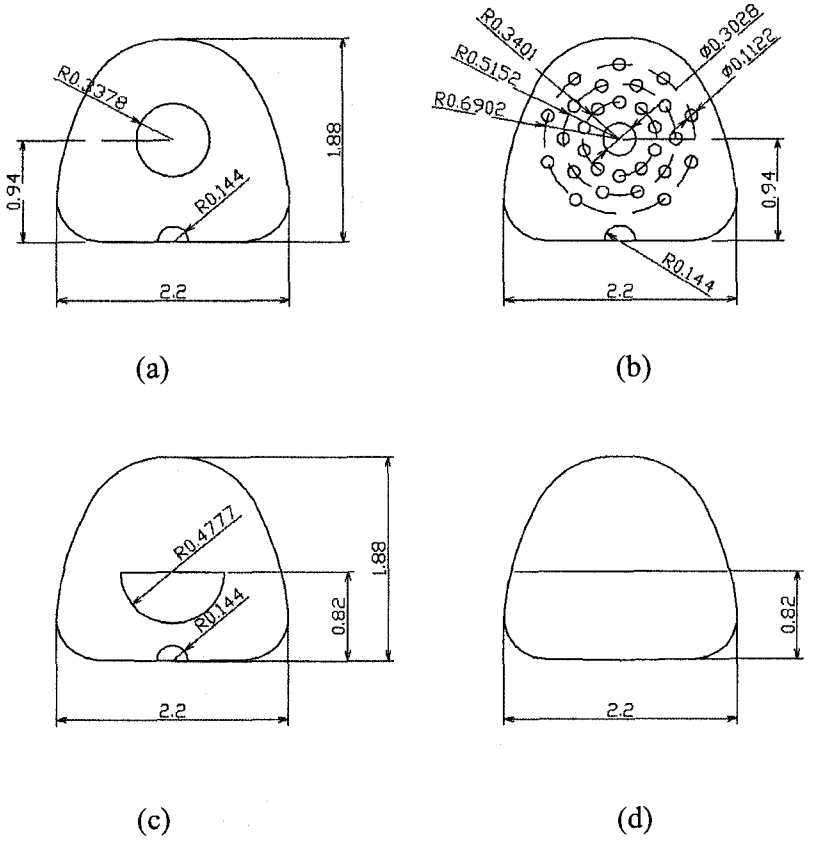


Figure 4.3: Layout of baffle designs for the tanks: (a) 'T1' and 'T5'; (b) 'T2' (c) 'T3' and (d) 'T4'.

in Figure 4.3*b*. The sizes of orifices are designed to have the opening ratio of approximately 11% of tank cross-sectional area which matches the standard of CFR codes (the baffle opening area should be no more than 20% of total tank cross-sectional area). A small orifice is drilled on the baffle near the tank bottom, which acts as an equalizer to maintain the same height of liquid cargo in the neighboring baffled compartments. The equalizer opening is approximately 1% of the tank cross-sectional area. Thus, the total porosity of each of the two baffles ('B1' and 'B2') is 12% of the tank

cross-sectional area. The three dimensional perspective views of 'T1' and 'T2' tanks are shown in Figures 4.4*a* and *b*, respectively.

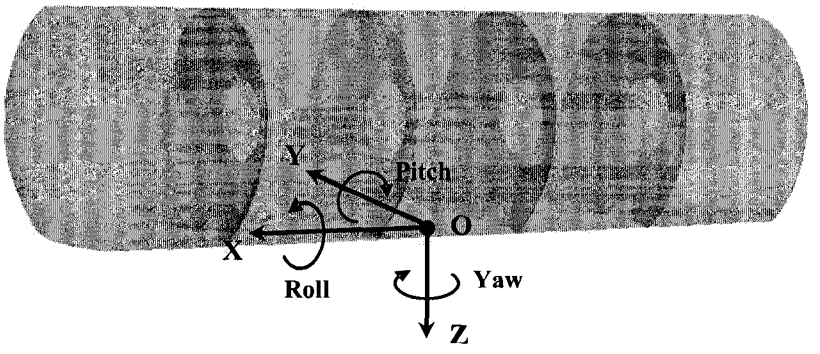


(a)

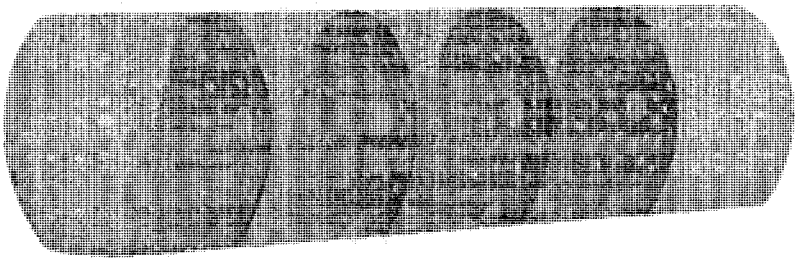

(b)

Figure 4.4: Perspective view of baffled tanks: (a) 'T1'; (b) 'T2'.

To explore the mechanism of enhanced anti-slosh effectiveness of the baffle designs, three novel baffle designs have been conceived: (*i*) single half-circle orifice baffle ('B3'), (*ii*) half-opening partial baffle ('B4'); and (*iii*) conical baffle ('B5'). The baffle opening area and curvature of baffles 'B3' and 'B4' are identical to those of baffle 'B1' to facilitate evaluating the effect of the new design in comparison with the conventional equivalent. To seek the possibility of more effective slosh suppression for

the intermediate and high fill levels, the orifice of baffle 'B3' is designed to be in a half-circle shape of diameter 0.48 m, as shown in Figure 4.3c. The horizontal upper edge of the orifice is 0.82 m from the tank bottom, which passes through the tank's cross-sectional *cg* position. The fluid free surface under 50% fill volume is thus in the same height level as the upper horizontal edge of the orifice. Therefore, when the tank is with 50% and higher fill volumes, the baffle orifice can be completely merged in the liquid cargo, and the top solid part of the baffle could prevent the liquid surface from the longitudinal motion.

The idea of baffle 'B4' is to seek the possibility of maintaining the baffle's anti-slosh effectiveness while cutting down on the baffle weight to obtain the benefit of increased payload capacity. To meet this goal, the ratio of the opening area is designed to be 50% and the opening is located in the lower part of the baffle, as illustrated in Figure 4.3d. In a fashion similar to baffle 'B3', the baffle bottom horizontal edge passes through the center of gravity of the tank cross section. The baffle curvature also remains the same as those of baffles 'B1' to 'B3'. Baffle 'B5' has a longer extrusion in the longitudinal direction due to its conical shape, as shown in Figure 4.2b, which is designed to achieve more effectiveness of slosh suppression in the lateral direction. To compare with the conventional baffle 'B1', baffle 'B5' possesses the same size circular orifice and equalizer, and the same orifice location as those of baffle 'B1'.

Furthermore, the baffle design factors, including effects of baffle equalizer and baffle opening area ratio, have also been investigated in the present dissertation research. The influence of baffle equalizer was studied by comparing the simulation results within the single-orifice baffled tank configuration equipped with and without the equalizers but

for the identical baffle opening area ratio of 12%. The effect of baffle opening was analyzed in a tank equipped with single-orifice baffles of the opening area ratios ranging from 4% to 20%.

## 4.3 SIMULATION MATRIX

The heavy tank vehicles are usually used to transport various fluid cargos. The fill volumes of fluid cargos thus vary due to the difference in the density and the payload regulation for a given vehicle. Analyses of dynamic fluid slosh within tanks with different fill volumes at the load capacity are thereby essential for the study of dynamic responses of road tank vehicles. In this study, three different liquids, sulfuric acid, dichloromethane and water are considered as fluid cargos such that their respective fill volumes of 38.1%, 52.1% and 69.5% of the total tank volume corresponding to the load limit (16400 kg) of the tank truck shown in Figure 4.1. Table 4.1 summarizes the properties of the three fluids which are notated as 'C1', 'C2' and 'C3', respectively.

Table 4.1. The properties of fluid cargos considered for the analysis of dynamic fluid slosh under different fill volumes corresponding to constant load.

| Fill volume | Fill depth (m) | Liquid cargo | Density ($kg/m^3$) | Viscosity (kg/m-s) |
|---|---|---|---|---|
| 38.1% | 0.633 | Sulfuric acid ('C1') | 1826.3 | 0.0255 |
| 52.1% | 0.85 | Dichloromethane ('C2') | 1326 | 0.00044 |
| 69.5% | 1.142 | Water ('C3') | 998.2 | 0.001003 |

The liquid slosh was analyzed under four types of maneuvers: steady turning, straight-line braking, steady turn-in-brake and lane-change. Steady turning and straight braking could be represented by ramp step acceleration input, while steady turn-in-brake could be represented by combination of two ramp step acceleration inputs in lateral and longitudinal directions. The lane-change could be represented by a lateral single-cycle sinusoidal acceleration input. Tables 4.2 and 4.3 show the details of the input functions applied to simulate the slosh within the three conventional tank configurations 'T0', 'T1' and 'T2'. The steady turning was simulated for 0.25g and 0.4g lateral ramp-step acceleration, while the braking maneuver was simulated for 0.3g and 0.6g longitudinal ramp-step acceleration. The brake-in-a-turn maneuver was simulated for three combinations of lateral and longitudinal ramp-step acceleration magnitudes: (0.25g, 0.6g), (0.4g, 0.6g) and (0.4g, 0.3g). The rise time is set at 0.5 s for all ramp-step acceleration

Table 4.2: The simulation excitations considered for the three regular tank configurations ('T0', 'T1' and 'T2') with the constant cargo payload.

| Type of excitation | Accel. applied | Steady turning | | Braking | | Brake-in-a-turn | | |
|---|---|---|---|---|---|---|---|---|
| Ramp-step | $a_y$ (g) | 0.25 | 0.4 | 0 | 0 | 0.25 | 0.4 | 0.4 |
| | $a_x$ (g) | 0 | 0 | 0.3 | 0.6 | 0.6 | 0.6 | 0.3 |

inputs. The simulations of lane-change maneuver were conducted for the single-cycle sinusoidal acceleration at 0.3 Hz and 0.4 Hz frequencies and 0.25g and 0.4g acceleration magnitudes. Since long computation time is required for 'T2' tank due to fine mesh of complex computation domain, only the extreme cases of maneuvers are simulated for that

tank, which include the ramp-step accelerations ($a_y$, $a_x$) of (0, 0.4g), (0.6g, 0) and (0.6g, 0.4g), and single-cycle sinusoidal acceleration at 0.4g magnitude and 0.4 Hz.

Table 4.3: The lane-change maneuvers considered for conventional tank configurations ('T1', 'T2' and 'T3') with the constant cargo payload.

| Excitation | $f$(Hz) | $a_y$(g) | |
|---|---|---|---|
| | | 0.25 | 0.4 |
| Single-sine | 0.3 | √ | √ |
| | 0.4 | √ | √ |

Since baffles 'B3', 'B4' and 'B5' are used to evaluate the influence of design factors on anti-slosh effectiveness, the slosh analyses of these baffles are performed to permit the comparison to the conventional tank configurations under the most interested conditions. The analysis of baffles 'B3' and 'B4' is focused on the intermediate and high fill volumes (52.1% and 69.5%), while the maneuvers are limited to the longitudinal ramp-step accelerations of 0.3g and 0.6g. Since the conical baffle 'B5' is designed for suppressing the lateral fluid slosh, its analysis is focused on high magnitude lateral ramp-step acceleration (0.4g) and single-cycle sinusoidal accelerations (0.25g at 0.3 Hz and 0.5 Hz), for intermediate and high fill volumes (52.1% and 69.5%).

Considering that single-orifice baffles are common in operation, the influences of baffle opening ratio and equalizer on slosh are studied for a tank equipped with this type of baffles. Each of the three baffle opening area ratios (4%, 12%, and 20%) are evaluated for the liquid cargos with the intermediate (52.1%) and high (69.5%) fill volumes under 0.3g and 0.6g longitudinal ramp-step acceleration excitations. The effect of equalizer is

studied for fluid cargo 'C2' with the intermediate fill volume (52.1%) under 0.3g longitudinal ramp-step excitation.

## 4.4 ANALYSIS METHOD

The simulations of fluid slosh under the above conditions are performed with the CFD VOF model developed and validated in Chapter 3. The dynamic slosh responses are analyzed in terms of the slosh frequency, slosh forces and moments. As described in Section 3.2, the sloshing forces are calculated by integrating the pressure distribution over the wetted tank and baffle boundaries, while the slosh moments are computed by integrating the product of force vectors and position vectors. The slosh natural frequencies are derived from the frequency spectrum analysis of the resulting horizontal slosh force in the tanks during free fluid slosh. The analysis is performed under different fill volumes and different directional modes. The free slosh simulations start with the condition that the ramp-step excitation simulations are terminated.

### 4.4.1 Parameters of Fluid Slosh

A disturbed fluid is known to settle down to a steady state, which may be different depending on the excitation type. The steady state of fluid slosh under a ramp-step acceleration excitation is linearly dependent upon the acceleration magnitude which can be derived from the quasi-static method (QS), while it returns back to the static state when the excitation is single-cycle acceleration. The amplification factor can be identified when the transient slosh behavior is analyzed in association with the steady-state. The responses of slosh forces and moments, under the ramp-step acceleration

excitations, are thus analyzed in terms of the ratio of the peak values to the steady-state values which are derived by time-averaging the transient values, and are equivalent to the QS solutions. For the single-cycle sinusoidal acceleration excitations, since the steady-state horizontal forces are zero, the peak slosh forces and moments are normalized by the values of the equivalent rigid cargo. The origin of the coordinate reference used in the study is located at the tank base centre, as shown in Figure 4.4a. Considering that the transient peaks of slosh parameters occur in the first few seconds of maneuvers (<10 s), the simulations were performed for 20 seconds for each maneuver.

The amplification factors of slosh forces ($M_{Fy}$, $M_{Fx}$ and $M_{Fz}$) and moments ($M_{Mx}$, $M_{My}$ and $M_{Mz}$) under lateral ramp-step excitations are defined as:

$$M_{Fy} = \frac{F_{y,Max}}{F_{y,QS}};\ M_{Fi} = \frac{F_{i,Max}}{mg} \quad (i=x, z) \tag{4.1}$$

$$M_{Mi} = \frac{M_{i,Max}}{M_{x,QS}} \quad (i=x, y, z) \tag{4.2}$$

where, $F_{i,Max}$ ($i$=$x$,$y$,$z$) are the maximum transient slosh forces in longitudinal, lateral and vertical directions. $M_{i,Max}$ ($i$=$x$,$y$,$z$) are the maximum transient slosh roll, pitch and yaw moments. $F_{y,QS}$ and $M_{x,QS}$ are the mean lateral force and roll moment, respectively, calculated in the steady-state range of the slosh, representing the QS estimations. $m$ is the mass of liquid cargo.

For the longitudinal ramp-step excitations, the amplification factors of slosh forces ($M_{Fy}$, $M_{Fx}$ and $M_{Fz}$) are defined as:

$$M_{Fx} = \frac{F_{x,Max}}{F_{x,QS}};\ M_{Fi} = \frac{F_{i,Max}}{mg} \quad (i=y, z) \tag{4.3}$$

Since the transient pitch moment does not show a peak during the longitudinal ramp-step excitations, the slosh pitch moments are not evaluated in the form of amplification, instead their transient behavior is analyzed.

Under the lateral single-cycle excitations, the amplification factors of slosh forces ($M_{Fy}$, $M_{Fx}$ and $M_{Fz}$) and moments ($M_{Mx}$, $M_{My}$ and $M_{Mz}$) are defined as:

$$M_{Fy} = \frac{F_{y,Max}}{F_{y,RP}};\ M_{Fi} = \frac{F_{i,Max}}{mg} \quad (i=x, z) \tag{4.4}$$

$$M_{Mi} = \frac{M_{i,Max}}{M_{x,RP}} \quad (i=x, y, z) \tag{4.5}$$

where, $F_{y,RP}$ and $M_{x,RP}$ are the peak lateral force and roll moment, respectively, yielded by the equivalent rigid cargo, which can be calculated as:

$$F_{y,RP} = m(a_P) \tag{4.6}$$

$$M_{x,RP} = m(a_P)(\bar{h}_{cg}) \tag{4.7}$$

where, $a_P$ is the magnitude of acceleration. $\bar{h}_{cg}$ is the *cg* height of the equivalent rigid cargo.

### 4.4.2 Mesh Refinement

The CFD simulation could be influenced by the mesh size in certain range. Therefore, it is important to select the mesh size, such that the simulation results are least sensitive to it. Assessment of mesh independence is thus conducted for the different tank configurations with the VOF fluid slosh model, as described in Chapter 3. The analyses were performed under the simultaneous lateral and longitudinal ramp-step excitation of high magnitudes, 0.4g and 0.6g, respectively. Three mesh sizes were evaluated for the

tank configurations 'T0', 'T1' and 'T2', as shown in Table 4.4. The hexahedral shape is selected as the cell shape for the meshes of tanks 'T0' and 'T1', while the computation domain of tank 'T2' is discretized with pentahedral wedge cells.

Table 4.4. The total number of cell for three meshes considered for the mesh independence assessment

| Tank | Grid-1 | Grid-2 | Grid-3 |
|---|---|---|---|
| T0, T1 | 32,498 | 75,038 | 126,199 |
| T2 | 53,810 | 140,444 | 285,010 |

Figure 4.5 illustrates the transient fluid slosh forces in tank 'T1' obtained from the three different meshes: (*i*) 32,498 (Grid-1); (*ii*) 75,038 (Grid-2); (*iii*) 126,199 (Grid-3). The simulations were performed for the tank with 50% fill volume of water and subject to the simultaneous 0.4g lateral and 0.6g longitudinal ramp step excitation. The figure shows that the slosh forces obtained from the three grids are in very close agreement, with negligible difference in peak and mean values, as well as the magnitude variation trends. It suggests that the coarse mesh with 32,498 cells (Grid-1) can generate reasonable mesh-independent results for the baffled 'T1' tank. Meshing of the unbaffled tank 'T0' can be readily achieved using the grids built for the baffled tank 'T1' by re-defining the wall faces of baffles as the interior faces. Analysis of mesh independence also shows that the Grid-1 is appropriate for the numerical calculations of fluid slosh in tank 'T0'.

Analysis of mesh independence for tank 'T2' is conducted for three different fine meshes, as listed in Table 4.4, due to the complexity of baffle geometry. Figure 4.6 shows

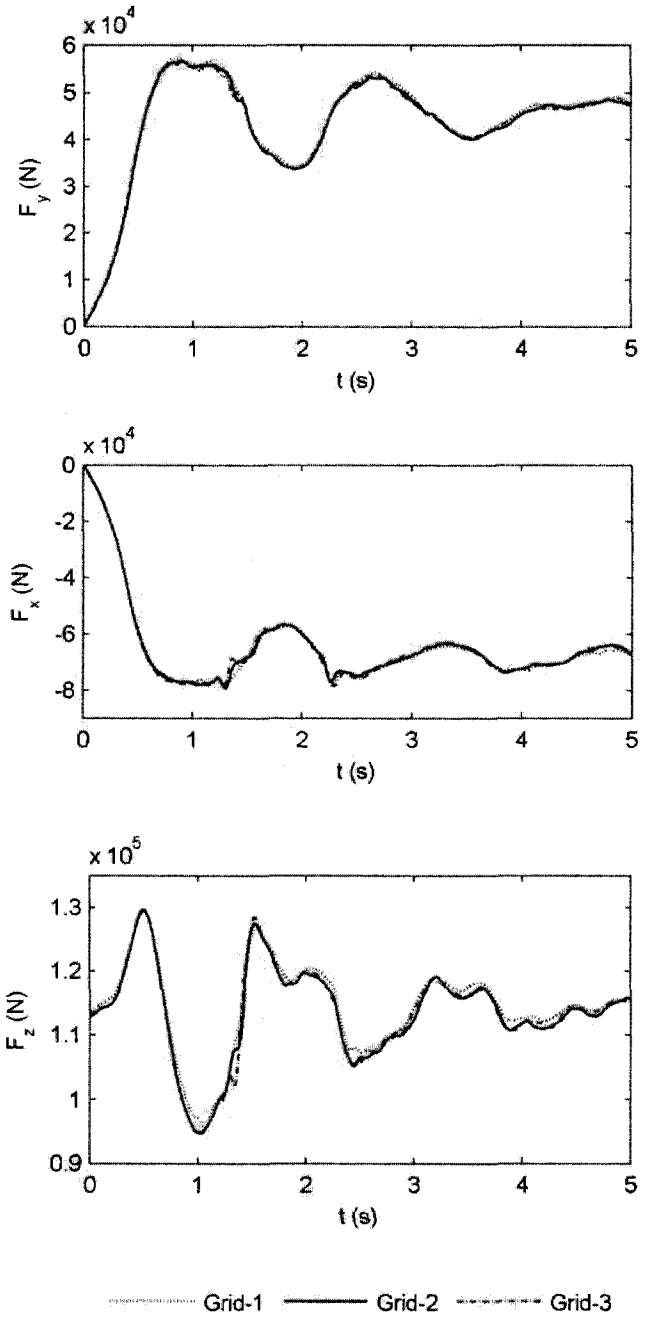


Figure 4.5: Comparison of simulation results attained using different discretization grids of the computation domain of the baffled 'T1' tank with 50% fill volume of water. (a) lateral force ($F_y$); (b) longitudinal force ($F_x$); (c) vertical force ($F_z$).

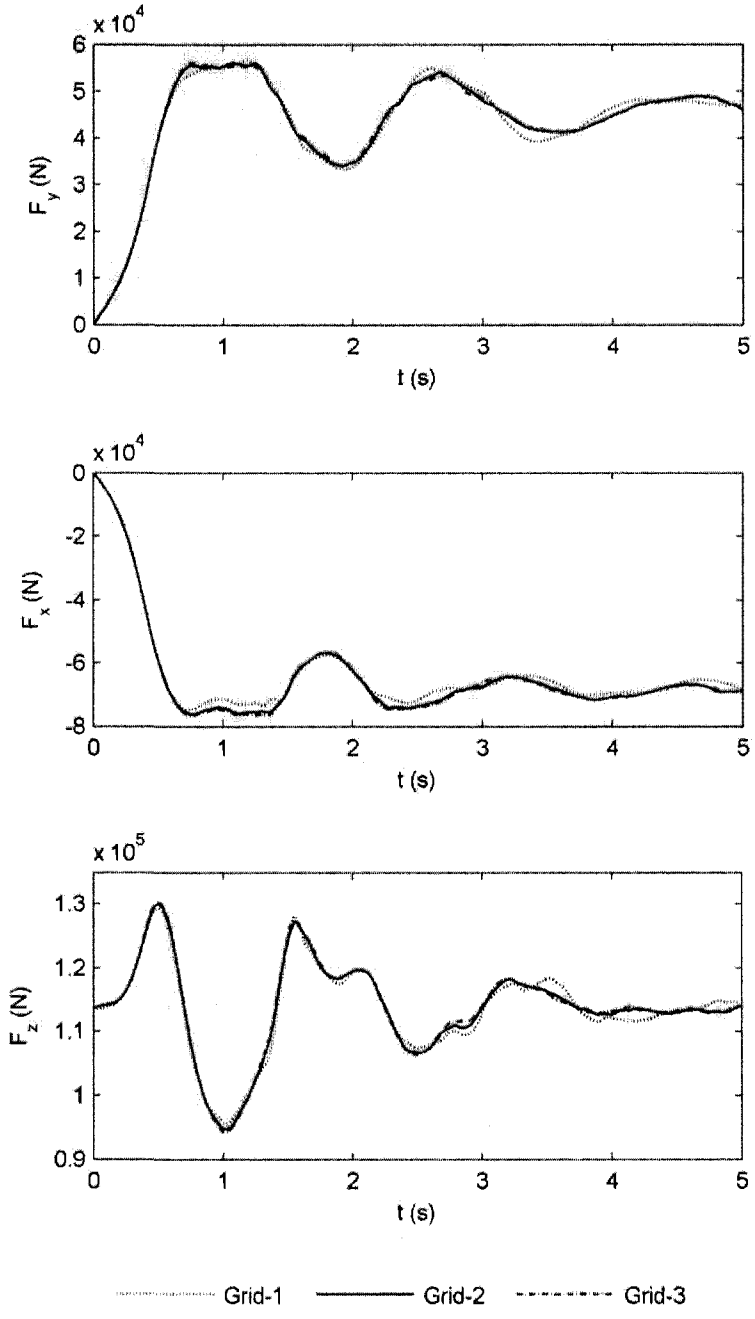


Figure 4.6: Comparison of simulation results attained using different discretization grids of the computation domain of the baffled 'T2' tank with 50% fill volume of water. (a) lateral force ($F_y$); (b) longitudinal force ($F_x$); (c) vertical force ($F_z$).

the slosh force obtained from the simulations in tank 'T2' for three size grids considered: (*i*) 53,810 (Grid-1); (*ii*) 140,444 (Grid-2); (*iii*) 285,010 (Grid-3). The simulations are performed with 50%-filled water subject to the same excitation as that used for the analyses of tanks 'T0' and 'T1'. The figure shows that Grid-2 and Grid-3 yield virtually identical results of transient slosh forces, while some deviations are observed for the coarsest mesh Grid-1. The results for Grid-1 show a slightly higher slosh frequency in the lateral force, and slightly smaller magnitudes of the longitudinal force. A slight deviation is also observed in the vertical force around t=4 s, compared to the results based on the finer meshes (Grid-2 and Grid-3). Thus, Grid-2 has been selected for the slosh simulation in tank 'T2'. The same mesh size is also used for tanks 'T3' to 'T5'.

## 4.5 ANALYSIS OF FLUID SLOSH

The slosh simulations have been conducted for the three regular tank configurations 'T0', 'T1' and 'T2' with three fill volumes (see Table 4.1), and subjected to a wide range of excitations, as shown in Tables 4.2 and 4.3. The slosh characteristics under these conditions are analyzed in terms of the natural frequency, slosh forces and moments.

### 4.5.1 Natural Frequency

The fundamental natural frequencies of fluid slosh in the lateral and longitudinal directions were computed from the frequency spectra with the resolution 0.0153 Hz of the slosh forces arising from the free slosh. The spectra invariably revealed a single dominant peak and the frequency corresponding to this peak was considered as the fundamental slosh natural frequency. Figure 4.7 presents the fundamental natural

frequencies in both lateral and longitudinal directions derived from the fluid slosh simulations for the un-baffled cleanbore tank ('T0'). As expected, the results show that a higher fill volume invariably yields a higher fundamental slosh natural frequency, irrespective of the direction. The lateral mode frequency ranges from 0.53 Hz to 0.67 Hz for fill volume from 38.1% to 69.5%, while the longitudinal mode frequency is considerably lower (0.17-0.23 Hz) due to significantly larger length of the tank compared to its width.

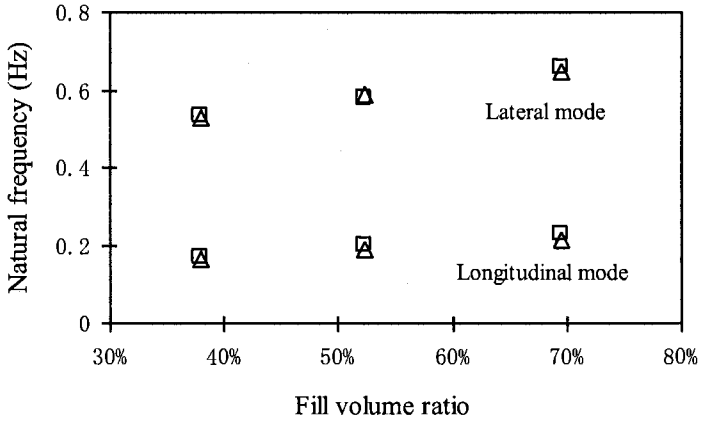


Figure 4.7: Comparisons of the fundamental slosh natural frequencies derived from the simulation and analytical calculation for the cleanbore tank ('T0') with different fill volumes (□, simulated; Δ, calculated).

In Figure 4.7, the simulation results are also compared with the slosh natural frequencies derived from the analytical calculations based on the free surface wavelength [13]. It is observed that the simulation results agree reasonably well with the analytical calculations for all fill volumes considered. The difference is less than 2% and 8% for the lateral and longitudinal modes, respectively. This agreement also serves as a validation of the CFD model in predicting fluid slosh within the full scale tanks.

Figure 4.8 shows the comparison of the fundamental natural frequencies of lateral and longitudinal fluid slosh in the cleanbore 'T0' and the baffled 'T1' tanks with different fill volumes. The baffled 'T2' tank is not included in this figure because the results exhibit identical frequency as that of the 'T1' tank, which is consistent with the experiment results discussed in Chapter 2. The results show that the lateral mode fundamental natural frequencies of both 'T0' and 'T1' tanks are almost identical for all three fill volume (Figure 4.8a), while the longitudinal mode frequencies for the baffled tank ('T1') are significantly higher than those of the cleanbore tank ('T0') for any given fill level (Figure 4.8b). The slosh frequencies of 'T1' tank are 3.7, 3.3 and 3.0 times those of 'T0' tank for 38.1%, 52.1% and 69.5% fill volumes, respectively. This trend is also observed in the experimental results with the scaled tanks, as discussed in Chapter 2. However, the variation of slosh frequency with the fill volume exhibits the same trend for both baffled and cleanbore tanks, that is, the fundamental natural frequency increases with the fill volume.

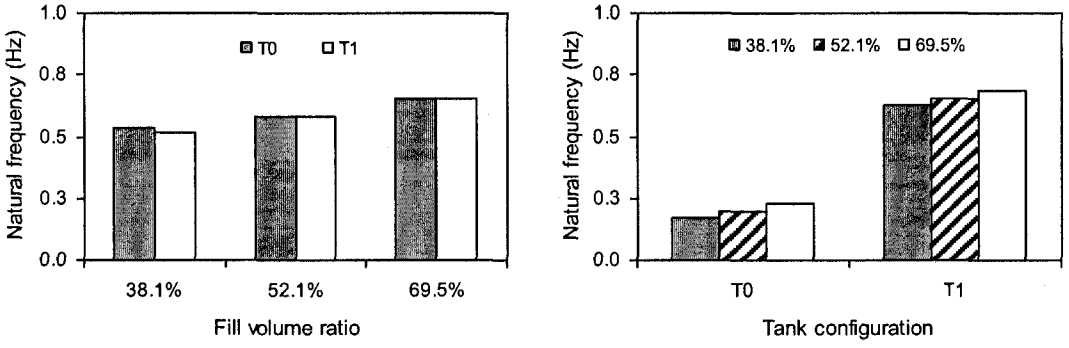


Figure 4.8: Comparisons of the fundamental natural slosh frequencies in the un-baffled 'T0' tank and the baffled 'T1' tank for different fill volumes: (a) lateral mode; (b) longitudinal mode.

### 4.5.2 Magnitudes of Slosh Forces and Moments

The fluid slosh simulations are conducted for tanks 'T0', 'T1' and 'T2' with three different fill volumes (38.1%, 52.1% and 69.5%) at a constant load. Fluid slosh responses are analyzed for four different types of excitations: (*i*) lateral ramp-step acceleration; (*ii*) longitudinal ramp-step acceleration; (*iii*) simultaneous lateral and longitudinal ramp-step accelerations; and (*iv*) lateral single-cycle sinusoidal acceleration. The four excitations permit for analysis of dynamic fluid slosh behavior in the tanks under steady-turning, braking, braking-in-turn and path change maneuvers, respectively.

**(1) Lateral Ramp-step Excitation**

Two lateral ramp-step acceleration excitations (0.25g and 0.4g) are considered for the analysis of fluid slosh responses. Figure 4.9 illustrates the peak amplification factors of the slosh forces in the cleanbore 'T0' tank and the baffled 'T1' and 'T2' tanks under the two excitations for fill volumes of 38.1%, 52.1% and 69.5%. The results show that a lower fill volume tends to yield larger peak amplification factors of lateral, longitudinal and vertical slosh forces, irrespective of the tank configuration and excitation magnitude. This is consistent with the experimental results for the scaled tanks previously discussed in Chapter 2.

The results also show that the peak lateral and vertical forces for the three tanks are of comparable magnitudes when filled with the same cargo and under the same excitation, suggesting that the baffles have negligible influence on these slosh force components when the tank is subjected to lateral ramp-step acceleration excitations. The results under the excitations of different magnitudes show that at the higher magnitude

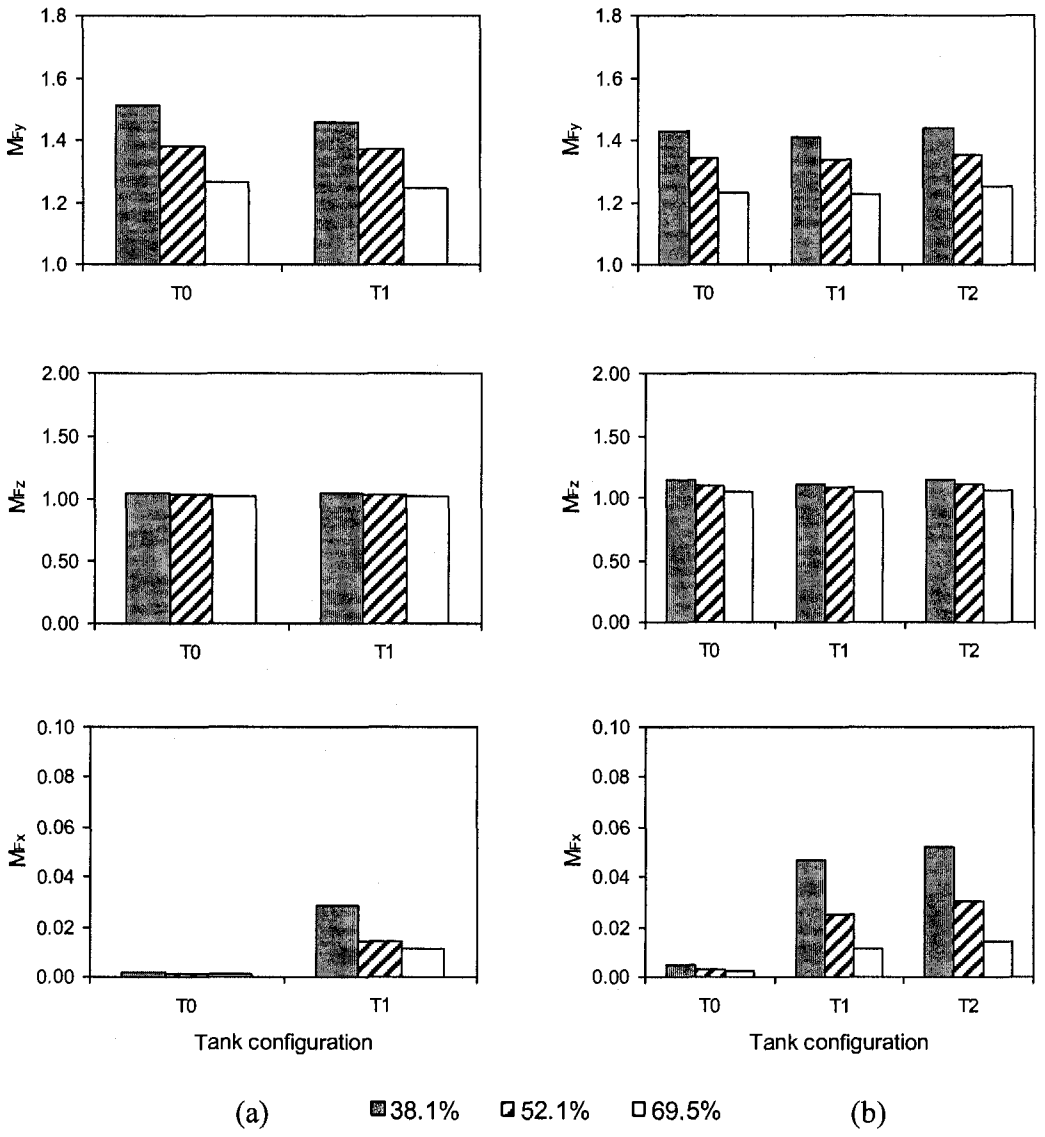


Figure 4.9: Peak amplification factors of lateral ($M_{Fy}$), longitudinal ($M_{Fx}$) and vertical ($M_{Fz}$) forces versus tank configurations for different fill cargos under pure lateral ramp-step excitations: (a) $a_y$=0.25g; (b) $a_y$=0.4g.

excitation (0.4g), the peak lateral force amplification factor is slightly smaller than that at the smaller magnitude excitation (0.25g), while the case is opposite for the peak vertical amplification factor. This is due to the reason that the amplification factor of lateral slosh force is attained from the normalization with respect to the QS estimation, which is linearly proportional to the acceleration, whereas the vertical force is normalized by the constant cargo weight. In dimensional form, however, the absolute lateral and vertical forces are obviously larger for the higher excitation magnitude. It is seen that the peak lateral force amplification factor approaches 1.51 for the cleanbore 'T0' tank with 38.1% fill volume and subjected to the lower excitation (0.25g), while it is slightly smaller (1.43) for the higher magnitude excitation (0.4g).

The results in Figure 4.9 further shows that the peak longitudinal slosh force amplification factor ($M_{Fx}$) is significantly small for all the three tanks considered, which is less than 0.06 for both the two excitations, suggesting that the slosh is predominantly a two dimensional phenomena under the given lateral excitations. Although in small magnitude, the longitudinal slosh force is relatively larger in the baffled 'T1' and 'T2' tanks than the unbaffled 'T0' tank, suggesting that the baffle curvature may induce the slosh motion in the longitudinal direction.

The responses of peak amplification factors of roll, pitch and yaw moments under the same excitations are illustrated in Figure 4.10. The results show that the three moments exhibit the same fill-volume dependency as the slosh forces. The peak roll moment amplification factors ($M_{Mx}$) are comparable for the three tanks with the same fill volume and excitation. Comparison of Figures 4.9 and 4.10 shows that the peak roll

moment amplification factor ($M_{Mx}$) is slightly higher than the peak lateral force amplification factor ($M_{Fy}$) for a given tank under the same fill volume and excitation. Under the lower fill volume (38.1%) and lower magnitude excitation (0.25g), $M_{Mx}$ approaches 1.57 for the cleanbore 'T0' tank, while $M_{Fy}$ is approximately 1.51. The figure also shows that the peak pitch ($M_{My}$) and yaw moment ($M_{Mz}$) amplification factors are significantly small, compared to $M_{Mx}$. Comparison of the results for different tank configurations shows that the higher peak pitch and yaw moments are yielded in the baffled 'T1' and 'T2' tanks compared to that in the unbaffled 'T0' tank, which is due to the longitudinal slosh induced by the baffle curvature.

As a summary, it can be concluded that when a tank is subjected to lateral ramp-step excitation, the lateral slosh force and the corresponding roll moment are significantly amplified, and are almost the same for baffled and un-baffled tanks. Fill volume has shown to influence the amplifications of almost all components of slosh force and corresponding moments. The amplifications of slosh forces and moments increase with a decrease in the fill volume.

**(2) Longitudinal Ramp-step Excitation**

The slosh responses to longitudinal ramp-step accelerations can be used to represent the dynamic fluid slosh behavior in straight-line braking maneuvers. In the present study, the slosh analyses are performed under two longitudinal ramp-step acceleration excitations (0.3 and 0.6g). Figure 4.11 presents the peak amplification factors of lateral and vertical slosh forces arising from different tank configurations for three fill volumes under the two excitations. The lateral force is not shown in the figure due to its significantly small

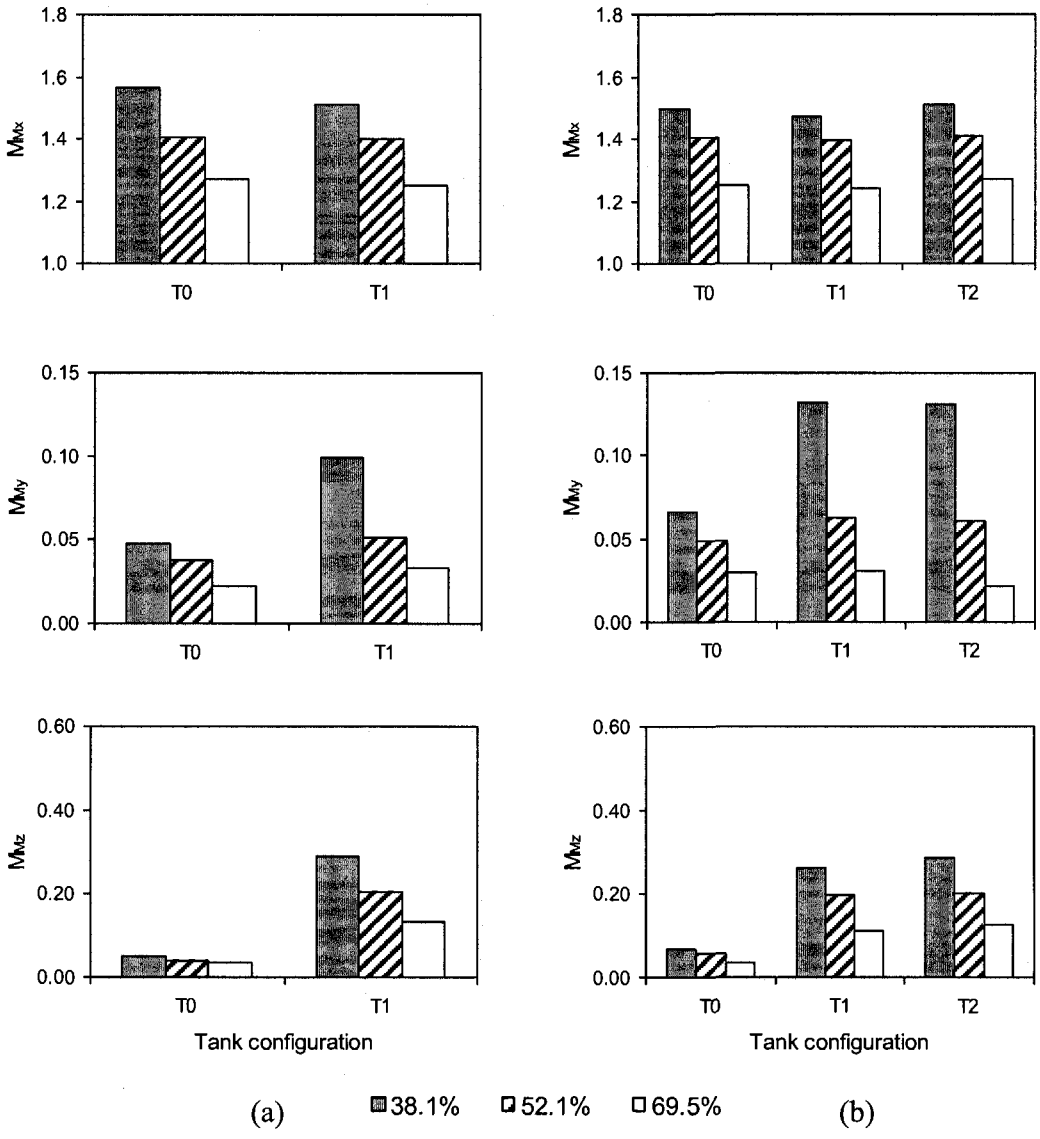


Figure 4.10: Peak amplification factors of roll ($M_{Mx}$), pitch ($M_{My}$) and yaw ($M_{Mz}$) moments versus tank configurations for different fill cargos under pure lateral ramp-step excitations: (a) $a_y$=0.25g; (b) $a_y$=0.4g.

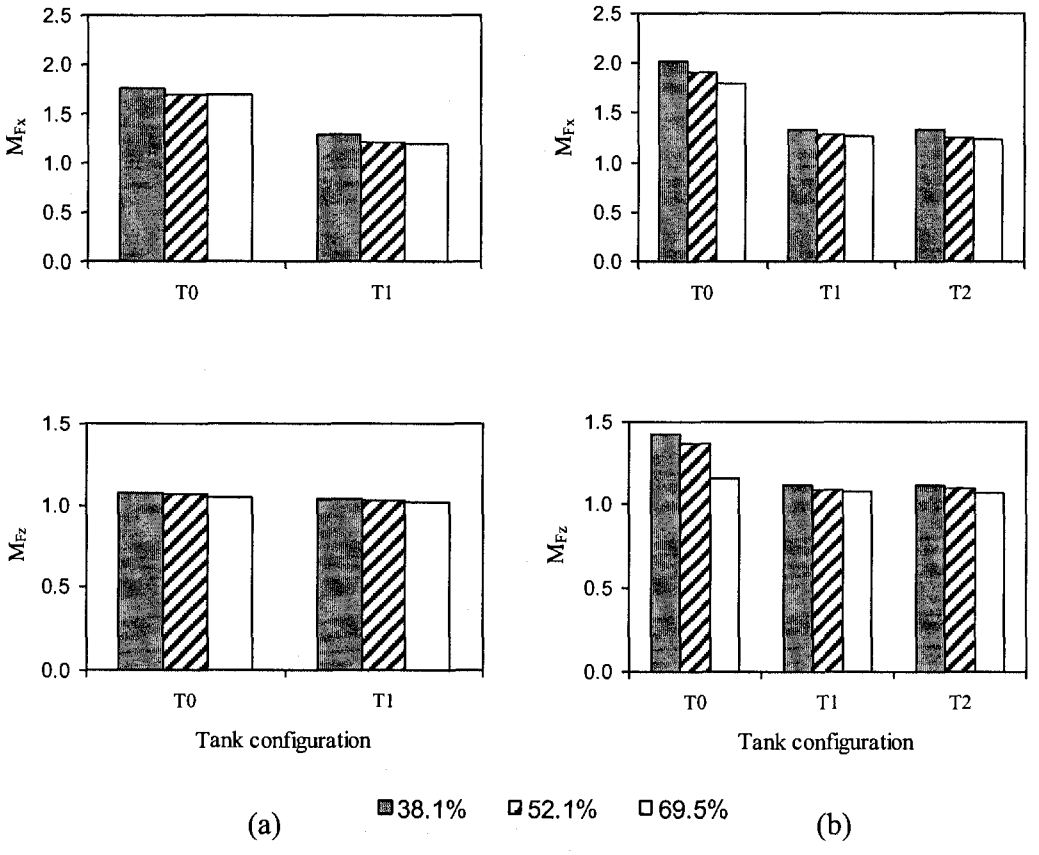


Figure 4.11: Peak amplification factors of longitudinal force ($M_{Fx}$) and vertical force ($M_{Fz}$) versus tank configurations for different fill cargos under pure longitudinal ramp-step excitations: (a) $a_x$=0.3g; (b) $a_x$=0.6g.

magnitude compared to the other two components. The results show that cargo with lower fill level invariably yields higher peak slosh forces than the liquid cargo with higher fill level, which is similar to that observed under lateral ramp-step excitations. The figure further shows that the longitudinal and vertical slosh forces are considerably smaller in the baffled 'T1' and 'T2' tanks than those in the unbaffled 'T0' tank for a given excitation magnitude and fill volume. At 38.1% fill volume under 0.6g excitation, the magnification of the longitudinal and vertical forces reduced from 2.02 and 1.42 in

the un-baffled 'T0' tank to 1.23 and 1.12 in the baffled 'T1' tank, respectively. The reduction rates are 39.1% and 21.1%, respectively. This suggests that the addition of baffles could effectively suppress the longitudinal slosh force.

Comparison of the results for the two baffled tanks ('T1' and 'T2') shows no significant difference in the peak amplification factors of longitudinal and vertical forces ($M_{Fx}$ and $M_{Fz}$), indicating an equivalent effectiveness of the two baffle designs on the slosh suppression. The results of the unbaffled 'T0' tank show that the peak longitudinal force amplification factor is larger under a higher magnitude excitation, which is not consistent with the results of peak lateral slosh force amplification factor observed for the same tank in the lateral ramp-step excitation (Figure 4.9). The results of the baffled tank 'T1' show a similar trend as that illustrated in Figure 4.9. Due to the long tank length, the boundary effect of tank walls in the pitch plane is less evident, thus causing significantly large slosh. Since the baffle spacing is close to the tank width, the boundary effect of the baffles in the pitch plane is almost equivalent to that of the tank walls in the roll plane.

The transient slosh pitch moment in the tanks with the intermediate fill volume (52.1%) under the same excitations are illustrated in Figure 4.12. The results for tank 'T0' under the lower magnitude excitation (0.3g) show oscillations with a frequency of 0.2 Hz which is the same as the slosh resonant frequency. Under the higher excitation (0.6g), the results of tank 'T0 show that the slosh pitch moment settles down rapidly after an overshoot around t = 2 s (Figure 4.10b). The recorded liquid surface motion shows that the slosh liquid hits one tank head with a strong impact and results in a large fluid free surface separation. This separated flow hits back to another tank head and bounced back into the main bulk flow, thus causing an abrupt increase of longitudinal force and

pitch moment. Owing to the large magnitude of the acceleration excitation, the flow settles down to the steady-state soon after this disturbance, with oscillations of small magnitude at a frequency considerably higher than that observed for the 0.3g excitation. This is due to the reason that the liquid free surface under the large longitudinal acceleration field becomes highly inclined. The liquid free surface length (i.e., fetch) thus is shorter than that under small magnitude excitation and thereby yields a relatively higher slosh frequency.

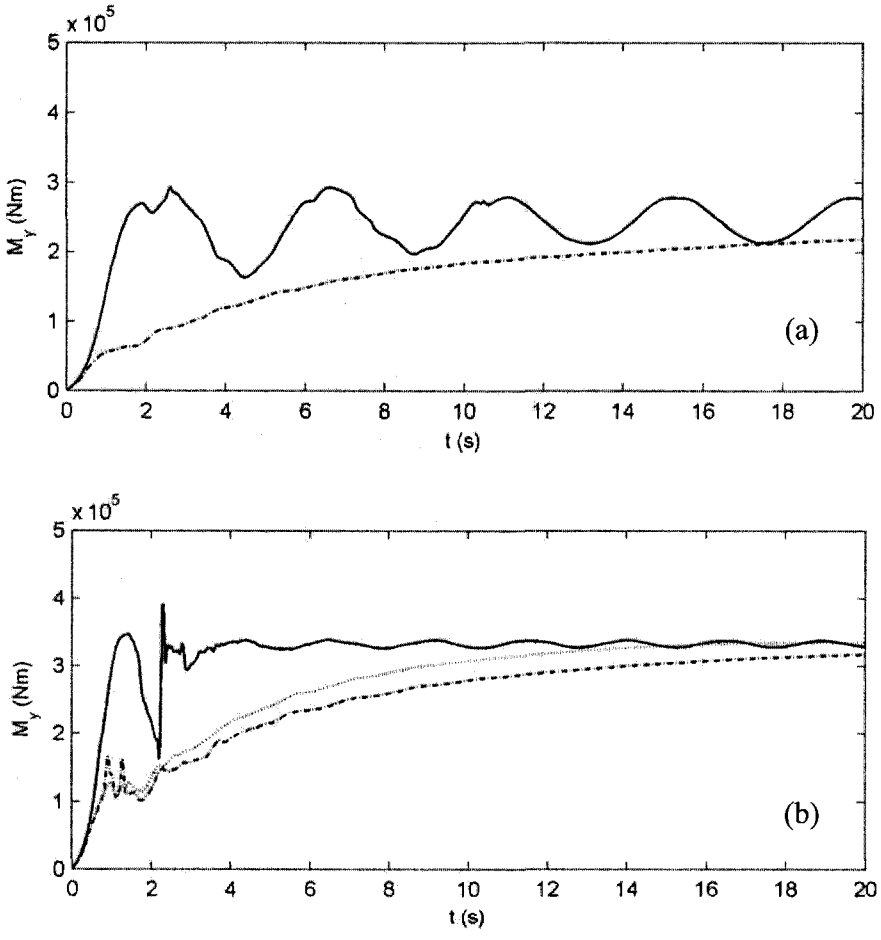


Figure 4.12: Comparison of slosh pitch moment yielded in the baffled and un-baffled tanks with 52.1%-filled dichloromethane ('C2') subject to pure ramp step accelerations: (a) $a_x = 0.3g$; (b) $a_x = 0.6g$. ——, 'T0' tank; –·–·–, 'T1' tank; ·····, 'T2' tank.

The pitch moment results for the baffled tanks 'T1' and 'T2' exhibit a slow increasing trend which asymptotically approaches the steady-state value practically without oscillations. The free surface results (not shown) reveal that due to the presence of baffles the liquid tends to accumulate gradually toward one end of the tank in the direction of acceleration, thus causing the asymptotical increment in the pitch moment. The steady-state, however, can not be observed for the limit time of simulation, which may need a considerably long time, particularly under the low magnitude excitation.

The results in Figure 4.12 also show that the magnitude of the slosh pitch moment in the baffled tanks 'T1' and 'T2' is much smaller than that in the unbaffled tank, especially during the first few seconds of excitations, indicating the effectiveness of baffles in slosh control. Comparison of the results for the two baffled tanks shows that the moment of tank 'T1' is slightly smaller than that of tank 'T2'. This is because the baffle part beneath the liquid free surface is more porous in the multiple-orifice baffle than in the single-orifice baffle and thus the cargo is more likely to permeate through the baffle. This suggests that the single-orifice baffle is slightly more effective than the multiple-orifice baffle in pitch moment suppression. The results also show that for a given tank and fill volume, the higher magnitude excitation (0.6g) yields larger pitch moment.

In summary, it can be concluded that when a tank is subjected to a longitudinal ramp-step acceleration, the longitudinal slosh force is significantly amplified for the cleanbore tank, while the presence of baffles can effectively reduces the amplification. The transient pitch moment shows oscillating behavior for the cleanbore tank, but asymptotical trend for the baffled tanks. The peak moment for the cleanbore tank is significantly larger than those for the baffled tanks, particularly during first few seconds

of excitations. The two baffles ('B1' and 'B2') have almost identical effectiveness in suppressing the longitudinal slosh force, however, the single-orifice baffle ('B1') can be more effective to reduce the pitch moment than the multiple-orifice baffle ('B2').

**(3) Combined Lateral and Longitudinal Ramp-step Excitation**

Fluid slosh characteristics under maneuvers of braking-in-turn can be analyzed using simultaneous lateral and longitudinal ramp-step acceleration excitations. The analysis of slosh responses under the excitations are conducted for three combinations of lateral and longitudinal ramp-step accelerations ($a_y$, $a_x$): (0.25g, 0.6g), (0.4g, 0.6g) and (0.4g, 0.3g), which are notated as Case-1, Case-2 and Case-3, respectively. Figure 4.13 illustrates the peak lateral and longitudinal force amplification factors for tanks 'T0' and 'T1' with three different fill volumes for excitations Case-1, 2 and 3. The results of baffled tank 'T2' are not included in the figure since they are comparable to those of baffled tank 'T1'. The results in Figure 4.13 show that under the combined excitations, the fluid slosh yields the same fill volume dependency of the peak lateral and longitudinal force amplification factors ($M_{Fy}$ and $M_{Fx}$) as previously shown for the pure single-axis acceleration excitations, irrespective of the tank configuration. The results also show that the addition of baffle can significantly reduce the peak longitudinal slosh force amplification factors ($M_{Fx}$) for a given fill volume, which is consistent with the results observed under the pure longitudinal excitation. The amplification factor $M_{Fx}$ for the unbaffled tank 'T0' with the low fill volume (38.1%) is 2.01, 2.00 and 1.72 for excitations Case-1 to Case-3, respectively, while the respective values are reduced by 41.5%, 42.8% and 28.2% for the baffled tank 'T1'. Furthermore, the peak lateral slosh force amplification factor ($M_{Fy}$) is

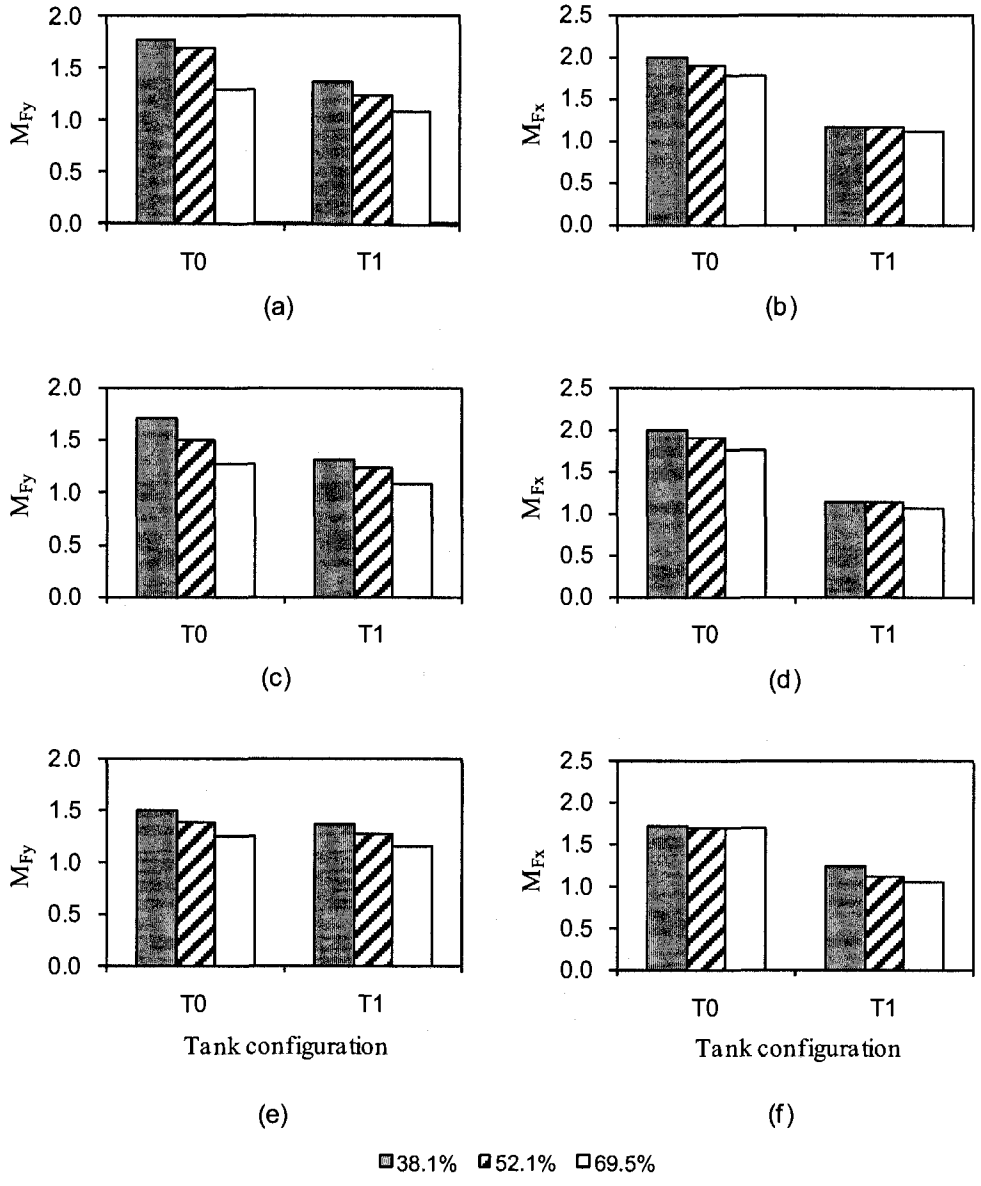


Figure 4.13: Peak amplification factors of lateral force ($M_{Fy}$), and longitudinal force ($M_{Fx}$) versus tank configuration with three different fill volumes under combined lateral and longitudinal ramp-step excitations: (a-b) Case-1; (c-d) Case-2; (e-f) Case-3.

also considerably reduced in the presence of baffles, particularly when the combined excitations involve a high magnitude longitudinal excitation (i.e., Cases-1 and 2), which is not observed in the results attained for the pure lateral excitations. This suggests that the baffles not only suppress the longitudinal slosh force, but also help in reducing the lateral slosh force. The reduction of $M_{Fy}$ is more evident at a lower fill volume where the slosh is more severe. $M_{Fy}$ factors for tank 'T0' with 38.1% fill volume are 1.79, 1.72 and 1.50 for excitations 'Case-1' to 'Case-3', respectively, while the respective values are decreased by 28.8%, 30.1% and 9.8% for tank 'T1'.

The peak amplification factors of all three force components at the low fill volume (38.1%) under the three excitation cases for tanks 'T0' and 'T1' are shown in Figure 4.14. This is the fill volume under which a more severe slosh is observed as compared to other two fill volumes. The results show that Case-1 yields higher amplification in lateral and vertical forces than Case-2 for the cleanbore tank ('T0'), while the longitudinal force is practically the same due to the identical longitudinal acceleration for the two cases. This indicates that in a brake-in-turn maneuver, the less turning centrifugal acceleration but identical braking effort could generate higher amplification in lateral and vertical forces for the cleanbore tank, although the absolute values increase with an increase of the excitation magnitude. The results further show that Case 2 generates higher amplification in all three force components than Case-3 for tank 'T0', suggesting that in a brake-in-turn maneuver, higher braking effort but identical turning centrifugal acceleration may give rise to higher amplification in the lateral, longitudinal and vertical slosh forces ($M_{Fy}$, $M_{Fx}$ and $M_{Fz}$). The amplification factors $M_{Fy}$, $M_{Fx}$ and $M_{Fz}$ for the baffled 'T1' tank, however, exhibit small variations with the

excitations, suggesting that the amplification factors of slosh forces under the three combined excitations are comparable, and lower than that in the cleanbore tank under similar condition.

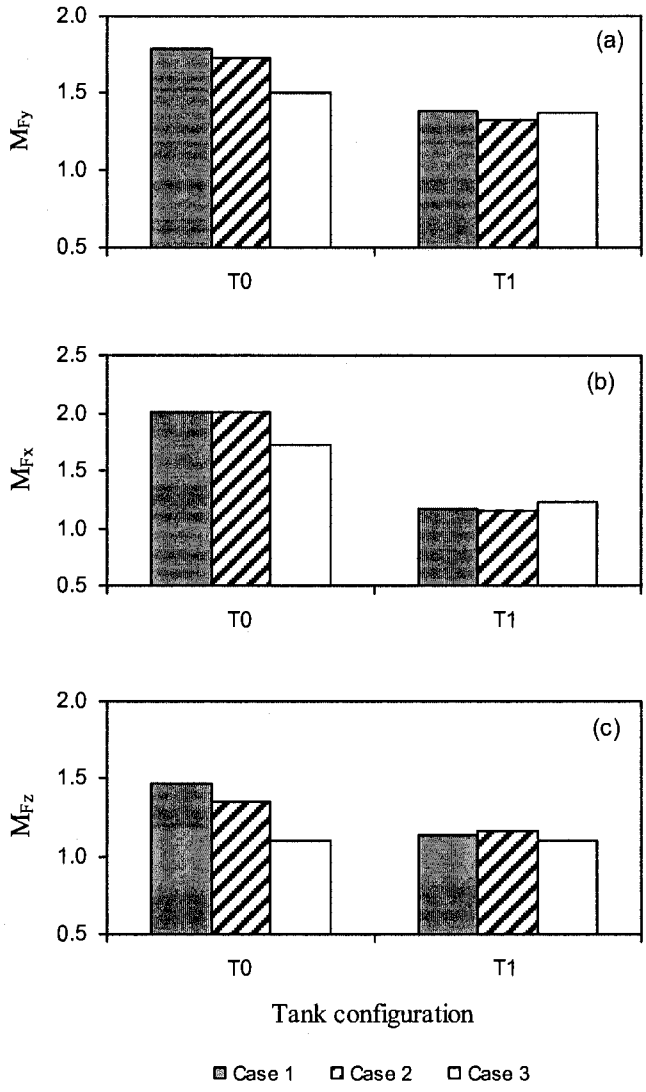


Figure 4.14: Peak amplification factors of lateral force ($M_{Fy}$), and longitudinal force ($M_{Fx}$) and vertical force ($M_{Fz}$) versus tank configurations with the low fill volume (38.1%) under combinations of different lateral and longitudinal ramp-step excitations ($a_y$, $a_x$): (a) Case-1 (0.25g, 0.6g); (b) Case-2 (0.4g, 0.6g); (c) Case-3 (0.4g, 0.3g).

Figure 4.15 illustrates the peak roll amplification factor ($M_{Mx}$) for tanks 'T0' and 'T1' at the low fill volume (38.1%) under the three excitation cases. The results exhibit a trend similar to that of the lateral slosh force shown in Figure 4.14*a*. For a given combined excitation, the baffled tank 'T1' yields lower $M_{Mx}$ than the unbaffled tank 'T0', suggesting that the transverse baffle can considerably suppress the peak roll moment under a braking-in-turn manoeuvre. The results for the cleanbore tank show that excitation 'Case-2' yields lower $M_{Mx}$ than 'Case-1' due to a larger normalization factor, while it generates higher $M_{Mx}$ than 'Case-3' when the two excitations have the same lateral acceleration component, suggesting a larger longitudinal slosh can help reduce the lateral slosh. The results for the baffled tank, however, show small variations of $M_{Mx}$ with the excitations and this trend is not obvious.

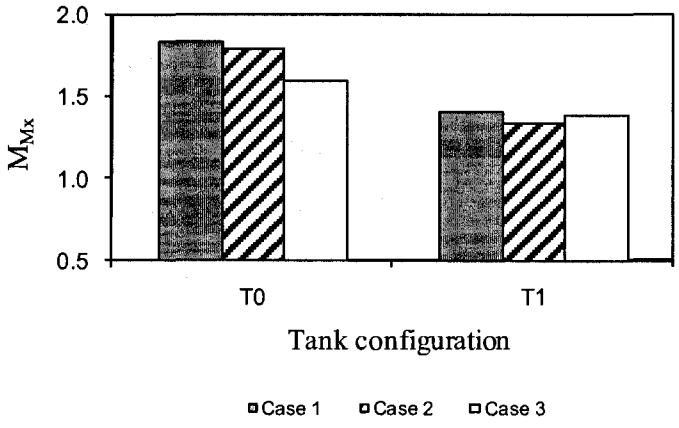


Figure 4.15: Peak amplification factors of roll moment ($M_{Mx}$) versus tank configurations for tanks 'T0' and 'T1' with the low fill volume (38.1%) subject to combinations of different lateral and longitudinal ramp-step excitations ($a_y$, $a_x$): (a) Case-1 (0.25g, 0.6g); (b) Case-2 (0.4g, 0.6g); (c) Case-3 (0.4g, 0.3g).

The transient slosh moment responses to the combined excitations are shown in Figure 4.16, which depicts the time-histories of transient roll, pitch and yaw moments for the baffled tank 'T1' with the low fill volume (38.1%). The results of roll moment ($M_x$) show variations with dampened magnitudes and about constant steady-state values at all three excitations. The mean values of variations (i.e., steady-state values) are practically identical for Cases-2 and 3 due to the same lateral acceleration component ($a_y$) of the excitations, while it is significantly smaller for 'Case-1' due to the smaller $a_y$. The oscillation frequencies are found to be close to the resonant frequency (0.53 Hz) during the initial time of excitation. However, the slosh frequency tends to increase under the excitations 'Case-1' and '-2', while it remains nearly identical for the excitation 'Case-3'. For the excitations 'Case-1' and '-2', the liquid free surface becomes highly inclined due to the large longitudinal acceleration ($a_x$=0.6g), and this should affect the slosh frequency response since the results of $M_x$ under the two excitations show almost the same frequency behaviour.

The results of pitch moment ($M_y$) show asymptotical increasing tendencies toward the steady-states, with very small oscillations. The asymptotical trend is due to the effect of fluid accumulation within a baffled tank under a longitudinal acceleration field. The results under the excitations 'Case-1' and '-2' are virtually the same owing to the identical longitudinal acceleration component, suggesting negligible influence of lateral acceleration on the pitch moment. The pitch moment under the excitation 'Case-3' is significantly smaller due to the smaller longitudinal acceleration.

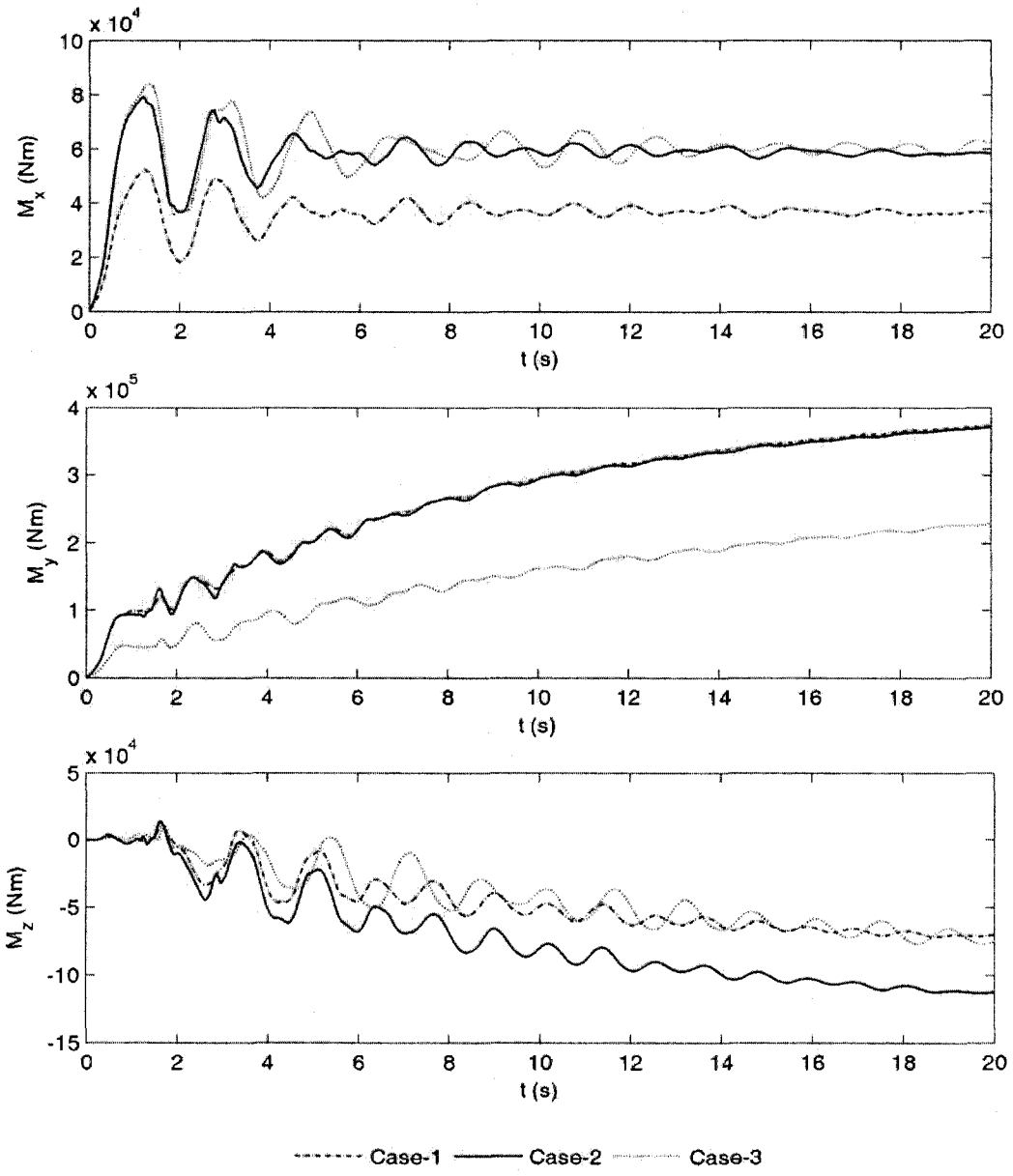


Figure 4.16: Transient responses of slosh roll ($M_x$), pitch ($M_y$) and yaw ($M_z$) moments for the baffled tank 'T1' with the low fill volume (38.1%) subject to combinations of different lateral and longitudinal ramp-step excitations ($a_y$, $a_x$): Case-1 (0.25g, 0.6g); Case-2 (0.4g, 0.6g); Case-3 (0.4g, 0.3g).

The results of yaw moment ($M_z$) also show asymptotical trends for all the three combined excitations considered, while the oscillation frequencies behave like those of the roll moment. This indicates that the slosh yaw moment is influenced by both lateral and longitudinal slosh motions. The results of the yaw moment also show that the excitation 'Case-2', due to the high accelerations in both the lateral and longitudinal directions (0.4g, 0.6g), yields larger yaw moment than the other two excitations.

In a nutshell, under a combined lateral and longitudinal acceleration excitation, a lower fill volume tends to yield more severe slosh. The presence of transverse baffles can considerably reduce the peak amplification factors in the longitudinal force ($M_{Fx}$) and pitch moments ($M_{My}$), as well as lateral force ($M_{Fy}$) and roll moment ($M_{Mx}$). For the cleanbore tank, smaller lateral ($a_y$) but identical longitudinal ($a_x$) accelerations tend to generate higher amplification in the slosh forces and moments, which is also the case for higher $a_x$ but identical $a_y$. The amplification factors $M_{Fy}$, $M_{Fx}$, $M_{Fz}$, and $M_{Mx}$ for the baffled 'T1' tank, however, exhibit small variations with the combined excitations. The transient slosh pitch moment is negligibly influenced by the magnitude of $a_y$ component when $a_x$ is the same. The transient slosh yaw moment is influenced by both $a_x$ and $a_y$ components.

**(4) Single-cycle Sinusoidal Excitation**

The single-cycle sinusoidal excitations can be used to represent the path change manoeuvres. The slosh simulations under this type of excitation are conducted for two cases with constant magnitude (0.25g) but different frequencies: 0.3 and 0.4 Hz. Hereafter these cases are denoted as 'Case 4' and 'Case 5', respectively. The excitation

frequencies are chosen such that they can represent the possible lane-change maneuvers in the extreme case (i.e., near resonance). Figure 4.17 presents the peak amplification factors of slosh forces ($M_{Fy}$, $M_{Fx}$ and $M_{Fz}$) in tanks 'T0' and 'T1' subjected to these two excitation cases. The figure shows that the excitation at higher frequency ('Case 5') yields higher peak slosh amplification factors in all three force components compared to the excitation of lower frequency ('Case 4'), irrespective of the cargo fill volume. As discussed in Section 4.5.1, the fundamental lateral resonant frequency ranges from 0.53 Hz to 0.67 Hz for fill volume from 38.1% to 69.5%. The higher peak amplifications observed for the excitation 'Case 5' is thus due to the reason that the excitation frequency is closer to the resonant frequency. The results also show decreasing slosh forces as fill volume increases, confirming the influence of fill volume in the slosh forces which has been observed for the other excitations.

In Figure 4.17, the results for the cleanbore tank 'T0' show very small $M_{Fx}$ at all three fill volumes of fluid cargos (<0.004), suggesting that the fluid slosh is predominantly two-dimensional in this maneuver. Relatively large magnitude of $M_{Fx}$ (<0.13) is observed for the baffled tank 'T1', confirming that the effect of transverse baffle curvature induces the slosh in the longitudinal direction, as observed under the lateral ramp-step acceleration excitations. The comparison further shows that the magnifications of lateral and vertical slosh forces in the cleanbore 'T0' tank are slightly larger than those in the baffled 'T1' tank when the fill volume and excitation are the same.

The peak amplification factors of moments ($M_{Mx}$, $M_{My}$ and $M_{Mz}$) under the same excitations are shown in Figure 4.18. Similar to the behavior of slosh forces, the peak amplification factors of moments, particularly $M_{My}$ and $M_{Mz}$, are larger under the

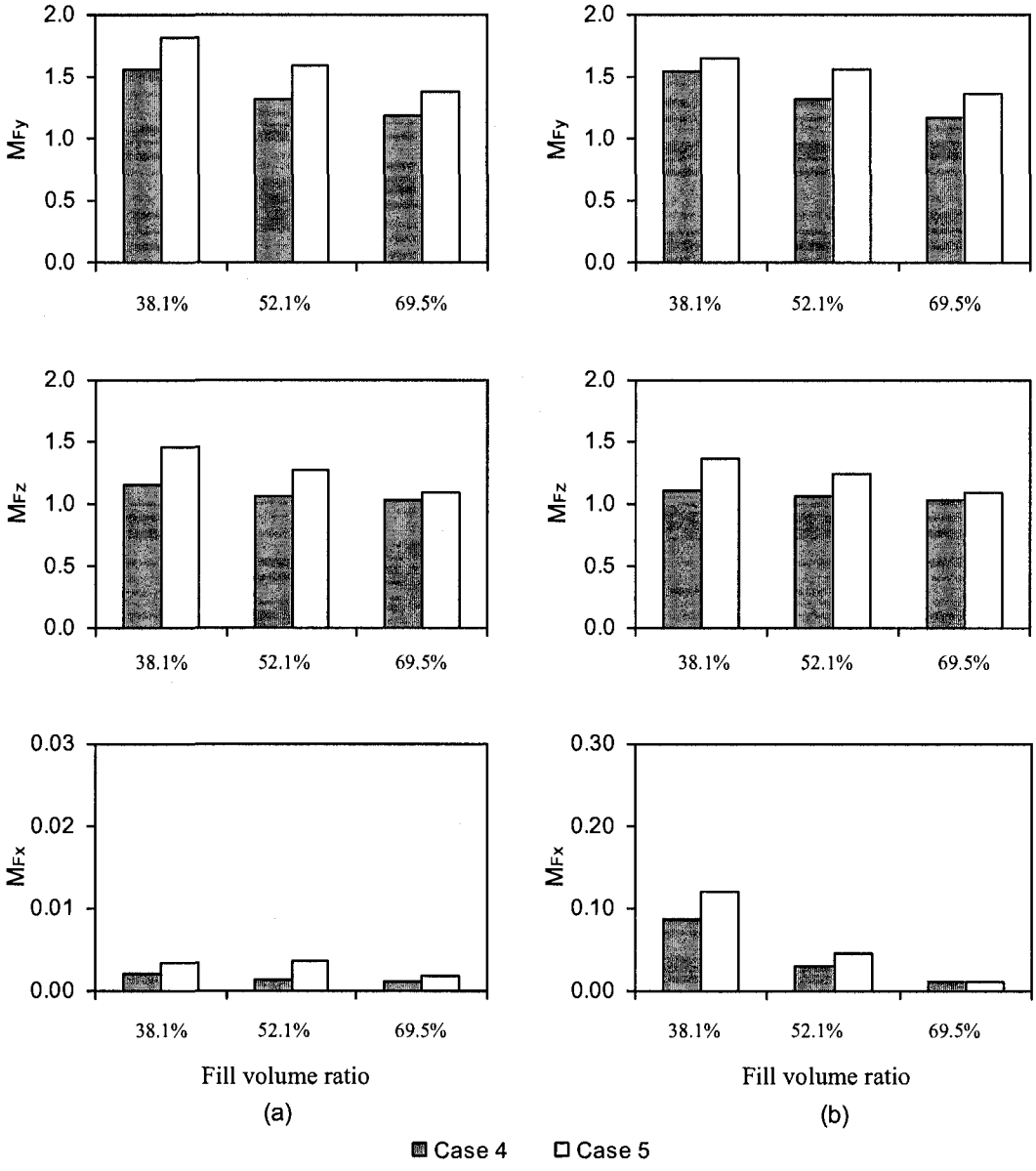


Figure 4.17: Peak amplification factors of lateral ($M_{Fy}$), vertical ($M_{Fz}$) and longitudinal ($M_{Fx}$) forces versus cargo fill volume for tanks: (a) 'T0' and (b) 'T1'. (Excitation: Case-4, 0.25g at 0.3 Hz; Case-5, 0.25g at 0.4 Hz).

excitation 'Case 5' which is near the resonant frequency for both the baffled and unbaffled tanks, as compared to those under 'Case-4'. Comparison of Figure 4.17 and Figure 4.18 shows that the amplification factor in roll moment is considerably higher than that in the lateral force, suggesting that there are other factors that contribute to the roll moment, such as vertical force and fluid *cg* translation. It is seen that $M_{Mx}$ can approach as large as 5, while $M_{Fy}$ is less than 2 for the fluid slosh in the cleanbore 'T0' tank with the low fill volume (38.1%). However, such large difference is not observed for the ramp-step excitations shown in Figures 4.9 and 4.10. The results in Figure 4.18 further show that the pitch and yaw moments are significantly higher in the baffled 'T1' tank than in the unbaffled 'T0' tank, suggesting relatively more severe 3D slosh due to the effect of baffle curvature.

As a summary, the fluid slosh tends to be more severe when an excitation is near resonant frequency. The fluid slosh under a pure lateral single-cycle sinusoidal acceleration excitation is predominantly two-dimensional. The baffle curvature tends to induce the longitudinal fluid slosh. Similar to other excitation cases, the slosh resulting forces and moments tend to be larger at a lower fill volume.

## 4.6 ANALYSIS OF BAFFLE DESIGN FACTORS

While fluid slosh in a partly filled tank is known to be affected by the size of baffle opening area, it is also influenced by other factors associated with the baffle design, such as baffle curvature, and shape and location of orifice. A better understanding of the influence of these factors is therefore essential in order to improve the baffle design

aiming to minimize the fluid slosh and consequently improve the safety of road tank vehicles.

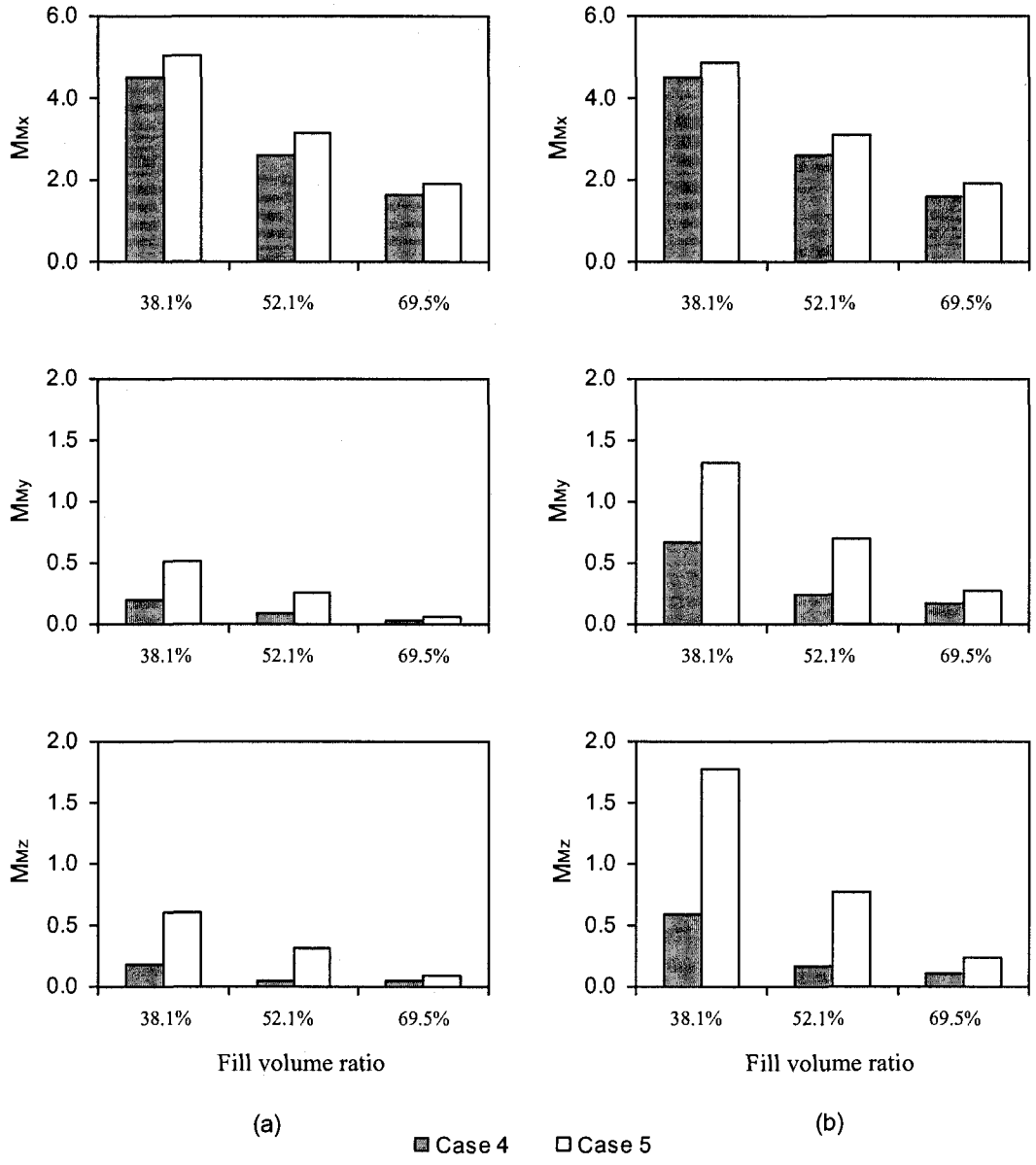


Figure 4.18: Peak amplification factors of roll moment ($M_{Mx}$), pitch moment ($M_{My}$) and yaw moment ($M_{Mz}$) versus cargo fill volume for tanks: (a) 'T0' and (b) 'T1'. (Excitation: Case-4, 0.25g at 0.3 Hz; Case-5, 0.25g at 0.4 Hz).

### 4.6.1 Effect of baffle equalizer

Equalizer is a small opening located at the bottom of the baffles to equalize the fluid cargo in the adjacent compartments separated by the baffles. The effect of the baffle equalizer is analyzed using a modified single-orifice baffle in which the equalized is removed while the central orifice size is enlarged to maintain the opening ratio identical to that of 'B1' (nearly 12%). The slosh analyses are performed for the low and intermediate fill volumes (38.1% and 52.1%) and under a pure longitudinal acceleration excitation (0.3g). Figure 4.19 presents the peak amplification factors of lateral and vertical forces ($M_{Fy}$ and $M_{Fz}$) arising from the slosh under the conditions. The results show almost identical values of $M_{Fy}$ and $M_{Fz}$ for the baffle configurations with and without equalizers, suggesting negligible influence of the device on the slosh forces. The influence, however, is observed in the slosh pitch moment, as evident in Figure 4.20. It is seen in Figure 4.20 that the slosh pitch moment yielded by the tank configuration without equalizers is lower than that with equalizer, particularly when the fill volume is low (38.1%). The results show that the difference is small within 2 seconds after the beginning of the maneuver, but it increases with time. The discrepancy between the two configurations approaches approximately 42% around t = 20 s at the low fill volume. The pitch moment difference for the two configurations is significantly reduced for the intermediate fill volume (52.1%), which is due to the reason that at the low fill volume (38.1%) due to the lower height of the liquid free surface, almost the entire fluid shift between the two adjacent compartments, occur through the equalizer opening. However, at the intermediate fill volume (52.1%) the liquid cargo permeate mostly through the large central orifices due the high level of liquid surface. Therefore, the pitch moment at

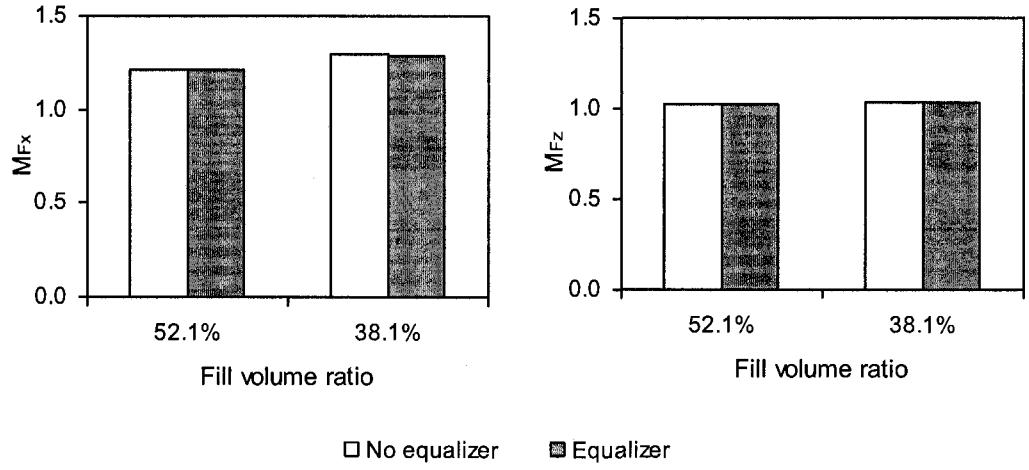


Figure 4.19: Peak amplification factors of longitudinal force ($M_{Fx}$) and vertical force ($M_{Fz}$) generated by fluid cargos with 38.1% and 52.1% fill volumes under the 0.3g longitudinal ramp-step acceleration.

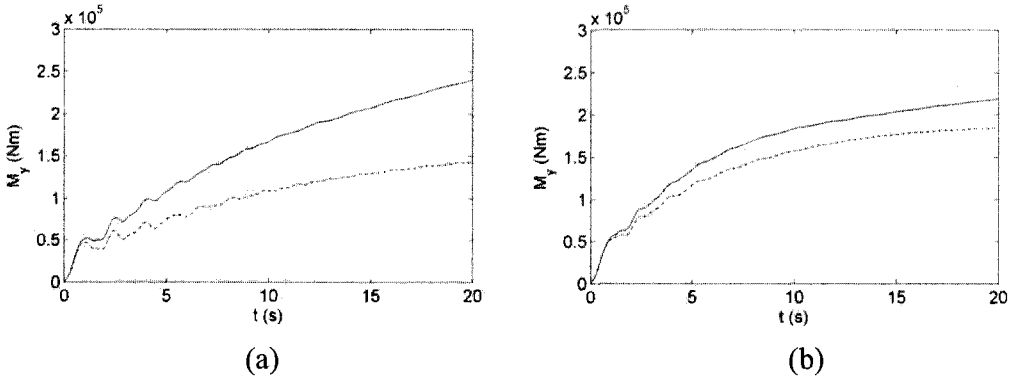


Figure 4.20: Transient responses of pitch moment ($M_{My}$) to the 0.3g longitudinal ramp-step acceleration excitation for the fluid cargos with fill volumes: (a) 38.1%; (b) 52.1%. ——, Equalizer; –·–·–, No equalizer.

the intermediate fill volume nearly approached the steady-state values within the simulation time, while it is not the case at the low fill volume. Thus, it can be concluded that the effect of equalizer is highly associated with the liquid cargo fill volume and it is more evident at the low fill volumes. It would thus be desirable to devise a closure function for the baffle equalizer such that the devices can be closed when high density fluid cargo is transported with low fill level.

In summary, the equalizer has negligible influence on the slosh forces, while the effect on the slosh pitch moment is also small, particularly for the initial time of excitation.

### 4.6.2 Effect of Baffle Porosity

The influence of baffle porosity is analyzed for single-orifice baffles of different diameters. Three orifice diameters are considered that correspond to the baffle opening area to total tank cross-section area ratio of 0.04, 0.12 and 0.2. The analysis is conducted with the intermediate and high fill volumes (52.1% and 69.5%) and subject to two longitudinal ramp-step acceleration excitations (0.3g and 0.6g). Figure 4.21 illustrates the peak amplification factors of longitudinal slosh force ($M_{Fx}$) for the three orifice diameters under two fill volume conditions and excitations. The figure also includes the results for the cleanbore tank configuration (i.e., 100% baffle opening) for comparison. The results show small variations with the baffle openings (ranging from 4% to 20%) for the two excitations, while they are significantly smaller than that for the cleanbore tank. This suggests that for the baffle porosity less than 20%, the orifice diameter has no significant

effect on the longitudinal force, which is in agreement with the results reported by Popov [40] for a 2-D baffled rectangular tank.

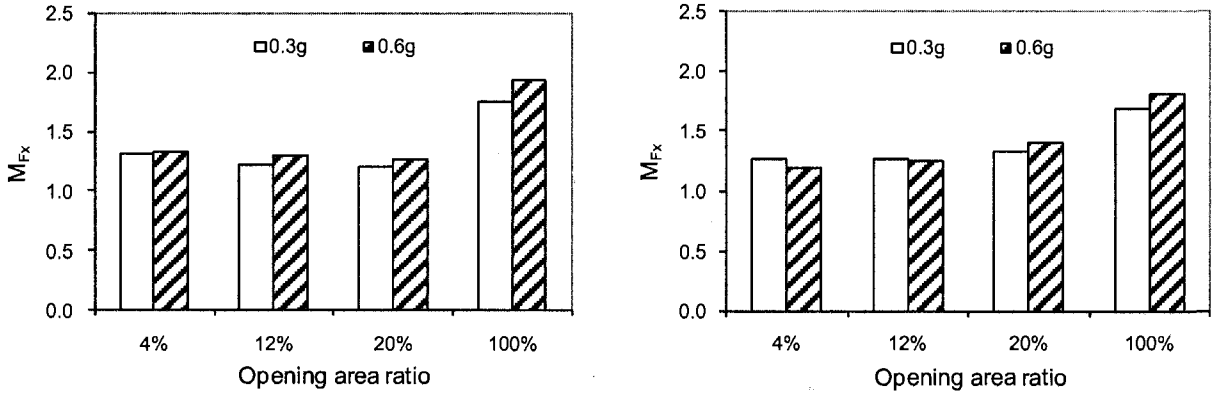


Figure 4.21: Variations of peak amplification factors of longitudinal force ($M_{Fx}$) with baffle opening ratio under the longitudinal ramp-step accelerations of 0.3g and 0.6g and for different fill volumes: (a) 52.1% and (b) 69.5%.

The transient responses of slosh pitch moments for the same excitation cases are shown in Figure 4.22. The plot indicates a significant influence of the baffle porosity on the slosh pitch moment. The results show that a baffle of smaller opening orifice tends to yield a lower pitch moment, irrespective of the fill volume. The results of the cleanbore tank clearly show transient variations with time about constant steady-state values at the frequencies near the resonant frequencies for the two fill volumes, while those of the baffled tank exhibit asymptotical tendency towards the steady-states. It is seen that the slosh in the tank with larger orifice baffles tends to approach the steady-state more rapidly, particularly under the high fill volume (69.5%), thus causing significantly larger pitch moment. The difference in the pitch moment between different baffle openings tends to be more evident after t = 1 s for both fill volumes.

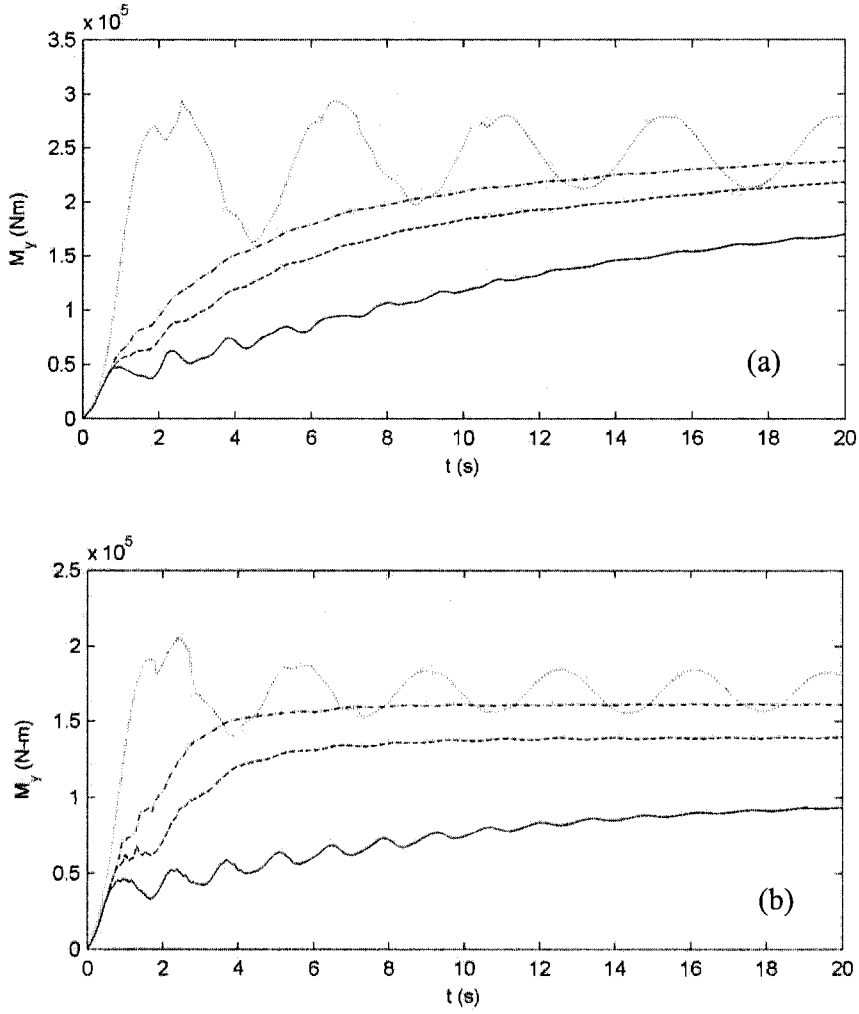


Figure 4.22: Transient responses of pitch moment to a longitudinal ramp-step acceleration (0.3g) in the tank equipped with the baffles of different orifice sizes with two different fill volumes: (a) 52.1%; (b) 69.5%. ——, 4%; ----, 12%, –·–·, 20%,; ·····, 100%.

The results also show that for the three baffled cases, the pitch moment do not reach the same steady-state values after 20 seconds. These values are also different from the steady-state level for the cleanbore tank. This suggests that the fluid slosh may end up with the different free surface positions in the tank with different baffle porosities due to the difference in the orifice position relative to the liquid free surface. Comparison of

the results with different fill volumes shows that the slosh pitch moment is considerably larger for the intermediate fill volume (52.1%) than for the high fill volume (69.5%) for the tank with a given-size baffle.

In summary, it could be stated that when the baffle opening area to tank cross-sectional area ratios are in the range of less than 20%, the baffle porosity has very small influence on the longitudinal slosh force. However, its effect on the pitch moment is quite significant. The baffle with smaller orifice tends to more effective in suppressing the pitch moment.

### 4.6.3 Effects of Baffle Designs

Three novel baffle designs, 'B3', 'B4' and 'B5', as described in Section 4.2, are devised to explore the mechanism to enhance the role of baffle in slosh suppression. The three baffles have different design goals: (*i*) increase the baffle effectiveness using different orifice shape and location ('B3'); (*ii*) reduce the baffle weight while maintain the baffle effectiveness ('B4'); (*iii*) enhance the slosh's role in the lateral slosh suppression ('B5').

**(1) Half-circle Orifice Baffle Design ('B3')**

The slosh analysis for this baffle ('B3') shown in Figure 4.3*c* is performed at the intermediate and high fill volumes (52.1% and 69.5%) subjected to two longitudinal ram-step acceleration excitations (0.3g and 0.6g). Figure 4.23 illustrates the peak amplification factor of the longitudinal slosh force ($M_{Fx}$) under these conditions for the baffled 'T3' tank equipped with baffles 'B3'. The results for 'T1' tank are also included in this figure for comparison. The results show no obvious difference in $M_{Fx}$ between the

two baffle designs at the higher fill volume (69.5%), while at the intermediate fill volume, the amplification in the longitudinal force ($M_{Fx}$) is slightly larger (within 7%) with baffle 'B3' compared to that with baffle 'B1'.

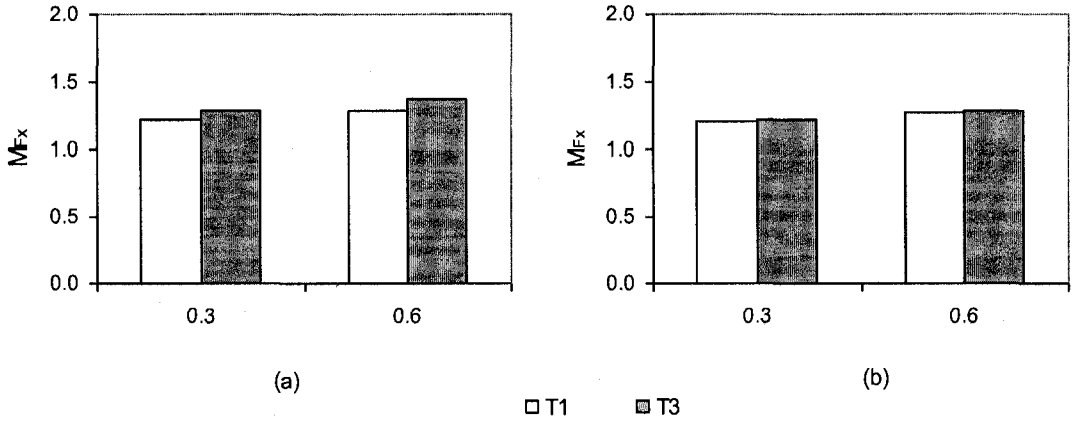


Figure 4.23: Comparison of peak amplification factor of longitudinal slosh force ($M_{Fx}$) between tanks 'T1' and 'T3' with different fill volumes: (a) 52.1%; (b) 69.5%

The transient pitch moment response to the same excitation cases are illustrated in Figure 4.24. The results indicate a significant reduction in the pitch moment in the presence of baffle 'B3' compared to baffle 'B1', particularly under high fill volume condition. Figure 4.24 also shows that the pitch moment for tank 'T3' rapidly approach the steady-state, compared to that for tank 'T1'. The steady-state magnitude of pitch moment for tank 'T3' is almost 30% smaller than that for tank 'T1' at the high fill volume. At the same fill volume, for tank 'T3' the pitch moment shows oscillations at the frequency near the natural slosh frequency ($\approx 0.69$ Hz) with no asymptotical trend, suggesting very little liquid accumulation occurred in this case.

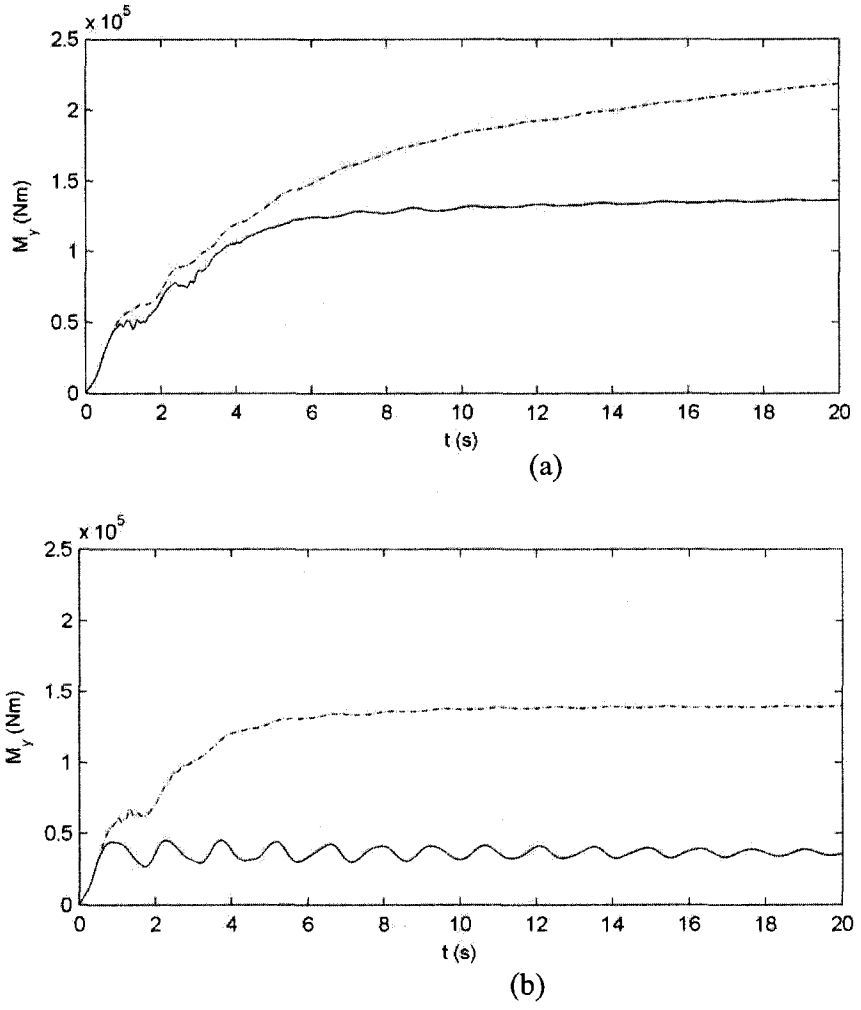


Figure 4.24: Comparison of transient slosh pitch moment for the tanks 'T1' and 'T3' with two different fill volumes (a) 52.1% and (b) 69.5% subjected to 0.3g longitudinal ramp-step acceleration excitation. ——, 'T3' tank; –·–·, 'T1' tank.

The high anti-slosh effect of baffle 'B3' under the high fill volume is also evident in the results of fluid cargo *cg* position, as shown in Figure 4.25. The results show smaller magnitudes of fluid cargo *cg* positions in both longitudinal and vertical directions for the tank equipped with baffles 'B3'. The difference tends to be significantly large after t=2 s. The steady-state value of longitudinal *cg* position is about 0.7 m for the

conventional tank design 'T1', while it reduces to below 0.1 m for tank 'T3' with the novel baffle design 'B3'.

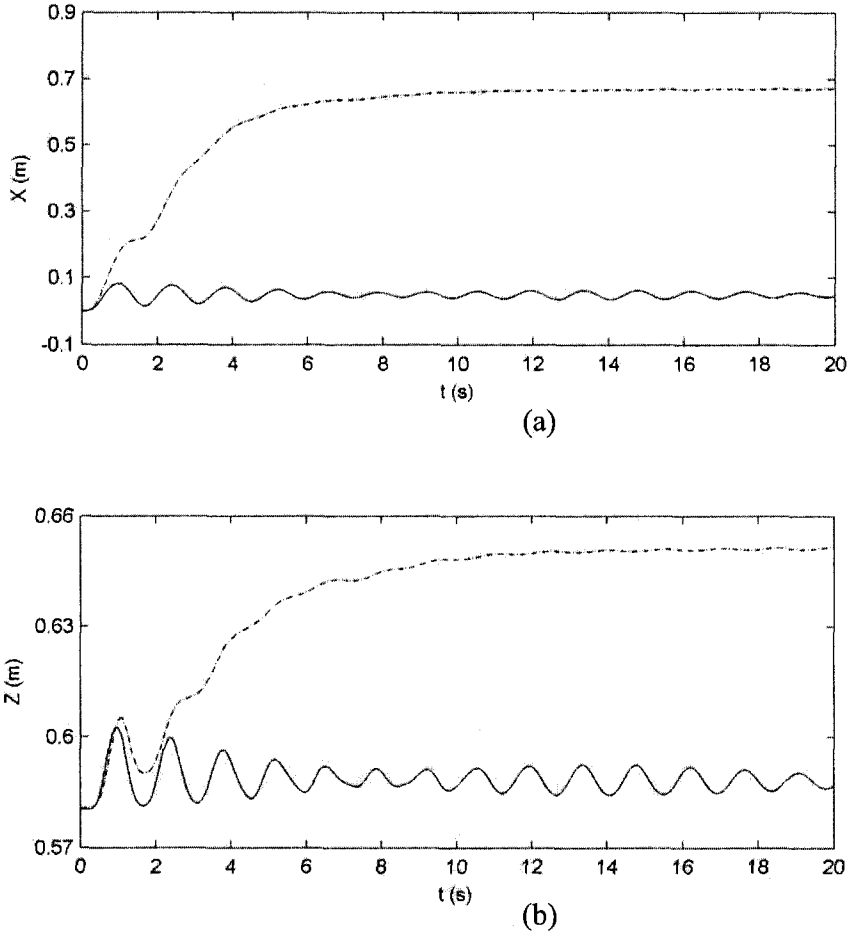


Figure 4.25: Comparison of transient longitudinal ($X$) and vertical ($Z$) fluid cargo *cg* coordinates between tanks 'T1' and 'T3' with 69.5% fill volume subjected to 0.3g longitudinal ramp-step acceleration excitation. ——, tank 'T3'; –·–·, tank 'T1'.

The non-asymptotical trend and the rapid approach to steady-state by the transient pitch moment and longitudinal fluid *cg* position for tank 'T3' indicate that with this baffle design, very little liquid cargo shifts between the baffled compartments. This is also

evident through the visualization of the liquid free surface patterns from the simulations. The transient liquid free surface positions for tanks 'T1' and 'T3' with 52.1% and 69.5% fill volumes under the same excitation at $t \approx 20$ s (i.e., at steady-state) are illustrated in Figure 2.26. The plots show that the fluid cargo tends to accumulate towards the left head of the tank, while the accumulation is significantly more evident in tank 'T1' than tank 'T3', and at the intermediate fill volume than that at the high fill volume. At higher fill volume in tank 'T3' (Figure 4.26b), the results show that the free surfaces are uniform in all baffled compartments, suggesting a behavior similar to that in a compartmented tank with solid baffles. This indicates that baffle 'B3' due to its top half solid part can yield highly effective resistance to the fluid slosh motion when the fluid fill volume is high. The resistance is believed to arise from the adverse air pressure gradient generated between compartments due to the liquid accumulation along the acceleration direction. Since baffle 'B3' differs from baffle 'B1' in terms of the baffle orifice shape and location (relative to liquid free surface), it further suggests that these two factors are essential for the effective baffle design.

As a summary, it can be stated that significant reduction in pitch moment could be achieved by introducing the novel half-circle orifice baffle design. Since lower pitch moment implies smaller longitudinal normal load transfer, the presence of baffle 'B3' can significantly reduce the risk of wheel lockup and consequently improve the vehicle's directional stability. Furthermore, the benefit of this baffle design is more obvious for the higher liquid fill level in which the baffle orifice is well immersed in the liquid. It also suggests that the baffle orifice location has significant influence on the slosh control. The

2-D slosh analysis by Popov [40], however, showed that the baffle orifice location is insignificant if the orifice is fully immersed in the liquid.

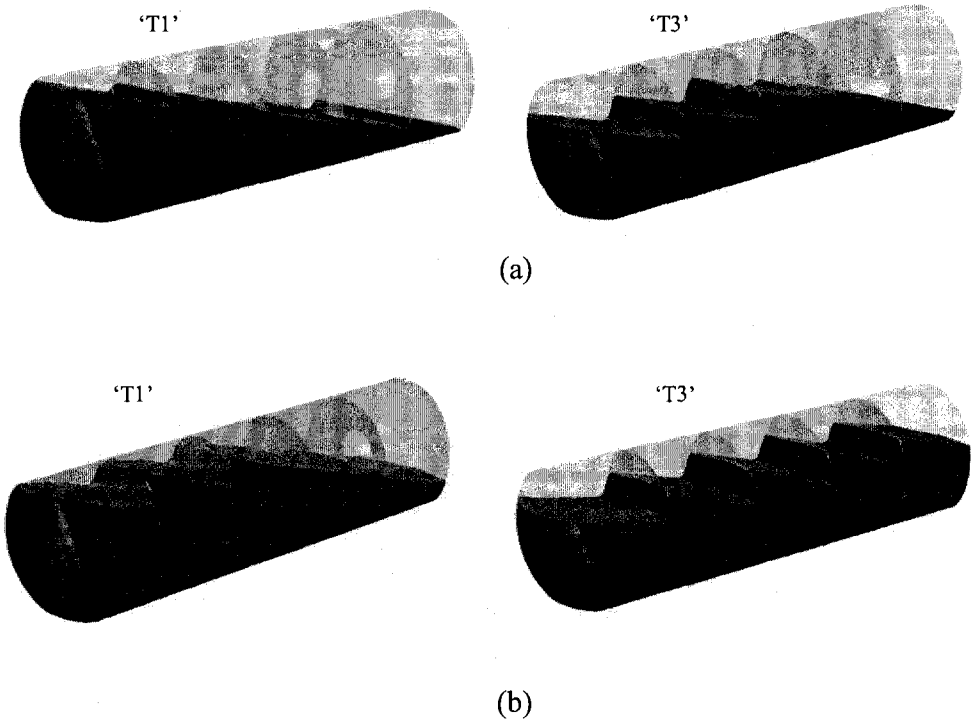


Figure 4.26: Comparison of free surface position of liquid cargos in tanks 'T1' and 'T3' with (a) 52.1% and (b) 69.5% fill volumes subjected to 0.3g longitudinal ramp-step acceleration excitation.

**(2) Half-opened Partial Baffle ('B4')**

The design goal of the half-opened baffle 'B4' sketched in Figure 4.3*c* is to reduce the baffle weight while maintaining its effectiveness. The fluid slosh analysis is conducted for the tank 'T4' which is equipped with the baffles ('B4') under the same conditions as those for tank 'T3'. Figure 4.27 shows the peak amplification factor of lateral slosh force ($M_{Fy}$) for tank 'T4' under the 0.3g and 0.6g longitudinal ramp-step accelerations. The

data for the conventional tank 'T1' is also plotted for comparison. The results show that at the intermediate fill volume, the fluid slosh within tank 'T4' yields a considerably larger $M_{Fy}$ (about 20%) than that in tank 'T1', while they are comparable at the high fill volume (69.5%). This suggests that baffle 'B4' with larger orifice opening in the lower portion can have the anti-slosh effect similar to that of the conventional small orifice baffle 'B1' under the high fill volume (69.5%), but not at the intermediate fill volume.

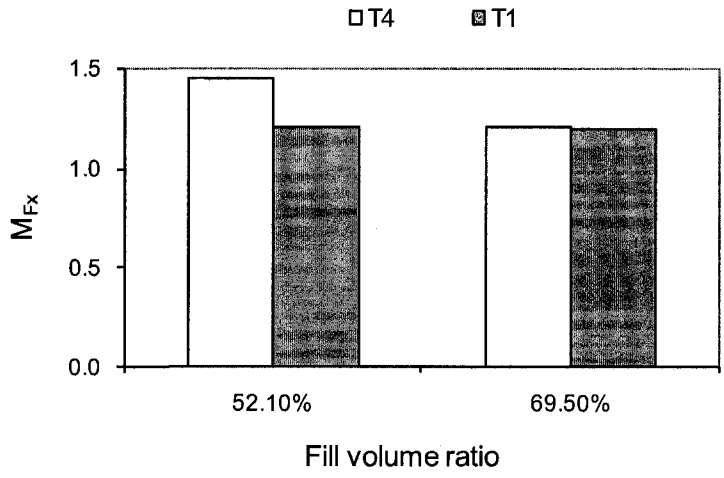


Figure 4.27: Peak amplification factor of longitudinal slosh force ($M_{Fx}$) for the tanks 'T4' and 'T1' filled with 52.1% and 69.5% fill volumes under 0.3g longitudinal ramp-step acceleration.

The transient slosh pitch moment responses to 0.3g longitudinal ramp-step excitation are shown in Figure 4.28. The results show that the slosh pitch moment in tank 'T4' approaches the peak rapidly ($t \approx 2.5$ s) and tends to oscillate about the constant steady-state value. This behavior is very similar to that observed for the cleanbore tank 'T0'. Comparison with the results in Figure 4.12 for the cleanbore tank 'T0', shows that the peak and mean values of the slosh pitch moment for tank 'T4' is considerably lower

than those of cleanbore tank 'T0', suggesting some anti-slosh benefit of the partial baffle, under the intermediate fill volume (52.1%). The results further show that the pitch moment under the high fill volume (69.5%) with the partial baffle 'B4' is significantly smaller than that with the conventional baffle 'B1'. Comparison with the results for tank 'T3' (Figure 4.24*b*) shows comparable magnitudes fro the two tanks, suggesting similar anti-slosh influence of baffles 'B4' and 'B3'.

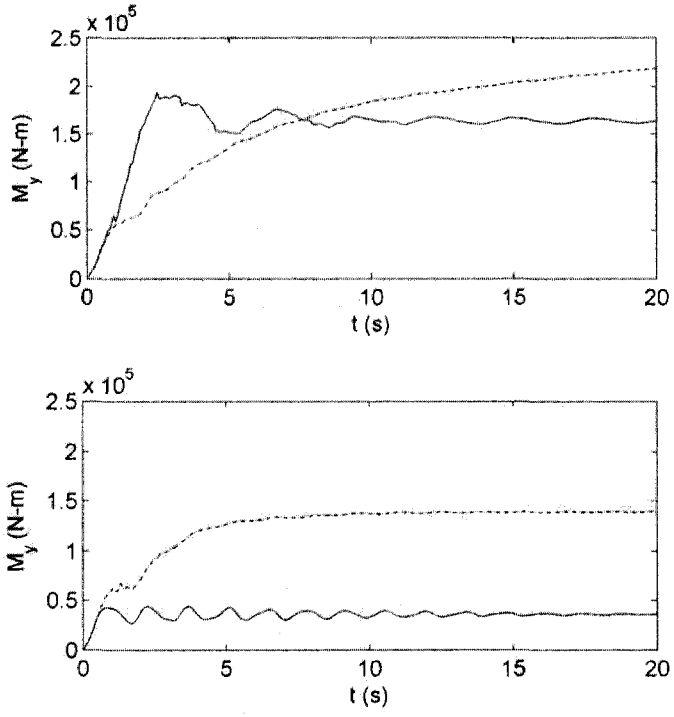


Figure 4.28: Comparison of transient slosh pitch moment for tanks 'T4' and 'T1' with fill volumes (a) 52.1% and 69.5% subjected to 0.3g longitudinal ramp-step acceleration excitation. ——, 'T4' tank; –·–·, 'T1' tank.

The liquid free surface position shown in Figure 4.29 also indicates the high effectiveness of the partial baffle 'B4' as an anti-slosh device. In the figure, the liquid cargo below the free surface is intentionally not shown to have a perspective view of the

tank configuration. The free surface shows nearly the same slope and height for different baffled compartments, suggesting very little liquid passed through the baffles. This behavior is similar to that observed for tank 'T3'. Thus it can be concluded that the half-opened partial baffle could help suppress the slosh magnitude, particularly at higher cargo fill volume. This benefit, however, is not observed under the high excitation magnitude (0.6g). It could partly due to the high longitudinal body force of liquid arising from the high magnitude acceleration excitation and partly due to the large opening of the baffles.

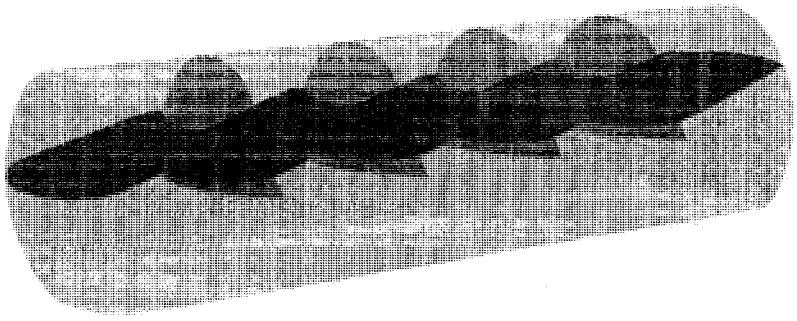

Figure 4.29: Free surface position of liquid slosh at t=20 s for tank 'T4' with fluid cargo 'C3' under the high fill volume (69.5%) subjected to 0.3g longitudinal ramp-step acceleration excitation.

In summary, the half-opened partial baffle ('B4') can effectively suppressing the fluid slosh at the high fill volume (69.5%), which is of the same order as that observed for the single half-circular orifice baffle ('B3') with smaller opening area ratio (12%). The role of suppressing slosh was not observed for the baffle under the intermediate fill volume (52.1%).

### (3) Conical Baffle ('B5')

The idea of the conical baffle 'B5' shown in Figure 4.2*b* is based on the possibility to develop a novel device that can effectively suppress liquid cargo slosh in the lateral direction in the roll plane. Therefore, the analysis of this baffle is carried out under the lateral excitations and two volume conditions. Figure 4.30 shows the peak amplification factors of slosh forces ($M_{Fy}$, $M_{Fx}$ and $M_{Fz}$) and moments ($M_{Mx}$, $M_{My}$ and $M_{Mz}$) for tank 'T5' under lateral single- cycle sinusoidal acceleration of 0.25g and 0.5 Hz.

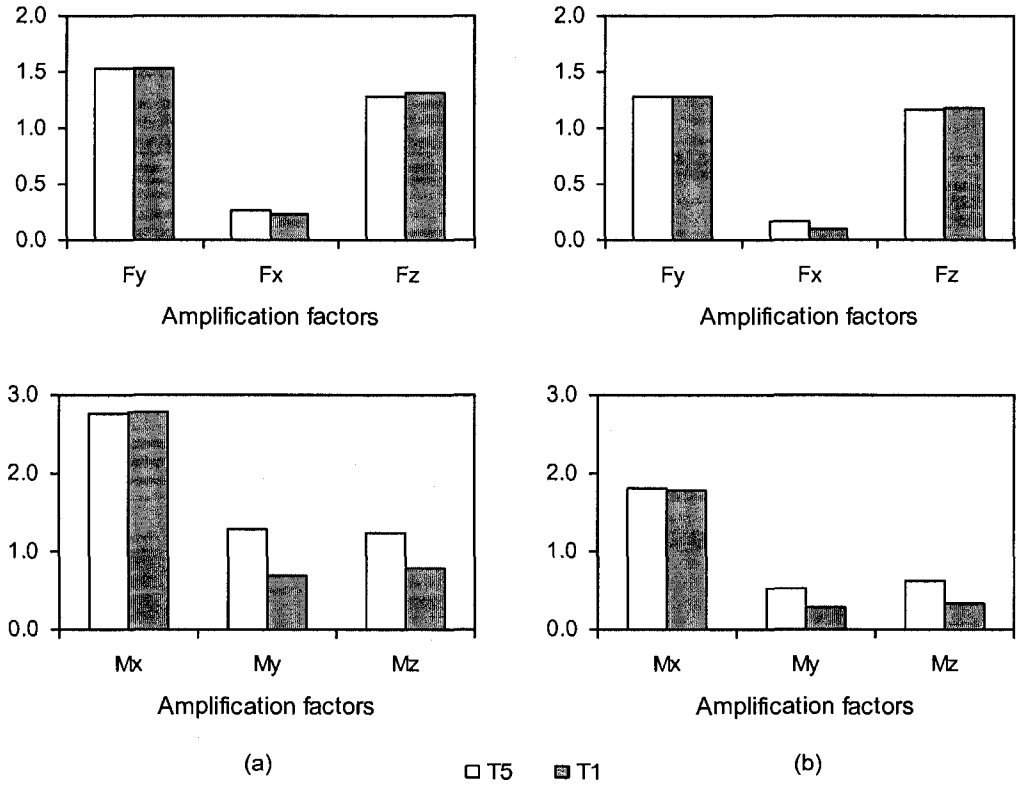


Figure 4.30: Comparison of peak amplification factors of slosh forces ($M_{Fy}$, $M_{Fx}$ and $M_{Fz}$) and moments ($M_{Mx}$, $M_{My}$ and $M_{Mz}$) for tanks 'T5' and 'T1' with (a) 52.1% and (b) 69.5% fill volumes under lateral single-cycle sinusoidal acceleration of 0.25g and 0.5 Hz

The results for tank 'T1' are also plotted for comparison. The results show that the peak force amplification factors $M_{Fy}$, $M_{Fx}$ and $M_{Fz}$, as well as the peak roll moment amplification factor ($M_{Mx}$), are comparable for both the two tank configurations at 52.1% and 69.5% fill volumes, while the peak pitch and yaw moments ($M_{My}$ and $M_{Mz}$) for tank 'T5' are larger than those in tank 'T1'. The larger $M_{My}$ and $M_{Mz}$ suggest a relatively more severe 3-D fluid slosh occurred in tank 'T5' due to the long extrusion of the conical baffle in the longitudinal direction of the conical baffle design. This is consistent with the results for the curved baffles. Similar trends are also observed for the fluid slosh simulations in the tank under 0.3 Hz lateral single-cycle excitation.

The fluid slosh responses to 0.4g lateral ramp-step excitation in tank 'T5' are illustrated in Figure 4.31 under the intermediate and high fill volumes (52.1% and 69.5%). The plot shows that the peak amplification factors of lateral and vertical forces ($M_{Fy}$, and $M_{Fz}$ ) and roll moment ($M_{Mx}$) are comparable for tanks 'T5' and 'T1' with 52.1% and 69.5% fill volumes. The peak amplification factor of longitudinal force ($M_{Fx}$) and pitch and yaw moments ($M_{My}$ and $M_{Mz}$) in 'T5' tank are significantly larger than those in 'T1' tank at both fill volumes. This trend is similar to that observed for the single-cycle sinusoidal acceleration excitations, suggesting that the fluid slosh behaves slightly more in a three dimensional manner.

As a summary, the slosh analyses of the conical baffle show that the baffle could not yield any benefit in the reduction of the slosh force and moment in the roll plane, as compared to the conventional single-orifice baffle. The longitudinal extrusion of the conical baffle tends to induce the three-dimensional fluid slosh when the tank is subjected to a pure lateral acceleration excitation.

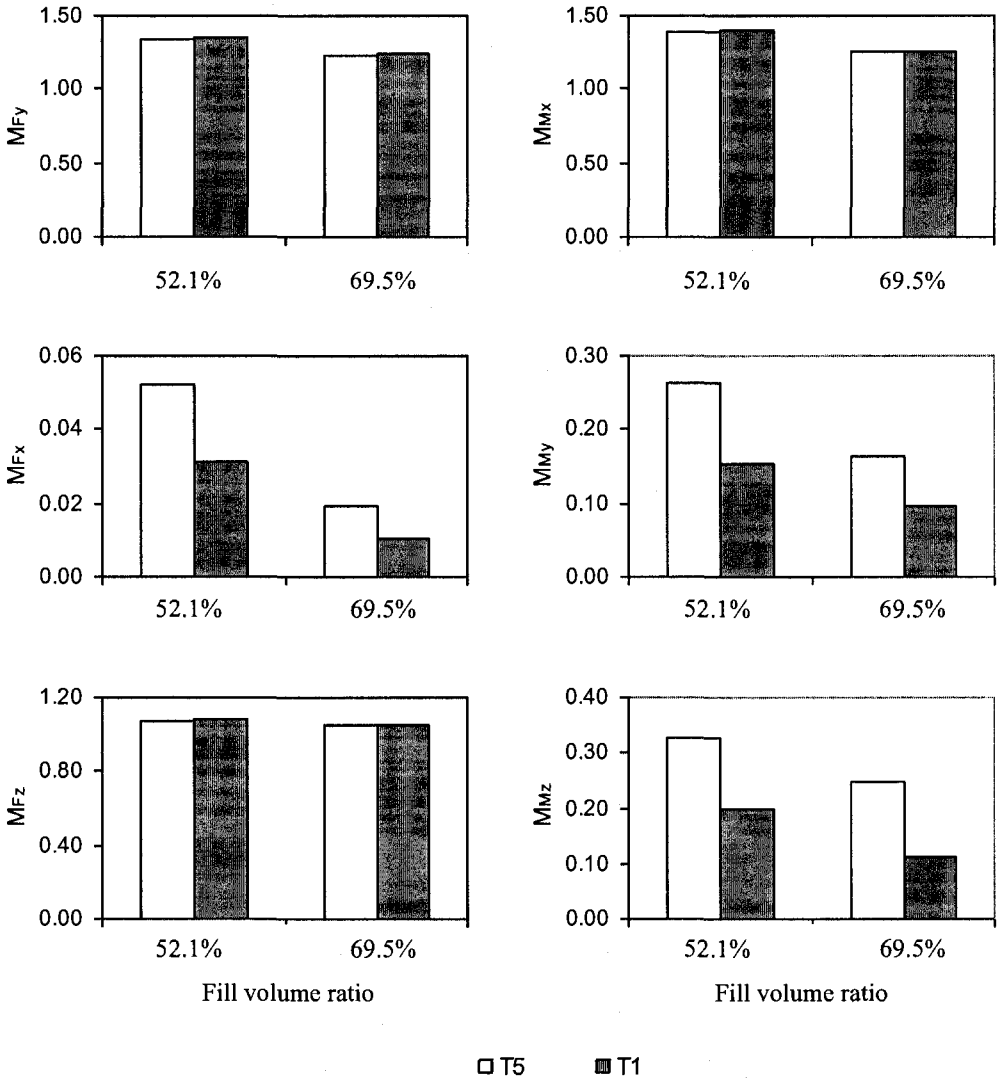


Figure 4.31: Comparison of peak amplification factors of slosh forces ($M_{Fy}$, $M_{Fx}$ and $M_{Fz}$) and moments ($M_{Mx}$, $M_{My}$ and $M_{Mz}$) for tanks 'T5' and 'T1' with 52.1% and 69.5% fill volumes under 0.4g lateral ramp-step acceleration.

## 4.7 SUMMARY

The three dimensional slosh has been studied within a partially filled fullscale road vehicle tank of the optimized "Reuleaux triangle" cross-section. The slosh characteristics were analyzed in terms of slosh frequency and slosh forces and moments, for cleanbore and baffled tank configurations with different fill volumes but corresponding a constant cargo load. Different baffle designs and baffle design factors have been evaluated at different fill volumes and selected excitations that represent steady-turning, straight-braking, braking-in-a-turn and lane change maneuvers.

The results showed that the curved baffles have no influence on the lateral slosh natural frequency but they cause a significant increase in longitudinal slosh frequency. The fundamental natural frequency of lateral slosh is in the range of 0.53~0.67 Hz for the baffled and unbaffled tank configurations with the fill volume range 38.1% to 69.5%. The longitudinal slosh in the cleanbore tank exhibits very low frequencies which are less than 0.23 Hz for the given fill volume range which increases significantly in the presence of baffles.

The results revealed that the baffle equalizer has negligible influence on the suppression of peak longitudinal slosh force, irrespective of the fill level. However, it increases the transient pitch moment at lower fill volumes. The peak longitudinal slosh force showed negligible variations with the baffle opening area ratio in the range from 4% to 20%. But the transient slosh pitch moment tends to increase with an increase in the baffle orifice diameter, while the steady-state value approaches more rapidly with higher baffle porosity.

The peak slosh forces and moments invariably tend to reduce with an increase in liquid cargo fill volume, irrespective of the excitation type and direction. The fluid in both the baffled and unbaffled tanks is characterized by a predominant two-dimensional slosh when subjected to a pure lateral ramp-step or lateral single-cycle excitation, which represents a steady-turning or lane-change maneuver. A lane-change maneuver occurring near the resonant frequencies tended to yield larger slosh forces and moments.

The addition of transverse baffles helps significantly to decrease the peak longitudinal slosh force and pitch moment under a pure longitudinal or a combined longitudinal and lateral ramp-step acceleration excitation. The installation of the single-orifice 'B1' baffle (12% opening area ratio) reduced the amplification factors $M_{Fx}$ and $M_{Fz}$ by 39.1% and 21.1%, respectively, for 38.1% fill volume and $a_x$= 0.6g. The presence of transverse baffles can also yield considerable reduction in the peak lateral slosh force when the tank is subjected to a simultaneous lateral and longitudinal ramp-step acceleration excitation. The presence of baffle 'B1' decreased the amplification factor $M_{Fy}$ by 22.4% for the baffled 'T1' tank with 38.1%-filled cargo under the combined excitation of $a_x$=0.25g and $a_y$=0.6g. The anti-slosh effect of the multiple orifice baffle ('B2') is practically identical to that of the single-orifice baffle ('B1'). The presence of transverse baffles, under a pure lateral excitation, tended to induce the longitudinal slosh, causing relatively larger longitudinal slosh force, pitch and yaw moments.

The single half-circle orifice baffle ('B3'), due to the lower orifice position and the horizontal upper orifice edge, demonstrated their highly effective anti-slosh role in reducing the transient peak and mean pitch moment, as compared to the conventional baffle design ('B1'). The slosh suppression effect is more evident at the high fill volume.

The half-opened partial baffle ('B4') showed a significant suppression of the pitch moment when the liquid cargo is filled with the high fill volume. The analysis also showed that the baffle orifice shape and location are important factors in improving the effectiveness of baffle to suppress the fluid slosh. The conical baffle ('B5') does not show additional benefit in reducing the slosh forces and moments, as compared to the baffle 'B1'.

# CHAPTER 5

# EFFECT OF FLUID SLOSH ON ROLLOVER THRESHOLD ANALYSIS OF PARTLY FILLED TANK TRUCKS

## 5.1 INTRODUCTION

Heavy vehicles are known to exhibit low directional stability and controllability limits compared to those of the other road vehicles. Rollover is considered to be the utmost concern for the highway and the heavy vehicle safety [1, 2]. The partly filled road tank vehicles exhibit even lower stability limits due to the destabilization arising from the dynamic fluid slosh [3]. The majority of the fluid slosh analyses have been performed with in-plane fluid slosh models, assuming quasi-static (QS) motion of the free surface of the inviscid liquid cargos, which do not permit for analysis of the transient behaviour of the fluid motion [110, 112, 142]. Only limited efforts have been made to integrate the dynamic slosh model of a tank to that of a heavy vehicle to study the impact of dynamic slosh forces on the directional responses of the tank vehicle, while the fluid slosh was mostly represented by a mechanical system analogy [110], which can not describe the non-linearity of fluid slosh accurately. The transient fluid slosh may be simulated using the computational fluid dynamics (CFD) models. A few studies have investigated the dynamic slosh forces using linear and nonlinear CFD models of fluids within the tanks [32, 54, 143, 144]. Only limited efforts, however, have been made to integrate the CFD fluid slosh models to the vehicle model to analyze the roll stability of the tank vehicles [7].

The dynamic analysis of a partly-filled tank vehicle involves complex coupling of the nonlinear liquid slosh with a three-dimensional model of the nonlinear motions of the vehicle. Considering that the roll stability of a vehicle is closely represented by its steady-turning rollover threshold acceleration, the task of coupling the two elaborate models can be simplified through consideration of roll moment equilibrium of the partly-filled vehicle, and the transient slosh forces and moment.

In this chapter, the transient slosh forces and roll moment caused by a time-varying lateral acceleration are evaluated using a roll-plane two-dimensional CFD slosh model. These slosh forces and moment are then incorporated into the roll moment equilibrium of an articulated vehicle to compute the roll stability limits of the partly-filled tank vehicle system, as functions of fill volume and magnitude of the applied acceleration. The analyses are performed for two tanks of different cross-section geometries: circular and "Reuleaux triangular", which are denoted as 'TC' and 'TR' tanks, respectively. The results attained are compared with those derived from the QS analyses to demonstrate the role of transient slosh loads on the roll stability limits.

## 5.2 FLUID SLOSH MODELING

### 5.2.1 Quasi-static (QS) Slosh Model

The static and dynamic roll properties of partially-filled tank vehicles have been evaluated by combining the QS roll plane model of the tank with the comprehensive three-dimensional vehicle models [10, 110]. The quasi-static model, which is based on the hydrostatic theory, yields an accurate estimation of the steady-state *cg* position of the liquid cargo, when subjected to a steady lateral acceleration. In this model, the liquid free

surface is assumed to be stationary, as shown in Figure 5.1a, while the surface gradient $\phi$ is related to the tank roll angle ($\theta_s$) and lateral acceleration ($a_y$), such that:

$$\phi = \frac{a_y + \theta_s}{1 - a_y \theta_s} \tag{5.1}$$

where, $a_y$ and $\theta_s$ in the above equation are in $g$ and *rad*, respectively, while the contribution of the roll angle is significantly smaller than that of the lateral acceleration [112]. The gradient of the free surface may thus be directly related to lateral acceleration, such that $\phi \approx a_y$.

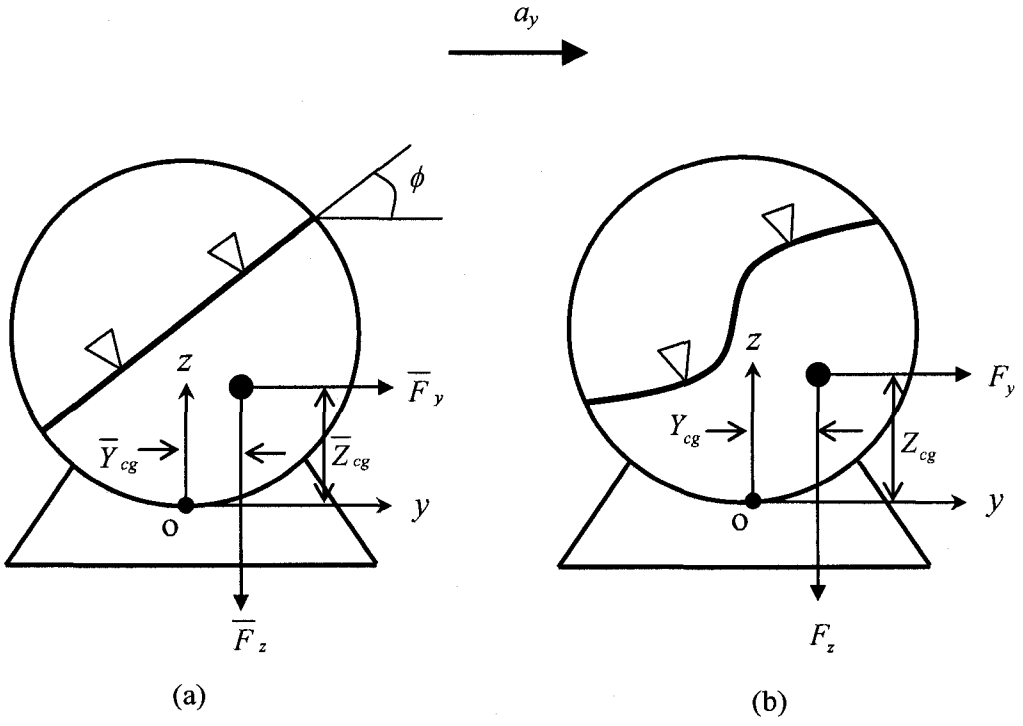


Figure 5.1: Comparisons of free surfaces of liquid in the roll-plane of a tank subject to a lateral acceleration field: (a) quasi-static slosh and (b) dynamic slosh.

The coordinates of the liquid load *cg* are then computed from the following area integrals, assuming homogeneous incompressible fluid:

$$\overline{Y}_{cg} = \frac{\iint_{\Omega} y dy dz}{\iint_{\Omega} dy dz}; \qquad \overline{Z}_{cg} = \frac{\iint_{\Omega} z dy dz}{\iint_{\Omega} dy dz} \tag{5.2}$$

where $\Omega$ is the liquid domain, which is dependent on the tank geometry, and $\overline{Y}_{cg}$ and $\overline{Z}_{cg}$ are the lateral and vertical coordinates of the liquid cargo *cg* with respect to the origin 'O', as shown in Figure 5.1a.

The body forces and the roll moment due to cargo shift are assumed to be constant for a given lateral acceleration. The resulting forces acting on the tank wall and the roll moment, can be computed from [10]:

$$\overline{F}_y = m(a_y g); \qquad \overline{F}_z = mg \tag{5.3}$$

$$\overline{M}_x = \overline{F}_z \overline{Y}_{cg} + \overline{F}_y \overline{Z}_{cg} \tag{5.4}$$

where $m$ is the mass of liquid cargo, $\overline{F}_y$ and $\overline{F}_z$ are the lateral and vertical forces, respectively, and $\overline{M}_x$ is the roll moment about the origin of the coordinate system defined in Figure 5.1a.

The QS model yields an accurate prediction of the mean values of the *cg* coordinates and thus the load shift in the steady state mode of the disturbed fluid flow. The QS formulation, however, cannot provide the *cg* translation in the transient state and thus the transient load shift behaviour. Popov *et al.* [143] demonstrated that the peak translation of the instantaneous *cg* coordinates is considerably higher than the corresponding steady-state mean value, when the tank is subjected to moderate to high

levels of lateral acceleration. The higher magnitudes of the lateral load shift caused by transient oscillations of the fluid (as shown in Figure 5.1b and later in Figure 5.11 in Section 5.5.2) could yield considerably lower roll stability limits. Solaas [79] argued that the low viscosity disturbed fluids require significantly long periods to approach a steady-state. Thus, the QS formulation is not capable of investigating the influence of transient oscillatory fluid slosh phenomenon on the vehicle responses.

### 5.2.2 Transient CFD Fluid Slosh Model

The earlier experimental and simulation results, as discussed in Chapters 2 and 3, showed that the fluid slosh loads under a pure lateral ramp-step acceleration input can be estimated by considering two-dimensional flows for a three-dimensional downscale flat-head tank. The dominant two-dimensional behaviour was observed only in the roll plane due to relatively smaller lateral dimension of the tank and absence of longitudinal baffles. Moreover, the two-dimensional behaviour was also observed to be predominant in the fluid slosh within the fullscale 7.62 m-long tank with curved heads (see Chapter 4).

The fluid slosh in this study is modeled using the CFD VOF method presented in Chapter 3. The computations were performed in the two-dimensional domain within the tank cross-section geometry in the roll plane. As described previously, the pressure distribution over the wetted tank wall due to the fluid slosh were integrated to compute the transient slosh responses in terms of the lateral and vertical slosh forces, and roll moment. The instantaneous free surface curvature is used to estimate the coordinates of the cargo *cg*. Transient variations in the coordinates of cargo *cg*, slosh forces and roll

moment were computed from the coordinates of individual cells, and pressure distributions over the wetted surface of the tank in the following manner:

$$Y_{cg}(t) = \frac{\sum_{\Omega}(Y_{ci}A_i)}{\sum_{\Omega} A_i} \quad , \quad Z_{cg}(t) = \frac{\sum_{\Omega}(Z_{ci}A_i)}{\sum_{\Omega} A_i} \tag{5.6}$$

$$F_y(t) = \sum_{\partial\Omega}(P_i A_{yi}) \, , \; F_z(t) = \sum_{\partial\Omega}(P_i A_{zi}) \tag{5.7}$$

$$M_x(t) = \sum_{\partial\Omega}\left\{(P_i A_{zi})Y_{f_i} + (P_i A_{yi})Z_{f_i}\right\} \tag{5.8}$$

where, $Y_{cg}$ and $Z_{cg}$ are the lateral and vertical coordinates of the liquid *cg*, respectively. $F_y$ and $F_z$ are the slosh forces along the lateral and vertical directions, respectively. $M_x$ is the roll moment about the origin. $\Omega$ is the domain of the liquid occupied cells and $\partial\Omega$ is the domain of liquid-wetted faces on the wall boundary, $Y_{ci}$ and $Z_{ci}$ are the coordinates of the $i^{th}$ cell centroid, $Y_{fi}$ and $Z_{fi}$, are the coordinates of the centroid of the $i^{th}$ face cell, $P_i$, is the pressure at the $i^{th}$ face centroid, $A_i$ is the area of the $i^{th}$ face, and $A_{yi}$ and $A_{zi}$ are the components of the area vector of the $i^{th}$ face in the lateral and vertical directions, respectively.

In this study, two tank cross-sections, a circular and a "Reuleaux triangular", are considered with identical cross-sectional area to equip a tractor-semitrailer tank truck. The parameters of the tanks and vehicles are described in Section 5.4. The computational domains of the two tanks were descretized into the meshes consisting of quadrilateral cells. The influence of mesh size was evaluated to attain the refined mesh appropriate for the numerical simulations. Figure 5.2 depicts comparison of the lateral and vertical slosh forces within the 50%-filled circular tank obtained from the simulations for three

different grid sizes: (*i*) 3483 (Grid-1); (*ii*) 7207 (Grid-2); and (*iii*) 13580 (Grid-3). The comparison reveals only small differences in the slosh forces, in terms of both the magnitude and the frequency. The peak differences in the lateral and vertical forces are less than 1% for the three grid sizes considered. The computational domain was thereby discretized into 3483 cells (Grid-1) for the circular tank ('TC'), while the "Reuleaux triangular" tank ('TR') used a mesh in the same order of size (3490 cells). The time steps in the simulation runs varied from 0.001 to 0.01 s for different levels of the lateral acceleration excitation and the fill volume, in order to obtain solutions within a reasonable computational time, while the residual criterion was selected as $10^{-4}$.

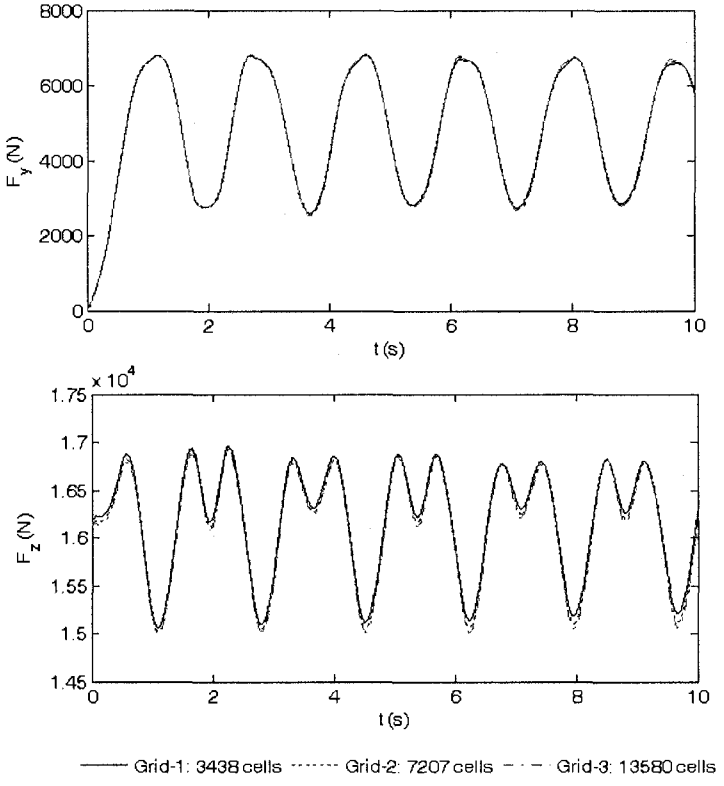


Figure 5.2: Dependence of the fluid slosh forces derived from the CFD simulations on the mesh size for the circular tank under 50% fill volume.

The validity of the two-dimensional CFD slosh model of the partly-filled tank was examined under different lateral acceleration inputs, ranging from 0.1g to 0.5g. The model responses were evaluated to deduce steady-state slosh forces, roll moment and coordinates of the cargo mass centre (*cg*), which were compared with those derived from the QS model using Equations (5.2) to (5.4). As an example, Figure 5.3 illustrates the

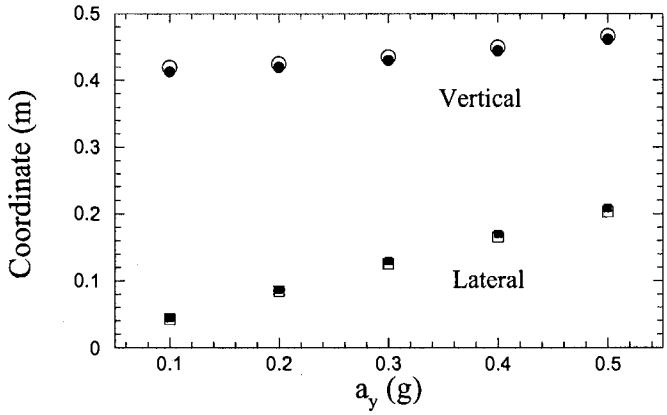


Figure 5.3: Comparisons of mean lateral and vertical *cg* coordinates derived from the dynamic slosh model for 50%-filled 'TR' tank subject to different magnitudes of lateral acceleration with those estimated from the quasi-static method (Lateral coordinate: ■-mean dynamic, □-QS; vertical coordinate: ●-mean dynamic, ○-QS).

comparisons of the mean or steady-state values of the vertical and lateral coordinates of the liquid load *cg*, derived from the dynamic fluid slosh analyses, with the coordinates $\overline{Y}_{cg}$ and $\overline{Z}_{cg}$, computed from the QS model. The results are presented for the "Reuleaux triangular" tank ('TR') with 50% fill volume, subjected to lateral ramp-step acceleration of magnitude ranging from 0.1g to 0.5g. The results obtained from the two approaches show very good agreement in both lateral as well as vertical coordinates. The maximum difference between the mean dynamic and QS results was observed to be less than 4%.

Similar agreements were also observed between the mean values of the vertical and lateral slosh forces, and roll moment derived from the dynamic slosh model, with those derived from the QS model using Equations (5.3) and (5.4). These results also provide validation of the mesh size used in the present study. The mean values of the responses obtained from the dynamic slosh model are therefore used to represent the quasi-static estimations for all simulation runs in the study.

## 5.3 VEHICLE ROLL STABILITY MODEL

A six-axle tractor-semitrailer tank truck is considered to investigate the impact of transient slosh behaviour on its rollover threshold acceleration. The vehicle combination comprises a three-axle tank semi-trailer and a three-axle tractor, as shown in Figure 5.4. The static and dynamic roll properties of such vehicles with rigid cargos have been extensively evaluated using comprehensive nolinear models [8, 12]. The static or steady-turning roll stability of a heavy vehicle is generally evaluated in terms of static roll over threshold using the static roll plane model [8, 11]. An alternate simple method based on roll moment equilibrium [11] has also been employed, which yields rollover threshold values comparable to those derived from the comprehensive models. The roll stability limit of a coupled partly-filled tank and vehicle combination under the influence of transient slosh can be conveniently evaluated by integrating the fluid slosh forces and roll moment to the moment equilibrium or the vehicle. Such an approach would allow independent CFD analysis of the partly-filled tank under steady levels of lateral acceleration. The method has been applied to derive analytical solutions for the steady-turning rollover threshold of vehicles with partly-filled circular, modified-oval and elliptical tanks, while considering the QS slosh forces and roll moment [112]. The effect

of transient slosh forces and roll moment on the steady-turning rollover threshold of the partly-filled tank vehicle can also be evaluated using the same approach, where the primary overturning moment would be based on the transient responses attained from the dynamic slosh analysis.

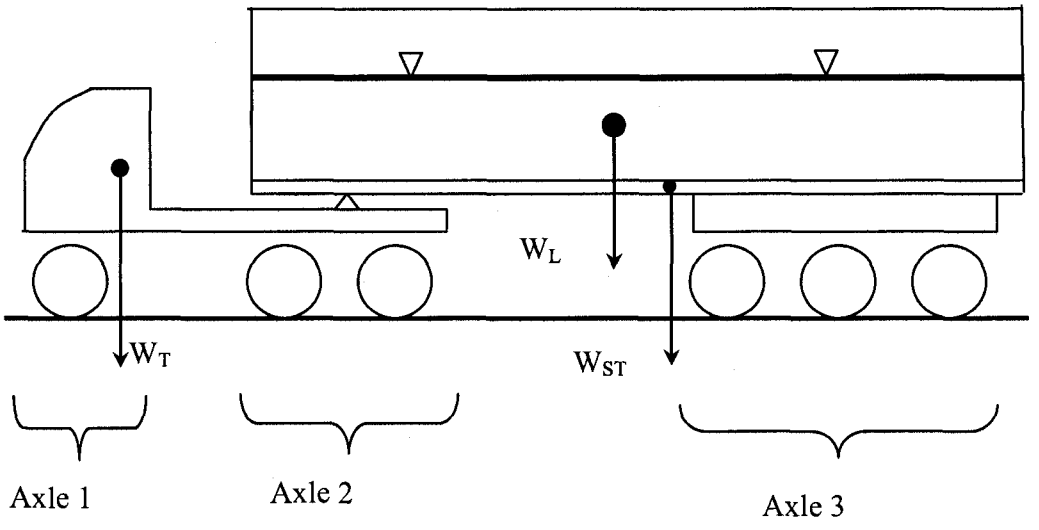


Figure 5.4: Schematic of the 6-axle tractor-semitrailer tank vehicle in the pitch plane.

The roll stability limit of the tractor-semitrailer tank truck is analyzed by decomposing the vehicle into three composite axle sections, in a manner similar to that described in [112]. The groups of semi-trailer and tractor drive axles are lumped together to represent each group by a single equivalent axle, assuming similar properties of individual axles within the group. The combination is thus, considered as a three-axle articulated vehicle. The tractor sprung weight is modeled as two rigid masses supported by the front and composite drive axle coupled through the torsional compliance of the chassis frame, while the masses due to the semi-trailer structure and liquid cargo are

supported by the trailer composite axles, as described in [112]. Each of the sprung and composite unsprung weight is represented in the roll plane, as illustrated in Figure 5.5.

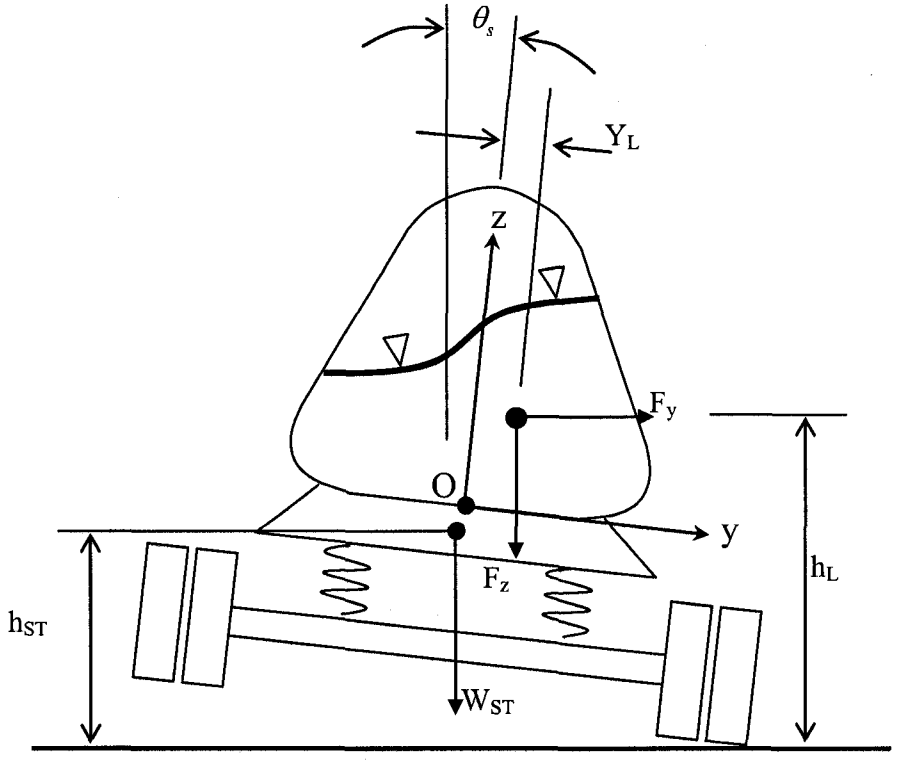


Figure 5.5: Roll plane representation of a partly filled six-axle tractor semitrailar tank vehicle.

It is known that the liquid sloshing and suspended tank structure interact in a very complex manner. Owing to the considerable complexities associated with the integration of the dynamic slosh model to the vehicle model, the analysis is simplified by assuming small roll angles and small unsprung weights relative to the sprung weights. The roll moment equilibrium is derived by considering three components for each sprung weight: the primary overturning moment ($M_{1i}$) arising from the centrifugal acceleration; lateral

displacement moment ( $M_{2i}$ ) caused by lateral *cg* translation due to roll deflection of the sprung weight; and restoring moment ( $M_{3i}$ ) due to the lateral transfer of vertical load from inner to outer tires. The subscript *i* in the moment components refers to the sprung weight on the composite $i^{th}$ the axle ($i$=1, 2, 3). Figure 5.6 illustrates the moment equilibrium for a rigid-cargo multi-axle articulated vehicle combination [11]. The primary overturning moment, $M_{1i}$ and lateral displacement moment, $M_{2i}$, increase linearly with the lateral acceleration ($a_y$) and sprung weight roll angle, respectively. The components $M_{31}$, $M_{32}$ and $M_{33}$ are the suspension and tire restoring moments due to the three composite axles. The figure further shows the rollover threshold accelerations $a_y$*, when the primary overturning moment exceeds the net restoring moment (i.e., $\sum M_{1i} >> \sum M_{2i} + \sum M_{3i}$ ).

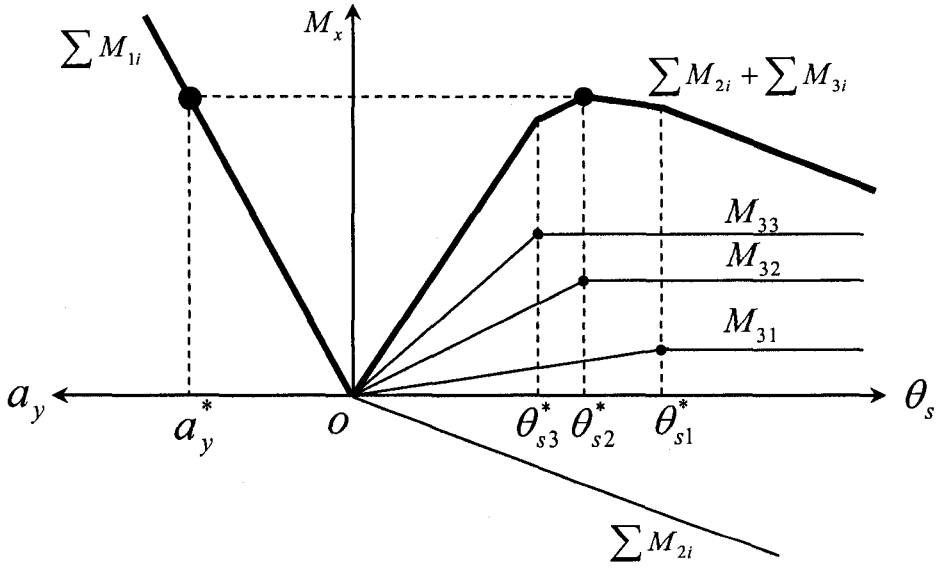


Figure 5.6: The roll moment diagram of the three composite axle tank vehicle model.

A moment equilibrium model may also be formulated for the partly-filled liquid tank vehicle by considering the roll moments due to the transient slosh forces. The maximum primary overturning moment arising from the lateral acceleration can be expressed as the sum of overturning moments due to sprung weights supported by three composite axles. The overturning moment imposed on each composite sprung weight can be derived from:

$$M_{11} = W_1 h_1 a_y^*$$

$$M_{12} = (W_{2T} h_{2T} + W_{2ST} h_{2ST} + C_{Fy} W_{2L} h_L) a_y^* + C_{Fz} W_{2L} Y_L \text{ ; and}$$

$$M_{13} = (W_{3ST} h_{3ST} + C_{Fy} W_{3L} h_L) a_y^* + C_{Fz} W_{3L} Y \tag{5.9}$$

where $W_1$, $W_2$ and $W_3$ are sprung weights supported on composite axles 1, 2 and 3, respectively. The sprung weight $W_2$ comprises tractor weight supported by the rear axle ($W_{2T}$), and portions of the rigid tank semitrailer structure weight ($W_{2ST}$) and the liquid cargo ($W_{2L}$). The sprung weight $W_3$ also comprises portions of weights due to tank semitrailer structure ($W_{3ST}$) and the liquid cargo ($W_{3L}$), such that $W_2 = W_{2L} + W_{2T} + W_{2ST}$, $W_3 = W_{3L} + W_{3ST}$, and $W_L = W_{2L} + W_{3L}$ being the total liquid cargo load. $a_y^*$ is the lateral acceleration corresponding to the relative rollover condition, when primary overturning moment approaches the net restoring moment, and the tractor-rear and semi-trailer composite axles lift off the ground. In the above equation, $h_1$, $h_{2T}$, $h_{2ST}$ and $h_{3ST}$ are the *cg* heights of $W_1$, $W_{2T}$, $W_{2ST}$ $W_{3ST}$, respectively, with respect to the ground. $h_L$ is the vertical coordinate of the liquid cargo *cg*, corresponding to the peak roll moment, as derived from $Z_{cg}$ in Equation (5.6), and $Y_L$ is the corresponding lateral coordinate $Y_{cg}$

derived from Equation (5.6). Coefficients $C_{Fy}$ and $C_{Fz}$ are defined as the ratios of the lateral and vertical sloshing forces (attained from Equation 5.7) at the instant of the maximum roll moment, to the corresponding mean values, respectively, which are used to account for the transient lateral and vertical forces arising from fluid slosh.

The roll moments caused by lateral translations of sprung weights ($M_{2i}$, $i$=1,2,3), corresponding to relative rollover condition, expressed by lift-off of tires of axles 2 and 3 at roll angles, $\theta_{s2}^*$ and $\theta_{s3}^*$, are expressed as:

$$M_{21} = W_1 h_1 \theta_{s2}^*$$

$$M_{22} = (W_{2T} h_{2T} + W_{2ST} h_{2ST} + C_{Fz} W_{2L} h_L)\theta_{s2}^* \text{; and}$$

$$M_{23} = (W_{3ST} h_{3ST} + C_{Fz} W_{3L} h_L)\theta_{s2}^* \tag{5.10}$$

In the above equations, the relative rollover condition is considered to occur when the tractor rear axle experiences lift off corresponding to angle $\theta_{s2}^*$ [11]. At this moment, the restoring moments caused by the composite axle suspension 2 and 3 attain their maximum values of $W_2 T_2$ and $W_3 T_3$, respectively, as evident in Figure 5.6. The restoring moment due to axle 1, however, approaches $W_1 T_1 (\theta_{s2}^* / \theta_{s1}^*)$, which is considerably smaller than those of axle 2 and 3 due to lower front axle load and softer suspension. The restoring moments ($M_{3i}$, $i$=1,2,3), may thus be expressed as:

$$M_{31} = -W_1 T_1 \frac{\theta_{s2}^*}{\theta_{s1}^*};$$

$$M_{32} = -W_2 T_2$$

$$M_{33} = -W_3 T_3 \tag{5.11}$$

where $T_1$, $T_2$, $T_3$ are the half tire tracks of the three composite axles, respectively.

The roll moment equilibrium for the combination corresponding to relative rollover condition may be expressed as:

$$\sum M_{1i} + \sum M_{2i} + \sum M_{3i} = 0 \tag{5.12}$$

Substituting for the moments from Equations (5.9) to (5.11), the moment equilibrium equation is obtained as:

$$M_t a_y^* + C_{Fz} W_L Y_L = W_3 T_3 + W_2 T_2 + W_1 T_1 \frac{\theta_{S2}^*}{\theta_{S1}^*} - M_t \theta_{s2}^* \tag{5.13}$$

where

$$M_t = W_T h_T + W_{ST} h_{ST} + C_{Fy} W_L h_L \tag{5.14}$$

In the above formulation, the slosh parameters ($Y_L$, $h_L$, $C_{Fy}$ and $C_{Fz}$) corresponding to peak roll moment are functions of lateral acceleration $a_y$ for a given fill volume, which are derived on the basis of the polynomial regression (see Section 5.5.3).

The roll angles corresponding to wheel lift-off in the above equations are determined from equivalent roll stiffness of tires and the suspension springs [112], as:

$$\theta_{Si}^* = W_i T_i \left( \frac{1}{K_{Si}^*} + \frac{1}{K_{Ti}^*} \right) - \frac{W_i h_{rci}}{K_{Si}^*} a_y^*; \ (i = 1,2,3) \tag{5.15}$$

where $K_{Si}^*$ and $K_{Ti}^*$ are the equivalent roll stiffnesses of the $i^{th}$ axle suspension springs and tires, respectively, and $h_{rci}$ is the roll center height of the $i^{th}$ axle. The equivalent torsional stiffness of the $i^{th}$ axle suspension springs and tires can be computed, respectively, from:

$$K_{Si}^* = k_{si} S_i^2 + K_{\theta i}; \text{ and } K_{Ti}^* = k_{ti} T_i^2, \quad (i = 1,2,3) \tag{5.16}$$

where $k_{si}$ and $k_{ti}$ are the constant vertical stiffness coefficients due to suspension springs and tires, respectively, and $K_{\theta i}$ is the auxiliary roll stiffness of the $i^{th}$ axle, and $S_i$ is half the suspension track.

## 5.4 SIMULATION CONDITIONS AND ANALYSIS METHOD

The transient fluid slosh behaviour is analyzed in the roll plane for tanks of circular and "Reuleaux triangular" cross-section shapes, which are of identical cross-section area (approximately 3.3 $m^2$), as illustrated in Figure 5.7. The tanks are used to equip a tractor-semitrailer shown in Figure 5.4. Each tank is 12.5 m in length. The height and the maximum width of the "Reuleaux triangular" tank ('TR') are 1.88 m and 2.2 m, respectively, and the diameter of the circular tank ('TC') is 2.05 m.

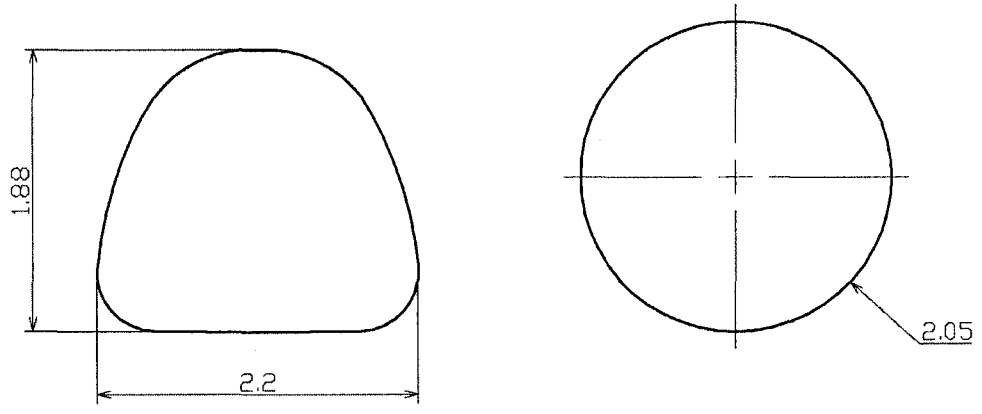


Figure 5.7: The cross-section geometry of the tanks used in the study: (a) "Reuleaux triangular" tank ('TR') and (b) circular tank ('TC').

The transient fluid slosh parameters (i.e., dynamic fluid cargo *cg* coordinates and peak slosh force factors) are incorporated into the simplified 3-axle vehicle model of a tractor-semitrailer tank truck to derive the roll stability limit of the vehicle coupled with the two tanks under different fill conditions. The analyses of the vehicle roll stability are performed for two loading conditions:

*(i)* Approximately constant payload but varying fill volume (44% volume of sulphuric acid and 80% volume of water), which resulted in payloads of 323 kN for both the 'TR' and 'TC' tanks;

*(ii)* Variable cargo load (50% and 80% volume filled with water), where the 50% fill condition resulted in payload of 202 kN.

Table 5.1 Parameters of the 6-axle semitrailer tank vehicle used for analysis.

| **Tractor (three axles)** | | **Semitrailer (tri-axle)** | |
|---|---|---|---|
| Tractor weight (kN) | 85.4 | Trailer and tare tank weight (kN) | 80.1 |
| Wheelbase (m) | 6.2 | Wheelbase (m) | 9.8 |
| Front axle suspension stiffness (kN/m) | 289.5 | Tank length (m) | 12.5 |
| Rear axle suspension stiffness (kN/m) | 700.7 | Tanks cross-section area ($m^2$) | 3.30 |
| Auxiliary roll stiffness- rear axle (kNm/rad) | 514.5 | Auxiliary roll stiffness (kNm/rad) | 514.5 |
| Tire vertical stiffness (kN/m) | 948.3 | Suspension stiffness (each axle, kN/m) | 700.7 |

The analyses are also performed on the basis of QS analysis of the fluid, and rigid cargo with identical loads and *cg* heights. The results are compared to demonstrate the effect of transient fluid slosh. The vehicle parameters used in the analyses are summarized in Table 5.1. The tractor weight is 85.4 kN. The trailer and tare tank weight

is 80.1 kN. The wheelbases of tractor and semitralier are 6.2 m and 9.8 m, respectively. Table 5.2 illustrates different fluid cargos considered and their corresponding fill volumes and loads. For each fill volume, the fluid slosh simulations were carried out for five different magnitudes of steady lateral ramp-step accelerations ($a_y$ = 0.1, 0.2, 0.3, 0.4, 0.5g) with the rise time of 0.5 s, as shown in Figure 5.8.

Table 5.2 The cargo loads of different liquid cargos with different fill volumes considered in the simulation.

| Cargo | Density ($kg/m^3$) | Viscosity (kg/m-s) | Fill volume (%) | Cargo load (kN) |
|---|---|---|---|---|
| Sulphuric acid | 1826.3 | 0.0255 | 44 | 323 |
| Water | 998.2 | 0.001003 | 50 | 202 |
| | | | 80 | 323 |

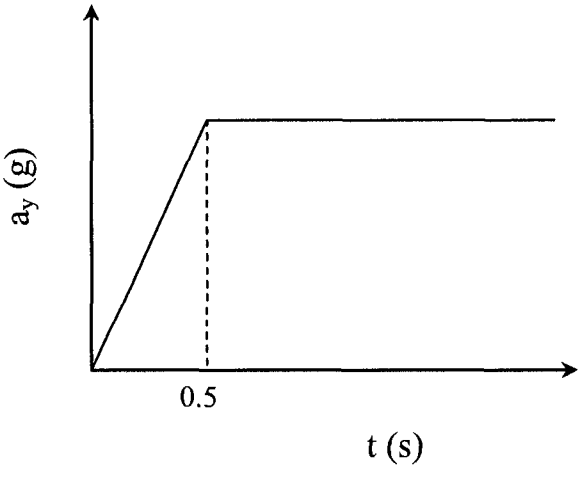


Figure 5.8: The time-varying ramp-step lateral acceleration excitation.

The dynamic fluid slosh is analyzed in terms of the frequency and magnitude of variations in slosh forces, moment and fluid *cg* coordinates for the two tanks under different fill volumes. The fluid slosh frequencies are derived on the basis of frequency spectrum analysis of the transient fluid slosh forces. Based on the sampling rate and FFT window size applied, the frequency resolution of the spectra is 0.0305 Hz. The transient peaks in the fluid *cg* coordinates, lateral and vertical slosh forces and roll moment are computed under each condition of fill volume and acceleration to analyze the dynamic fluid slosh behaviour. The peak responses of fluid slosh are subsequently incorporated into the vehicle roll stability model to derive the roll stability limit corresponding to transient fluid slosh. Considering the phase differences between the slosh forces, and the lateral and vertical coordinates of the cargo *cg*, their peak values are not considered in the analysis. The results obtained from the fluid slosh analysis are evaluated to identify the instance of peak roll moment corresponding to each tank, fill volume and lateral acceleration combination. The coordinates of the cargo, vertical and lateral slosh force amplification factors, corresponding to the same instance are considered to derive the relationship with the lateral acceleration magnitude under the given fill volumes. These transient fluid slosh parameters can be expressed as second-order polynomial regression functions in lateral acceleration ($a_y$) for the three different fill volumes and thus the transient peak slosh responses can be incorporated into the vehicle model described in Equations (5.9), (5.10) and (5.14). Equations (5.9) thru (5.16) are subsequently solved in an iterative manner until a convergent solution is obtained in the rollover threshold $a_y^*$.

## 5.5 DYNAMIC RESPONSES OF FLUID SLOSH

The fluid slosh within partly filled circular and "Reuleaux triangular" cross-section tanks is analysed in the roll plane using the two-dimensional CFD VOF model. The analysis of fluid slosh emphasizes on the magnitude and frequency of variations in the fluid *cg* coordinates, slosh forces and roll moment.

### 5.5.1 Slosh Frequency

The fluid slosh simulations under lateral ramp-step acceleration excitation yield the transient variations in the fluid *cg* coordinates, fluid slosh forces and the roll moment. The frequency spectra of the transient lateral slosh force generally exhibit a single predominant peak for a given fill volume, irrespective of the tank geometry. This frequency was thus considered as the natural slosh frequency for the respective fill volume.

Figure 5.9 illustrates the natural slosh frequencies for the 'TC' and 'TR' tanks under different fill volumes. The validity of the simulation results is further demonstrated by comparing the computed frequencies with those derived from the analytical method [28] reported for the circular cross-section tanks. It should be noted that a method for estimating the frequencies of slosh in the "Reuleaux triangular" tank has not yet been reported. The simulation results for the circular tank (Figure 5.9a) show that a higher fill volume tends to yield high slosh frequency, which agrees well with the analytical solutions. The peak difference between the frequencies estimated from the slosh force responses and the analytical method is less than 2.5% for the fill volumes considered. Similar trend is also observed in the slosh frequency for the 'TR' tank, as shown in

Figure 5.9b. The slosh natural frequency is found to be nearly identical for the two tanks under the intermediate fill volumes (44% and 50%) due to the comparable tank width at the height of free surface under these fill conditions, while the higher fill volume (80%), due to the relatively narrow design of the top section yields a slight higher frequency (by 4.5%) for the "Reuleaux triangular" tank than the circular tank.

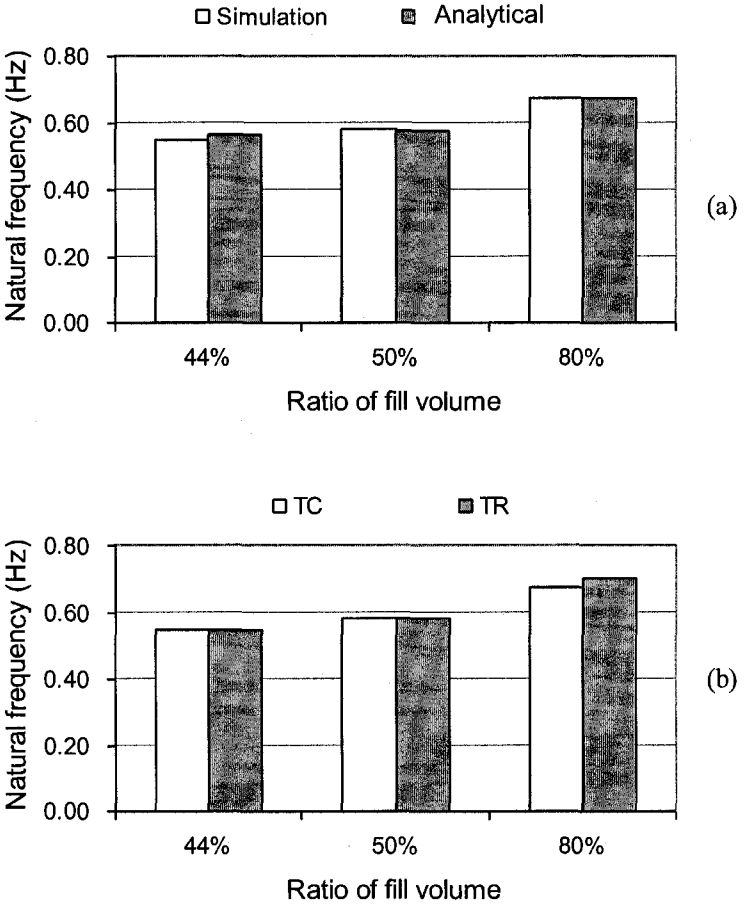


Figure 5.9: Comparisons of lateral mode natural frequencies of fluid slosh of the 'TC' and 'TR' tanks estimated from the spectral components of the slosh forces with those derived form the analytical method: (a) Circular tank; (b) 'TC' and 'TR' tanks.

### 5.5.2 Magnitudes of Slosh Forces and Moment, and *cg* Coordinates

The amplitude of transient fluid slosh can be characterized by the instantaneous *cg* coordinates and the slosh forces. Figure 5.10 illustrates variations in the dynamic lateral and vertical coordinates of the liquid *cg* and the lateral and vertical slosh forces for the 50% volume-filled 'TR' tank with water subject to 0.3g lateral ramp-step acceleration. The results show considerably large amplitudes of the *cg* coordinates and slosh forces, while the oscillatory fluid slosh continues over a long duration with relatively small rate of decay. The mean values of the *cg* coordinates and slosh forces, which represent the solutions derived from the QS model, using Equations (5.6) and (5.7), are also plotted in the figure. It is evident that the magnitudes of dynamic slosh forces are significantly larger than those derived from the QS model. The results also indicate that the large amplitude forces are imposed on the tank structure and vehicle for a sustained duration, which could lead to roll instability at the given acceleration level well below the rollover threshold limits that are estimated from the QS solution [3, 32]. The results further show that the variations in the lateral direction are significantly large as compared to those in the vertical direction, suggesting larger lateral load shift under steady acceleration. The dynamic fluid slosh yields nearly 70% larger deviation in the lateral *cg* coordinates compared to the QS solution. The corresponding difference between the peak and mean values for the vertical coordinates is in the order of 10%. The transient peak magnitude of the lateral slosh force approaches nearly 140% of the respective mean value for the 50% volume-filled condition at $a_y$ = 0.3g, while the mean value is comparable to the QS force. The corresponding magnification of the vertical force, however, is relatively small, which is in the order of 106%. The non-linearity of fluid slosh can also be observed from the

transient free surface position, as evident in Figure 5.11. The figure clearly shows the non-linear waveform of the free surface at time t=1.16s when the peak lateral slosh force occurred.

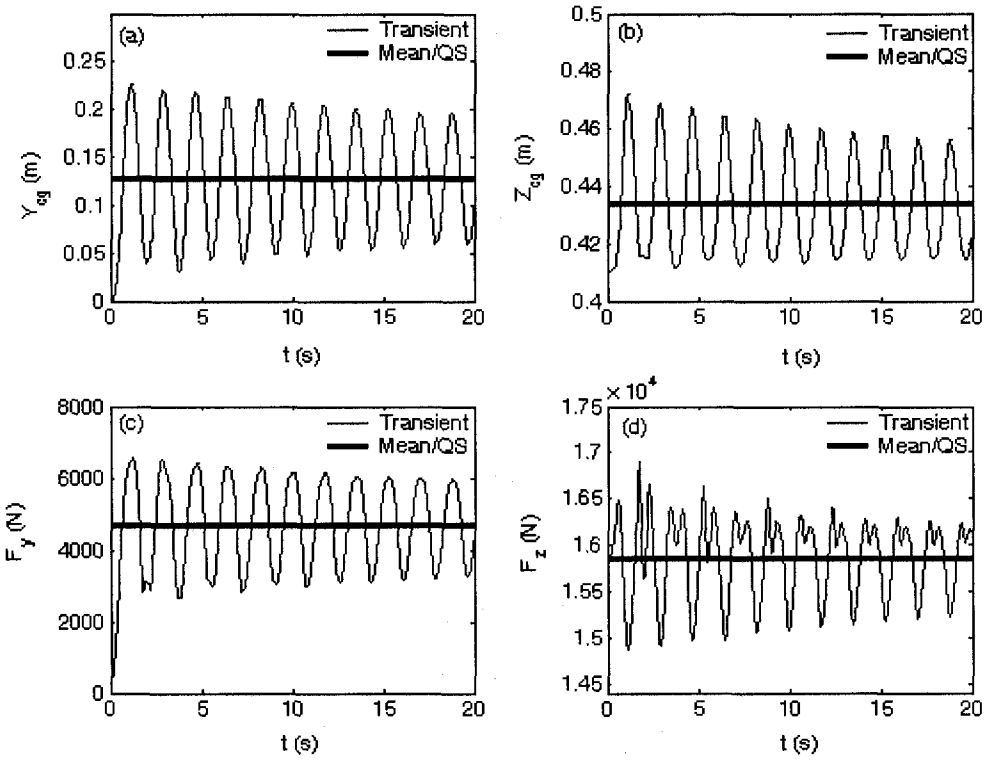


Figure 5.10: Time histories of *cg* coordinates, and lateral and vertical forces for 50% volume-filled 'TR' tank and $a_y$ = 0.3g: (a) lateral *cg* position; (b) vertical *cg* position; (c) lateral slosh force; and (d) vertical slosh force.

The variations in the roll moment derived from the fluid slosh are also compared with that estimated Equation (5.8) under the same conditions, as shown in Figure 5.12. The results show large variations in the roll moment and relatively slow decay of oscillations, similar to that observed for the lateral slosh force response. The peak roll moment is nearly 1.4 times the mean/QS moment, which is sustained over a long period. From these results, it can be concluded that an analysis based on the steady-state (i.e. QS) values

substantially undermines the impact of these parameters on the roll stability of the tank vehicles.

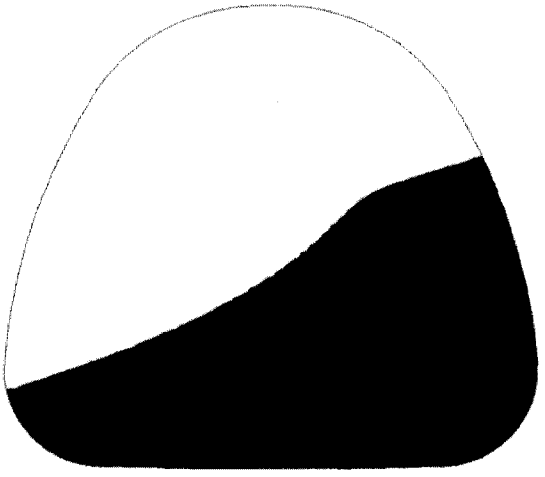

Figure 5.11: The free surface position of the sloshing fluid at t = 1.16 s when the peak lateral slosh force occurred for the 50% volume-filled 'TR' tank at $a_y$ = 0.3g.

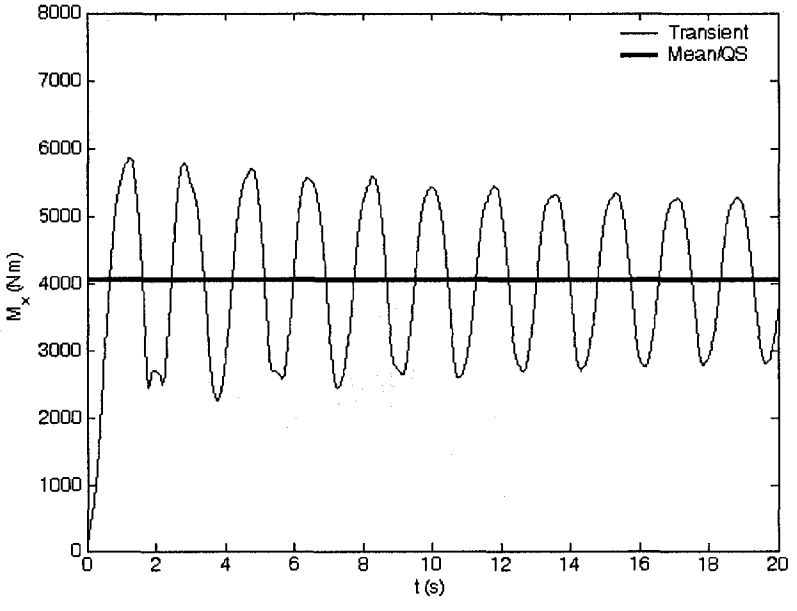


Figure 5.12: Ttime history of the roll moment of the liquid cargo sloshing within the 50% volume-filled 'TR' tank under $a_y$ = 0.3g, together with the quasi-static roll moment.

The variations in the coordinates of the cargo *cg* serve as the primary measure of the slosh phenomenon. The transient deviations in the lateral *cg* coordinates directly relate to the transient lateral load shift, which is more closely related to the relative rollover condition for the heavy vehicles. The variations in the *cg* coordinates are thus considered to describe the transient slosh phenomenon under different fill and lateral acceleration conditions. The analyses are performed for both tanks and fill volumes of 44% (sulphuric acid) and 80% (water), which provided constant cargo loads of approximately 323 kN for both the 'TC' and 'TR' tanks.

Figures 5.13 and 5.14 present the mean and peak values of the lateral and vertical *cg* coordinates for 'TC' and 'TR' tanks under the two fill volumes of constant load, subject to varying magnitudes of lateral acceleration. The results, as expected, show smaller amplitude of sloshing under higher fill volume or less severe lateral excitation. The circular tank ('TC') is observed to exhibit larger *cg* translations than the 'TR' tank in almost all cases, except for the lateral translations under the smaller fill volume (44%). The lower mean and peak values of the vertical *cg* coordinate of the 'TR' tank are attributed to its wider bottom design. The lower values of the lateral coordinate under a higher fill volume are due to the narrower width of the 'TR' tank in the upper half. The results clearly show that the amplitude of fluid slosh can be considerably reduced by the "Reuleaux triangular" cross-section tank for fill volumes in excess of 50%. The amplitude or severity of transient fluid slosh can be further assessed in terms of the ratio of maximum to mean values of the coordinates. This ratio could reach as high as 1.83 for the lateral *cg* translation, and 1.25 for the vertical *cg* translation for the 44% sulphuric

acid filled 'TR' tank. The highest values of this ratio for the circular tank ('TC') in this situation are 1.86 and 1.17, respectively.

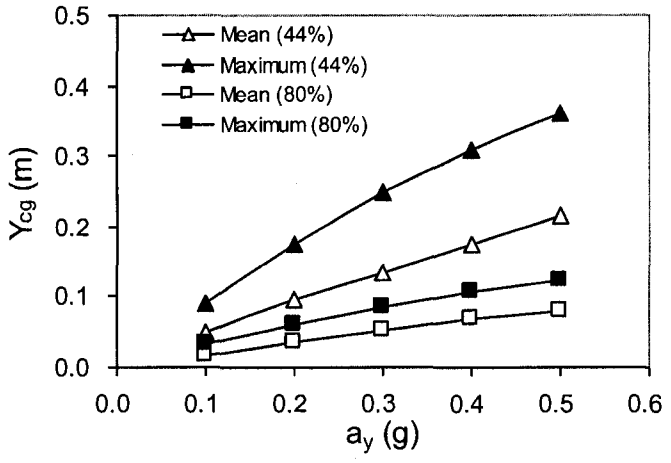


(a)

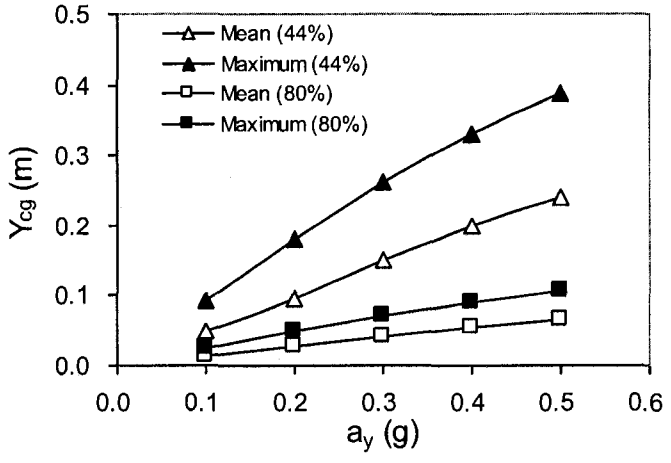


(b)

Figure 5.13: Variations in the mean and maximum values of the lateral *cg* coordinates of liquid cargos as a function of the lateral acceleration excitation and fill volume: (a) 'TC'; and (b) 'TR'.

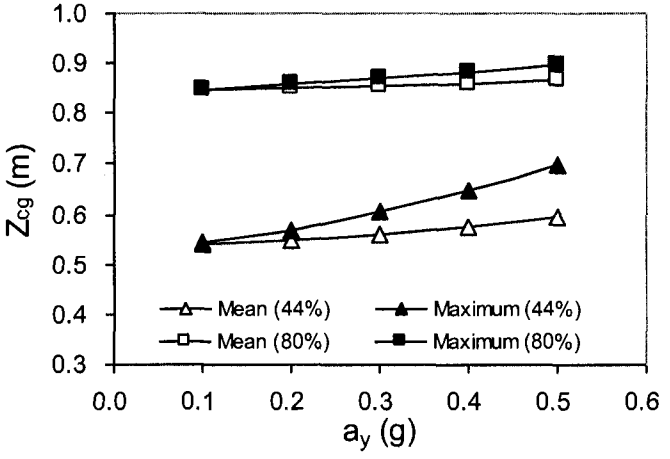


(a)

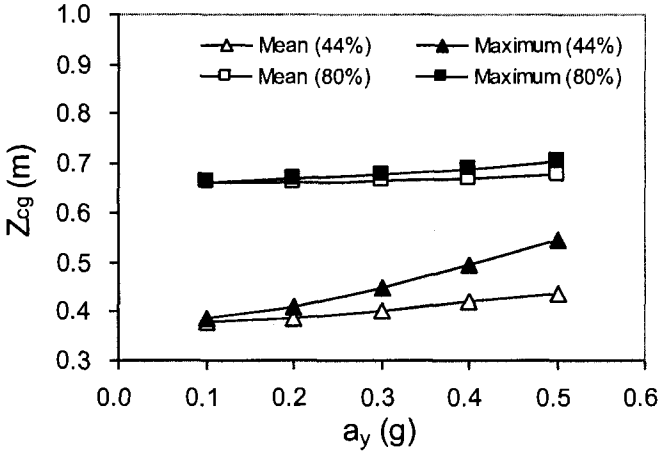


(b)

Figure 5.14: Variations in the mean and maximum values of the vertical *cg* coordinates of liquid cargos as a function of the lateral acceleration excitation and fill volume: (a) 'TC'; and (b) 'TR'.

The sloshing phenomenon is also characterized by the unsteady lateral slosh forces generated due to the impact of the liquid motion on the tank walls. The magnitudes of slosh forces depend on the lateral acceleration, fill volume and tank shape. Figure 5.15 shows the dependency of the peak lateral sloshing force ($F_y$) on the lateral acceleration, fill volume and tank shape. For the circular tank ('TC'), the mean lateral force does not vary with the fill volume, but increases linearly with magnitude of lateral acceleration. The mean/QS lateral slosh force under 44% fill, however, tends to be slightly higher for the 'TR' tank. The amplification of the lateral force, defined as the ratio of the peak force to the mean/QS value, increases with a decrease in the fill volume, suggesting that the uncertainty associated with the QS model increases as the fill volume decreases and yields more severe slosh. The peak lateral force exhibits a rapid change as $a_y$ increases from 0.4g to 0.5g for 'TR' tank, which may be caused by the occurrence of free-surface separation.

The peak and mean magnitudes of vertical slosh forces for both tanks under the same conditions are illustrated in Figure 5.16. The magnitudes of peak as well as mean vertical slosh forces are considerably lower for the circular tank, irrespective of the fill condition and lateral acceleration. The peak magnitudes increase with an increase in the acceleration level, while the rate of increase is significantly higher for the 'TR' tank. It should be noted that the payload for the 'TR' tank is 1.9% higher than that for the circular tank for the 44% fill volume. Consequently, the mean vertical force for the 'TR' tank is slightly higher (by about 2.2%) for the low fill volume (44%) than the high fill volume (80%). For the 44% fill condition, the static free surface lies in the lower coarse mesh zone, which provides slightly higher value of the mean/static mass and is mostly

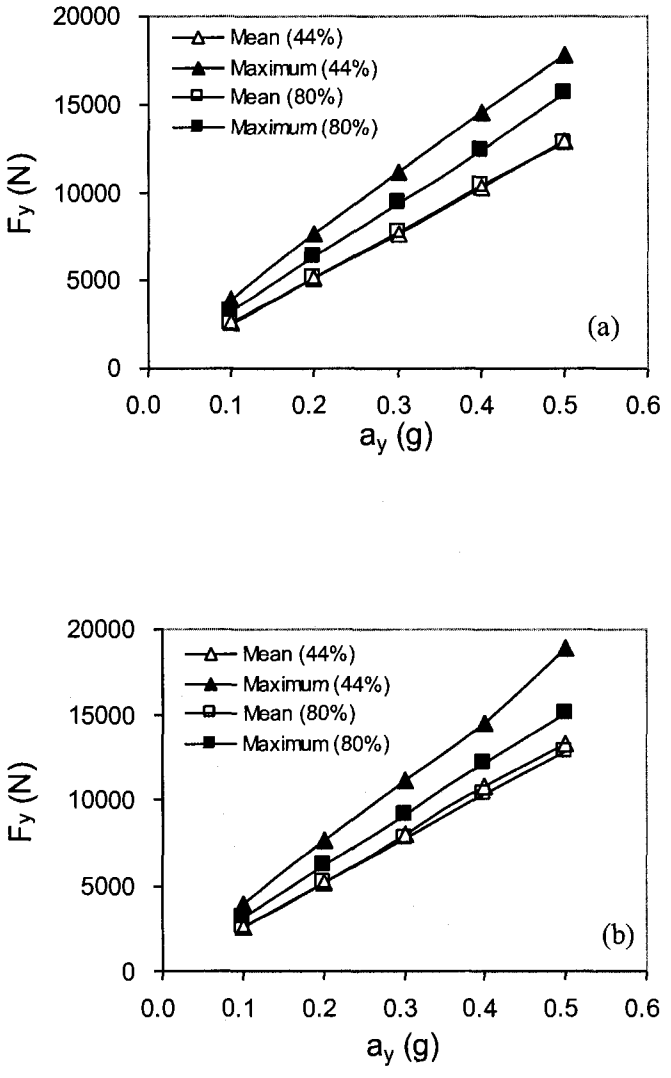


Figure 5.15: The mean and maximum lateral slosh force as a function of lateral acceleration and fill volume: (a) 'TC'; and (b) 'TR'.

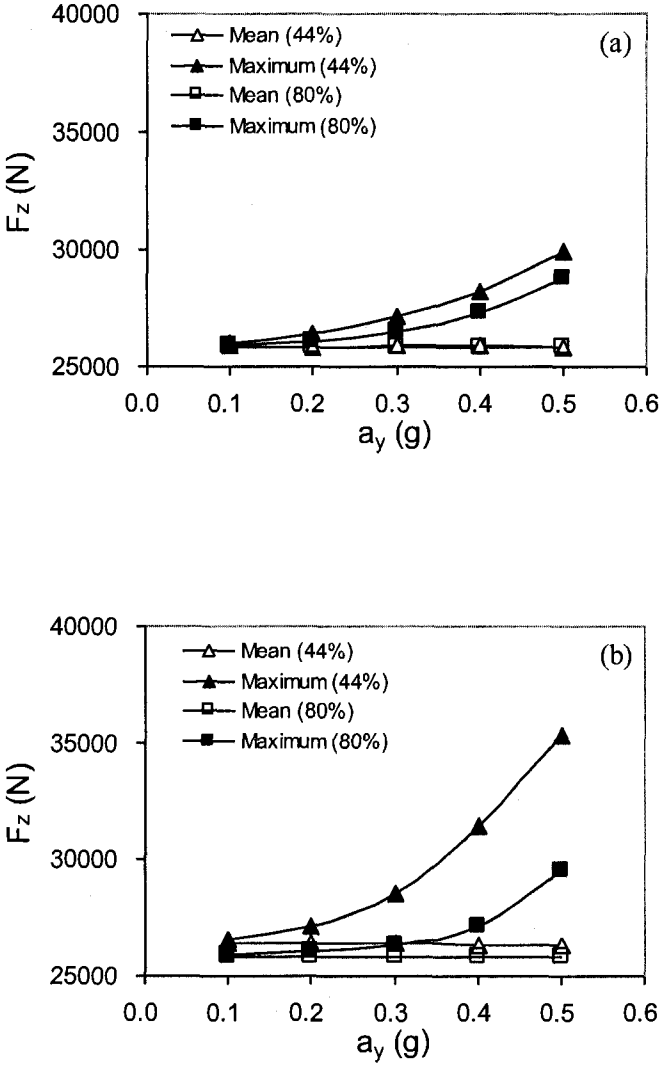


Figure 5.16: The mean and maximum vertical slosh force as a function of lateral acceleration and fill volume: (a) 'TC'; and (b) 'TR'.

attributed to poor initial treatment of partly filled cells in Figure 5.16b. This difference is attributed to relatively coarse mesh used in the wider bottom of the 'TR' tank relative to the narrow top, and the treatment of partly-filled cells and round-off errors with the Fluent software. The narrowing upper section of 'TR' tank encourages relatively larger movement of the free surface along the vertical direction and thus yields considerably larger variations in the wetted surface area, specifically for a lower fill volume and higher acceleration. This tends to create larger dynamic variations in the vertical force, which is derived from the pressure distributions over relatively wider wetted surface.

Roll moment is the most significant measure that directly determines the roll stability. It reflects the combined effects of slosh forces, *cg* translation and tank shape on the roll stability. Figure 5.17 illustrates the peak transient and mean/QS values of the roll moment for both the tanks under same fill conditions and lateral acceleration levels. The figure shows that the slosh forces within the partly-filled circular tank generate higher mean as well as peak roll moment than the 'TR' tank. For the constant cargo load considered in the study, a lower fill volume yields significantly higher peak roll moment, while the 'TR' tank yields considerably lower roll moment than the circular tank. The circular tank yields identical roll moment for both fill conditions, while the 'TR' tank causes higher mean roll moment for the lower fill volume (44%). The magnitudes of mean roll moment of the 'TR' tank, however, remain below those of the circular tank for the entire range of lateral acceleration considered. For both tank geometries, the roll moment increases with an increase in the lateral acceleration. The results further indicate that a 'TR' tank could provide better roll stability than the circular tank of the same cross-sectional area.

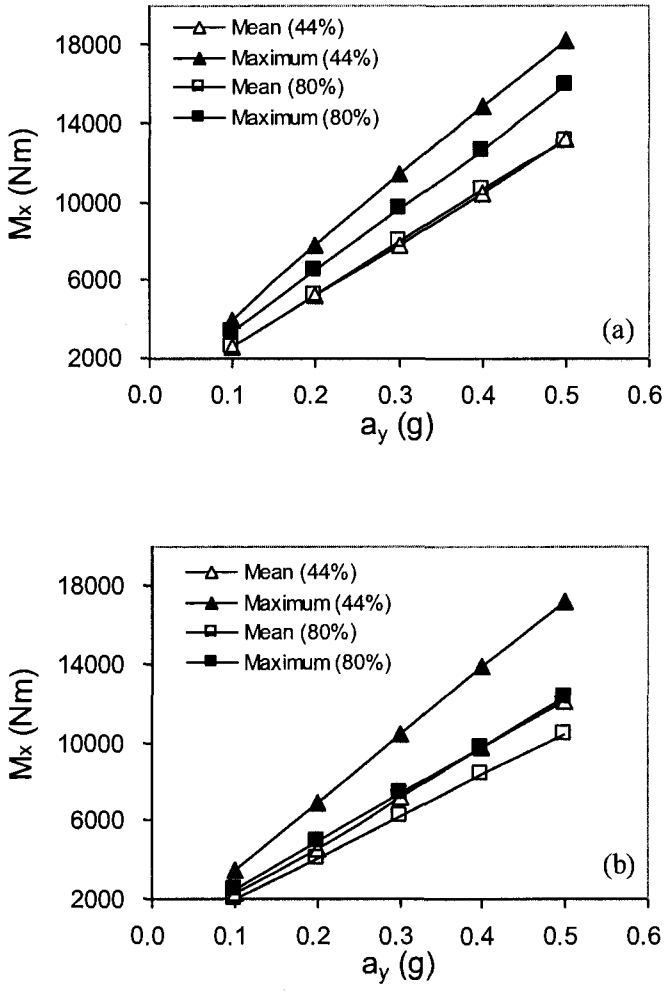


Figure 5.17: The mean and maximum roll moment about the tank base as a function of lateral acceleration and fill volume: (a) 'TC'; and (b) 'TR'.

### 5.5.3 Regression Functions of Slosh Parameters

The slosh parameters ($Y_L$, $h_L$, $C_{Fy}$ and $C_{Fz}$) in Equations (5.9), (5.10), (5.13) and (5.14) are derived on the basis of the second order polynomial regression using the instantaneous these parameter values corresponding to the transient peak roll moments for given lateral acceleration excitations (0.1g to 0.5g) and fill volumes (44%, 50% and

80%). These parameters can be thus expressed as functions of lateral acceleration $a_y$ in the form of $y = a_2 x^2 + a_1 x + a_0$ for a given fill volume. The regression coefficients $(a_2, a_1, a_0)$ may vary depending on the different tank geometries and fill volumes. As an example, Table 5.3 shows the coefficients for the circular and "Reuleaux triangular" tanks with 50% fill volume.

Table 5.3: Polynomial regression coefficients of the slosh parameters for the tanks with 50% fill volume.

| | Circular tank | | | "Reuleaux triangular" tank | | |
|---|---|---|---|---|---|---|
| | $a_2$ | $a_1$ | $a_0$ | $a_2$ | $a_1$ | $a_0$ |
| $Y_L$ | -0.4857 | 0.8468 | 0.0007 | -1.2364 | 1.2638 | -0.0386 |
| $h_L$ | 0.2921 | 0.1218 | 0.5854 | -0.3243 | 0.4280 | 0.3739 |
| $C_{Fy}$ | 0.4586 | -0.6881 | 1.5796 | 3.7975 | -2.1127 | 1.6567 |
| $C_{Fz}$ | -0.1373 | -0.1983 | 1.0114 | 0.5346 | -0.4610 | 1.0354 |

## 5.6 ANALYSIS OF ROLL STABILITY

The rollover threshold of tank vehicles was studied by incorporating the dynamic sloshing model into the simplified 3-axle vehicle model of a 6-axle tractor-semitrailer tank truck. The influence of transient slosh forces on the vehicle roll stability was investigated by solving the moment equilibrium Equation (5.13), which incorporates the regression functions in coordinates of the liquid mass centre, and amplification factors of the vertical and lateral slosh forces, derived from the dynamic slosh analyses. The sloshing effects on roll instability were investigated from two aspects: varying cargo load

with varying fill volume; constant cargo load but varying fill volume. The first case was simulated by 50% and 80% tank volume filled with water, and the second case was realized by loading the tanks with 44% and 80% fill volumes of sulphuric acid and water, respectively. The rollover threshold ( $a_y^*$ ) was computed for both cases, considering different tank shapes (circular and "Reuleaux triangular"), and different liquid states, i.e. the transient maximum (based on the peak roll moment), the steady-state (based on the mean or QS values of the liquid cargo *cg* variations, and additionally in the absence of fluid slosh, considering the cargo to be rigid.

Figure 5.18 illustrates the rollover threshold accelerations of the articulated vehicle when equipped with tanks of circular ('TC') and 'Realeaux angular' ('TR') shapes for different fill volumes. The rollover threshold accelerations for each case were computed for three treatments of fluid cargo that correspond to: (*i*) equivalent rigid cargo; (*ii*) liquid cargo at steady-state using mean/QS slosh forces; (*iii*) transient liquid cargo by using the peak t slosh forces and liquid *cg* positions. The results show that for the same fill-volume, cargo load and tank shape, the rollover threshold is highest for the rigid cargo (as expected), which is followed by the limits attained from the mean/QS analysis, while the consideration of peak transient slosh forces yields lowest values of lateral acceleration threshold, irrespective of the tank geometry. These results clearly indicate that the quasi-static model underestimates the rollover threshold. This is mainly attributed to the lack of consideration of transient forces that are significantly large, and occur over a sustained duration after the application of the manoeuvre. As shown previously in Figure 5.12, the transient peak roll moment could be up to 40% larger than the mean roll moment under a manoeuvre-induced steady acceleration of 0.3g. Therefore, the rollover threshold based

on the mean or quasi-static condition could be considered as an underestimation of the rollover risk, particularly when the slosh forces occur over a sustained period. The results show that the differences between the rollover thresholds predicted from the QS and transient slosh analyses approach as large as 30% and 31%, respectively, for the 'TC' and 'TR' tanks, when both tanks contain 44% fill-volume of sulphuric acid. These differences reduce to 15% and 17%, respectively, for the 80% fill volume. This indicates that the underestimation of the roll stability limit by the QS model is larger for the lower fill volume under which the sloshing amplitude is larger. Comparison of results attained from the analyses of transient slosh and equivalent rigid cargo suggests that the rollover threshold under transient slosh could be as low as 56% of the equivalent rigid cargo vehicle under medium fill volume (44%) for both tanks, while it increases to near 79% under larger fill volume (80%). This, however, holds true when the transient slosh forces and moment occur over a sustained period. The rollover threshold of the vehicle, however, can be considered to lie between the two values corresponding to transient and steady-state forces and moment.

The results further show that the 'TR' tank yields higher rollover threshold values under all fill conditions, particularly under higher fill volume, as compared to those of the circular tank, irrespective of the analysis method used. This is in agreement with the results reported in [142]. Although the 'TR' tank yields larger lateral cargo *cg* shift and higher vertical slosh force under the lower fill volume (44%), these adverse factors do not lead to any disadvantage in terms of the rollover threshold as compared to that for the circular tank. This is attributed to the lower *cg* height of the wide bottom 'TR' tank and smaller lateral slosh force due to its narrower top.

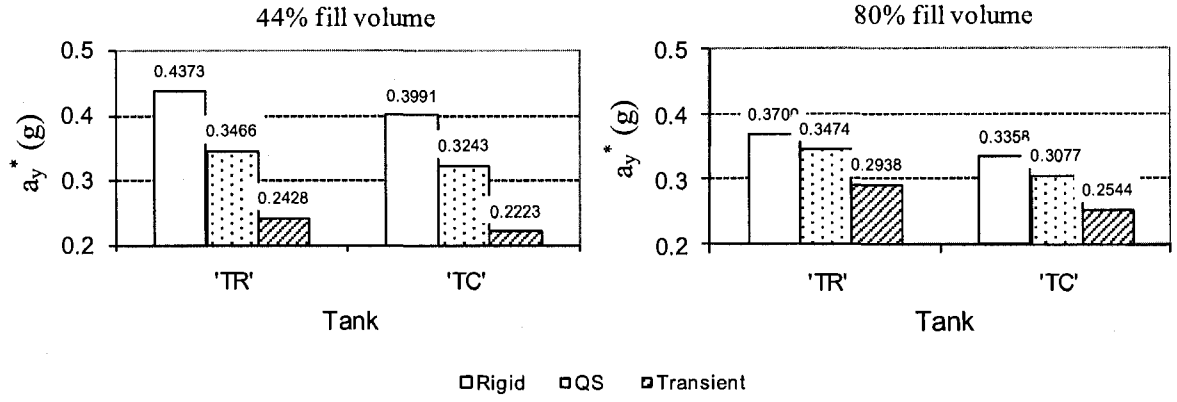


(a)

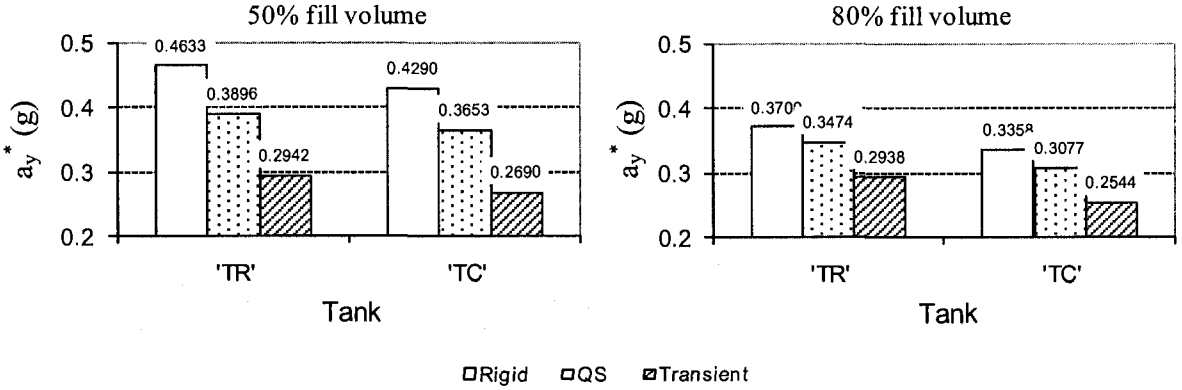


(b)

Figure 5.18: Comparisons of rollover threshold acceleration values predicted from different methods for the 6-axle tractor-semitrailer tank vehicle equipped with the 'TC' and 'TR' tanks carrying different liquid cargos with different fill volumes: (a) constant load; (b) variable load. The value of the rollover threshold for each case is presented above the corresponding bar.

The results derived from the transient slosh analysis for the constant cargo load (Figure 5.18a) show that rollover threshold value for the 'TR' tank under lower fill volume (44%) is 9.2% higher than that for the circular tank, while the difference increases to 15.5% under higher fill volume (80%), suggesting that the 'TR' tank has more pronounced advantage in rollover limit over the 'TC' tank under high fill conditions. Similar trends can be seen in the results attained from the QS and equivalent rigid cargo

analyses. Using the QS approach, due to the inability to consider transient slosh, the above difference is slightly lower, approximately 6.9% and 12.9% under the two fill volumes, respectively. Comparison of the results under different fill volumes of constant load show that lower fill volume (44%) yields lower threshold values than the high fill volume (80%), when transient slosh is considered. This trend, however, is not evident from the results attained from the analyses with mean/QS method and equivalent rigid cargo treatment. This is attributed to more severe sloshing under 44% fill volume, as illustrated in Figures 5.13 to 5.16.

The results attained under variable loading conditions (Figure 5.18b) show similar trends with respect to the effect of transient slosh forces, although the effect is far more pronounced for the 50% fill volume condition, despite the lower associated load. Under the influence of transient slosh, the rollover threshold of the 50% volume filled 'TR' tank is 9.4% higher than that of the circular tank, while it is 6.7% higher when analyzed with the QS approach. The results attained in the QS and equivalent rigid cargo approaches show that this particular fill condition yields considerably higher threshold values than the higher fill volume (80%) for both tanks, which is attributed to relatively smaller load. This gain in the rollover threshold, however, is not evident, when transient fluid slosh is considered, suggesting that the fluid slosh would be the major contributing factor.

## 5.7 SUMMARY

Sloshing phenomenon induced inside a partially loaded tank subject to a steady lateral acceleration is numerically investigated using 2-D roll plane VOF fluid slosh model. The fluid slosh response to a ramp-step acceleration is characterized by the variable *cg*

translation of the cargo and unsteady slosh forces, and consequently the variable roll moment. The transient fluid slosh exhibits variations at the fluid slosh natural frequency which depends on the fill volume and tank geometry. The results shows that the lateral fluid slosh frequency in the roll plane increases as fill volume increases, irrespective of the tank cross-section geometry. The slosh frequency in the 'TR' tank is higher than that in the 'TC' tank under higher fill volume (80%), while they are comparable under intermediate fill volumes (44% and 50%).

The magnitudes of transient fluid slosh depend on the acceleration magnitude, fill volume and tank shape. The results unveil a considerably high ratio of the transient maximum to mean values of lateral cargo *cg* shift and lateral sloshing force, where the mean values are known to correspond with those derived from the quasi-static analysis. The quasi-static method could be considered acceptable for cases involving high fill volume and low lateral excitation, where the magnitude of transient fluid slosh is relatively small. Moreover, the decay rate of the oscillatory transient fluid slosh is extremely small, which may increase for higher viscosity fluids. The transient fluid slosh forces thus occur over a sustained period of time, thereby, the effect cannot be neglected for roll stability analysis of a partially filled tank trucks subject to moderate or high lateral acceleration during steady turning. The severity of the transient slosh is dependent on the tank shape, fill volume and excitation magnitude. The simulation results show that the 'TR' tank exhibits smaller vertical *cg* translation and lateral slosh force, when compared to the circular tank. In terms of lateral *cg* translation and vertical slosh force, however, the former is slightly inferior to the latter. The roll dynamic response of a partly-filled tank truck, however, relies more on roll moment caused by fluid slosh. The

analyses of roll moment show that the 'TR' tank is superior to the circular one, and it thus yields higher rollover threshold, under the influence of transient slosh forces, although the results are comparable for both tanks under 44% fill condition. The same trend is also evident when a quasi-static slosh is considered.

The results of the integrated sloshing model and roll-plane vehicle model verify that partially filled liquid cargo tank trucks have much lower rollover threshold than rigid cargo trucks, when transient slosh effect is considered. Under identical cargo load, a lower fill volume, despite its lower *cg* height, yields lower threshold acceleration, which suggests that the fluid slosh is a major contributory factor from the perspective of roll stability of partly-filled tank trucks. This trend is not as evident when quasi-static analysis is considered. Under variable load conditions, a lower fill volume yields threshold limits that are comparable with those attained at higher fill volume. Considering that the *cg* height and cargo load associated with low fill volume are considerably lower, the results further emphasize the significance of transient fluid slosh effects. The results show that the rollover threshold of the 'TR' tank is higher than that of the 'TC' tank for all the three fill volumes considered, irrespective of the analysis method. The difference is more evident under higher fill volume (80%), which can approach 15.5%.

# CHAPTER 6

# EFFECT OF TRANSIENT FLUID SLOSH ON BRAKING PERFORMANCE ANALYSIS

## 6.1 INTRODUCTION

Fluid cargo and the vehicle body system are the two primary dynamic units of a partly filled tank vehicle, which interact in a highly complex and non-linear fashion under directional maneuvers and road disturbances. The fluid slosh forces and moments arising from a road disturbance or a maneuver induce motions of the vehicle body along the translational and rotational axes. The resulting vehicle motions may subsequently induce the fluid slosh and cause significant variations in the slosh forces and moments. The analysis of such complex interactions of the fluid and the vehicle in a tank-vehicle combination is thus quite difficult, particularly due to nonlinearities of the vehicle system and the fluid slosh.

The previous efforts in this field are hence mostly limited to either quasi-static or mechanical analogy approach to model the fluid slosh for simplicity and convenience of integration with the vehicle models [10, 102, 104-106, 109, 111, 113, 145]. While the quasi-static analysis cannot account for the transient nature of the fluid slosh, the mechanical analogy representations are difficult to reflect the nonlineary in fluid slosh [101]. The CFD fluid slosh models, on the other hand, have rarely been attempted for full integration with the dynamic vehicle models. Only a few studies [7, 55, 150] could be found in the published literature, which attempted to accomplish the integration. The

methodology proposed in [55] was based on updating of the vehicle state using transient fluid slosh forces and moments derived from a CFD fluid slosh model, while the studies in [7, 150] considered the fluid-structure interaction through continuously updating of the values of parameters of both the vehicle and fluid slosh models. The fluid slosh models in their studies, however, were limited to the two-dimensional domain, while the validity of the models was not evaluated. Moreover, only limited results were presented from the models and significantly simple tank geometries were considered.

In Chapter 5, the fluid slosh model developed in this study was incorporated within the static roll plane model of vehicle based upon the static equilibrium equations. This integration, however, did not permit for consideration of the dynamic interactions between the sloshing fluid and the moving vehicle. Moreover, it has been shown that the fluid slosh within a partly filled tank occurs in the three dimensions. Analysis of performance characteristics of a partly filled tank vehicle necessitates the consideration of transient three-dimensional fluid slosh, and integration of the slosh model to the dynamic vehicle formulations such that the dynamic fluid-structure interaction could be taken into account appropriately.

In this Chapter, a 7-DOF pitch-plane vehicle braking model is formulated and integrated with the 3-D fluid slosh model of a partly-filled tank with and without the baffles. The integration of the two models is attained by solving both the models simultaneously while continuously updating the input parameters of the models in the computational process. The braking performance of a tridem tank truck (Figure 4.1) equipped with a tank of a 'Reuleaux triangle' cross-section is evaluated under different

straight-line braking maneuvers. The use of the 3-D slosh model also permits for analysis of effectiveness of the anti-slosh devices, such as transverse baffles.

## 6.2 DEVELOPMENT OF VEHICLE BRAKING MODEL

The entire tank vehicle can be modeled as a multi-body system, which consists of two subsystems: the tank vehicle without the fluid cargo and the fluid cargo within the tank. The two components could be represented by a rigid body vehicle model and a fluid slosh model, respectively. The analyses of the coupled system could thus be performed using the modular simulations of the two subsystems.

The dynamics of a tank vehicle during braking maneuvers could be described by the equations of motion characterizing the motions of different bodies. The equations of motion are formulated by considering the floating fluid as an external object to the vehicle. Thus the forces and moments arising from the fluid slosh are regarded as the external forces and moments acting on the vehicle sprung mass. With regard to the vehicle, a number of pitch-plane and three-dimensional models have been reported in the literature [10, 19-21, 146], as described in Section 1.2.1. In view of the high computational demand of the CFD code, it is desirable to formulate a simple, yet credible, pitch-plane model of the vehicle to simulate for the straight-line braking maneuvers. The analysis under simultaneous application of steering and braking, however, would require a comprehensive three-dimensional vehicle model. In this study, a pitch-plane model of the vehicle is formulated to study the influence of fluid slosh on the braking performance of the vehicle in the presence of a straight-line braking maneuver. A seven-DOF model of the vehicle is formulated by considering longitudinal,

vertical and pitch motions of the sprung mass, vertical motions of unsprung masses, and angular motions of the wheels.

The tank vehicle model is formulated upon considerations of the following simplifying assumptions:

*(i)* The vehicle pitch motion is small, which occurs about the sprung mass cg position;

*(ii)* The fluid cargo undergoes pitch motion identical to that of the vehicle sprung mass;

*(iii)* The sprung mass cg position is assumed to be fixed relatively to the sprung mass structure;

*(iv)* The unsprung masses are rigidly coupled to the sprung mass in the longitudinal direction. The relative longitudinal motion between the sprung and unsprung masses is thus neglected;

*(v)* The tridem rear-axles possess identical properties, and thus lumped together as a composite single unsprung mass;

*(vi)* The properties (stiffness and damping) of the vehicle suspensions and tires are assumed to be linear.

### 6.2.1 Coordinate Systems

The equations of the vehicle motion are formulated in relation to the inertial coordinate system (*xyz*), as seen in Figure 6.1. The origin '*O*' is assumed to be located at the static sprung mass cg position, when a braking maneuver is initiated. Since the vehicle and the fluid slosh models are formulated using different coordinate systems, the coordinate

transformations are used to consider the fluid-vehicle interactions and facilitate the data exchange between the two models. It is thus necessary to define the moving references relative to the inertial coordinate system. Two floating references, $(xyz)^S$ and $(xyz)^B$, are defined with a moving origin attached to the sprung mass cg position ('$O_s$'), as shown in Figure 6.1. The axis system $(xyz)^S$ coincides with the inertial reference, while the $(xyz)^B$ is the body-fixed coordinate system. The $y^B$-axis of the body-fixed coordinate coincides with the $y^S$-axis, assuming negligible lateral, yaw and roll motions under the straight-line braking maneuver. The body-fixed axis system can thus be related to $(xyz)^S$ through the body pitch rotation.

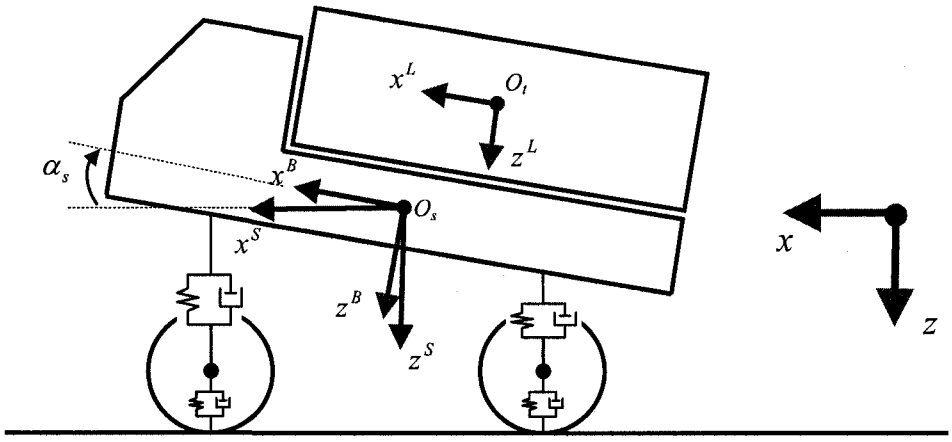


Figure 6.1: Coordinate system used in the vehicle model formulation.

An additional coordinate system $(xyz)^L$ with the origin '$O_t$', attached to the geometric centre of the tank, is also defined to describe the resultant fluid slosh forces and moments. The liquid cargo coordinate system is considered to be merely a translation

of the body-fixed axis system, since the tank structure and the fluid bulk is assumed to undergo same pitch rotation.

### 6.2.2 Equations of Motion of the Vehicle Model

The sprung mass ($m_s$) of the vehicle is considered to be composed of two components: sprung mass due to the chassis structure and sprung mass due to the tare mass of the empty tank. Figure 6.2 illustrates the forces and moments acting on the vehicle sprung and unsprung masses. The fluid slosh forces and moments are considered as the external inputs to the vehicle sprung mass.

The translational motions of the sprung mass along the $x$- and $z$-axes of the inertial reference can be described by the following equilibrium equations:

$$\begin{aligned} \overline{F_{xl}} - \left(F_{xbf} + F_{xbr}\right) - \left(m_s g + m_l g + F_{zl}\right)\alpha_s &= \left(m_s + m_{uf} + m_{ur} + m_l\right)\ddot{x}_s \\ \overline{F_{zl}} - \left(F_{zsf} + F_{zsr}\right) + \left(m_s + m_l\right)g &= \left(m_s + m_l\right)\ddot{z}_s \end{aligned} \tag{6.1}$$

The rotational motion of the sprung mass about the $y^S$-axis can be expressed as:

$$\overline{M}_{yl} + F_{zsf}L_f - F_{zsr}L_r - \left(H_s - z_s\right)\left(F_{xbf} + F_{xbr}\right) = \left(I_{yys} + I_{yyl}\right)\ddot{\alpha}_s \tag{6.2}$$

where $\overline{F_{xl}}$ and $\overline{F_{zl}}$ are the resultant longitudinal and vertical forces due to sloshing liquid cargo, $\overline{M_{yl}}$ is the resultant pitch moment due to the fluid slosh. The resultant slosh forces and moment are computed along the $(xyz)^L$ coordinate system and transformed to the inertial reference, as illustrated in Figure 6.1. The resultant pitch moment due to the slosh forces is computed about the sprung mass cg position ('$O_s$'). The resultant slosh forces and moments are derived from the absolute slosh forces and moment by appropriately adjusting for the inertial forces and moment due to an equivalent rigid cargo.

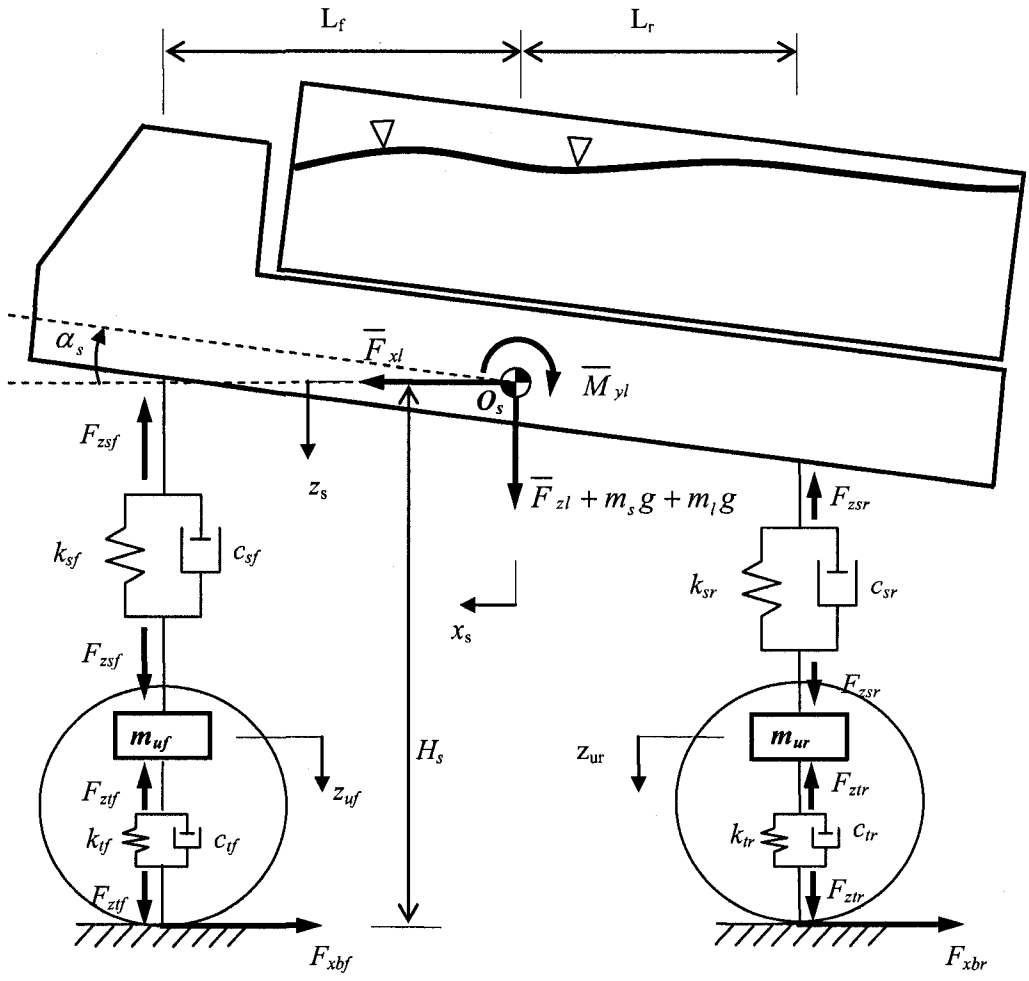


Figure 6.2: Pitch-plane model representation of the tank truck

In the above equations, $F_{xbf}$ and $F_{xbr}$ are the braking forces developed at the front and rear tire-road interfaces, respectively, due to the applied braking efforts. The fluid cargo mass is represented by $m_l$, and $m_{uf}$ and $m_{ur}$ are the front and rear unspung masses, respectively. $I_{yys}$ and $I_{yyl}$ are the mass moment of inertias of the sprung mass and the floating fluid mass about the lateral axis ($y^B$), respectively. Variable $z_s$ describes the

vertical displacement of the sprung mass cg from its static position and $\alpha_s$ is the pitch deflection of the sprung mass. $H_s$ is the sprung mass *cg* vertical position at the static state, and $L_f$ and $L_r$ are the longitudinal positions of the front and rear axles, respectively, from the static sprung mass *cg*, as illustrated in Figure 6.2. $F_{zsf}$ and $F_{zsr}$ are the vertical forces developed due to the front and rear suspensions, respectively. Assuming linear stiffness and damping properties of the suspension system, the suspension forces are derived from:

$$\begin{aligned} F_{zsf} &= k_{sf}(z_s - L_f\alpha_s - z_{uf}) + c_{sf}(\dot{z}_s - L_f\dot{\alpha}_s - \dot{z}_{uf}) \\ F_{zsr} &= k_{sr}(z_s + L_r\alpha_s - z_{ur}) + c_{sr}(\dot{z}_s + L_r\dot{\alpha}_s - \dot{z}_{ur}) \end{aligned} \tag{6.3}$$

where $k_{si}$ and $c_{si}$ are the stiffness and damping coefficients of the suspension at wheel $i$ ($i$=$f$, $r$), and $f$ and $r$ refer to the front and rear axles, respectively. $z_{ui}$ $(i = f, r)$ is the vertical displacement of the unsprung mass $i$ from its respective static position.

The braking forces developed at the wheels are related to the applied braking torque and the tire properties. The braking properties of the tire are known to be highly nonlinear dependent upon the slip, load and physical tire properties. Pacejka [125] proposed a tire model on the basis of measured physical characteristics to describe the braking and cornering properties of the tires. The model, referred to as 'the Magic Formula', has been widely used in vehicle dynamics [9, 10, 55, 146]. Assuming no wheel lockup and application of braking alone, the longitudinal forces, $F_{xbi}$, developed by the tires on the $i^{th}$ axle can be expressed as:

$$F_{xbi} = D\sin\{C\arctan[B(i_s + S_h) - E(B(i_s + S_h) - \arctan B(i_s + S_h))]\} + S_v \quad (i = f, r) \tag{6.4}$$

where $B$, $C$, $D$ and $E$ are empirical coefficients, referred to as stiffness factor, shape factor, peak factor and curvature factor, respectively, which are functions of tire normal load. The variable $i_s$ is the longitudinal slip in percentage and is considered to be a negative value. $S_v$ and $S_h$ are the empirical coefficients representing the offsets in the force-slip characteristics of the tires. The coefficients of the Magic Formula tire model in this dissertation are obtained from the heavy vehicle tire data reported in [149].

The equations of motion for the unsprung masses, $m_{uf}$ and $m_{ur}$, describing the vertical motion can be expressed from the suspension and inertial forces, such that:

$$F_{zsi} - F_{zti} + m_{ui}g = m_{ui}\ddot{z}_{ui} \qquad (i = f, r) \tag{6.5}$$

where $F_{zti}$ is vertical force due to the tires on the $i^{\text{th}}$ axle $(i = f, r)$. Assuming linear vertical stiffness and damping properties of the tires, the vertical tire forces are derived from:

$$F_{zti} = k_{ti}z_{ui} + c_{ti}\dot{z}_{ui} \qquad (i = f, r) \tag{6.6}$$

where $k_{ti}$ and $c_{ti}$ ($i$=$f$, $r$) are the tire stiffness and damping coefficients, respectively.

The angular motions of the wheels depend upon the applied braking torque, road friction, forward vehicle speed and the braking force developed by the tires. Figure 6.3 illustrates the forces and moments acting on a wheel/tire assembly. Assuming uniform tire-road adhesion and that the braking forces remain below the limit of tire-road adhesion (i.e., no wheel lockup), the angular motion of the wheel/tire combination can be related to the braking force in the following manner:

$$F_{xbi}R_i - T_i = I_i\dot{\Omega}_i \qquad (i = f, r) \tag{6.7}$$

where $T_i$ is the braking torque applied to wheel $i$ ($i = f$, $r$), as shown in Figure 6.3. It is assumed that the torque distribution is proportional to the static normal load distribution

at the front and rear axles [9, 146]. The torque is applied via a braking system with a treadle pressure input. $R_i$ is the effective rolling radius of wheel $i$ ($i=f, r$) and $I_i$ is the polar mass moment of the tire-wheel assembly $i$.

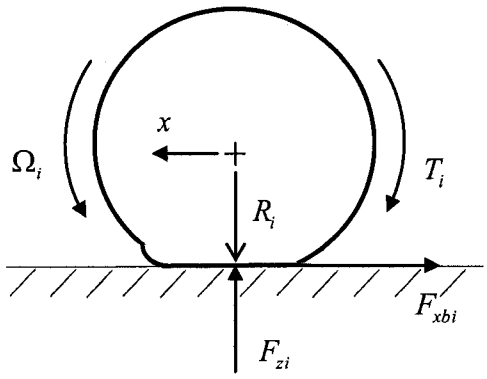


Figure 6.3: Forces and torque acting on the tire ($i=f$ and $r$, indicating front and rear wheel-tires, respectively).

## 6.3 FLUID SLOSH MODEL

The fluid cargo slosh is modeled assuming the 3-D fluid slosh, as described in Chapter 4. Although a straight-braking maneuver may cause only longitudinal dynamics of the tank structure and the vehicle, the fluid slosh in the three-dimension would be expected, particularly in the presence of the baffles. This was observed from the experiments conducted on the scale model tank and the simulation results presented in Chapters 2 and 4. The fluid slosh model is developed for the full scale tank of a typical tridem tank truck, as depicted in Figure 4.1. The tank geometry has been described in Chapter 4. The model simulations are performed using the identical refined mesh and step size that was established in Chapter 4. The analyses, however, were performed by considering the

reference coordinate system located at the tank geometry centre, rather than the tank base that was used for the earlier results.

Apart from the longitudinal acceleration excitation arising from a straight-line braking maneuver, the tank structure in a tank-vehicle combination experiences considerable vertical and pitch motions. The position and orientation of the tank structure thus need to be altered along with the vehicle body during the maneuvers, when the fixed coordinate system (*xyz*) is considered. The implementation of both types of motions to the fluid slosh model in the fixed coordinate system is quite complex as it requires re-meshing of the fluid domain during the computational process. Alternatively, the fluid slosh model can be solved in the tank-fixed coordinate system $(xyz)^{L}$, while the resulting accelerations applied on the fluid cargo can be derived through transformation of the acceleration responses of the vehicle sprung mass ( $\ddot{x}_s$ , $\ddot{z}_s$ and $\ddot{\alpha}_s$ ) onto the $(xyz)^{L}$ coordinate system. This methodology is described in the following section.

## 6.4 INTEGRATION OF FLUID SLOSH AND VEHICLE MODELS

As stated earlier that the motions of the fluid cargo and the vehicle body are strongly coupled and the two subsystems exhibit significant dynamic interactions. The models thus need to be integrated to achieve the real-time simulations of these interactions, particularly the effects of transient fluid slosh forces and moments on the vehicle motions. In the present dissertation, the integration of the two models is realized by updating the input parameter required for each model at every time step in the process of computation, as illustrated in Figure 6.4. The vehicle model is initially solved assuming static fluid condition and a given forward initial velocity. The time varying braking

torque is subsequently applied assuming a rounded ramp-step change in the brake treadle pressure, as illustrated in Figure 6.5.

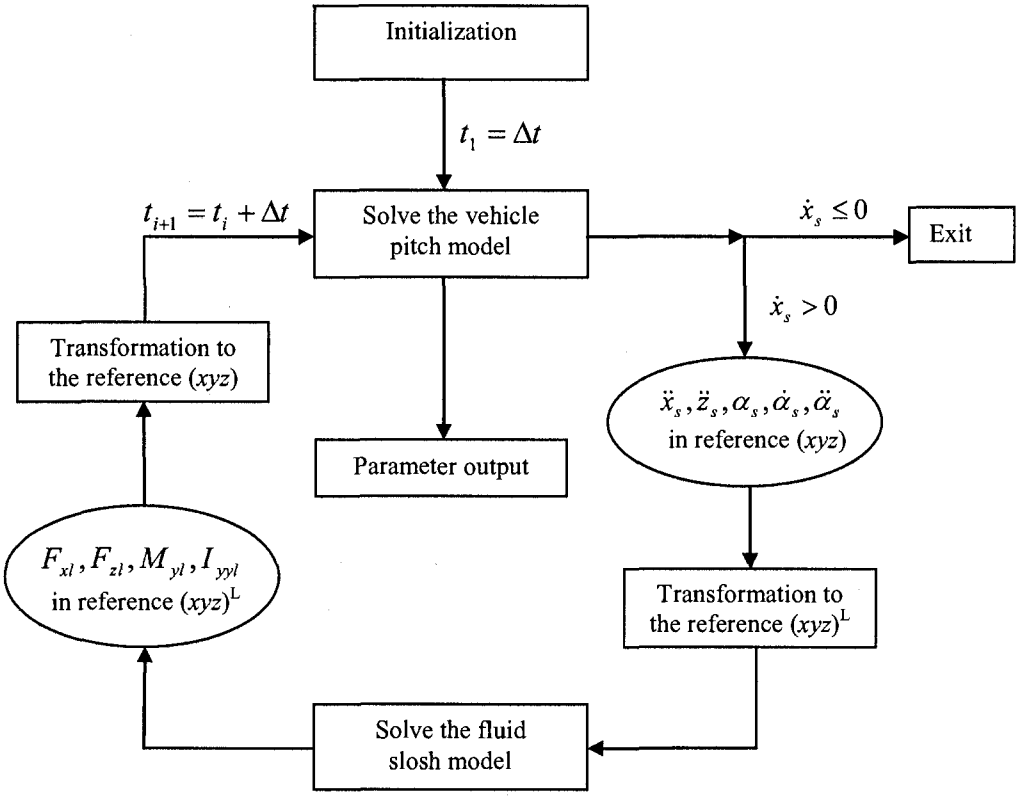


Figure 6.4: Computation procedure of the coupled fluid slosh and vehicle models.

The vehicle responses ( $\ddot{x}_s, \ddot{z}_s, \alpha_s, \dot{\alpha}_s, \ddot{\alpha}_s$ ) computed in the inertial coordinate system (*xyz*) are transformed to the resultant accelerations imposed on the fluid cargo at the geometric centre of the tank. The fluid slosh model is subsequently solved to determine the slosh forces and pitch moment, and the pitch mass moment of inertia, with reference to the $(xyz)^L$ axis system, as shown in Figure 6.4. The instantaneous fluid slosh responses are transformed onto the fixed coordinate system (*xyz*) and applied to the

vehicle model at the subsequent instant. The process is continued until when the vehicle forward velocity has diminished.

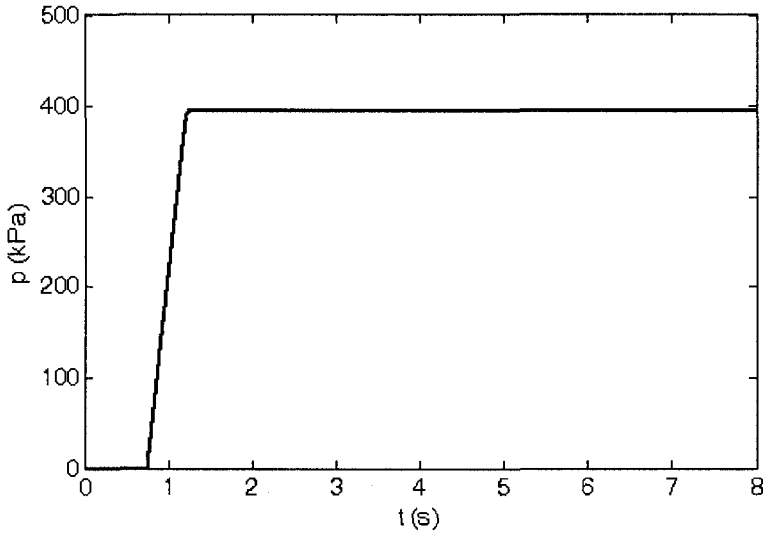


Figure 6.5: The braking treadle pressure input representing a straight line braking maneuver.

The straight-line braking maneuvers are simulated with a rounded ramp-step braking treadle pressure, as illustrated in Figure 6.5. The rise time of the braking system of the vehicle is assumed to be 0.5 s. The driver's reaction time and the braking system time lag are assumed to be 0.75 s [147, 148]. The braking torque gain of the braking system is set as 98.2 Nm/kPa [148].

### 6.4.1 Transformation of Acceleration Responses

As introduced in Section 6.3, the fluid slosh model is analyzed under resultant accelerations, while the tank orientation is held fixed. The vertical, longitudinal and pitch

acceleration responses of the vehicle sprung mass, computed along the coordinate system $(xyz)$, are thus transformed to the tank attached axis system $(xyz)^{L}$. The tank geometric centre ('$O_t$') can be regarded as a virtual point on the tank structure. Since the tank geometry centre ('$O_t$') is not coincident with the truck sprung mass centre '$O_s$', the point '$O_t$' will be subjected to both angular and translational (longitudinal and vertical) accelerations in the pitch plane. The angular acceleration at the tank geometry centre ('$O_t$') is the same as that at the sprung mass cg position ('$O_s$'), since the two axis systems are fixed to the respective sprung mass structures. The translational accelerations of the tank centre are derived from the translational accelerations of the sprung mass cg position '$O_s$' superposed by the components due to the angular motion.

With the floating body-fixed reference $(xyz)^{B}$ rotated by a pitch angle $\alpha_s$ with respect to the fixed reference $(xyz)^{S}$, the position of a point '$P$' in the reference $(xyz)$ can be expressed:

$$X_p = X_{Os} + X_p^S = X_{Os} + [A]X_p^B \tag{6.8}$$

where $X_p = \begin{Bmatrix} x_p \\ z_p \end{Bmatrix}$ is the position vector of '$P$' in the inertial reference, $X_{Os} = \begin{Bmatrix} x_s \\ z_s \end{Bmatrix}$ is the position vector of the origin '$O_s$' of the floating reference $(xyz)^{S}$ in the reference $(xyz)$, $X_p^S = \begin{Bmatrix} x_p \\ z_p \end{Bmatrix}^S$ and $X_p^B = \begin{Bmatrix} x_p \\ z_p \end{Bmatrix}^B$ define the positions of point '$P$' in the floating references $(xyz)^{S}$ and $(xyz)^{B}$, respectively, and $[A]$ is the transformation matrix due to the rotation:

$$[A] = \begin{bmatrix} \cos\alpha_s & \sin\alpha_s \\ -\sin\alpha_s & \cos\alpha_s \end{bmatrix} \tag{6.9}$$

Differentiating Equation (6.9) with respect to time yields:

$$\dot{X}_p = \dot{X}_{Os} + [\dot{A}]X_p^B + [A]\dot{X}_p^B \tag{6.10}$$

Further differentiating Equation (6.10) with respect to time yields:

$$\ddot{X}_p = \ddot{X}_{Os} + [\ddot{A}]X_p^B + 2[\dot{A}]\dot{X}_p^B + [A]\ddot{X}_p^B \tag{6.11}$$

Thus the acceleration at the tank geometry centre '$O_t$', in the reference ($xyz$) can be expressed as:

$$\ddot{X}_{Ot} = \ddot{X}_{Os} + [\ddot{A}]X_{Ot}^B + 2[\dot{A}]\dot{X}_{Ot}^B + [A]\ddot{X}_{Ot}^B \tag{6.12}$$

Since the position of tank centre '$O_t$' is fixed relative to the body-fixed axis system $(xyz)^B$, its position, velocity and acceleration in this axis system are derived as:

$$X_{Ot}^B = \begin{Bmatrix} x_{Ot} \\ z_{Ot} \end{Bmatrix}^B ;\ \dot{X}_{Ot}^B = 0;\ \ddot{X}_{Ot}^B = 0 \tag{6.13}$$

where $\begin{Bmatrix} x_{Ot}^B \\ z_{Ot}^B \end{Bmatrix}$ is the position vector of the tank geometry centre ('$O_t$') in the body-fixed reference $(xyz)^B$. Considering that

$$[\ddot{A}] = \begin{bmatrix} -\ddot{\alpha}_s \sin(\alpha_s) - \dot{\alpha}_s^{\,2} \cos(\alpha_s) & \ddot{\alpha}_s \cos(\alpha_s) - \dot{\alpha}_s^{\,2} \sin(\alpha_s) \\ -\ddot{\alpha}_s \cos(\alpha_s) + \dot{\alpha}_s^{\,2} \sin(\alpha_s) & -\ddot{\alpha}_s \sin(\alpha_s) - \dot{\alpha}_s^{\,2} \cos(\alpha_s) \end{bmatrix} \tag{6.14}$$

The acceleration vector at the tank centre ('$O_t$') in the inertial reference ($xyz$) can be expressed as:

$$\begin{Bmatrix} \ddot{x}_{Ot} \\ \ddot{z}_{Ot} \end{Bmatrix} = \begin{Bmatrix} \ddot{x}_{Os} \\ \ddot{z}_{Os} \end{Bmatrix} +$$

$$\begin{Bmatrix} x_{Ot}^B(-\ddot{\alpha}_s \sin(\alpha_s) - \dot{\alpha}_s^{\,2} \cos(\alpha_s)) + z_{Ot}^B(\ddot{\alpha}_s \cos(\alpha_s) - \dot{\alpha}_s^{\,2} \sin(\alpha_s)) \\ x_{Ot}^B(-\ddot{\alpha}_s \cos(\alpha_s) + \dot{\alpha}_s^{\,2} \sin(\alpha_s)) + z_{Ot}^B(-\ddot{\alpha}_s \sin(\alpha_s) - \dot{\alpha}_s^{\,2} \cos(\alpha_s)) \end{Bmatrix}$$

(6.15)

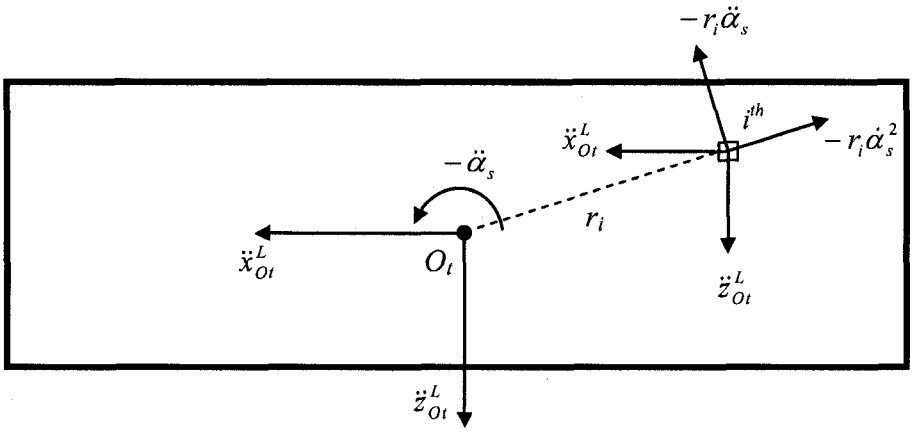


Figure 6.6: The accelerations imposed on a fluid 'cell' within the computational domain of the tank

The accelerations imposed on a fluid 'cell' located at '$O_t$' in the reference $(xyz)^L$, can be derived from the following transformation with consideration of the pitch rotation:

$$\begin{Bmatrix} \ddot{x}_{Ot} \\ \ddot{z}_{Ot} \end{Bmatrix}^L = -[A]^{-1} \begin{Bmatrix} \ddot{x}_{Ot} \\ \ddot{z}_{Ot} \end{Bmatrix} \tag{6.16}$$

The negative sign indicates that the fluid acceleration field is in the direction opposite to that of the vehicle structure. Owing to the pitch rotation of the tank structure, a fluid cell, other than that located at '$O_t$', is subjected to both the centripetal and tangential accelerations ($r_i\dot{\alpha}_s^2$ and $r_i\ddot{\alpha}_s$) in addition to the above translational accelerations, as illustrated in Figure 6.6, where $r_i$ is the position vector of the $i^{th}$ fluid 'cell' in the $(xyz)^L$ reference. The resultant acceleration imposed on the $i^{th}$ fluid 'cell' is thus expressed as:

$$\begin{Bmatrix} \ddot{x}_i \\ \ddot{z}_i \end{Bmatrix}^L = \begin{Bmatrix} \ddot{x}_{Ot} \\ \ddot{z}_{Ot} \end{Bmatrix}^L - \begin{Bmatrix} z_i{}^L\ddot{\alpha}_s - x_i{}^L\dot{\alpha}_s \\ -x_i{}^L\ddot{\alpha}_s - z_i{}^L\dot{\alpha}_s \end{Bmatrix} + \begin{Bmatrix} -g\sin\alpha_s \\ g\cos\alpha_s \end{Bmatrix} \tag{6.17}$$

where $x_i^L$ and $z_i^L$ are the coordinates of the $i^{th}$ fluid cell within the tank in the tank axis system $(xyz)^L$. The last term on the right side of the equation relates to the components of acceleration due to gravity.

### 6.4.2 Transformation of Slosh Force and Moment Responses

The forces and pitch moment due to the fluid slosh are computed from the analysis of the fluid slosh model in the tank-fixed axis system $(xyz)^L$. These responses are subsequently transformed into the vehicle inertial reference $(xyz)$ to serve as the disturbances to the vehicle model. The slosh forces acting on the sprung mass cg location ('$O_s$') of the vehicle can be related to those developed at the tank centre ('$O_t$'), such that:

$$\begin{Bmatrix} F_{xl} \\ F_{zl} \end{Bmatrix}_{Os} = [A] \begin{Bmatrix} F_{xl} \\ F_{zl} \end{Bmatrix}_{Ot}^{L} \tag{6.18}$$

The pitch moment at the location '$O_s$', in a similar manner, is related to the fluid slosh moment and slosh forces developed at '$O_t$':

$$M_{yl,Os} = M_{yl,Ot} + \vec{F}_{l,Ot} \times \vec{r}_{Ot} \tag{6.19}$$

where $M_{yl,Ot}$ is the resultant fluid slosh pitch moment at the tank centre ('$O_t$'), $\vec{F}_{l,Ot} = \begin{Bmatrix} F_{xl} \\ F_{zl} \end{Bmatrix}_{Ot}$ is the slosh force vector at the tank centre, and $\vec{r}_{Ot}$ is the position vector of the tank centre in the axis system $(xyz)^B$.

The instantaneous pitch mass moment of inertia of the floating fluid about the sprung mass cg position ('$O_s$') is also computed with respect to the tank reference system $(xyz)^L$ but about the position '$O_s$' of the vehicle from the following volume integral:

$$I_{yyl} = \iiint_V \rho[(z - |z_{Os}^L|)^2 + (x - |x_{Os}^L|)^2] dV \tag{6.20}$$

where $V$ is fluid occupied volume domain, and $x_{Os}^{L}$ and $z_{Os}^{L}$ are the longitudinal and vertical coordinates of '$O_s$' with respect to the origin of the $(xyz)^{L}$ axis system.

## 6.5 SIMULATION PARAMETERS AND VEHICLE MODEL VALIDATION

The simulation parameters of the baseline tridem tank truck (Figure 4.1) are summarized in Table 6.1. The sprung mass of the vehicle without the cargo is 5250 kg, while its full payload capacity is 16,400 kg. The wheelbase of the vehicle considering the single composite rear axle is 6.65 m. The length of tank is 7.62 and its cross-section area is 3.26 $m^2$, which is identical to the tank defined in Chapter 4.

The straight-line braking responses of the truck are analyzed considering two tank configurations: (*i*) the un-baffled cleanbore tank 'T0'; and (*ii*) the baffled tank 'T1' with the single orifice baffles, as described in Section 4.2. The tank-truck combinations employing the two tanks are also denoted as 'T0' and 'T1', respectively. The vehicle models are formulated for three different liquid cargos, but constant cargo load, to realize different fill conditions. The liquid cargos considered include sulfuric acid, dichloromethane and water, which correspond to the fill volume ratios of 38.1%, 52.1% and 69.5%, respectively. As presented in Chapter 4, the three fluid cargos are denoted as 'C1', 'C2' and 'C3', respectively. The properties of these fluids have been presented in Section 4.3.

Table 6.1: The simulation parameters of the baseline tridem tank truck

| | |
|---|---|
| Sprung mass (including tare tank), $m_s$ –kg | 5250 |
| Fluid cargo load (rated), $m_l$ –kg | 16400 |
| Front Unsprung mass, $m_{uf}$ –kg | 550 |
| Rear Unsprung mass, $m_{ur}$ –kg | 3640 |
| Suspension stiffness | |
| Front axle, $k_{sf}$ –N/m | 2.89e5 |
| Rear axle, $k_{sr}$ –N/m | 3.53e5 |
| Suspension damping coefficient | |
| Front axle, $c_{sf}$ –Ns/m | 1.57e4 |
| Rear axle, $c_{sr}$ –Ns/m | 2.87e4 |
| Tire | |
| Vertical stiffness, $k_{tf}$, $k_{tr}$ –N/m | 9.48e5 |
| Vertical damping coefficient, $c_{tf}$, $c_{tr}$ –Ns/m | 2.0e3 |
| Radius –m | 0.56 |
| Sprung mass cg position | |
| From the front axle, $L_f$ –m | 5.28 |
| From the rear axle, $L_r$ –m | 1.37 |
| From the ground, $H_s$ –m | 1.4 |
| Overall truck length –m | 11 |
| Overall truck height –m | 3.5 |
| Wheel base –m | 6.65 |
| Tank length –m | 7.62 |
| Tank cross-section area –$m^2$ | 3.26 |

Table 6.2 summarizes the simulation matrix used for analysis of straight-line braking responses of the partly-filled tank truck. The braking maneuvers are simulated by applying ramp-step braking treadle pressures, as shown in Figure 6.5. Two different magnitudes of braking treadle pressures are implemented with the vehicle running on the dry and wet road surface conditions with the road adhesion coefficients of 0.9 and 0.5, respectively. The two road surfaces are denoted as 'S0.9' and 'S0.5'. The intensity of braking is varied by considering two different magnitudes of the treadle pressure: (*i*) 395

and 680 kPa for braking on the dry surface condition; and (*ii*) 235 and 415 kPa on the wet surface condition. The braking actions are denoted as 'P395', 'P680', 'P235' and 'P415', respectively. The braking pressures are chosen such that the adhesion limit is not exceeded and the wheel lockup does not occur. The braking simulations corresponding to higher treadle pressure (i.e., 680 and 415 kPa) are not performed for the cleanbore tank truck ('T0') due to occurrence of the wheels lockup.

Table 6.2: Simulation matrix (the superscripts [1] and [2] denote that the braking treadle pressures are applied during braking on the dry and wet road surfaces).

| Tank | Fill volume ratio | Liquid cargo | Braking treadle pressure (kPa) | | | |
|---|---|---|---|---|---|---|
| | | | $395^{[1]}$ | $680^{[1]}$ | $235^{[2]}$ | $415^{[2]}$ |
| 'T0' | 38.1% | Sulfuric acid ('C1') | √ | - | √ | - |
| | 52.1% | Dichloromethane ('C2') | √ | - | √ | - |
| | 69.5% | Water ('C3') | √ | - | √ | - |
| 'T1' | 38.1% | Sulfuric acid ('C1') | √ | √ | √ | √ |
| | 52.1% | Dichloromethane ('C2') | √ | √ | √ | √ |
| | 69.5% | Water ('C3') | √ | √ | √ | √ |

### 6.5.1 Model Validation

The validity of the pitch plane tank-vehicle model was initially examined using the experimental data reported in [146] for a rigid cargo truck with gross vehicle weight of 17,300 kg. The simulations were performed using the reported model parameters, while

the excitations due to the fluid slosh were suppressed. The simulations performed under the selected treadle pressures and road adhesion coefficients to derive the stopping distance, while the initial speed was assumed as 100 km/h. Figure 6.7 compares the predicted stopping distance responses for the rigid cargo truck on the dry and wet road

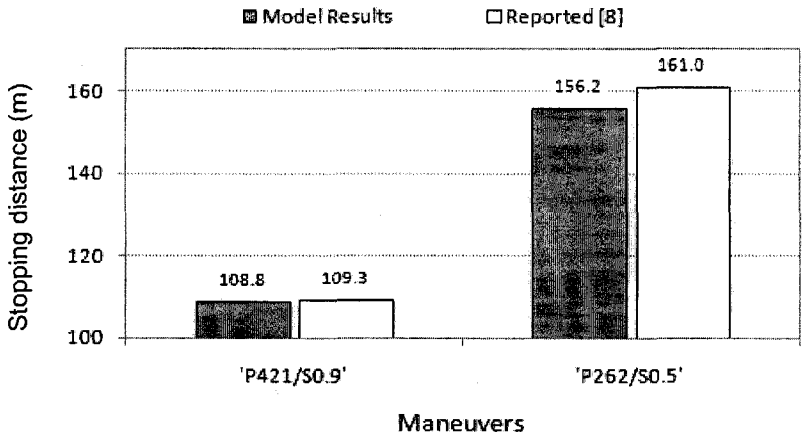


Figure 6.7: Predicted stopping distance for a rigid cargo truck with initial forward speed 100 km/h in 'P421/S0.9' and 'P262/S0.5' maneuvers, in comparison with the results from reference [146].

surfaces undergoing two braking maneuvers with those reported in [146]. It should be noted that the simulations were performed with parameters identical to those of the reported results, except for the suspension properties. A non-linear suspension was employed in the reported study [146], while a linear suspension is assumed in the present model. Simulation results were obtained using 421 and 262 kPa treadle pressures on the dry ($\mu$=0.9) and wet ($\mu$=0.5) road surfaces, respectively, which are denoted as 'P421/S0.9' and 'P262/S0.5' maneuvers. The results show reasonably good agreements with the reported data, while the model underestimates the stopping distance, particularly

on the wet surface. Approximately 0.46% and 3.13% errors are obtained for the dry and wet surface maneuvers, respectively.

The model of the tank-vehicle combination with liquid cargo was verified by comparing its braking responses with those of a rigid cargo vehicle. A completely filled tank vehicle is expected to respond identical to that of a rigid cargo vehicle in the absence of motion of the free surface of fluid. The simulations for the tank vehicle were performed using the methodology described in Figure 6.4. The comparison permitted for verification of the analysis methodology for the coupled liquid tank-vehicle model. The simulations were performed for the baffled tank vehicle ('T1') filled with fuel oil equal to 98.8% of the total volume. The braking responses are evaluated in terms of dynamic load factors (DLF) of the front and rear axles, defined as the ratio of the instantaneous axle load to the static axle load, and the vehicle longitudinal deceleration ($a_x$). Figure 6.8 presents the comparison of responses of the 'T1' tank-vehicle combination with those of the equivalent rigid-cargo vehicle subjected to an identical braking maneuver of 680 kPa treadle pressure on the dry road ($\mu$=0.9). The comparisons show nearly identical responses of tank truck and the equivalent rigid cargo vehicle in terms of deceleration and dynamic load factors of the front and rear axles. Similar degree of agreement was also obtained in the stopping distance (results not shown). The excellent agreement in the responses validates the proposed simulation methodology.

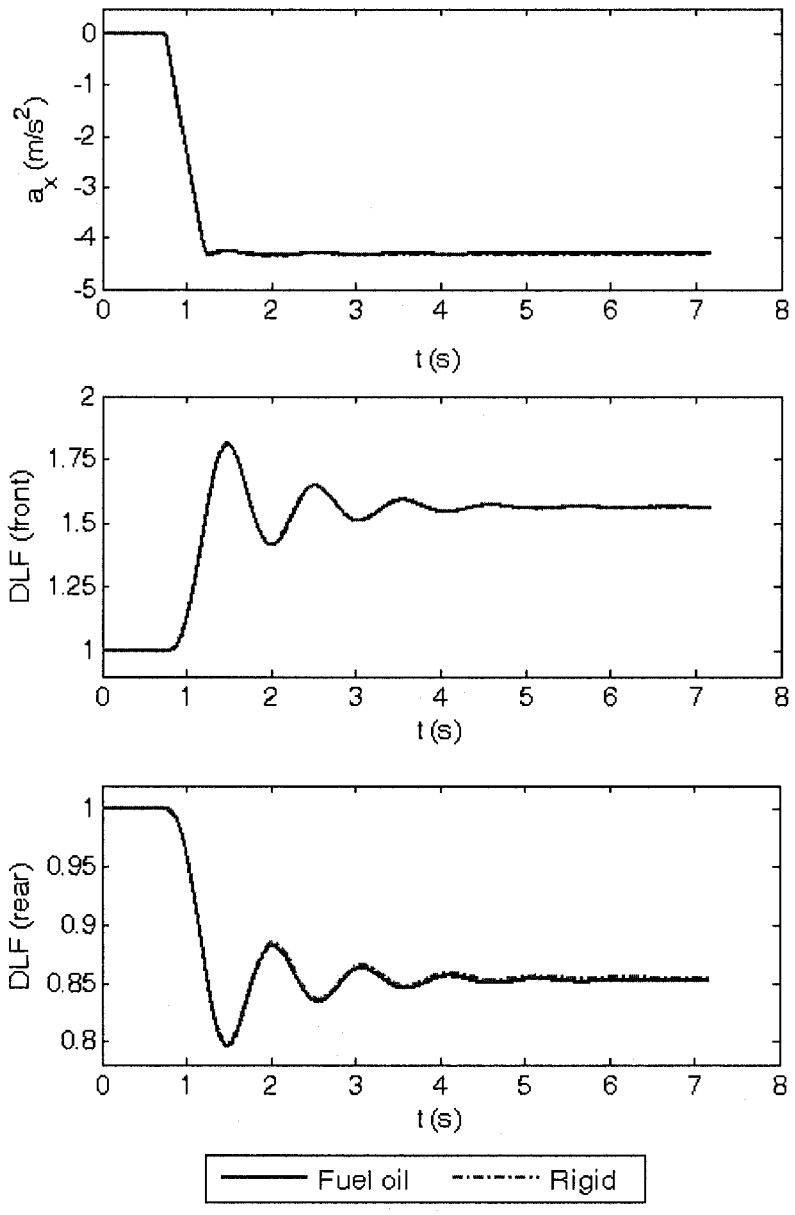


Figure 6.8: Comparisons of braking responses of the nearly completely filled tank truck ('T1') with those of the equivalent rigid cargo vehicle under a straight-line braking maneuver (treadle pressure: 680 kPa; road adhesion: 0.9).

## 6.6 ANALYSES OF BRAKING RESPONSES

The straight-line braking responses of the partly filled tank truck are evaluated under defined braking inputs using the methodology described in Figure 6.4. The responses are presented and discussed to highlight the influences of fluid slosh, fill volume, braking severity, baffles and tire-road adhesion.

### 6.6.1 Effect of Fluid Slosh

Figure 6.9 illustrates the braking dynamic responses of the tank trucks equipped with a cleanbore ('T0') and a baffled ('T1') tank filled with dichloromethane ('C2'). The fill volume is 52.1% of the total volume to achieve the nominal payload of 16,400 kg. The braking maneuver is synthesized under a 395 kPa treadle pressure on the dry road surface ($\mu$=0.9). The braking responses are presented in terms of variations in the sprung mass pitch angle ($\alpha_s$), and longitudinal and vertical coordinates of the vehicle ($x_s$ and $z_s$). The responses of the equivalent rigid cargo truck are also presented in the figure to illustrate the influence of fluid slosh. The dynamic fluid slosh responses to this maneuver are illustrated in Figure 6.10, which depict the additional longitudinal and vertical forces and pitch moment arising from the fluid slosh.

The vehicle responses (Figure 6.9a) reveal a negative pitch angle of the sprung mass, irrespective of the type of cargo and tank configuration, indicating a dynamic load transfer to the front axle. The pitch angle responses of the fluid cargo tank trucks, irrespective of tank configuration, are considerably greater than that of the equivalent rigid cargo truck. This is due to the additional longitudinal force and pitch moment arising from the liquid slosh, as shown in Figure 6.10. The results in Figure 6.9

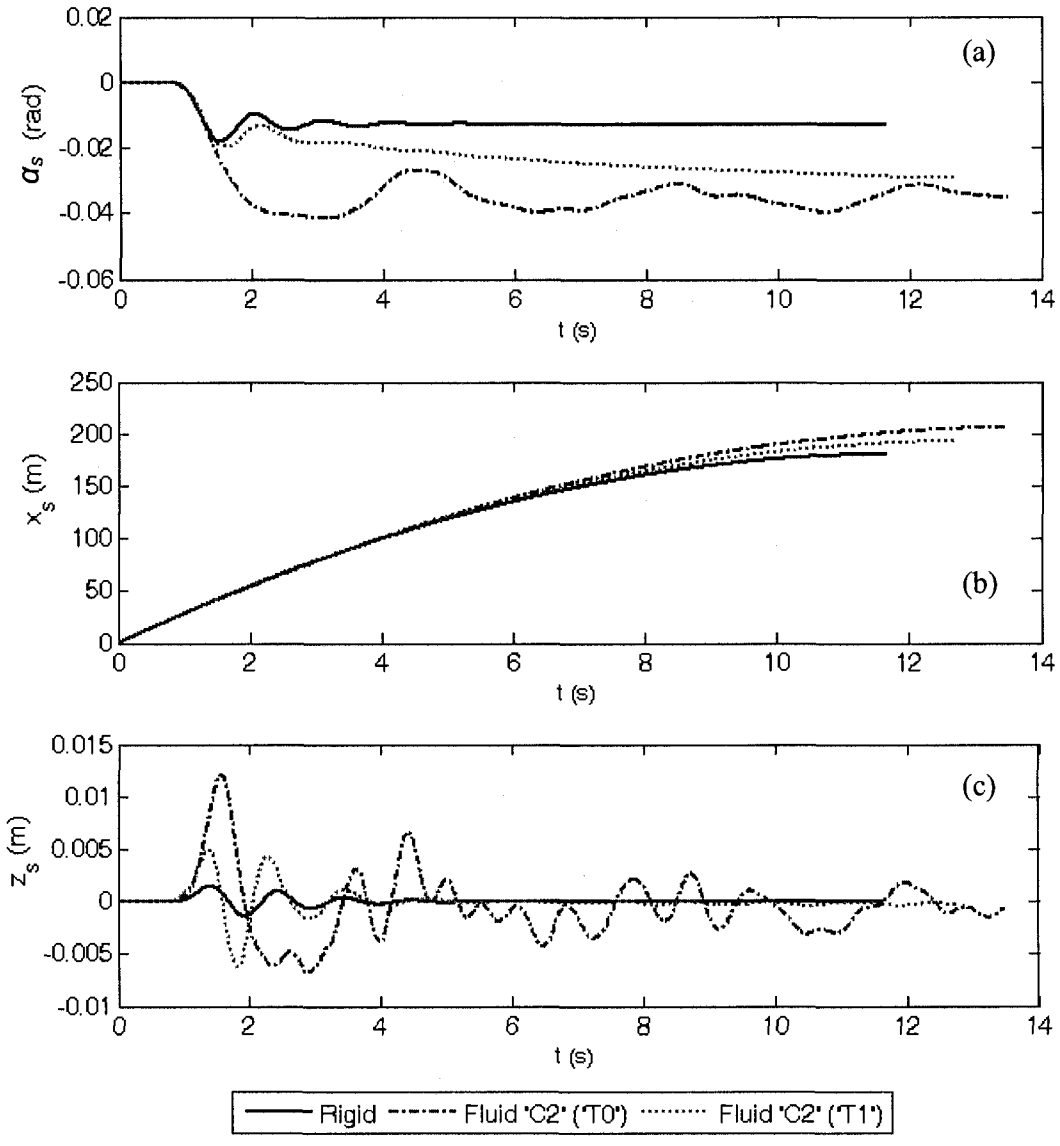


Figure 6.9: Comparisons of variations in the pitch angle ($\alpha_s$), longitudinal ($x_s$) and vertical ($z_s$) displacement responses of the sprung mass of the partly-filled tank trucks (ratio of fill volume = 52.1%) and the equivalent rigid cargo vehicle (Treadle pressure = 395 kPa; initial speed = 100 km/h; $\mu = 0.9$).

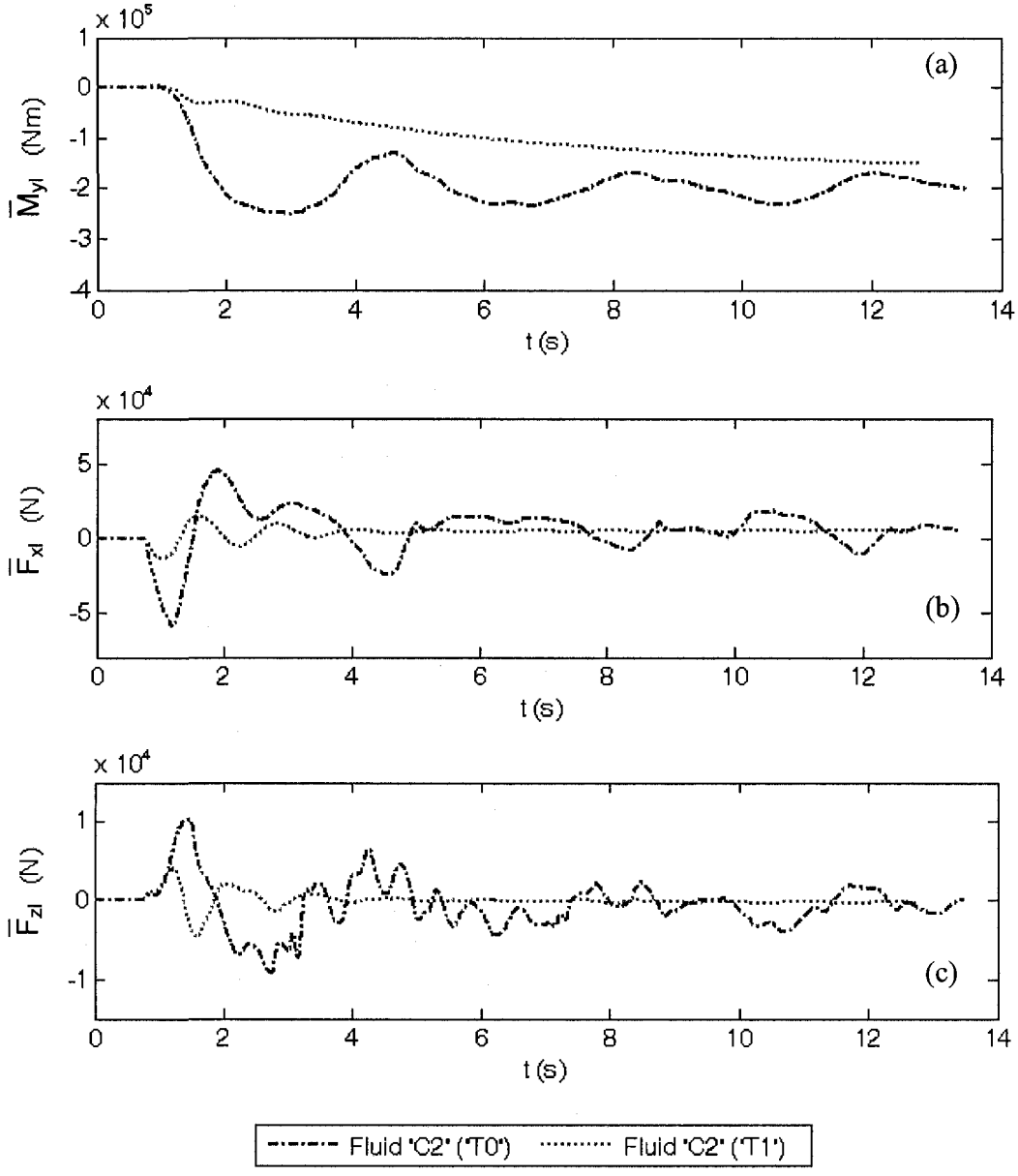


Figure 6.10: Comparisons of net pitch moment ($\overline{M}_{yl}$) and longitudinal ($\overline{F}_{xl}$) and vertical ($\overline{F}_{zl}$) forces due to the fluid slosh in the baffled and unbaffled tank trucks (Ratio of fill volume = 52.1%; Treadle pressure = 395 kPa; Initial speed = 100 km/h; $\mu$ = 0.9).

also show that the vehicle with a 52.1%-filled cleanbore tank yields significantly larger magnitude of the pitch moment, which oscillates at a frequency of approximately 0.25 Hz, which is near the fundamental pitch plane slosh frequency ($\approx$0.2 Hz) derived from the free slosh oscillations within the same tank (Chapter 4). It should be noted that the free slosh simulations were performed for the tank fixed at its base, while in a moving truck it is subject to the translational and pitch motions. The results of the equivalent rigid cargo truck exhibit nearly identical sprung mass pitch and bounce mode frequencies, which are approximately 1 Hz. In the present study, the angular acceleration of pitch was considered in the acceleration field that the fluid is exposed to, as evident in Equations (6.15) to (6.17).

Both the slosh pitch moment and the sprung mass pitch responses of the cleanbore tank truck reveal oscillations at the frequency near the fundamental slosh frequency (0.20 Hz), which suggests that the pitch and thus the dynamic load transfer responses of the tank vehicle are essentially influenced by the fluid slosh. The sprung mass pitch angles of tank vehicles 'T0' and 'T1' asymptotically approach comparable steady-state values, which are twice that of the equivalent rigid cargo vehicle. The asymptotical trend in the pitch moment due to the fluid slosh has also been observed for the same baffled tank in Chapter 4 and has also been reported by Modaressi [128] for a baffled circular tank. The presence of baffles, however, tends to reduce the tank vehicle pitch and thus the dynamic load transfer. Excessive transient load transfer to the front axle of a cleanbore tank truck may cause lockup of the rear wheels and thus degrade the directional performance and stability. The magnitudes of the transient peaks in pitch moment and pitch angle are significantly smaller, when compared to those of the unbaffled tank vehicle ('T0'),

suggesting the anti-slosh effectiveness of the baffles. The lower magnitudes of transient responses of the baffled tank truck are also attributed to its relatively higher slosh frequency. The oscillations in the responses of the baffled tank truck decay more rapidly than the unbaffled tank truck, which is partly attributed to the higher slosh frequency of the baffled tank and partly to the resistance offered by the baffles. It should be noted that the simulation results were attained until the vehicle speed diminished. The slosh forces and moment responses, however, continue to exhibit oscillations, even after the vehicle approaches the stop, particularly for the cleanbore tank, as seen in Figure 6.10. A significantly longer simulation time is required to observe the steady-state fluid slosh responses.

The cleanbore tank truck also yields considerably larger magnitudes of vertical and longitudinal slosh forces than the baffled tank truck, as shown in Figures 6.11b and c. The magnitudes of the transient peak forces are particularly large for the unbaffled tank truck. The presence of baffles tends to dampen the magnitudes of oscillations and helps to suppress the peak forces and moment. Consequently, the baffled tank truck yields considerably lower vertical and pitch responses of the vehicle sprung mass, as seen in Figure 6.9.

The fluid slosh also induces considerably larger vertical motions of the sprung mass of the fluid tank vehicles, as seen in Figure 6.9c, when compared to that of the equivalent rigid cargo vehicle. The peak magnitudes of vertical motions of the tank trucks 'T0' and 'T1' are approximately 8.0 and 3.3 times that of the equivalent rigid cargo truck, respectively. Owing to the increased slosh frequency by addition of baffles, the time corresponding to the peak vertical slosh force for the baffled tank truck (at $t \approx 1.4$ s)

appears to be slightly smaller than that of the unbaffled tank truck ($t \approx 1.6$ s). It is also observed that the vertical responses of the 'T0' tank truck oscillate at a very low frequency near the fundamental slosh frequency ($\approx 0.2$ Hz), superposed by a high frequency ($\approx 1.1$ Hz), which is close to the vehicle bounce mode frequency. These results are also evident from the vertical slosh force illustrated in Figure 6.10*c*, suggesting highly coupled motions of the sloshing fluid and the vehicle body. The vertical slosh force responses of the baffled tank truck ('T1') vanish rapidly, while that of the unbaffled tank truck ('T0') decays relatively slowly.

The sprung mass longitudinal position responses (Figure 10b) show that the stopping time of the baffled tank truck is less than that of the unbaffled tank truck. The stopping times of the baffled and unbaffled tanks are approximately 12.74 s and 13.51 s, respectively, which are larger than that of the equivalent rigid cargo vehicle (11.65 s). The larger stopping time and thus the stopping distance of the partly-filled tank trucks, compared to the equivalent rigid cargo truck, is attributed to greater longitudinal load transfer and additional longitudinal force arising from the fluid slosh, as evident in Figure 6.10*b*. The results show that the cleanbore tank truck ('T0') yields larger magnitude of the net longitudinal slosh force than the baffled tank truck ('T1'), and thereby the longer stopping time and stopping distance. Figure 6.9b further suggests that the partly-filled fluid cargo tank trucks exhibit larger stopping distance compared to the equivalent rigid cargo truck subjected to identical braking efforts. The stopping distance for the truck with the unbaffled tank is approximately 14.1% longer than that of the equivalent rigid cargo truck. The presence of baffles can reduce the stopping distance considerably (by about 6.3%).

The velocity and deceleration responses of the liquid and equivalent rigid cargo tank trucks subjected to the same barking maneuver are compared in Figure 6.11, while the dynamic load factor responses are shown in Figure 6.12. The results clearly show that the presence of fluid slosh deteriorates the deceleration performance of the vehicles, particularly for the unbaffled tank truck ('T0'). Although the excessive load transfer due to the fluid slosh yields relatively larger peak magnitude of deceleration of the unbaffled tank vehicle ('T0') compared to the equivalent rigid cargo truck, the steady state deceleration response is considerable lower, which is partly attributed to the longitudinal slosh force (Figure 6.10*b*). A comparison of results presented in Figures 6.12*a* and 6.11*b* suggests that the deceleration response is highly dependent on the longitudinal slosh force for both the baffled and un-baffled tank trucks. The results show identical oscillation frequencies of the deceleration and the longitudinal slosh, irrespective of tank configuration. For the unbaffled tank truck, the frequency is approximately 0.25 Hz, which is consistent with that observed from the pitch motion and is slightly higher than the slosh frequency of fluid in a fixed tank ($\approx$0.2 Hz). The presence of baffles yields a high frequency ($\approx$ 0.83 Hz), which is also greater than the fundamental fluid slosh frequency ($\approx$0.66 Hz) derived from the free slosh within a fixed tank. These results suggest that the fluid slosh frequency in a tank mounted on a truck is affected by the sprung mass motions and is considerably higher than that derived on the basis of the fixed tank.

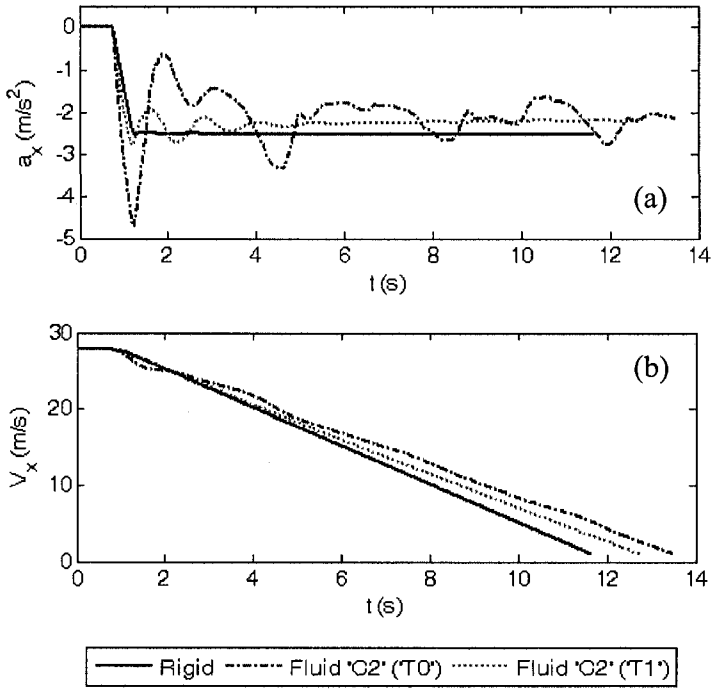


Figure 6.11: Velocity ($V_x$) and deceleration ($a_x$) responses of the vehicle with 50%-filled baffled and unbaffled tanks, and equivalent rigid cargo (Ratio of fill volume = 52.1%; Treadle pressure = 395 kPa; Initial speed = 100 km/h; $\mu = 0.9$).

The deceleration responses show sharp transient peaks for both the fluid tank trucks, which are caused by the rounded step treadle pressure input in the vicinity of large rate of change in the treadle pressure. A slight overshoot in the deceleration responses of the rigid cargo vehicle can also be observed near t=1.25 s. The results show that the peak-to-peak variations in the deceleration response for the cleanbore tank truck range from -4.6 to -0.6 m/s$^2$ compared to -1.9 to -2.7 m/s$^2$ for the baffled tank truck. The deceleration response of the rigid cargo truck rapidly approach a steady value of nearly -2.55 m/s$^2$. The velocity of the fluid cargo vehicle also decreases in an oscillatory fashion for the unbaffled tank truck due to large variations in the deceleration magnitude. The forward

velocity response of the baffled tank truck, however, decreases nearly linearly similar to the rigid cargo truck, which is attributed to the relatively smaller oscillation in the deceleration response. The overall rate of reduction in the forward velocity for both the fluid cargo tank trucks are observed to be smaller than that of the equivalent rigid cargo truck, while it is relatively higher for the baffled tank truck compared to that of the unbaffled tank truck.

As previously mentioned, the presence of fluid slosh causes greater pitch motion, and consequently yields larger longitudinal load transfer, as seen in Figure 6.12. The results show that the dynamic load factors (DLF) of the front axle of all the three vehicles remain well above the unity value over the entire simulation period, while those of the rear axle are less than unity. The magnitudes of the DLF of both the axles of the liquid cargo vehicles are significantly greater than those of the equivalent-rigid cargo vehicle. Both the tank trucks ('T0' and 'T1') with fluid cargo exhibit significantly higher peak and mean values of DLF of the front axle than the equivalent rigid cargo truck, while those of the unbaffled 'T0' truck are considerably higher than those of the baffled 'T1' truck. This suggests that the baffles greatly help to limit the dynamic load transfer, particularly in the transient state, which is attributed to the reduced sprung mass pitch response (Figure 6.9a). The peak magnitudes of transient DLF of the front and rear axles of the cleanbore tank truck approach 2.05 and 0.69, respectively, which are considerably larger than those of the baffled 'T1' tank truck (1.51, 0.84). The respective peak values of DLF of the rigid cargo vehicle axles are 1.47 and 0.88, which are comparable to those of the baffled tank truck. These results suggest that the excessive load transfer associated

with the fluid slosh within an unbaffled tank truck causes the normal load on the rear axle tires to diminish. Application of a severe braking may cause the rear wheels to lockup.

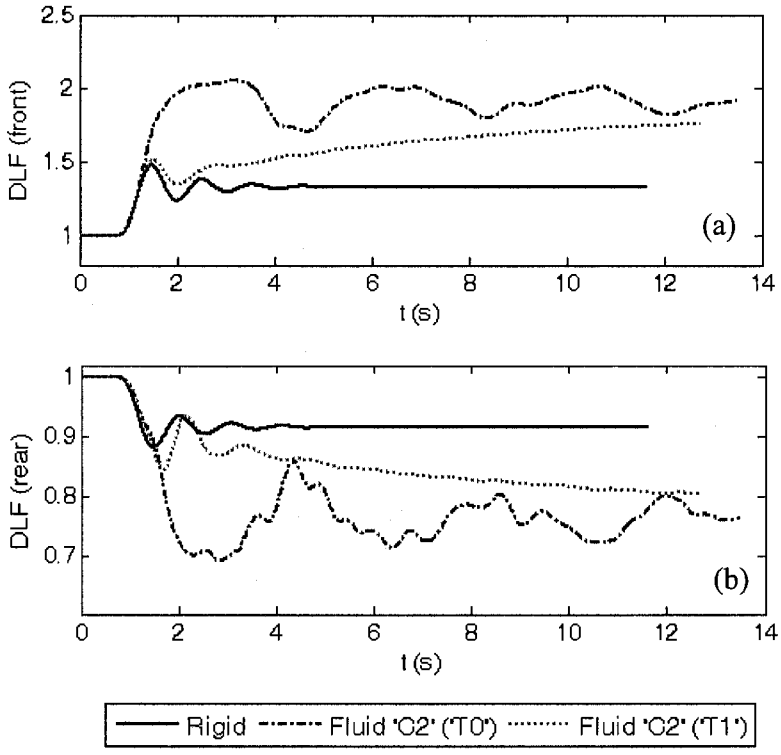


Figure 6.12: Dynamic load factor (DLF) responses of the vehicle with 50%-filled baffled and unbaffled tanks, and equivalent rigid cargo (Ratio of fill volume = 52.1%; Treadle pressure = 395 kPa; Initial speed = 100 km/h; $\mu = 0.9$).

A comparison of Figures 6.13 with Figure 6.9*a* reveals that the DLF responses of the vehicles are closely associated with the pitch motion of the sprung mass. The front and rear axle load responses of the unbaffled tank truck suggest dominant oscillation near 0.25 Hz, which is the same as that of the vehicle pitch response. The pitch oscillations, however, occur about the mean or steady-state values. The DLF responses of the baffled tank reveal oscillations near 0.83 Hz, which is consistent with the slosh frequency within

the baffled tank mounted on the truck. The magnitudes of the oscillations are significantly small and are more evident in the initial stage of the rear axle responses, which may be partly attributed to the nature of the input. Unlike the DLF responses of the 'T0' tank vehicle, which oscillate about the mean values, the responses of the 'T1' tank vehicle continue to increase in a non-oscillatory manner for $t>3$ s and asymptotically approach their respective steady-state values. This behavior is attributed to the damping effect of the baffles and accumulation of fluid within the compartments below the baffle orifice level. The same trends can also be observed in the slosh pitch moment and sprung mass pitch response (Figures 6.10a and 6.11a).

### 6.6.2 Influence of Fill Volume

Tank trucks, employed in general purpose bulk liquid transportation, often carry different types of products with varying weight density. This loading practice thus yields varying fill volume, while the payload is held near the regulated vehicle capacity. The magnitudes of dynamic load transfer and thus the braking responses of the tank trucks strongly depend upon the fill volume and the load. In this dissertation study, the cargo load is held constant, while the variations in fill volume are achieved by varying the weight density of the liquid cargo. Three different liquid products are selected to achieve 38.1%, 52.1% and 69.5% fill volumes, as summarized in Table 6.2. The braking responses are evaluated for both 'T0' and 'T1' tank trucks subject to different braking pressures, while the initial speed is held as 100 km/h, as summarized in Table 6.2. The vehicle configurations with different loads are denoted as 'C1', 'C2' and 'C3', respectively, which correspond to 38.1%, 52.1% and 69.5% of total tank volume.

Figure 6.13 illustrates the straight-line braking responses in terms of deceleration ($a_x$), and DLF of the cleanbore tank truck ('T0') with three different fill volumes, under a treadle pressure of 395 kPa on the dry road ($\mu$=0.9). The results show considerable oscillations in the responses, while oscillations decay rapidly under a high fill volume. The lower fill volume of 38.1% invariably yields higher transient peak and lower frequency of oscillation. This can be attributed to higher slosh forces and lower slosh frequency due to lower fill volume, which were observed from both the experimental and simulation results obtained for the tanks alone (Chapters 2 and 4). The results show oscillation frequencies ranging from 0.22 to 0.30 Hz for the fill volume range considered (38.1% to 69.5%), which are slightly higher than the fluid slosh frequencies (0.17-0.23 Hz) derived from free slosh within the fixed tank for the same fill volume range. It should be noted that the vehicles approach a stop at the end of the simulation run (13 s < t <14 s), while the deceleration responses continue to oscillate, irrespective of the fill volume, which is attributed to residual fluid slosh and is also evident in the DLF responses. While the mean deceleration responses corresponding to the three fill volumes are comparable, the higher fill volumes yield lower transient peak and stopping time.

The deceleration response of the vehicle with the high fill volume (69.5%) exhibits a sharp peak near t=5 s (Figure 6.13a). From the examination of the free surface, it was concluded that this peak was caused by the impact of the slosh fluid against the tank ceiling, Such an impact was not observed for the lower fill volumes. The fluid impact under the higher fill volume caused an abrupt increase in the transient vertical slosh force relative to the tank coordinate system $(xyz)^L$, which resulted in a sharp increase in the longitudinal slosh force with reference to the vehicle coordinate system

$(xyz)^S$. This peak is not evident in the DLF responses, which is most likely due to the filtering provided by the low frequency suspensions and tires.

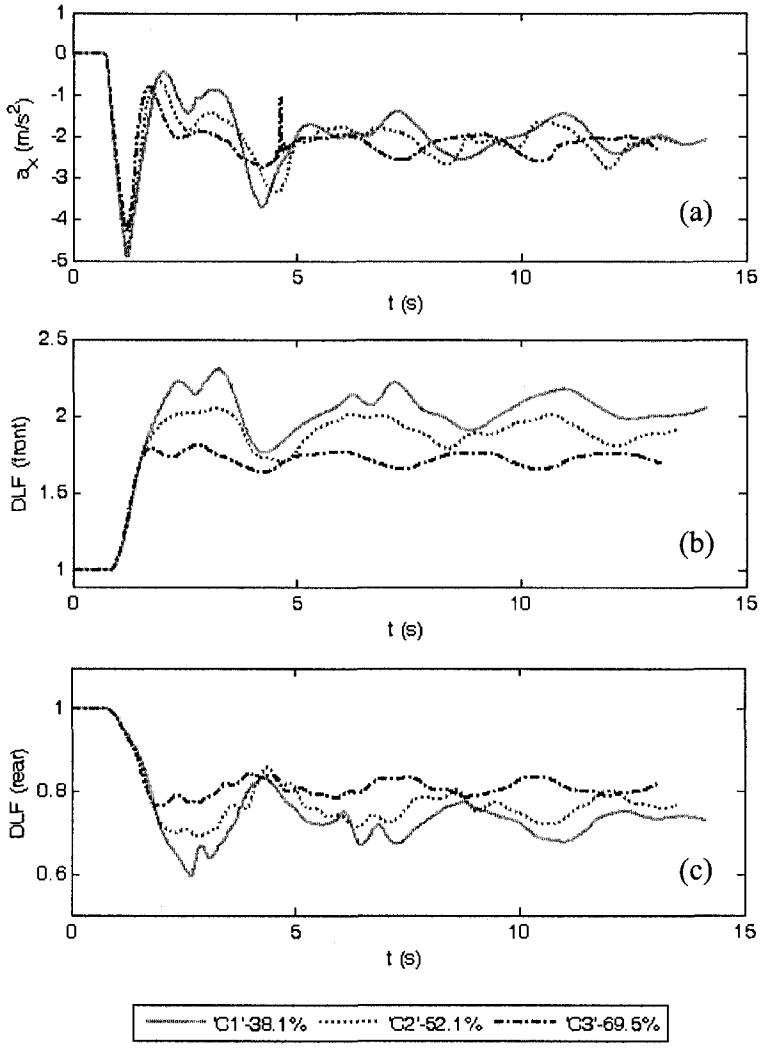


Figure 6.13: Variations in the braking deceleration and dynamic load factor responses of the un-baffled tank truck with different fill volumes (Initial speed=100 m/s; Treadle pressure=395 kPa; $\mu$=0.9).

The DLF responses also exhibit oscillations near the respective slosh frequencies. The rate of decay of oscillations tends to be higher for the higher fill volume. The

magnitudes of DLF responses are higher for the lower fill volume, while the frequency is lower. This is attributed to higher slosh pitch moment and longitudinal slosh force caused under a lower fill volume. The peak and mean DLF responses of the front axle tend to be larger for the fluid cargo filled under lower fill volume due to more severe fluid slosh, while it is opposite for the rear axle. This suggests that a lower fill volume may yield larger load transfer and thus is more likely to cause the lockup of the rear axle. Moreover, the relatively larger load transfer under a lower fill volume may result in lower braking efficiency and longer stopping time and distance, which is evident from the deceleration response. It is also shown in Figures 6.14b and c that the peaks at the front and rear axles do not coincide, which may be partly attributed to the different suspension properties of the two axles and partly due to the difference in the instantaneous position of the vehicle sprung mass cg from the two axles.

Figure 6.14 shows the peak dynamic load factors as a function of the liquid fill volume for the cleanbore tank truck ('T0'). The results are presented for two different braking maneuvers corresponding to treadle pressures of 395 and 235 kPa, on the dry and wet road surfaces, respectively, which are denoted as 'P395/S0.9' and 'P235/S0.5' maneuvers. The figure illustrates maximum values of DLF for the front axle and minimum values for the rear axle. The figure also shows the peak DLF magnitudes of rigid-cargo truck, equivalent to the 52.1%-filled liquid cargo, since the respective values for other two fill volumes are very close. The results clearly show that the peak values of DLF of the front axle of the fluid cargo tank trucks are considerably higher than that of

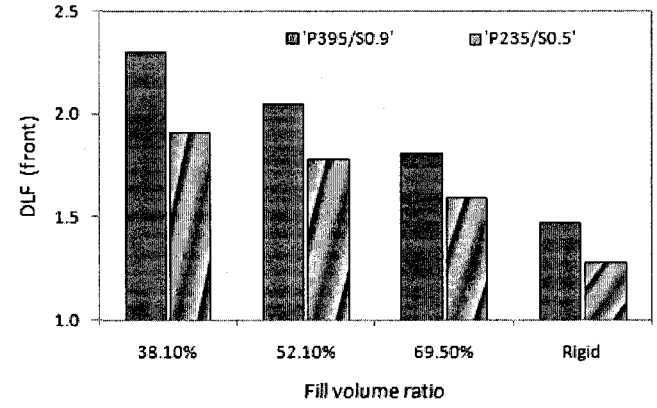


(a)

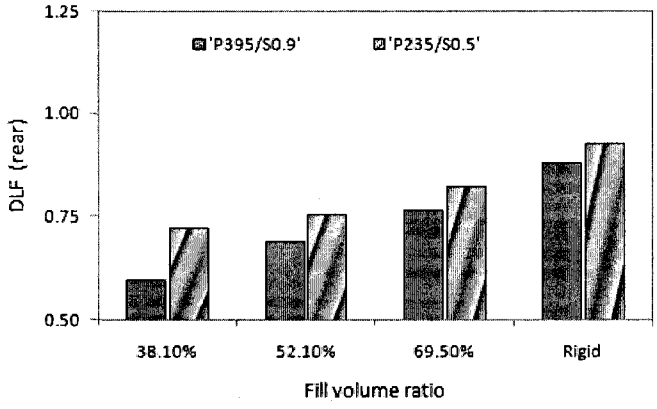


(b)

Figure 6.14: Variations in peak values of DLF responses with fluid cargo fill volume for the cleanbore tank truck ('T0'). (a) front axle; (b) rear axle.

the equivalent rigid cargo truck, irrespective of the braking input and the road condition, while the peak values under lower fill volume tend to be significantly larger. In the extreme case of 38.1% fill volume ('C1'), the peak magnitudes of LDF of the front axle approach as high as 2.3 and 1.92 under 'P395/S0.9' and 'P235/S0.5' braking maneuvers, respectively, which are 1.56 and 1.49 times the respective peak values of the equivalent rigid cargo truck. The peak magnitudes of DLF of the rear axle are significantly lower for the lower fill volume, as seen in Figure 6.14b. The results suggest that a cleanbore tank

truck with lower fill volume is more likely to encounter the lockup of the rear axle, irrespective of the road surface condition. The peak values of DLF of the rear axle of the 38.1% filled tank truck are 0.60 and 0.73 corresponding to 'P395/S0.9' and 'P235/S0.5' maneuvers, respectively, which are 0.68 and 0.78 times the respective peak values of the equivalent rigid truck.

The influence of fill volume on the responses of the baffled tank truck ('T1') are illustrated in Figure 6.15, which depicts the transient and steady-state characteristics of DLF in a maneuver under a straight-line braking input on wet road surface (treadle pressure = 235 kPa). The results show only small magnitude oscillations in the DLF responses, which asymptotically approach the respective steady-state values. The oscillations in the DLF responses are more evident for the low fill volume (38.1%) due to higher slosh forces and pitch moment. Lower fill volume also yields higher transient peak in DLF of the front axle and lower peak in DLF of the rear axle. Furthermore, the oscillation frequency tends to be higher as the fill volume increases, which vary from 0.80 to 0.87 Hz for the fill volume range considered and are slightly higher than the fundamental slosh frequencies (0.63-0.70 Hz) derived from free slosh occurring in the fixed tank for the same fill volume range.

The figure shows strong influence of the fill volume on the steady-state DLF responses of the two axles of the baffled tank truck. The DLF responses corresponding to higher fill volume of 69.5% rapidly approach their steady-state values near t = 5 s with only small oscillations. As discussed in Chapter 4, the orifice of either one or two baffles under the higher fill volume could be immersed in the liquid. The air pressure in the

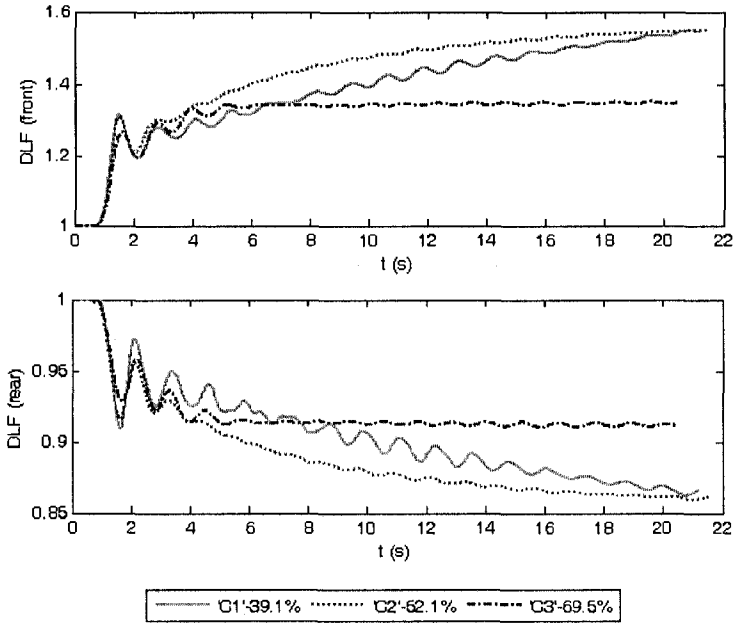


Figure 6.15: Variations in the dynamic load factor (DLF) responses of the baffled 'T1' tank truck with different cargo fill volumes (Initial speed=100 m/s; Treadle pressure=235 kPa; $\mu$=0.5).

compartment near one of the two tank heads tends to increase rapidly due to the addition of the liquid from the other compartments. An adverse air pressure gradient forms along the acceleration direction between different baffled compartments, causing increased resistance to the liquid movement through the baffles. In contrast, for the intermediate (52.1%) and low fill (38.1%) volumes, the liquid surface remains well below the upper edge of the baffle central orifice. The DLF responses of the vehicle with two lower fill volumes (52.1% and 38.1%) approach steady-state values beyond the simulation time considered or after the vehicle has approached a stop. This is attributable to relatively larger slosh forces and pitch moment under lower fill volumes. It is interesting to note that the steady–state DLF magnitudes tend to be higher for the 52.1% fill volume, compared to the 38.1% fill volume. This is attributed to the free surface below the lower

edge of the orifice and entrapment of the liquid within the compartments under the lowest fill volume. Additional simulations were thus performed to explore the settling time under lower fill volumes. Figure 6.16 illustrates the DLF responses of the two axles under the lowest fill volume (cargo 'C1' – 38.1%) over the simulation period of 51 s. The result show that the DLF responses almost approach their steady-state values long after the vehicle approaches the stop. Figure 6.17 further shows the fluid time (t =21.5 s) and the final time (t = 51 s). It can be seen that the free surface is below the lower edge of the baffle central orifice for the rear two baffles at t=21.5 s. The liquid translation for the two baffled compartments thus entirely relies on the small equalizer orifices located at the bottom, and consequently takes a long time to approach the steady state.

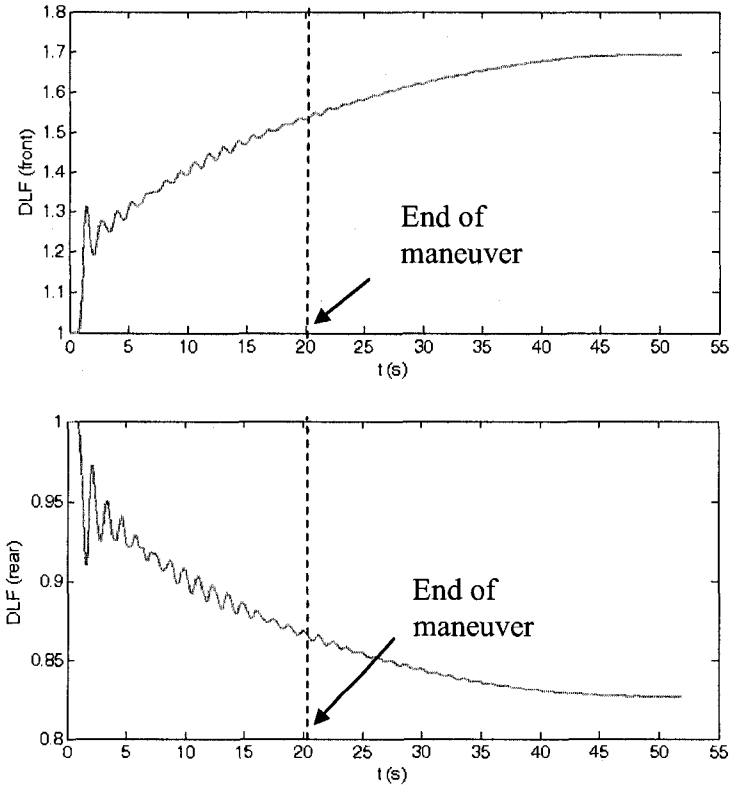


Figure 6.16: Dynamic load factor responses of the baffled tank truck ('T1') with 38.1% fill volume under a longer simulation period of 51 s (Initial speed=100 m/s; Treadle pressure=235 kPa; μ=0.5).

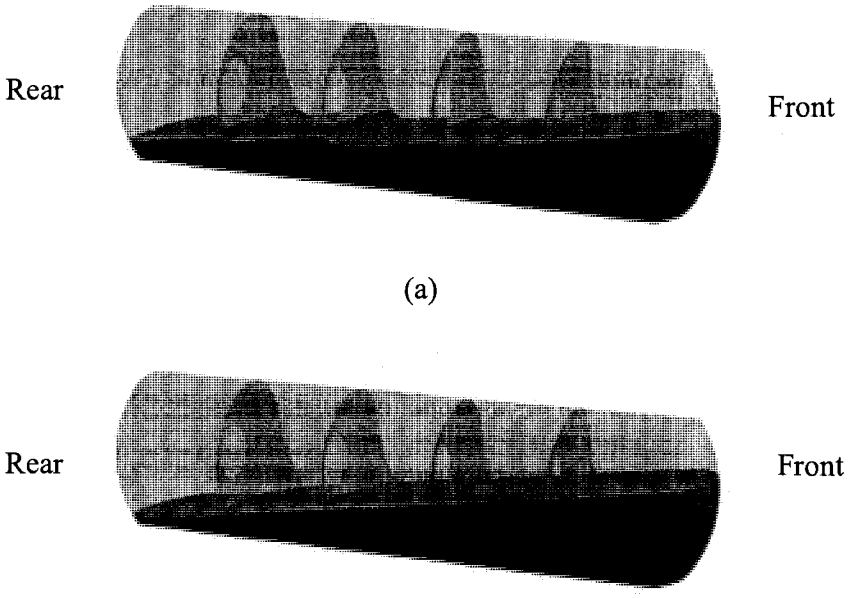


Figure 6.17: Evolution of liquid free surface patterns in the baffled tank truck ('T1') with 38.1% fill volume (Initial speed=100 m/s; Treadle pressure=235 kPa; $\mu$=0.5): (a) t=21.5 s when the vehicle is stopped; (b) the final simulation time t=51 s.

The deceleration responses of the baffled tank truck baffled under the three different fill volumes and subjected to the same maneuver are illustrated in Figure 6.18. The results show only small oscillations in the deceleration due to the presence of baffles, although the magnitudes of oscillations tend to be higher under lower fill volume owing to the larger slosh resulting forces. The vehicle deceleration response corresponding to higher fill volume of 69.5% approaches the steady-state value rapidly (t>5 s), as observed in the DLF responses in Figure 6.15. The steady-state deceleration also tends to be higher for the higher fill volume compared to those for the lower fill volumes. The results further show that the stopping time under the intermediate fill volume (52.1%) is slightly

longer than that under the lower fill volume (38.1%), suggesting that a longer stopping distance may result.

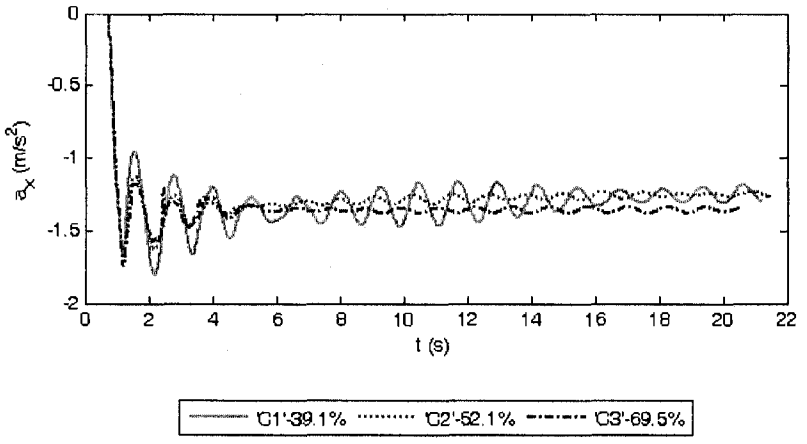


Figure 6.18: Variation in the deceleration response of the baffled 'T1' tank truck with different cargo fill volumes (Initial speed=100 m/s; Treadle pressure=235 kPa; $\mu$=0.5).

Figure 6.19 shows the variations in the stopping distance of the baffled 'T1' and unbaffled 'T0' tank trucks with the three fill volumes and subjected to two different straight-line braking maneuvers. The maneuvers were performed under 395 and 235 kPa treadle pressures on the dry and wet road surfaces, respectively. The figure also illustrates the stopping distances of the equivalent rigid-cargo vehicle. It is seen that the stopping distances for both the baffled and unbaffled fluid tank trucks ('T1' and 'T0') are longer than that of the equivalent rigid cargo truck under the two maneuvers, irrespective of the fill volume. The addition of baffles can considerably reduce the stopping distance. Under the low fill volume (38.1%), the stopping distance for the unbaffled tank truck ('T0') is 19.1% and 35.1% larger than that of the equivalent rigid truck under 'P395/S0.9' and

'P235/S0.5' maneuvers, respectively. The respective stopping distances are reduced by 10.7% and 12.6% when the truck tank is equipped with baffles.

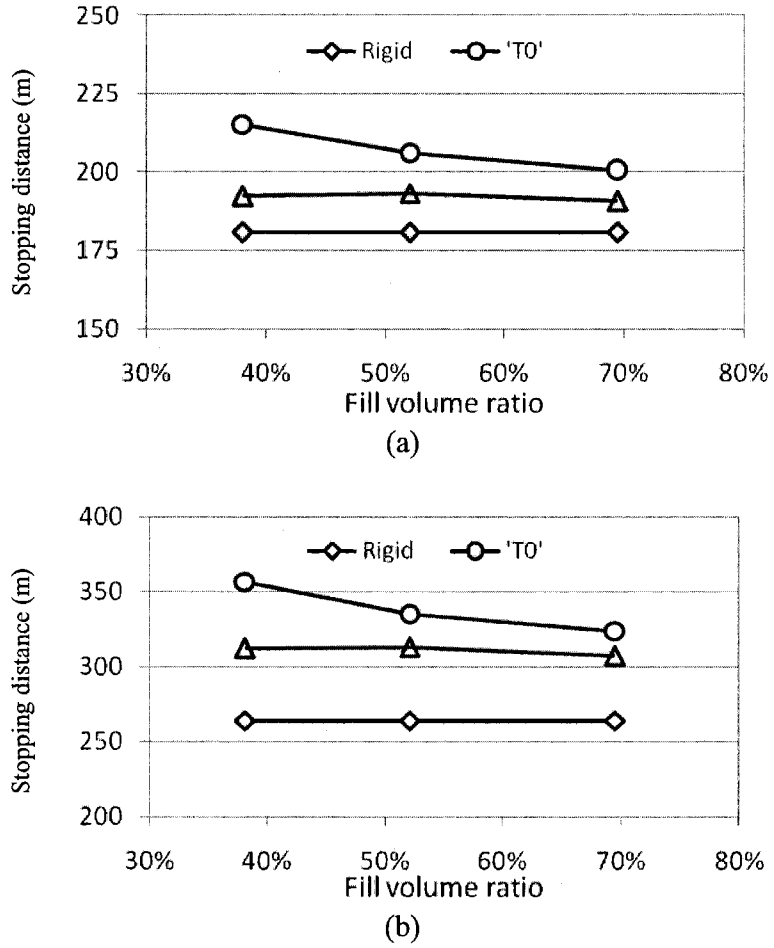


Figure 6.19: Comparisons of stopping distance responses of the baffled 'T1' and unbaffled 'T0' liquid-cargo trucks with equivalent rigid-cargo truck under different fill volumes and subjected to two different braking maneuvers: (a) P=395 kPa, $\mu$=0.9; (b) P=235 kPa, $\mu$=0.5.

The results further show that the stopping distance of the un-baffled tank vehicle ('T0') invariably decreases as the fill volume increases under the two maneuvers due to smaller slosh forces and moments under higher fill volumes. For the baffled tank truck ('T1'), however, the results show relatively smaller variations with fill volume compared

to those for the unbaffled tank truck, while the intermediate fill volume (52.1%) yields slightly larger stopping distance than the lower fill volume (38.1%). The results suggest that a baffled tank truck would yield poor braking performance under the intermediate fill volume.

### 6.6.3 Effect of Braking Severity

The braking performance of partly-filled tank trucks is also dependent upon the severity of braking. The effect of braking severity on the braking responses is investigated by considering tow different values of the treadle pressure. The analyses are performed the baffled and unbaffled tanks with different fill volumes and two braking treadle pressures on the dry and wet road surface conditions with initial vehicle velocity 100 km/h, as illustrated in Table 6.2. For the baffled tank, the higher treadle pressures are selected as 680 and 415 kPa for the dry and wet road conditions, respectively, such that the wheel lockup does not occur. The lower treadle pressures are selected as 395 and 235 kPa for the dry and wet road conditions, respectively. The analyses are also conducted for the equivalent rigid-cargo truck, and the results are compared to illustrate the effect of fluid slosh.

Figure 6.20 illustrates the vehicle responses of the baffled tank truck ('T1') with the intermediate fill volume (fluid 'C2'-52.1%) subject to straight-line braking maneuvers exerted with treadle pressures of 395 and 680 kPa on the dry road surface ($\mu$=0.9). The results are presented in terms of deceleration and the DLF of the front and rear axles. Higher magnitude of treadle pressure can generate larger braking torque and thus greater vehicle deceleration, as shown in Figure 6.20a. The results reveal that higher

treadle pressure yields a significantly higher absolute value of deceleration in terms of mean and peak of the variations. The peak deceleration under the 680 kPa maneuver is -4.6 m/s$^2$, which is approximately 1.7 times of that attained under the 395 kPa maneuver, while the difference in the mean decelerations is also in the same order. The results show oscillations in the deceleration response, which decay in a gradual manner, while the higher treadle pressure causes larger oscillations in the responses. The oscillation frequencies of the responses are almost identical for the two maneuvers.

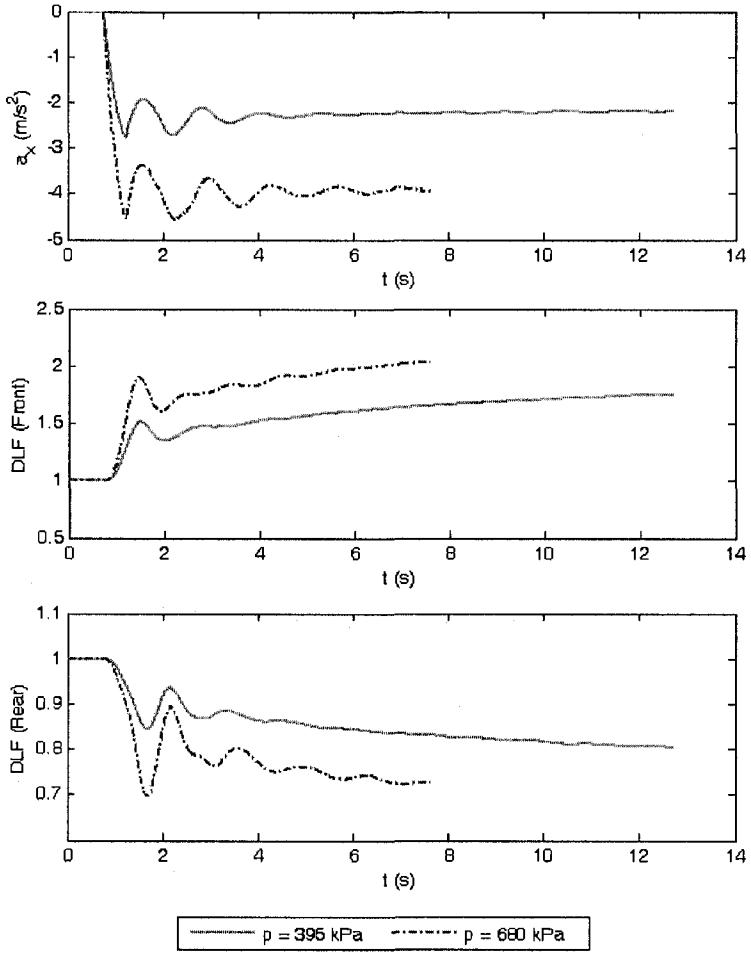


Figure 6.20: Comparisons of the deceleration and DLF responses of the baffled tank vehicle ('T1') subject to different braking treadle pressures (Ratio of fill volume=52.1%; $\mu$=0.9)

Larger deceleration of the vehicle under the higher treadle pressure can generate larger slosh force and pitch moment, causing larger pitch motion of the vehicle sprung mass and thus the dynamic load transfer, as evident in Figures 6.21*b* and *c*. The results show that the braking maneuver exerted under higher treadle pressure yields larger peaks in the DLF responses of the front and rear axles. The transient peak DLF value of the front axle under the maneuver of 680 kPa treadle pressure approaches 1.91, which is 1.27 times greater than that under the 395 kPa maneuver. The transient peak DLF response of the rear axle under the higher treadle pressure approaches 0.70, which is 17.7% less than that under the lower pressure maneuver. The results thus suggest that a braking maneuver exerted under a higher treadle pressure is more likely to cause the lockup of the rear axle wheels.

The results further show that the higher treadle pressure yields notably shorter stopping time (t=7.64 s), which is significantly less (by 40%) than that under the lower treadle pressure. The higher magnitude of deceleration and shorter stopping time under the higher treadle pressure thereby results in a shorter braking distance, as illustrated in Figure 6.21. The figure shows the stopping distance responses of the baffled tank vehicle ('T1') subjected to braking maneuvers under different treadle pressures on the dry and wet road surface conditions, together with those of the equivalent rigid-cargo vehicles. The braking distance of the tank vehicle was evaluated under the three fill volumes (38.1%, 52.1% and 69.5%). The results reveal that a higher treadle pressure under an emergent situation yields significantly shorter stopping distance, irrespective of the road surface condition, provided that the vehicle does not encounter wheel lockup. Furthermore, for a given braking treadle pressure, the intermediate fill volume (52.1%)

yields the longest stopping distance for the maneuvers exerted on both the dry and wet road surfaces. For the baffled tank truck carrying fluid cargo with this fill volume, the stopping distance under the 680 kPa treadle pressure maneuver on the dry road surface is 121.73 m, which is 37.0% less than that under the 395 kPa braking pressure. On the wet road, the stopping distance under the 415 kPa braking pressure is 184.90 m, which is 40.9% less than that under the 235 kPa pressure.

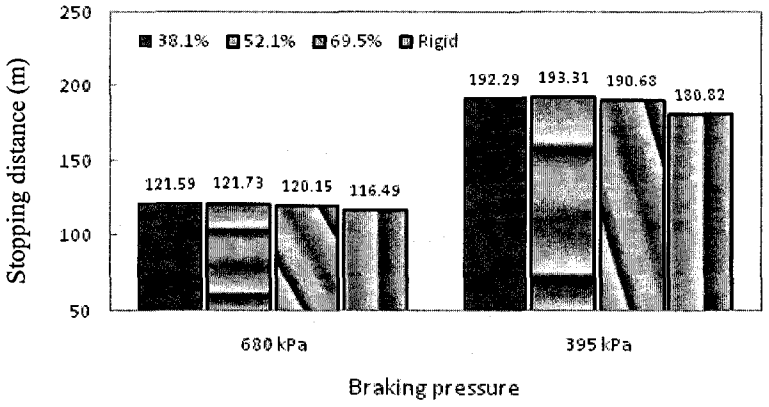


(a)

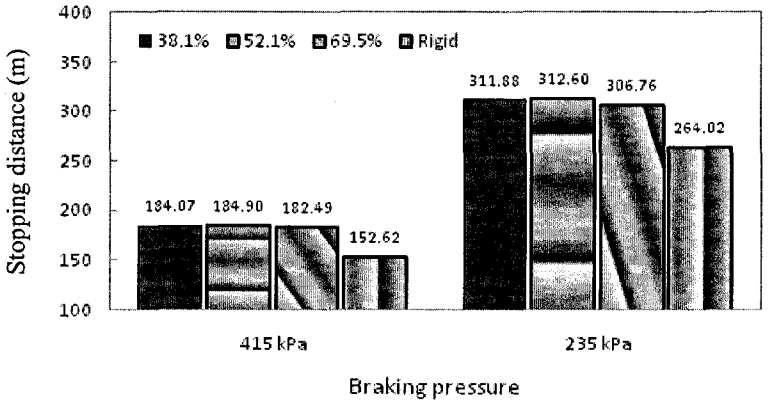


(b)

Figure 6.21: Comparisons of stopping distance responses of the baffled tank truck ('T1') under different fill volumes and braking pressures on dry and wet road surfaces: (a) $\mu$=0.9; (b) $\mu$=0.5.

The results show only small variations in the stopping distance with the fill volume for the baffled tank truck ('T1'), particularly under the higher treadle pressure, irrespective of road surface condition, which is consistent with the results discussed in the previous section. The stopping distances for the tank truck filled with fluid cargo are closer to those of the equivalent rigid cargo truck, when the braking maneuvers are exerted on the dry road, particularly under higher treadle pressure, suggesting greater effectiveness of the baffles as anti-slosh devices. On the wet road, however, the tank truck reveals greater stopping distances than the equivalent rigid cargo truck. The stopping distances for the 52.1%-filled baffled tank truck are 4.5% and 6.9% longer than those of the equivalent rigid cargo truck under 'P680/S0.9' and 'P395/S0.9' maneuvers, respectively, while they are 21.2% and 18.4% greater under 'P415/S0.5' and 'P235/S0.5' maneuvers, respectively. The results further show that the stopping distance of the tank vehicle under the high fill volume (69.5%) invariably approaches those of the equivalent rigid cargo vehicle for all maneuvers considered.

Figure 6.22 illustrates the deceleration and DLF responses of the unbaffled tank truck ('T0') with the intermediate fill volume (fluid 'C2'-52.1%) subject to straight-line braking maneuvers exerted with treadle pressures of 295 and 395 kPa on the dry road ($\mu$=0.9). The results show that a higher magnitude of treadle pressure yields larger peak and mean values of the transient deceleration and DLF. The peak deceleration under the higher treadle pressure (395 kPa) approaches 4.68 m/s$^2$, which is significantly higher (31.1%) than that under the lower braking pressure (295 kPa). However, the difference in the peak DLF is not so significant for the two braking pressures. The peak DLF of the front axle under the higher treadle pressure is 2.05, which is 6.2% higher than that under

the lower treadle pressure, while the results for the rear axle exhibit the same order difference. Moreover, the results also show that the higher treadle pressure causes larger magnitude oscillation in deceleration, while this trend is not observed in the DLF.

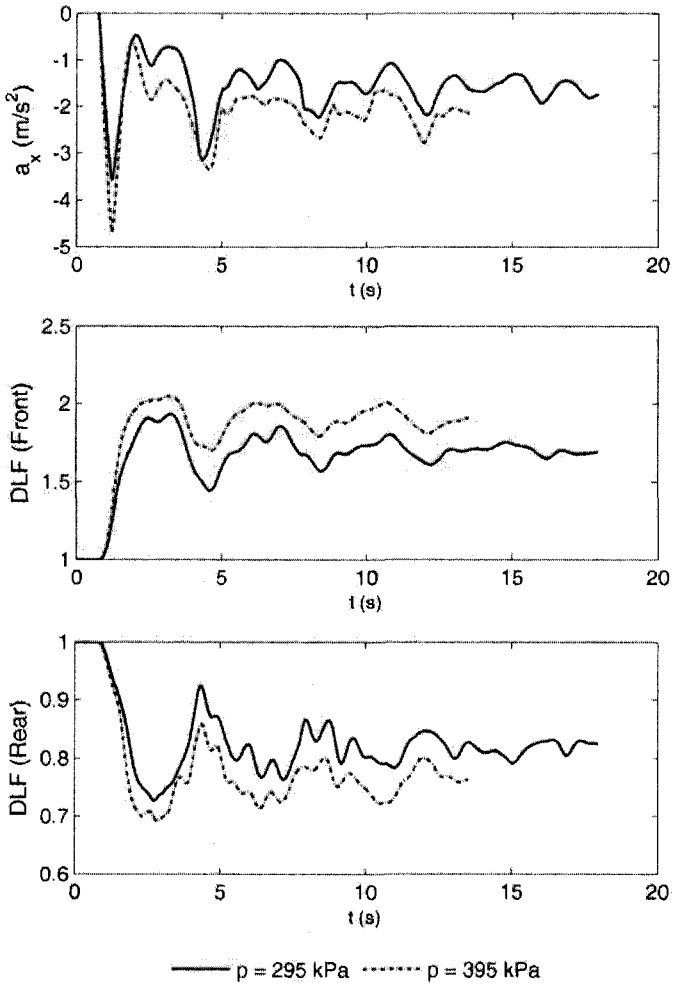


Figure 6.22: Comparisons of the deceleration and DLF responses of the cleanbore tank vehicle ('T0') subject to different braking treadle pressures (Ratio of fill volume=52.1%; $\mu$=0.9)

The vehicle responses also show that the higher magnitude of braking pressure tends to yield a significant shorter time approaching the stop, which is obviously attributed to the larger peak and mean deceleration. This behavior consequently results in

a shorter stopping distance, as shown in Figure 6.23, irrespective of the fill volume. The figure depicts the stopping distance for the same unbaffed tank with different fill volumes subject to the same two treadle pressures. Again, the results show the same trend of fill volume dependence as observed for the baffled tank truck. For a given fill volume, the lower magnitude of braking pressure invariably tend to yield a shorter stopping distance, which is also consistent with that observed for the baffled tank truck.

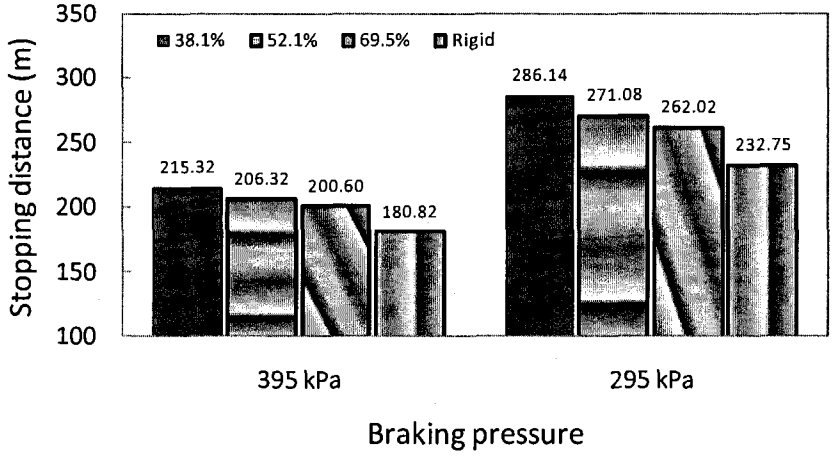


Figure 6.23: Comparisons of stopping distance responses of the cleanbore tank truck ('T0') under different fill volumes and braking pressures (Ratio of fill volume=52.1%; $\mu$=0.9).

## 6.7 SUMMARY

A 7-DOF pitch plane vehicle model was formulated and integrated with the 3-D fluid slosh model to analyze the braking characteristics of partly filled tank-trucks. The integration of the two models was realized through continuously updating the values of input parameters of both the models in the computational process. The parallel simulations allow the real-time transient interactions between the sloshing fluid and the

dynamics of the vehicle. The validity of the integrated model was examined for an equivalent rigid truck and a completely filled fluid-cargo truck.

The vehicle responses to straight-line braking maneuvers were studied with the integrated model applied to a tridem tank truck. The analyses were performed under different treadle pressures and two different road surface conditions. Two tank configurations (baffled and unbaffled) were used to equip the truck so as to analyze the effect of baffle. Three different fluid cargos were considered to realize different fill volumes but constant load.

The braking responses of the vehicle were analyzed in terms of transient dynamic load transfer, deceleration and the stopping distances. The results showed that the braking characteristics of the tank vehicles are closely associated with the behavior of the fluid slosh occurring in the tanks. The fluid slosh responses in the tank trucks are slightly different from those occurring in the fixed tank. The difference lies essentially in the slosh frequencies, which are slightly higher for moving tank compared to the tank with the fixed base that was analyzed in Chapter 4. The results showed that the baffles can help suppress the magnitudes of slosh forces and moment, and thereby reduce the vehicle responses in terms of longitudinal load transfer, deceleration and stopping distance.

The presence of fluid slosh in the partly-filled tank trucks, particularly when equipped with the unbaffed tank, yields larger pitch responses and thus larger normal load transfer, compared to those of the equivalent rigid cargo truck. The oscillations in the dynamic load transfer (DLF) occurred at frequencies close to the fundamental slosh frequencies, irrespective of tank configuration and fill volume. The DLF responses of the cleanbore tank truck ('T0') revealed considerably high magnitude of oscillations about

the steady-state values and relatively slow decay, compared to those of the baffled tank truck. Lower fill volume can yield lower peak and mean DLF values of the rear axle, while the case is opposite for the front axle, which represents larger load transfer. The addition of baffles can cause significant reductions in the transient DLF of the front and rear axles, indicating smaller load transfers. For the baffled tank vehicle ('T1'), the transient DLF response is characteristic of small magnitude oscillations, which are more notable in the initial time of maneuver and the results tend to asymptotically approach their steady-state values. The settling time is significantly shorter under a higher fill volume, while it is considerably long under a lower fill volume. Unlike the fill volume effect for the unbaffled tank truck, for the baffled tank truck the intermediate fill volume may yield the greatest transient variations in the DLF responses of the rear and front axles. Higher magnitude of braking treadle pressure generates larger transient variations in the DLF responses. Higher magnitudes of braking treadle pressure can also yield higher deceleration, provided that the wheels do not encounter lock up.

The stopping distance was observed to be affected by the tank configuration, fluid fill volume and the treadle pressure. Owing to the influence of fluid slosh, the stopping distance of the partly-filled fluid tank vehicles, particularly when equipped with the unbaffled tank, is longer than that of the equivalent rigid cargo truck. For the cleanbore tank truck, lower fill volume tends to generate longer stopping distance. The addition of baffles can considerably reduce the stopping distance. The results of stopping distance of the baffled tank truck show small variations with fill volume, while the intermediate fill volume may yield the longest stopping distance compared to the low and high fill volumes. Higher braking treadle pressure yields larger magnitude of deceleration and

thus shorter stopping distance. The role of the baffle in anti-slosh is more effective when the baffled tank truck is subject to an emergent braking maneuver, particularly on the dry road surface.

# CHAPTER 7

# CONCLUSIONS AND RECOMMENDATIONS

## 7.1 HIGHLIGHTS OF THE STUDY

The fluid slosh within partly filled tanks is known to be highly non-linear, particularly under severe braking- or steering-induced manoeuvres. The slosh phenomena largely depend on the tank geometry, fill volume and nature of external excitation. While the experimental observations serve as vital means to identify and understand the fluid slosh characteristics, the computational fluid dynamics (CFD) is considered as a powerful and effective approach to model this complex flow. Previous experimental works on fluid slosh were mostly focused on the study of limited parameters using small scale model tanks. The previous CFD studies emphasized on the exploration of algorithms appropriate for fluid slosh modeling, while their applications in tank vehicle dynamics, particularly with baffled tank configurations, were rare. The primary objective of this dissertation research is to contribute towards the in-depth understanding of transient fluid slosh within partly-filled cleanbore as well as different baffled tanks. The numerical and experimental studies were performed for the analyses of fundamental natural frequency, transient nature of forces and moments caused by the fluid slosh in the presence of time-varying external excitations, and the influence of transient fluid slosh on the directional performance and stability limits of partly-filled tank vehicles.

The present research comprised both experimental and numerical slosh investigations. The experimental investigations were conducted in scaled models of the cleanbore and

baffled tanks. The analysis of transient fluid slosh was performed under different fill volumes and a wide range of excitations arising from braking as well as steering inputs. The measured responses were thoroughly analyzed to identify the natural slosh frequencies, and the influences of excitation frequency and magnitude on the slosh forces and moments imposed on the tank strucures. For numerical investigation, two- and three-dimensional CFD fluid slosh models of the scaled tank were developed and validated using the experiment data attained from the laboratory study. The validity of the numerical model was demonstrated over a wide range of fill and excitation conditions. The validated tank model was then used to study the transient slosh behaviors within different designs of full scale vehicle tanks and the influences of baffle design factors. The tank model was subsequently applied to study the directional dynamics and roll stability limits of tank vehicles in the presence of transient slosh forces and moments. The two-dimensional slosh model was integrated with a static roll plane model of a tank vehicle to derive the rollover limits and the influences of transient lateral force and roll moment. The three-dimensional slosh model was integrated into a pitch plane model of the vehicle to study the braking responses of partly filled tank trucks as functions of the fill volume, braking severity and road adhesion limit.

## 7.2 MAJOR CONCLUSIONS

The systematic studies carried out in this dissertation lead to the development of a dynamic fluid slosh model that could provide a better understanding of the transient fluid slosh in baffled and unbaffed partly-filled tanks, and their influence on the roll stability

and braking characteristics of the partly filled tank vehicles. The major conclusions drawn from the study are summarized below:

- Fluid slosh is highly dependent on the tank configuration, fill volume and nature of excitation. Under the condition of constant cargo load, a lower fill volume tends to yield greater magnitudes of slosh forces and moments compared to those developed under higher fill volumes.
- The slosh forces and moments responses generally oscillate near the resonant frequencies under single-cycle sinusoidal or ramp-step acceleration inputs. The magnitudes of such oscillations decay gradually, while the rate of decay for the unbaffled tanks is substantially lower than that for the baffled tanks. The high magnitude transient slosh forces and moments can thus sustain over longer durations.
- The anti-slosh effect of transverse baffles is minimal for the transient lateral slosh force and roll moment. The baffles, however, can effectively alter the fluid slosh in the longitudinal direction. The most significant effect of baffles is observed in the pitch moment due to slosh. Under a longitudinal ramp-step acceleration excitation, the pitch moment due to fluid slosh within a cleanbore tank exhibits oscillations similar to those observed in the lateral force in the roll plane, while the pitch moment due to slosh within a baffled tank asymptotically approaches its steady value with minimal or no oscillations.
- The peak slosh forces and moments occur in the vicinity of slosh natural frequency under continuous as well as single-cycle sinusoidal excitations, which can be largely amplified in comparison to those of the equivalent rigid mass. The

slosh amplification effects are more significant in moments than in forces. Under harmonic excitation at an excitation frequency above the resonant frequency, the magnitude of fluid slosh force can be less than the inertial force developed by an equivalent rigid mass. Under a ramp-step acceleration excitation, the slosh forces and moments are also considerably amplified relative to the steady-state values (or quasi-static solutions).

- Liquid slosh contains a number of frequency contents, which include the excitation frequency, natural frequency and the vibration frequency. When the excitation frequency is close to the natural frequency of slosh, the magnitude of slosh force may vary periodically at the beating frequency.
- The fundamental slosh natural frequency depends on the fill volume and the tank configuration. For a given tank configuration, this frequency, in both lateral and longitudinal modes, increased with the fill volume. For a given fill volume, the addition of transverse baffles causes a significant increase in the longitudinal mode natural frequency, while the lateral mode frequency is not affected.
- Fluid slosh is predominantly two-dimensional when the tank is subjected to a pure lateral ramp-step or lateral single-cycle acceleration excitation, while it is three-dimensional under a simultaneous lateral and longitudinal acceleration excitation. It is also three-dimensional under harmonic excitations along single-axis in the vicinity of the resonant frequency.
- The presence of lateral baffles (curved or planar) can significantly reduce the peak magnitudes of longitudinal slosh force and pitch moment. The addition of transverse baffles results in a considerable reduction of the peak lateral slosh force

when the tank is subjected to a simultaneous lateral and longitudinal ramp-step acceleration excitation. The transverse curved baffles, under a pure lateral excitation, tend to induce the longitudinal slosh, thus causing relatively larger longitudinal slosh force, pitch and yaw moments.

- The baffle equalizer has negligible influence on the suppression of peak longitudinal slosh force, and pitch moment. The baffle porosity ranging from 4% to 20% yields negligible variation in the peak longitudinal slosh force. However, a larger baffle orifice size tends to yield larger slosh pitch moment, which was observed to rapidly approach the steady-state.
- The baffle orifice shape and location are significant factors in controlling the effectiveness of baffle for slosh suppression. The single half-circle orifice baffle and the half-opened partial baffle are highly effective in reducing the transient pitch moment, particularly when the fill volume is high. The anti-slosh effect of the multiple orifice baffle is practically identical to that of the single-orifice baffle of identical porosity. The conical baffle does not show additional benefit in reducing the slosh forces and moments, as compared to the single orifice baffle.
- Dynamic fluid slosh in roll plane yields a considerably high ratio of the transient maximum to the mean values of the cargo *cg* shift, slosh forces and moments, under a ramp-step acceleration. These high amplifications are major contributory factors to the roll destabilization of partly filled tank vehicles, which result in significantly lower rollover threshold, compared to those of rigid cargo trucks.
- Both the transient and quasi-static slosh analyses show that the "Reuleaux triangular" tank has considerably higher rollover threshold than the circular tank,

irrespective of the cargo fill volume. Lower fill volume yields smaller rollover threshold limit.

- Transient fluid slosh in pitch plane is also a significant factor that affects the braking characteristics of partly filled tank vehicles. The high amplitude slosh force and moment observed in the cleanbore tank tend to cause lockup of the rear axle wheels, and yield large magnitude variations in the deceleration. The magnitude of slosh forces and moment can be significantly suppressed by the addition of transverse baffles, thereby reducing the vehicle responses in the dynamic load factor, deceleration and stopping distance. The slosh frequency is slightly higher in the tank trucks than in the tank alone with the fixed base.
- The stopping distance is affected by the tank configuration, fluid fill volume, treadle pressure and road surface adhesion. The stopping distance of partly-filled tank vehicles, particularly when equipped with the unbaffled tank, is considerably longer than that of the equivalent rigid cargo truck. For the cleanbore tank truck, lower fill volume tends to generate longer stopping distance. For the baffled tank, the fluid cargo filled with the intermediate fill volume may yield longer stopping distance compared to those with the low and high fill volumes. Higher braking treadle pressure yields shorter stopping distance.

In summary, it can be concluded that the fluid slosh is highly dependent on the tank configuration, fill volume and nature of excitation. Large amplitude slosh may occur when a partly-filled tank is subjected to an excitation near the resonant frequency or in high magnitude. Large amplitude fluid slosh exhibits highly non-linear oscillatory characteristics, which causes large amplified slosh forces and moments compared to the

results attained from the QS or equivalent rigid cargo. The amplifications significantly destabilize the roll stability and degrade the braking performance of partly filled tank trucks. Addition of baffles can significantly increase the longitudinal mode slosh frequency, and decrease the peak slosh forces and moments, thus enhancing the braking performance of tank vehicles.

## 7.3 MAJOR CONTRIBUTIONS

The literature review has indicated very limited studies on the transient behavior of the fluid slosh. This is attributed mainly to the challenges in both experimental and numerical investigations on the subject. As a result, the transient fluid slosh behavior and its impact on the road tank vehicle stability is poorly understood. The present dissertation research provided a thorough insight into this complex phenomenon, which leads to a better understanding of its influence on the road tank vehicle stability and eventually contributes towards the development of safer road tank vehicle systems. The major contributions of the present research are summarized below:

- The characterization of transient three-dimensional fluid slosh is accomplished through the experimental investigation in a scaled tank model. The experimental analysis of fluid slosh involve many significant control parameters that may affect the slosh phenomenon, which include excitation parameters such as frequency, magnitude and direction, as well as different tank configurations and fill volumes. The slosh characteristics are quantified in terms of the responses of all relevant parameters, including the slosh frequency and the transient three-dimensional forces and moments.

- An effective three-dimensional fluid slosh model is attained in this dissertation research, which is proven to be applicable under a wide range of conditions. The slosh model is analyzed for baffled and unbaffled tank configurations, different fill volumes and excitations. The frequency and time responses of the slosh forces and moments, which are vital for the road tank vehicle dynamics, are analyzed in detail.
- The investigation of transient three-dimensional slosh in the fullscale "Reuleaux triangular" tank is conducted for the first time. The study involves cleanbore and baffled configurations and different fill volumes. The baffle design factors are also evaluated with a fullscale tank, while very little efforts have been previously undertaken in this field.
- The influence of transient fluid slosh on the destabilization of road tank trucks is analyzed in detail through coupled transient slosh model and dynamic vehicle model. The analyses of the roll stability and braking responses of road tank vehicles in case of the transient fluid slosh are considered in detail. The results have shown for the first time that the roll stability limits are significantly lower than when the transient fluid slosh effects are considered as compared to the widely used quasi-static analysis, and the strong interaction exists between the fluid and the vehicle body of a partly-filled tank truck under a braking maneuver.

## 7.4 RECOMMENDATIONS FOR THE FUTURE WORK

Owing to the complexity of the fluid slosh, substantial efforts have been made in the present dissertation research to experimentally and numerically investigate this

challenging phenomenon. The applications of the slosh model in the present work are limited to the preliminary investigation of baffle design factors, and the single-plane stability analysis of tank vehicles with considerable simplifications. The present study constitutes a preliminary but significant step to identify the transient fluid slosh characteristics and its influence on the destabilization of partly filled tank vehicles. Therefore, this work can be continued to obtain deep insight into the fluid slosh phenomenon, improve the baffle anti-slosh effectiveness and enhance the tank vehicle stability. Some future recommendations in this regard are summarized as follows:

- The experimental slosh investigations in conventional circular tanks are important for further understanding of the fluid slosh dynamics in different tanks. The experimental data can be also very helpful to distinguish the fluid slosh characteristics for the conventional circular tank from those of the optimal "Reuleaux triangular" tank.
- The developed fluid slosh model can be further used to explore the high effective anti-slosh lateral baffles in suppressing the longitudinal slosh. The present study showed that the baffle orifice shape and location play significant role in reducing the slosh moments. Thus, the baffle design could be analyzed for more vertical orifice locations and other types of shapes so as to identify an optimized mechanism for all fill volumes, if possible.
- The present study is limited to the static roll stability analysis. Due to strong interaction between the sloshing liquid and the dynamic vehicle body, the analysis of dynamic roll characteristics would be essential in the study of roll stability of tank vehicles, which can be realized with the slosh model integrated to a dynamic

roll plane vehicle model. This study will allow the roll stability analysis of tank vehicles under path-change maneuvers.

- The effect of transient three-dimensional fluid slosh on a tank-vehicle system needs to be investigated. For this purpose, the three-dimensional fluid slosh model should be integrated into a three-dimensional vehicle model. This comprehensive integrated model can be used for the analysis of vehicle responses under braking-in-turn maneuvers, under which the fluid slosh is highly three-dimensional. In this case, the influence of slosh on the vehicle is complex and involves all components of slosh forces and moments.

# REFERENCES


[1] Campbell, K.L.; Sullivan, K.P. (1991) "Heavy truck cab safety study," Proceedings of the 35th Stapp Car Crash Conference, Univ of Michigan Tran Res Inst, MI, USA, pp.199-225.

[2] Winkler, C. (2000) "Rollover of heavy commercial vehicles," UMTRI Research Review, University of Michigan Transportation Research Institute, October-December, vol.31, no.4

[3] Strandberg, L. (1978) "Lateral stability of Road Tankers", National Road & Traffic Res Inst Report 138A, Sweden.

[4] Woodrooffe, J. (2000) "Evaluation of dangerous goods vehicle safety performance," Transport Canada Report, TP 13678 E.

[5] Abramson, H.N. (1966) "The dynamic behavior of liquids in moving containers," NASA SP-106.

[6] Nalecz, A.G. and Genin, J. (1984) "Dynamic stability of heavy articulated vehicles," Int. J. of Vehicle Design, vol.5, no.4, pp.417-426.

[7] Ranganathan, R. (1990) "Stability analysis and directional response characteristics of heavy vehicles carrying liquid cargo," Ph.D. thesis, Concordia University, Montreal, Canada.

[8] Liu, P.J.; Rakheja, S.; Ahmed, A.K.W. (1998) "Dynamic rollover threshold of articulated freight vehicles", Heavy Vehicle Systems, Int. J. of Vehicle Design, vol.5, nos.3/4, pp.300-322.

[9] Wong, J.Y. (2001) "Theory of Ground Vehicles," John Wiley & Sons, INC., 3rd edition.

[10] Kang, X. D. (2001) "Optimal tank design and directional dynamic analysis of liquid cargo vehicles under steering and braking," Ph.D. thesis, Department of Mechanical and Industrial Engineering, Concordia University.

[11] Ervin, R.D. (1983) "The influence of size and weight variables on the roll stability of heavy duty trucks," SAE paper, no.831163.

[12] Verma, M.K. and Gillespie, T.D. (1980) "Roll dynamics of commercial vehicles," Vehicle System Dynamics, vol.9, pp.1-17.

[13] Jindra, F. (1965) "Handling characteristics of tractor-trailer combinations," SAE paper, no.650720.

[14] Mallikarjunarao, C. and Fancher, P. (1978) "Analysis of the directional response characteristics of double tankers," SAE paper, no.781064.

[15] Vallurupalli, R.K. (1993) "Directional dynamic analysis of an articulated vehicle with articulation dampers and forced-steering," Master Thesis, Concordia University, Canada.

[16] Winkler, C.B.; Ervin, R.D. (1999) "Rollover of heavy commercial vehicles," Final Report, The University of Michigan Transportation Research Institute, UMTRI-99-19, August.

[17] ISO 14791. "Road vehicles – Heavy commercial vehicle combinations and articulated buses – Lateral stability test methods," International Organization for Standardization, Geneva, Switzerland.

[18] Winkler, C.B.; Bogard, S.E.; Bown, M.A.; Ganduri, S.M.; Lindquist, D.J. (1995) "An operational field test of long combination vehicles using ABS and C-dollies," Volume: final technical report, University of Michigan Transportation Research Institute, Report no. UMTRI-95-45-1.

[19] Mikulcik, E.C. (1971) "The dynamics of tractor-semitrailer vehicles: the jackknifing problem," SAE paper, no.710045.

[20] Mallikarjunarao.C. (1981) "Road tanker design: its influence on the risk and economic aspects of transporting gasoline in Michigan," PhD thesis, University of Michigan, December.

[21] Gillespie, T.D. and MacAdam, C.C. (1982) "Constant velocity yaw/roll program," User's Manual, Technical Report, The University of Michigan Transportation Research Institute (UMTRI), UMTRI-82-39, October.

[22] MacAdam, C.C.; Fancher, P.S.; Hu, G.T.; *et al.* (1980) "A computerized model for simulating the braking and steering dynamics of trucks, tractor-semitrailer, doubles and triple combinations," User's Manual, Phase IV, MVMA Project 1197, UM-HSRI-80-58, September.

[23] Ibrahim, R.A.; Pilipchuk, V.N.; and Ikeda, T. (2001) "Recent advances in liquid sloshing dynamics," Appl Mech Rev, vol.54, no.2, pp.133-198.

[24] Abramson, H.N., Chu, W.H. and Kana, D.D. (1966) "Some studies of nonlinear lateral sloshing in rigid containers," Journal of Applied Mechanics, Transactions of the ASME, vol.33, no.4, pp.777-784.

[25] Hutton, R.E. (1963) "An investigation of nonlinear, nonplanar oscillations of liquid in a cylindrical container," NASA Technical Note D-1870, May.

[26] Berlot, R.R. (1959) "Production of rotation in a confined liquid through translational motions of the boundaries," Journal of Applied Mechanics, vol.26, TRANS. ASME, vol.81, Series E. pp.513-516.

[27] Lam, C.P. (1986) "Comparison of simulation and test results for various truck combination configurations," Proc. Of Int. Symp. On heavy vehicle weight and dimension, pp.315-335.

[28] Budiansky, B. (1960) "Sloshing of liquids in circular canals and spherical tanks," Journal of the Aerospace Sciences, vol.27:3, pp.2601-2606.

[29] Sankar, S.; Ranganathan, R. and Rakheja, S. (1992) "Impact of dynamic fluid slosh loads on the directional response of tank vehicles," Vehicle System Dynamics, vol.21, no.6, pp.385-404.

[30] Silvermann, S. and Abramson, H. (1966) "Lateral sloshing in moving containers," in H.N. Abramson (ed) The Dynamic behaviour of liquids in moving containers, NASA SP-106.

[31] Romero, J.A.; Hildebrand, R.; Martinez, M.; Ramirez, O. and Fortanell, J.M. (2005) "Natural sloshing frequencies of liquid cargo in road tankers," Int. J. of Heavy Vehicle System, vol.12, no.2, pp.121-138.

[32] Su, T.C.; Lou, Y.K., Flipse, J.E. and Bridges, T.J. (1982) "A numerical analysis of large amplitude liquid sloshing in baffled containers," Ocean Engineering Program, Texas A&M University, College Station, Texas, USA, Report no. MA-RD-940-82046.

[33] Faltinsen, O.M. and Rognebakke, O.F. (2000) "Sloshing," NAV 2000: International Conference on Ship and Shipping Research, 13rd Congress, 19-22 September, Venice, Italy.

[34] Sankar, S.; Rakheja, S. and Ranganathan, R. (1989) "Directional response of partially filled tank vehicles," SAE paper, no.892481.

[35] Popov, G. (1991) "Dynamics of liquid sloshing in road containers," Ph.D. thesis, Department of Mechanical and Industrial Engineering, Concordia University.

[36] Modaressi, K. (2004) "Analysis of transient liquid slosh inside a partly filled tank subjected to lateral and longitudinal acceleration fields," M.S. thesis, Department of Mechanical and Industrial Engineering, Concordia University, Montreal, Canada.

[37] Uras, R.A. (1995) "Sloshing analysis of viscous liquid storage tanks," Fluid-sloshing and Fluid-structure Interaction, ASME Pressure Vessels and Piping Conf., PVP- vol.314, pp.63-72.

[38] Jitu K.; Chiba T.; Media T. (1994) "An experimental study of the effect of liquid viscosity on dynamic response of the fluid-filled co-axial cylinder," Sloshing, Fluid-Structure Interaction and Struct response Due to Shock and Impact Loads, ASME Pressure Vessels and Piping Conf., PVP- vol.272, pp.101-110.

[39] Case. K.; Parkinson, W. (1957) "Damping of surface waves in an incompressible liquid," J Fluid Mech., vol.2(2), pp.172-184.

[40] Popov, G.; Sankar, S. and Sankar, T. S. (1993) "Dynamics of liquid sloshing in baffled and compartmented road containers," Journal of Fluids and Structures, no.7, pp.803-821.

[41] Berlamont , J. and Vanderstappen, N. (1979) "The effect of baffles in a water tower tank," Proc 5th Int Conf Wind Eng, Ford Collins, CO.

[42] Wang, Z.; Rakheja, S. and Sun, C. (1995) "Influence of partition location on the braking performance of a partially filled tank truck," Society of Automotive Engineers, pp.75-84.

[43] Silverai, M.A.; Stephens, D.C. and Leonard, H.W. (1961) "An experimental investigation of damping of liquid oscillations in cylindrical tanks with various baffles," NASA, TND-715

[44] Summer, I.E. (1964) "Experimental investigation of slosh suppression effectiveness of annular ring baffles in spherical tanks," NASA TN D-2519.

[45] Stephens, D.G. (1966) "Experimental investigation of liquid impact in a model propellant tank," NASA TND-2913

[46] Stephens, D.G. and Scholl, H.F. (1967) "Effectiveness of flexible and rigid ring baffles for damping liquid oscillations in large scale cylindrical tanks," NASA TN D-3878.

[47] Dodge, F.T. (1971) "Eng study of flexible baffles for slosh suppression," NASA, CR-1880

[48] Lloyd, N.; Vaiciurgis, E.; and Langrish, T.A.G. (2002) "The effect of baffle design on longitudinal liquid movement in road tankers: an experimental investigation," Process Safety and Environmental Protection: Transactions of the Institution of Chemical Engineers, Part B, vol.80, n 4, July, pp.181-185.

[49] Wiesche, S.A.D. (2003) "Computational slosh dynamics: theory and industrial application," Computational Mechanics, Springer-Verlag, vol.30, pp.374-387.

[50] Harlow, F.H.; Welch, J.E. (1965) "Numerical calculation of time-dependent viscous incompressible flow of fluid with free-surface," Physics of Fluids, vol.8, no.12, pp.2182-2189.

[51] Mikelis, N.E.; Miller, J.K.; Taylor, K.V. (1984) "Sloshing in partially filled liquid tanks and its effect on ship motions: numerical simulations and experimental verification," A conference proceeding of The Royal Institution of Naval Architechs, April 11, pp.267-282.

[52] Hirt, C.W.; Nichols, B.D.; and Pomeroy, N.C. (1975) "SOLA – A numerical solution algorithm for transient fluid flows," Los Alamos Scientific Laboratory, Report LA-5852.

[53] Navickas, J.; Peck, J.C.; Bass III, R.L.; Bowles, E.B.; Yoshimura, N. and Endo, S. (1981) "Sloshing of fluids at high fill levels in closed tanks," ASME Winter Meeting, Washington D.C., pp191-198.

[54] Armenio, V.; La Rocca, M. (1995) "Numerical and experimental analysis of liquid sloshing in rectangular containers," Computational Mechanics Publ, pp.11-21.

[55] Rumold, W. (2001) "Modeling and simulation of vehicles carrying liquid cargo," Multibody System Dynamics, vol.5, pp.351-374.

[56] Wang, J.P.; Borthwick, A.G.L. and Taylar, R.E. (2004) "Finite-volume-type VOF method on dynamically adaptive quadtree grids," International Journal for Numerical Methods in Fluids, vol.45, pp. 485-508.

[57] Sames, P.C., Marcouly, D. and Schellin, T.E. (2002) "Sloshing in rectangular and cylindrical tanks," Journal of Ship Research, vol.46, no.3, Sept., pp.186-200.

[58] Okamoto, T. and Kawahara, M., (1990) "Two-dimensional sloshing analysis by Lagragian finite element method," Int. J. Numerical Methods Fluids, no.11, pp.453-477.

[59] Webb, D.C. and Kormi, K. (1999) "The use of the finite element method in the simulation of liquid sloshing," Proceedings of the Ninth International Offshore and Polar Engineering Conference, Brest, France, May 30-June 4, vol.3, pp.615-620.

[60] Kondo, N. (2000) "Three-demensional finite element analysis for incomprehensive viscous fluid with free surface," Theoretical and Applied Mechanics, vol.49: Proceedings of the 41st Japan National Congress for Applied Mechanics, pp.127-35.

[61] Wu, G.X.; Ma, Q.W. and Taylor, R.E. (1998) "Numerical simulation of sloshing waves in a 3D tank based on a finite element method," Applied Ocean Research, vol.20, pp.337-355.

[62] Pal, N.C.; Bhattacharyya, S.K.; Sinha, P.K. (1999) "Coupled slosh dynamics of liquid filled composite cylindrical tanks," J. Eng. Mech., ASCE, vol.125, pp.491-495.

[63] Nakayama, T. and Washizu, K. (1981) "The boundary element method applied to the analysis of two-dimensional nonlinear sloshing problems," International Journal for Numerical Methods in Engineering, vol.17, pp.1631-1646.

[64] Shiojiri H.; Hagiwara Y. (1990) "Development of a computational method for nonlinear sloshing by BEM, Fluid-structure Vibration and Sloshing," ASME Pressure Vessels and Piping Conf., PVP, vol.191, pp.149-154.

[65] Sugino, R.; Tosaka, N. (1992) "Sloshing analysis by boundary element method with direct differentiation procedure," Theoretical and Applied Mechanics, vol.41, pp.191-198.

[66] Landrini, M.; Grytoyr, G. and Faltinsen, O.M. (1999) "A B-Spline based BEM for unsteady free-surface flows," Journal of Ship Research, vol.43, no.1, pp.13-24.

[67] Dutta, S. and Laha, M.K. (2000) "Analysis of the small amplitude sloshing of a liquid in a rigid container of arbitrary shape using a low-order boundary element method," Int. J. Numer. Meth. Eng., vol.47, pp.1633-1648.

[68] Daly, B.J. (1969) "Numerical study of the effect of surface tension on interface instability," Phys. Fluids, vol.12, pp.1340.

[69] Kim, Y. (2001) "Numerical simulation of sloshing flows with impact load," Applied Ocean Research, vol.23, pp.53-62.

[70] Armenio, V. (1997) "An Improved MAC Method (SIMAC) for Unsteady High-Reynolds Free Surface Flows," International Journal for Numerical Methods in Fluids. vol.24, no.2, pp.185–214.

[71] Change, S.C. and To, W.M. (1992) "A brief description of a new numerical framework for solving conservation laws: the method of space-time conservation element and solution element," Proceedings of the 13th Int. Conf. On Numerical Methods in Fluid Dynamics, Rome, Italy, pp.396-400.

[72] Chan, R.K.C. and Street, R. L. (1970) "A computer study of finite-amplitude water waves," Journal of Computational Physics, vol.6, pp.68-94.

[73] Miyata, H.; Nishimura, S.; and Masuko, A. (1985) "Finite difference simulation of nonlinear waves generated by ships of arbitrary three-dimensional configuration," Journal of Computational Physics, vol.60, pp.391-436.

[74] Hirt, C.W. and Nichols, B.D. (1981) "Volume of fluid (VOF) method for the dynamics of free boundaries," Journal of Computational Physics, vol.39, no.1, pp.201-225.

[75] Partom, I.S. (1987) "Application of the VOF method to the sloshing of a fluid in a partially filled cylindrical container," International Journal for Numerical Methods in Fluids, vol. 7, no.6, pp.535-550.

[76] Celebi, M.S. and Akyildiz, H. (2002) "Nonlinear modeling of liquid sloshing in a moving rectangular tank," Ocean Engineering, vol.29, pp.1527-1553.

[77] Hadzic, I.; Mallon, F.; Peric, M. (2001) "Numerical simulation of sloshing, Proc. SRI-TUHH Mini Workshop on Numerical Simulation of Two-phase Flows," Ship Research Institute, Tokyo, Japan.

[78] Torrey, M.D.; Mjolsness, R.C.; Stein, R.L. (1987) "NASA-VOF3D: A three-dimensional computer program for incompressible flows with free surface," Tech. Rep. LA-11009MS, Los Alamos National Laboratory, July.

[79] Solaas, F. (1995) "Analytical and numerical studies of sloshing in tanks," Ph.D. thesis, The Norwegian Institute of Technology, Trondheim, Norway.

[80] Shahbazi, K.; Paraschivoiu, M. and Mostaghimi, J. (2003) "Second order accurate volume tracking based on remapping for triangular meshes," Journal of Computational Physics, vol.188, pp.100-122.

[81] Lafaurie, B.; Mardone, C.; Scardovell, R.; Zaleski, S.; Zanetti, G. (1994) "Modelling merging and fragmentation in multiphase flows with SURFER," Journal of Computational Physics, vol.113, pp.134-147.

[82] Hirt, C.W.; Cook, J.L.; Butler, T.D. (1970) "A Lagrangian method for calculating the dynamics of an incompressible fluid with free surface," Journal of Computational Physics, vol.5, pp.103.

[83] Hirt, C.W.; Amsden, A.A.; Cook, J.L. (1974) "An arbitrary Langrangian-Eulerian computing method for all flow speeds," Journal of Computational Physics, vol.14, pp.227.

[84] Nichols, B.D. and Hirt, C.W. (1971) "Calculating three-dimensional free surface flows in the vicinity of submerged and exposed structures", J. Comp. Phys., no.12, pp.234.

[85] Nichols, B.D.; Hirt, C.W. (1975) "Methods for calculating multidimensional, transient free surface flows past bodies," Proc. of the First International Conf. on Num. Ship Hydrodynamics, Gaithersburg, ML, Oct. 20-23.

[86] Solaas F.; Faltinsen O. M. (1997) "Combined numerical and analytical solution for sloshing in two-dimensional tanks of general shape," J Ship Res, vol.41, pp.118-129

[87] Faltinsen, O. M. (1974) "A nonlinear theory of sloshing in rectangular tanks," Journal of Ship Research, vol.18, no.4, Dec. pp.224-241.

[88] Moiseev, N.N. (1958) "On the theory of nonlinear vibrations of a liquid of finite volume," Applied Mathematics and Mechanics (PMM), vol.22, no.5, pp.860-872

[89] Faltinsen, O.M., Rognebakke, O.F., Lukovsky, I.A., Timokha, A.N. (2000) "Multidimensional modal analysis of nonlinear sloshing in a rectangular tank with finite water depth," J. of Fluid Mechanics, vol.407, pp.201-234.

[90] Faltinsen, O.M. and Timokha, A.H. (2001) "Adaptive multimodal approach to nonlinear sloshing in a rectangular tank," J. of Fluid Mechanics, vol.432, pp.167-200.

[91] Rognebakke, O.F. and Faltinsen O.M. (2003) "Coupling of sloshing and ship motions, J. of Ship Research," vol.47, no.3, pp.208-221.

[92] Faltinsen, O.M., Rognebakke, O.F. and Timokha, A.N. (2003) "Resonant three-dimensional nonlinear sloshing in a square-base basin," J. Fluid Mech., vol.487, pp.1-42.

[93] Faltinsen, O.M. and Timokha, A.N. (2002) "Asymptotic modal approximation of nonlinear resonant sloshing in arectanular tank with small fluid depth," J. of Fluid Mechanics, vol.470, pp.319-357.

[94] Lukovsky, I.A. and Timokha, A.N. (2002) "Modal modeling of nonlinear fluid sloshing in tanks with non-vertical walls, non-conformal mapping technique," International Journal of Fluid Mechanics Research, vol.29, no.2, pp.216-242.

[95] Miles, J.W. (1976) "Nonlinear surface waves in closed basins," J. of Fluid Mechanics, vol.75, pp.419-448.

[96] Lukovsky, I.A. (1976) "Variational method in the nonlinear problems of the dynamics of a limited liquid volume with free surface," In Oscillations of Elastic Constructions with Liquid, pp.260-264, Moscow: Volna (in Russian).

[97] Lukovsky, I.A. (1975) "Nonlinear oscillations of a fluid in tanks of complex shape," Naukova Dumka, Kiev, (in Russian).

[98] Dodge, F.T. (1966) "Analytical representation of lateral sloshing by equivalent mechanical models," Chapter 6, NASA SP-106.

[99] Graham, E.W. (1951) "The forces produced by fuel oscillations in a rectangular tank," Douglas Aircraft Co., SM-13748.

[100] Pinson, L.D. (1964) "Longitudinal spring constants for liquid propellant tanks with ellipsoidal tanks," NASA TN D-2220.

[101] Sayar, B.A. and Baumgarten, J.R. (1981) "Pendulum analogy for nonlinear fluid oscillations in spherical containers," Journal of Applied Mechanics, vol.48, pp769-772.

[102] Khandelwal, R.S. and Nigam, N.C. (1982) "Digital simulation of the dynamics of a vehicle carrying liquid cargo on a random uneven surface," Vehicle System Dynamics, vol.11, no.4, pp.195-214.

[103] Khandelwal, R.S. (1980) "Some problems in the sloshing of liquid in moving containers," PhD thesis, Department of Aeronautical Engineering, Indian Institute of Technology, Kanpur, India.

[104] Ranganathan, R.; Ying, Y. and Miles, J.B. (1993) "Analysis of fluid slosh in partially filled tanks and their impact on the directional response of tank vehicles," SAE paper, no.932942, pp.39-45.

[105] Mantriota, G. (2003) "Directional stability of articulated tank vehicles: a simplified model," Heavy Vehicle System, Int. J. of Vehicle Design, vol.10, nos.1/2, pp144-165.

[106] Ranganathan, R.; Ying, Y. and Miles, J.B. (1994) "Development of a mechanical analogy model to predict the dynamic behaviour of liquids in partially filled tank vehicles," SAE paper, no.942307.

[107] Yang, Y.S. (1992) "Directional response characteristics of liquid tank vehicles subjected to dynamic liquid load shift," M.S. thesis, University of Missouri, Columbia, US.

[108] Xu, L. and Dai, L. (2003) "A mechanical model for dynamic behavior of large amplitude liquid sloshing in partially filled tank vehicles," ASME International Mechanical Engineering Congress, Washington,D.C., November 15-21, pp.899-904.

[109] Rakheja, S.; Sankar, S. and Ranganathan, R. (1988) "Roll plane analysis of articulated tank vehicles during steady turning," Vehicle System Dynamics, vol.17, pp.81-104.

[110] Ranganathan, R.; Rakheja, S. and Sankar, S. (1990) "Influence of liquid cargo shift on the dynamic response of articulated tank vehicles," Vehicle System Dynamics, vol.19, pp.177-200.

[111] Ranganathan, R.; Rakheja, S. and Sankar, S. (1989) "Kineto-static roll plane analysis of articulated tank vehicles with arbitrary tank geometry," Int. J. of Vehicle Design, vol.10, no.1, pp.89-111.

[112] Rakheja, S. and Ranganathan, R. (1993) "Estimation of the rollover threshold of heavy vehicles carrying liquid cargo: a simplified approach," Heavy Vehicle Systems, Int. J. of Vehicle Design, vol.1, no.1, pp.79-98.

[113] Rakheja, S.; Sankar, S. and Ranganathan, R. (1989) "Influence of tank design factors on the rollover threshold of partially filled tank vehicles," SAE paper, No.892480.

[114] Hara F. (1989) "Experimental study on sloshing characteristics of a flowing liquid in a tank," Sloshing and Fluid Structure Vibration, The 1989 ASME Pressure Vessels and Piping Conference, JSME, PVP, vol.157, pp.133-141.

[115] Chen, K.H.; Kelecy, F.J.; Pletcher, R.H. (1994) "Numerical and experimental study of three-dimensional liquid sloshing flows," Journal of Thermophysics and Heat Transfer, vol.8, no.3, pp.507-513

[116] Kobayashi, N., Mieda, T.; Shibata, H.; and Shinozaki, Y. (1989) "A study of the liquid slosh response in horizontal cylindrical tanks," Transactions of the ASME, Journal of Pressure Vessel Technology, vol.111, February, pp.32-38.

[117] Pal, N.C.; Bhattacharyya, S.K.; Sinha, P.K. (2001) "Experimental investigation of slosh dynamics of liquid-filled containers," Experimental Mechanics, vol.41, no.1, pp.63-69.

[118] Rakheja, S.; Ranganathan, R. and Sankar, S. (1992) "Fielding testing and validation of directional dynamics model of a tank truck," Int. J. of Vehicle Design, vol.13, no.3, pp.251-275.

[119] Ranganathan, R. and Yang, Y.S. (1996) "Impact of liquid load shift on the braking characteristics of partially filled tank vehicles," Vehicle System Dynamics, vol.26, pp.223-240.

[120] Aquaro, M.; Mucino, V.H.; Gautam, M. and Salem, M. (1999) "A finite element modelling approach for stability analysis of partially filled tanker trucks," SAE paper, no.1999-01-3708.

[121] Mucino, V.; Gautam, M; Salem, M.; Saunders, E. and Aquaro, M. (1998) "Automotive stability of heavy-duty truck tractor tanker combinations," Final Report made to Frederick Manufacturing Division of SFA, December.

[122] Mangialardi, L. and Mantriota, G. (2001) "Stability of an articulated vehicle with suspended cargo," Heavy Vehicle Systems, vol.8, no.1, pp.83-102.

[123] Mantriota, G. (2002) "Influence of suspended cargoes on dynamic behavior of articulated vehicles," Heavy Vehicle Systems, vol.9, no.1, pp.52-75.

[124] Cho, J.R.; Lee, H.W. (2004) "Numerical study on liquid sloshing in baffled tank by nonlinear finite element method," Computer Method in Applied Mechanics and Engineering, vol.193, pp.2581-2598.

[125] Pacejka, H. And Bakker, E. (1993) "The magic formula tire model," in Tyre Models for Vehicle Dynamics Analysis, H. Pacejka (ed.), Swets & Zeitlinger, Amsterdam, 1-18.

[126] Mallikarjunarao, C.; Ervin, R.D. and Segal, L. (1982) "Roll response of articulated motor trucks during steady turning manoeuvres," ASME Winter Ann. Meet., Nov.

[127] Fancher, P.S. (1985) "The static stability of articulated commercial vehicles," Veh. Sys. Dyn., vol.14, pp.210-227.

[128] Modaressi-Tehrani, K.; Rakheja, S. ; Stiharu, I. (2007) "Three-dimensional analysis of transient slosh within a partly-filled tank equipped with baffles," Vehicle System Dynamics, vol.45, no.6, pp.525-548.

[129] Abramson, H. N. and Garza, L. R., 1965, "Liquid frequencies and damping in compartmented cylindrical tanks," AIAA, 2(3), pp.453-455.

[130] Lamb, S. H., 1945, "Hydrodynamics," 6th ed., Dover Publications, New York.

[131] Graham K. S., 2000, "Fundamentals of Mechanical Vibrations," Second Edition, The McGraw-Hill Companies, Inc.

[132] EI-Gindy, M., 1995, "An overview of performance measures for heavy commercial vehicles in North America," Int. J. Vehicle Design, **16**(4/5), pp.441-463.

[133] Rhee, S. H., 2005, "Unstructured grid based Reynolds-averaged Navier-Stokes method for liquid sloshing," J. Fluids Eng., 127, pp.572-582.

[134] Lee, Y.S.; Kim, H.S.; Lee, J.H. and Ko, S.H. (2003) "A study of the damping of the sloshing of storage tank using wing and diaphragm baffle," 10th International Congress on Sound and Vibration, Stockholm, Sweden, 7-10 July.

[135] Wendel, G.N.; Green, S.T. and Burkey, R.C. (2002) "Testing and validation of tank analysis," Phase 1 Report of "Coupled simulation of vehicle dynamics and tank slosh," Southwest Research Institute, SwRI Project No. 03.03227.14.

[136] Fluent (2001) "Tank sloshing validation," Example 161, Application Briefs From Fluent.

[137] Armenio, V. and La Rocca, M. (1996) "On the analysis of sloshing of water in rectangular containers: numerical study and experimental validation," Ocean Engineering, vol.23, no.8, pp.705-739.

[138] Ghorai, S. and Nigam, K.D.P. (2006) "CFD modeling of flow profiles and interfacial phenomena in two-phase flow in pipes," Chemical Engineering and Processing, vol.45, pp.55–65.

[139] Korang, M.-T. (2004) "Analysis of transient liquid slosh inside a partly filled tank subjected to lateral and longitudinal acceleration fields," Master's thesis, Concordia University.

[140] Issa, R.I. (1986) "Solution of Implicitly Discretized Fluid Flow Equations by Operator Splitting," J. Comput. Phys., vol.62, pp.40-65.

[141] Modaressi-Tehrani, K.; Rakheja, S. and Sedaghati (2006) "Analysis of the overturning moment caused by transient liquid slosh inside a partly filled moving tank," Proc. IMechE Vol.220, Part D: J. Automobile Engineering, pp.289-301.

[142] Kang, X., Rakheja, S. and Stiharu, I. (2002) 'Cargo Load Shift and its Influence on Tank Vehicle Dynamics under Braking and Turning', Int. J. of Heavy Vehicle Systems, 9(3), pp.173-203.

[143] Popov, G., Sankar, S., Sankar, T. S. and Vatistas, G. H. (1992) 'Liquid sloshing in rectangular road containers,' Computers Fluids, 21, No.4, pp. 551-569.

[144] Washizu, K., Nakayama, T., Ikegawa, M. and Tanaka, Y. (1984) 'Some Finite Element Techniques for the Analysis of Nonlinear Sloshing Problem,' Ch 17, pp. 357-376, Finite Elements in Fluids, 5, RH Gallagher, JT Oden, OC Zienkiewicz, and M Kawahara (eds), Jhon Wiley & Sons, New Yorks.

[145] Dai, L.; Xu, L.; and Setiawan, B. (2005) "A new non-linear approach to analysing the dynamic behaviour of tank vehicles subjected to liquid sloshing," Proc. IMechE Vol.219 Part K: J. Multi-body Dynamics, pp.75-86.

[146] Cao, D., Rakheja, S. and Su, C.-Y. (2007) "Pitch attitude control and braking performance analysis of heavy vehicle with interconnected suspensions," SAE paper, 2007-01-1347

[147] Delaigue, P. and Eskandarian, A. (2004) "A comprehensive vehicle braking model for predictions of stopping distance," Journal of Automobile Engineering, 218, pp.1409-1417

[148] Fancher, P.S., Ervin, R.D., Winkler, C.B. and Gillespie, T.D. (1986) "A factbook of the mechanical properties of the components for single-unit and articulated heavy trucks," UMTRI-86-12, The University of Michigan.

[149] Fancher, P.S. (1995) "Generic data for representing truck tire characteristics in simulations of braking and braking-in-a-turn maneuvers," UMTRI-95-34, The University of Michigan.

[150] Biglarbegian, M. and Zu, J.W. (2006) "Tractor-semitrailer model for vehicles carrying liquids," Vehicle System Dynamics, vol.44, no.11, pp.871-885.

[151] FLUENT 6.2.16 Documentation, 2005, User's Guide, Chapter 24, General Multiphase models.